Simulated alkaline hydrothermal vent environments to investigate prebiotic metabolism at the origin of life

By

Alexandra Whicher

The department of Genetics, Evolution and Environment

University College London

UK

Supervised by

Dr. Nick Lane

A thesis submitted for the degree of

Doctor of Philosophy

Division of Biosciences

Declaration

I, Alexandra Whicher, confirm that the work presented in this thesis is my own, except where the work that has formed part of a jointly-authored publication has been included. Where information has been derived from other sources, I confirm that this has been indicated in the thesis.

Abstract

There is still little agreement today about where life may have started on Earth. Prebiotic studies over several decades have successfully synthesised many molecules of life, yet the results display strikingly little congruence to the biochemistry of cells today. In contrast, alkaline hydrothermal vents offer conditions very similar to those harnessed by modern autotrophic cells, while providing a physical structure for a prebiotic metabolism that resembles the vectorial biochemistry of extant cells. Alkaline vents have not received much attention in experimental investigations, even though they have many features that point to their ability to drive prebiotic chemistry. This study set out to simulate inorganic, catalytic barriers equivalent to those that are thought to have existed inside early alkaline vent systems. These structures were then used to investigate the reduction of CO_2 by H_2, driven by natural proton gradients transecting semi-conducting barriers containing catalytic FeS minerals. Simple organics such as formaldehyde were successfully synthesised and observed to be closely associated with the precipitates. The next step examined potential prebiotic reactions that could have preceded modern metabolic processes. Methyl thioacetate and thioacetic acid have been suggested as possible precursors of acetyl-coenzyme A, therefore its synthesis from the 1-carbon precursors methyl sulphide and formate was attempted. Finally the synthesis of a plausible prebiotic analogue of ATP, acetyl phosphate, was demonstrated from the 2-carbon precursor thioacetate under ambient and mild hydrothermal conditions. Acetyl phosphate was shown to drive both phosphorylation and condensation reactions equivalent to ATP, in water, notably the formation of two key activated precursors of RNA synthesis, ribose phosphate and adenosine monophosphate. The results suggest that alkaline hydrothermal systems could indeed drive the beginnings of a prebiotic metabolism more congruent with living cells, and point to future research into this hypothesis.

Acknowledgements

First and foremost I would like to thank Nick Lane for giving me the opportunity to study the amazing subject that is the origin of life! His continual support and flow of thought provoking conversations is what kept me believing in my passion to solve the problem and come up with new, exciting ideas. I would also like to thank my second supervisors and thesis committee, John Ward, Julian Evans, and Finn Werner, who provoked new and fresh prospectives in our meetings. I would like to thank my fellow Lane Lab members Eloi, Victor and Barry for all their support throughout my time at UCL. Thanks to all in the 6th floor office for keeping me alive with our cake Mondays. I would also like to thank all the support staff, core facility technicians and PhD students who helped me with the different machines used in this project, particularly Kersti Karu and Benjamin Lichman. I thank the Leverhulme Trust for funding this research, enabling the foundations to be laid for some exciting new discoveries.

I would like to give a special thanks to my family and friends for their unending support and encouragement. Particularly to my sister Charlie for keeping me sane at home, listening to my problems and giving me perspective when things got tough, to my parents for their excitement and encouragement in my work and their amazing help in proof-reading my whole thesis, and finally to my boyfriend Alex for being such a big support during the write-up period.

Contents

List of Figures

List of Tables

List of Abbreviations

acetyl-CoA	Acetyl coenzyme-A
AcP	Acetyl phosphate
AMP	Adenosine monophosphate
ANOVA	One-way analysis of variance
ATP	Adenosine triphosphate
ATPase	Adenosine triphopshate synthase
cTMP	Cyclic trimetaphosphate
DKP	2,5-diketopiperazine or glycine anhydride
DNA	Deoxyribonucleic acid
DNPH	2,4-dinitrophenylhydrazine
Ech	Energy-converting hydrogenase
EDX	Energy-dispersive x-ray
ESI	Electrospray ionisation
FeS	Iron sulphide
FeSi	Iron silicate
FFT	Fast Fourier transform
GC-MS	Gas Chromatography - Mass Spectroscopy

HPLC	High Performance Liquid Chromatography
HSRC	Hydrogen sulphide removal column
IC	Inorganic carbon
LC-MS	Liquid Chromatography - Mass Spectrometry
LUCA	Last universal common ancestor
NADH	Reduced nicotinamide adenine dinucleotide
NMR	Nuclear magnetic resonance
NPOC	Non-purgable organic carbon
PFBOA	o-(2,3,4,5,6-pentafluorobenzyl)-hydroxylamine
pH	Measure of how acidic or basic a fluid is
POC	Purgeable organic carbon
PPi	Pyrophosphate
PXRD	Powder x-ray diffraction
RNA	Ribonucleic acid
SD	Standard deviation
SEM	Scanning Electron Microscope
TC	Total carbon
TEM	Transmission Electron Microscope
TOC	Total organic carbon
UV	Ultraviolet light

Chapter 1

Introduction

1.1 A fundamental question

'How and where did life originate on Earth?' remains one of the most fundamental questions for humanity, and has been a subject of contention for millennia. Until the 19th century, most people believed in spontaneous generation of life from non-living matter. It was believed that maggots in rotting meat or even mice in grain were spontaneously generated from decaying materials. It was not until Louis Pasteur found that tiny organisms were everywhere that this doctrine came into question. He showed, in a series of experiments, that these organisms grew very quickly in organic media, but could not grow in sterile media, disproving the idea of spontaneous generation (Pasteur, 1862; Schwartz, 2001; Ligon, 2002). This ultimately proved that all living organisms originate from other living organisms, bringing into question how life first started.

An issue we have to address here is what is 'Life'? Answers can differ dramatically, and some say suggesting definitions can cause problems from other counter arguments (Cleland and Chyba, 2002). However, there is a general agreement that living things have the ability to take in energy from the environment and transform it for growth and reproduction. Therefore life is a process of harnessing energy to make copies of itself, and when looking at the chemical evolution of life from the elements on the early Earth to free-living cells we need to recognise the need for a sustained source of energy (Martin, 2012).

One of the biggest problems for origin of life research is a lack of evidence to indicate what conditions on early Earth would have been like. What chemicals and energy sources would have been available to power the synthesis of simple inorganic molecules and their polymerisation, to more complex organic structures? This makes it difficult to understand what chemicals would have been available for life to have used as its building blocks. Some hypotheses try to avoid these problems by proposing that life came from an extraterrestrial source, known as panspermia, where cells or complex organics arrived on Earth by meteoritic impact. The first detailed hypothesis for panspermia came from Svante Arrhenius in 1908 (Arrhenius, 1908). This hypothesis removes the issue of the unknown period of time on Earth before habitability, when conditions were not favourable for the growth of micro-organisms. However, it also avoids the question of how life could have started anywhere else in the universe, and the whole origin of life question. If the universe had an origin, then the first appearance of any organisms must have occurred somewhere in the universe (Hartman, 1975). Given the fact that there is life on Earth today, and we know vaguely what the conditions on early Earth would have been like, it makes sense to look for its origin in a location where there are some environmental constraints rather than none.

If we can find conditions on Earth that could support synthesis of key molecules needed for life, applying Occam's Razor would suggest that life will originate in those conditions. This principle also suggests that life will take the most direct path from its basic chemical origins to complex biochemistry. There are two directions to go about investigating the transition from prebiotic to biotic, from the bottom up or from the top down (Peters and Williams, 2012). The most popular, 'Bottom-Up' approach, looks at the chemical and physical conditions of a prebiotic Earth, and applies the fundamental principles of chemistry, organic synthesis and molecular polymerisation to these conditions in experimental systems (Miller, 1953). Conversely, the 'Top-Down' approach looks at the biochemistry and phylogeny of extant ancient life and tries to find links back to a simpler biological system that could fit with the geological and chemical conditions on the early Earth (Woese, 2000). Although a valid solution

to this problem has yet to be found, there can be no doubt that considerable progress has been made in the last few decades, with laboratory experimental investigations being a major part of this progress, particularly the investigation into prebiotic chemistry (McCollom, 2013).

1.2 Origin of life research

1.2.1 Pioneering ideas and early experiments

Initial ideas for the origin of life came from Charles Darwin, where he supposed life could have begun in a warm little pond, with ammonia and phosphoric salts, along with a source of energy, such as light, heat or electricity. This he wrote in a letter to his friend Joseph D. Hooker in 1871 (contained in the Darwin project database; Darwin Correspondence Project, http://www.darwinproject.ac.uk). This was an amazing insight, considering it was decades before phosphorus was recognised as an essential element of energy metabolism and information storage (Follmann and Brownson, 2009). In the early 20th Century, Leduc (1911) suggested that inorganic osmotic membranes could have comprised the boundaries of the first living cells, encapsulating an ever-evolving chemical system. Many others came up with different hypotheses for the theoretical origin of life. The first comprehensively structured hypotheses for the origin of life were proposed independently by Oparin (in 1924) and Haldane (in 1929, before Oparin's first book was translated into English). They proposed similar ideas, that life arose from simple organic molecules which coalesced into a more complex state. Their theory relies on the early Earth having a reducing atmosphere of methane (CH_4), ammonia (NH_3), water (H_2O), and hydrogen (H_2), with UV radiation or lightning as the source of energy to create the first organic compounds within the atmosphere, which then dissolved into the oceans. The sea then became host to large populations of organic monomers and polymers, which further acquired lipid membranes that led to the first cells. Haldane coined the term 'prebiotic soup', which became a powerful driver for origin of life research.

The Oparin-Haldane ideas were backed up by pioneering experiments carried out by Stanley Miller and Harold Urey in the 1950's (Miller, 1953). This was known as the Miller-Urey experiment, and was the landmark experimental investigation of prebiotic chemistry, with the objective of testing this specific origin of life theory. The experiments consisted of an apparatus to circulate CH_4, NH_3, H_2O and H_2 past an electrical discharge, simulating the primordial atmosphere and ocean, with an energy input that might have been supplied by lightning strikes. The resulting mixture was found to contain five amino acids and several other simple organic compounds (Miller, 1953).

In the years since this pioneering work, experimental investigations have proliferated, so much so that it is beyond the scope of this review. Therefore the focus will remain on developments in geological understanding of the early Earth's conditions and how this has changed origin of life theories, touching only briefly on the prebiotic soup theories. It is understood that an inventory of chemical compounds would have been required on the early Earth to first form simple organic compounds, and from there build up to more complex structures which would act as precursors to the modern building blocks of life, such as amino acids, proteins, nucleic acids and membranes. The ingredients for life are important, but the environment in which they might then assemble and evolve is also crucial.

In the 1940's, prior to the Miller-Urey experiments, Victor Goldschmidt predicted a very different set of early atmospheric conditions than the reducing atmosphere proposed by Oparin and Haldane, and consequently a different view for how life could have started (published after his death by his friend N.W. Pirie; Goldschmidt, 1952). Goldschmidt disagreed with the idea of an atmosphere of carbon monoxide and gaseous hydrocarbons, and suggested an atmosphere of predominantly carbon dioxide (CO_2), which would have been exhaled from the interior of the Earth, providing ingredients for the formation of primitive molecules. Goldschmidt proposed that the formation of organics would be more likely if they were adsorbed onto surfaces or phase boundaries, with reactions being catalysed by minerals within these solid phases. Leduc (1911) previously had similar ideas, that these phase boundaries could have formed membranes to

encapsulate simple organics. Later evidence confirms Goldschmidt's view that the early atmosphere was unlikely to be reducing, but weakly oxidising (Holland, 1962; Wilde et al., 2001; Trail et al., 2011). The composition of the atmosphere and early Earth conditions in general, to this day, remain a mystery, and an issue of serious controversy, due to the fact that very little evidence remains from this early period in Earth history. There is no rock record surviving from the first 500 million years of Earth history, due to a continuously active crust (Arndt and Nisbet, 2012). However, we can gain clues about the Earth's early history from studying oxygen isotopes ($^{18}O/^{16}$ expressed as $\delta^{18}O$) in ancient zircon grains and the earliest Archaean rocks, that trap chemical data from the time they were formed (Wilde et al., 2001; Trail et al., 2011).

1.2.2 Early Earth conditions

The Earth is known to have formed by a series of accretion events, from grains and small planetesimals which had formed around a young star. This large number, and frequency of planetary collisions would have been large and the energy released would have been sufficient to raise the temperature of the Earth by thousands of degrees (Zahnle et al., 2007). The stage of Earth's accretion ends with the Moon-forming impact, where a Mars-sized planet collided in a glancing blow with the Earth, creating the Moon. Prior to this, Earth's atmosphere would have primarily formed from the captured gases of the solar nebula by gravity, like the gas giants of Jupiter and Saturn. This primary atmosphere would have been mostly lost after the Moon-forming impact, which would have melted the majority of the mantle and vaporised it (Zahnle et al., 2007). A secondary, prebiotic atmosphere would have formed after this event, when the loss of hydrogen to space meant the atmospheric carbon gases were relatively oxidised (Arndt and Nisbet, 2012). The ocean and atmosphere would have cooled quickly, within a few million years, depending on how quickly CO_2 was removed from the atmosphere by crust-mantle cycling (Sleep et al., 2001). However, there is some debate as to whether carbonates were subducted into the mantle at all; if they were then the CO_2 atmosphere would have been thin and the surface cold. If not, due to a lack

of continents on which to store carbonate rocks, CO_2 would have remained in the atmosphere and surface temperatures could have reached $\sim$200 ^{o}C (Sleep et al., 2001; Zahnle et al., 2007).

The Late Heavy Bombardment (LHB) is a period in Earth's history when the Solar System was thought to have been bombarded with many large impacts around 3.8 Ga and would have played a key role in defining the physical characteristics of the early Earth, and therefore the environments in which early life could have colonised (Nisbet, 1985; Nisbet and Sleep, 2001). This event has been postulated as being so catastrophic that conditions on Earth would have been too harsh to support life in a geological environment, therefore the open ocean was the only viable location for the origin of life. There has been much debate regarding the period of time this bombardment may have occurred; some believe that the Solar System was affected by large impacts around 3.8 Ga, while others think such impacts were spread more evenly over approximately 4.3 to 3.8 Ga. The controversy revolves around two impact basins, found on the Moon. However, recent evidence from the isotopic dating of these craters has found that there may have been a mistake in the dating of the ejecta and perhaps the LHB did not occur at all (Spudis et al., 2011). This would improve chances of life evolving in the oceans, or on land.

The atmosphere is now generally accepted to have been a mixture of mainly carbon dioxide (CO_2) and nitrogen (N_2), with negligible levels of oxygen (O_2) (making it anoxic), and only minor levels of reducing gases such as hydrogen (H_2), methane (CH_4), carbon monoxide (CO), hydrogen sulphide (H_2S), ammonia (NH_3) and phosphine (PH_3) (Holland, 1962; Kasting, 1993; Zahnle et al., 2010; Russell et al., 2010; Trail et al., 2011). These gases would have come from outgassing of volcanic systems of the crust and mantle (Catling and Claire, 2005). The Operin-Haldane theory, that life originated in a reducing atmosphere with hydrogen or methane making up the major constituents, could only be sustained if volcanic outgassing was much more reducing that modern emissions. The upper mantle would have needed to contain metallic iron to have supplied these reducing gases to the atmosphere, which is not found to be the case, therefore

the proportion of gases being outgassed is predicted to be relatively similar to modern day (Catling and Claire, 2005; Trail et al., 2011). This debate continues to cause controversy in the field, and for some justifies certain chemical approaches to the origin of life. If the exact conditions on Earth are not constrained then any number of experiments can be carried out, using different prebiotic chemical reactions to find a route to the synthesis of the requisite biopolymers. Even after considering this body of geological evidence, and the fact that CO_2 is assimilated by nearly all autotrophic cells today, current prebiotic chemical theories disregard CO_2 and use more reactive, but less likely, precursors (Lane, 2014; Sojo et al., 2016).

The origin of water on Earth is a topic that is still under debate. The young sun would have been hot enough to vaporise any ice that was present on the early planet, therefore it has always been assumed that the Earth must have acquired its water through meteoritic bombardment (Abe et al., 2000). Recent studies suggest that this may not have been the case (de Leeuw et al., 2010; Hallis et al., 2015). Theoretical studies predicted that water may have been on Earth from its beginning, as water molecules were adsorbed onto the coalescing dust particles (mainly Mg-rich forsterite) that formed the Earth (de Leeuw et al., 2010). Recently Hallis et al. (2015) have shown evidence, from deuterium/hydrogen ratios of water inclusions in ancient lavas in Iceland, that suggest this theory could be correct.

Archaean (4 - 2.5 Ga) ocean temperatures have been inferred as relatively hot (50 - 70 ^{o}C), along with a hot climate by Knauth and Lowe (2003) and Robert and Chaussidon (2006), who used oxygen isotope evidence from Archaean cherts. These hot temperatures raise a few questions about how this temperature could be sustained, especially as there is no sedimentary evidence of extreme weather that would be brought about by these high temperatures. Another point raised is if oxygen levels in seawater in the Archaean were less than today, the temperatures would actually be lower than predicted, closer to modern temperatures (Arndt and Nisbet, 2012; Shields and Kasting, 2007). Blake et al. (2010) suggest much lower ocean temperatures and Jaffrés et al. (2007) predict average surface tem-

peratures between 10 °C to 30 °C, after combining oxygen and hydrogen isotope ratios of cherts, along with oxygen isotope ratios of dissolved inorganic phosphate. Evidence for temperatures or conditions in the Hadean (4.6 - 4 Ga) is much harder as this is the time before before the rock record. Therefore, conditions have to be predicted from the conditions though to be present in the Archaean.

Heat production in the Hadean was probably at least 5 times that of the present day (Turcotte, 1980), indicating that the mantle would have been much hotter. This would have lead to dehydration of the lower mantle and consequently most of Earth's water would have been contained in the oceans, resulting in an increased volume of up to twice that of today's oceans (Wilde et al., 2001; Russell and Arndt, 2005; Russell et al., 2010). This greater ocean area would have increased the amount of water percolating through cracks in the oceanic crust, increasing the hydration of olivine, a process known as serpentinisation (Fyfe, 1988, 1994). This process would have had significant implications for hydrothermal activity on the early Earth, altering the composition of the oceans and increasing the number of alkaline hydrothermal vents, a location suggested by some, and examined in this thesis, as ideal for the origin of life. Alkaline hydrothermal vents and their possible location for the origin of life will be discussed later.

1.2.3 Heterotrophic origins

Those in the 'Prebiotic Soup' camp suggest that a select few molecules were important in comprising the building blocks of life: water, ammonia (NH_3), hydrogen cyanide (HCN), formaldehyde (CH_2O), acetonitrile (CH_3CN), acrylonitrile (CH_2CHCN), cyanogen (C_2N_2) and cyanoacetylene (C_3HN) (Eschenmoser and Loewenthal, 1992). Cyano compounds have been shown to be relatively abundant in outer space, thus justifying its use as a source of carbon in these prebiotic experiments, especially given the known meteorite bombardment (Sutherland and Whitfield, 1997), but there is no evidence of a high cyanide atmosphere on earth. Miller showed that formaldehyde and hydrogen cyanide were key components in the synthesis of glycine (Miller, 1957). These observations led to the work of Oró and colleagues, who discovered that adenine, a component of deoxyribonucleic

acid (DNA), ribonucleic acid (RNA) and adenosine triphosphate (ATP), can be synthesised by hydrogen cyanide polymerisation, under early Earth conditions (Oró, 1960). Molecular structures of some of these key building blocks are shown in Figure 1.1.

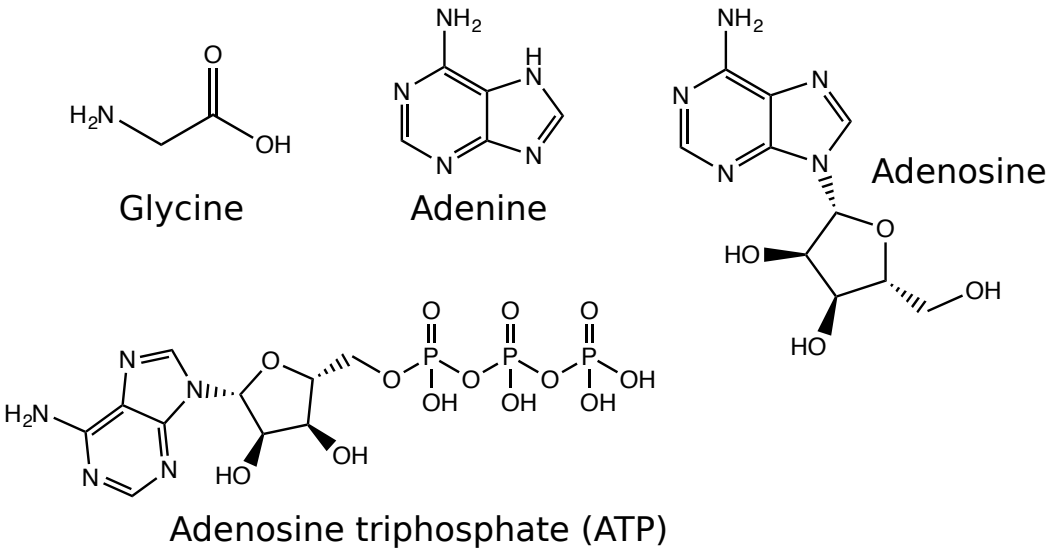

Figure 1.1. Molecular structures of some key building blocks of DNA and RNA. The amino acid glycine, the nucleobase adenine, the nucleoside adenosine (adenine plus the sugar ribose), and the energy currency adenosine triphosphate (ATP; the nucleoside adenosine plus three phosphate groups).

The majority of prebiotic chemistry research has assumed the first life was heterotrophic (obtaining carbon for growth and energy from complex organic compounds), originating in a broth of organic molecules synthesised in a reducing atmosphere (Oparin, 1924; Benner et al., 2010; Sutherland and Whitfield, 1997). The source of energy for this synthesis could have come from either visible and ultraviolet (UV) light or atmospheric electrical discharge (lightning). Visible light is the most abundant energy source, and is used by many life processes today (Deamer and Weber, 2010), however phylogenetic data show that this photosynthetic system is only seen in a small selection of bacterial ancestors, and not in any archaea. In fact, photosynthesis almost certainly derived from respiration (a process in living organisms involving the production of energy, typically with the intake of oxygen and the release of CO_2 from the oxidation of complex organic substances), as it uses the same respiratory proteins, proton gradients, redox centres and ATP synthase as respiration, but respiration (a

process in living organisms involving the production of energy, typically with the intake of oxygen and the release of carbon dioxide from the oxidation of complex organic substances) is universal across all life (Lane, 2015).

Recent abiotic synthesis of nucleotides (a compound consisting of a nucleoside linked to a phosphate group) using UV radiation and phosphate (Powner et al., 2009) suggests the idea of a primordial ocean filled with nucleotides, which spontaneously polymerise into RNA, catalysing their own replication. The problem with ionising UV radiation is that it breaks down and destroys organics, as much as it can drive their synthesis, and, more significantly, no extant life uses this process to metabolise (Lane et al., 2010).

Electrical discharge is another plausible source of energy for organic synthesis, however the amount of lightning needed to supply enough energy to synthesise enough organics to enable amino acid accumulation would have to be far greater than could have been physically possible on the early Earth, and again it is not a process used by extant life (Lane, 2015). Overall, no life on Earth today uses cyanide as a source of carbon or nitrogen, and no life uses UV radiation or electrical discharge as a source of energy (Lane, 2015).

A number of alternative hypotheses take into account a less reducing atmosphere and the need for a chemical potential between reactants. One example of these experiments focuses on condensation reactions, where chemically activated monomers (although no suggestion of their source is suggested), with catalysts present, can be linked into biologically relevant polymers (Rajamani et al., 2008; Deamer and Weber, 2010). It has been shown that condensation of mononucleotides and hydrolysis of their polymers can occur within a lipid matrix in the anhydrous phase of hydration-dehydration cycles. These cycles are theorised to have occurred in aqueous pools found in hydrothermal fields (temperatures of $60 - 100\,^{\circ}\mathrm{C}$ and acidic pH $2 - 3$) on the early continents of Earth. These pools would undergo evaporation and refilling with precipitation, and it is proposed that the concentrating effect and chemical potential made available by these cycles of hydration and dehydration would be sufficient to drive synthesis of ester bonds (Rajamani et al., 2008; DeGuzman et al., 2014). In this instance the activated

monomers are imidazole esters, which are shown to readily polymerise nucleotides (Rajamani et al., 2008). Nonetheless, as with cyanide and UV radiation, no life today uses these activated monomers for any biochemical processes.

In general, the heterotrophic hypotheses focus little attention on the geochemical constraints of a primitive planet. Life is a complex set of coupled exergonic and endergonic reactions that release and utilise energy, and this energy flux is vital to its existence (Lane et al., 2010). It is possible that the earliest prebiotic chemistry was replaced by subsequently derived, complex metabolic pathways, however the simpler, and more logical, interpretation that life assimilated CO_2 (which was prevalent in the Hadean atmosphere) from the very start, as it does today, has received very little attention (Sojo et al., 2016). This alternative, autotrophic hypothesis, assumes that life derived from inorganic molecules in CO_2-rich, less reducing Earth conditions, using an energy source in the local geochemical environment, such as proton gradients, plus a redox disequilibrium of H_2 in hydrothermal fluids and CO_2 in the ocean. This energy was captured, transferred to energy carriers (such as ATP does today), and then ultimately to the activated monomers, required for catalysing polymerisation (Deamer and Weber, 2010; Lane et al., 2010).

1.2.4 Autotrophic origins

As noted earlier the Archaean mantle is commonly thought to have been much hotter than the modern mantle, due to internal sources of heat being far greater than they are today (Richter, 1988; Franck, 1998; Nisbet et al., 1993; Nisbet and Sleep, 2001; Arndt and Nisbet, 2012). Circulation of seawater through the hot oceanic crust would have created a variety of hydrothermal vent environments (Abbott and Hoffman, 1984; Macleod et al., 1994; Arndt and Nisbet, 2012). There are a number of different types of deep-sea hydrothermal vents. First discovered in the late 1970's were black smokers, located on oceanic spreading zones, directly above magma chambers and driven by the interaction of seawater with hot magma. These vents produce iron- and sulphide-rich fluids in excess of

300 °C, chemically altered and very acidic (pH 1 - 2). They are rich in hydrogen sulphide and dissolved metals, but are very low in H_2 (Spiess et al., 1980).

An alternative hypothesis for the origin of life, suggested by Wächtershäuser (1988), predicts that life could have emerged from the direct reactions of chemicals derived from reduced fluids interacting with catalytic transition metal sulphides (Wächtershäuser, 1988, 1990). Wächtershäuser proposed a theory of origin by catalytic metabolism, using positively charged mineral surfaces, such as pyrite (FeS_2) produced by ferrous sulphide (FeS) and hydrogen sulphide (H_2S), at a hot water interface in black smoker vents. This he called the iron-sulfur world hypothesis or pyrites-pulling (Wächtershäuser, 1988, 1990). The adherence of molecules to a positively charged mineral surface (pyrite) is not the result of adsorption, but that of in situ autotrophic growth of anionic components, and could have provided a viable source of energy for the first life. He predicted that the reaction of FeS with H_2S was highly exergonic under standard conditions (Equation 1.2.1, Gibb's free energy calculated by Wächtershäuser, 1990, subsequent calculations with more recent thermodynamic data report this as slightly less by Schoonen et al., 1999) and therefore should have the potential to drive otherwise endergonic reactions when coupled together. For example the reduction of CO_2 to form formic acid is endergonic (Equation 1.2.2) unless it is coupled with the formation of pyrite (Equation 1.2.3; Wächtershäuser, 1988). However, Schoonen et al. (1999), although they agreed that these reactions would be thermodynamically viable, they suggest that the electron transfer from FeS to CO_2 was probably not feasible under standard conditions.

$$FeS + H_2S \rightarrow FeS_2 + H_2 (\triangle G^o = -38.4 \text{ kJ/mol}) \quad (1.2.1)$$

$$CO_2(aq\cdot) + H_2 \rightarrow HCOOH (\triangle G^o = +30.2 \text{ kJ/mol}) \quad (1.2.2)$$

$$CO_2(aq\cdot) + FeS + H_2S \rightarrow HCOOH + FeS_2 + H_2O (\triangle G^o = -8.2 \text{ kJ/mol}) \quad (1.2.3)$$

These black smoker systems are not only very short-lived (in the order of decades), due to the transient nature of the ridge axis, but have violent flow rates and extreme temperatures (Sleep et al., 2011), therefore they are not ideal for fostering the origin of complex organic molecules and their evolution. By contrast another type of deep sea hydrothermal vent was proposed, long before its discovery on the basis of fossil marine hydrothermal systems and small terrestrial equivalents, by Russell et al. (1988). These vents were suggested to have formed by a process known as serpentinisation, producing fluids of higher pH as seawater chemically interacts with the mantle rock olivine (Russell et al., 1988, 1989). Alkaline hydrothermal vents were eventually discovered in 2000 by Deborah Kelley, and the vent field was called Lost City. This type of vent offers much more favourable conditions for life's origin; unlike the black smokers, which are relatively short-lived, alkaline vents can be stable for long geological time scales. Lost City has been active for over 120,000 years, has much milder temperatures, slower flow rates and is much more reducing, being rich in H_2 gas, than black smokers (Ludwig et al., 2011).

Russell et al. (1988) predicted a very different scenario from Wächtershäuser based on iron-sulphur catalytic barriers within alkaline hydrothermal vent systems (Russell et al., 1988, 1989). This approach is more geochemical, based on a vent system which exhaled warm, alkaline fluids (50 - 90 ^{o}C, pH 9 - 11), rich in H_2, into a CO_2-rich, acidic ocean, which would precipitate an FeS, microporous structure (predominantly composed of greigite) (Russell et al., 1988). This structure would have acted as a catalytic barrier between fluids of very different pH and reduction potential, producing proton gradients across the thin inorganic barriers bounding interconnected pores within the walls of the vent. This would allow for electron transport from H_2, in the alkaline fluid, to reduce CO_2, in the acidic ocean, forming simple organic molecules such as formate, formaldehyde and methane.

These alkaline vent systems could have been ideal locations for the origin of life and polymerisation of organics, having a range of closely-linked temperature and pH gradients. These conditions could have produced high concentrations of reduced gases, such as H_2 and possibly methyl sulphide (CH_3SHh), of which

there is no direct evidence at present but it is easily oxidised so could have been present in anoxic conditions. Both of these gases are important in modern metabolic pathways (Baross and Hoffman, 1985; Russell et al., 1988), however so far only found by biogenic origin. The alkaline hydrothermal vent hypothesis will be discussed in more detail in Section 1.4.

One of the main differences between the Wächtershäuser (1988) and Russell et al. (1988) hypotheses and those of the prebiotic soup is the idea that the first organism was autotrophic, synthesising all its constituents from inorganic compounds, notably CO_2 and H_2S or H_2. These autotrophic hypotheses predict that life started from chemical reactions of reduced fluids within hydrothermal vents, interacting with catalytic transition metal sulphides. At the core of both of these hypotheses is the concept that primitive CO_2 fixation would have been similar to that of the acetyl-CoA pathway and the reductive Krebs cycle (Russell et al., 1988, 1989; Wächtershäuser, 1988, 1990), using thiols and phosphate molecules to drive early metabolic processes. These autotrophic hypotheses hold more relevance to modern biochemistry, due to the fact that life today uses proton gradients to drive the reduction of CO_2 by H_2, and intermediary metabolism including ATP synthesis and the reverse Krebs cycle

1.2.5 Bottom-up or top-down approach

Some of the main differences in hypotheses for the origin of life on Earth have been discussed here. These hypotheses have been categorised according to their energetic pathways; heterotrophic and autotrophic, however, there is an alternative way of categorising origin of life theories. As briefly mentioned earlier, the bottom-up approach looks at the chemical and physical constraints of the early Earth, where it is predicted that an abundance of simple organic molecules arose in a reducing atmosphere, using energy sources such as UV radiation or lightning, and further polymerisation to amino acids was facilitated before the first cells were formed by alternative solvents, dehydration agents, such as cyanamide, or wet-dry cycles to drive evolution of more complex biomolecules (Miller, 1953; Oró, 1960; Orgel, 1998; Sutherland and Whitfield, 1997; Rajamani et al., 2008;

DeGuzman et al., 2014). Alternatively the top-down approach studies modern biochemical processes and uses phylogenetics and comparative biochemistry to try and understand how complex systems could have evolved from a process that was originally much simpler, but used the same basic mechanisms (de Duve, 1994; Martin and Russell, 2007; Nitschke and Russell, 2009; Lane et al., 2010; Martin et al., 2014). Phylogenetics indicate that life may have had an autotrophic origin, where life synthesises its constituents from inorganic compounds, using energy sources available geochemically (Russell et al., 1988; Wächtershäuser, 1988; Sojo et al., 2014).

Insight from life itself is what has been missing from origin of life experimental work since it began in 1953. This is in part because the reactions proposed do not occur easily; CO_2 does not react with H_2 very well using ATP without enzymes, and if it does occur it does not produce very high yields. This is where a top-down/bottom-up combined approach has its advantage; we can look at the most basic metabolic processes we see in contemporary biochemistry, that are conserved across all life, and extrapolate back to see how the last universal common ancestor (LUCA), and before that the first protometabolism, may have occurred. This early metabolism would have initially utilised inorganic compounds and must have used natural energy sources that are still conserved today, such as proton gradients, which would have been found occurring naturally in alkaline hydrothermal vents at 4 Ga.

1.3 From protometabolism to metabolism

1.3.1 What can phylogenetics tell us about the Last Universal Common Ancestor?

Extant life is divided into three domains; bacteria, archaea and eukaryotes. Accumulating phylogenetic evidence suggests that the three-domain tree may not be correct, but instead eukaryotes arose from an archaeal host with a bacterial endosymbiont. These results support a tree with only two primary domains of

life, the archaea and bacteria, with the eukaryotes arising through a partnership between them (Figure 1.2) (Williams et al., 2013). Therefore the archaea and the bacteria are the deepest divergence on the 'tree of life', and we call the organism that came before this divergence LUCA, which logically must have had traits that are shared in both the bacteria and archaea. Reconstructing these traits requires understanding the relationships between these two domains of life (Sojo et al., 2014). There is a problem here though; the prevalence of lateral gene transfer within and between the domains means the deepest branches may not be resolvable by phylogenetics alone (Martin, 1999, 2011). Nonetheless, we do know that bacteria and archaea share a core biochemistry; this includes the genetic code, transcription, and ribosomal translation. On the other hand, they differ in a number of fundamental traits: cell membranes, cell walls, glycolysis (Embden Meyerhof-Parnas pathway), ion pumping machinery and even DNA replication (Sousa et al., 2013; Sojo et al., 2014).

The differences in cell membranes are a major unresolved problem, with the main fundamental difference being the stereochemistry of the glycerol phosphate G-P head-groups. They differ in several respects, but there is no obvious selective reason for the difference in G-P head-group stereochemistry (Lombard et al., 2012; Sojo et al., 2014). Even though there is this fundamental difference between the two domains, interestingly, there is a universality in the core of their membrane bioenergetics (Lane and Martin, 2012). All cells power ATP synthesis by a process called chemiosmotic coupling. The ATP synthase (ATPase), located within the cells's membrane, is powered by the electrochemical difference in H^+ or Na^+ concentrations on either side of the membrane (Mitchell, 1961). Phylogenetic studies conducted by Stetter (2006) show that a few hyperthermophile species of bacteria and archaea derive from the deepest and shortest phylogenetic branches of the tree of life, nearest to LUCA. These ancient organisms, in almost completely anaerobic environments, exhibit a chemolithoautotrophic form of metabolism, this means that they gain their energy by inorganic redox reactions, with CO_2 as the only source of carbon. They fix CO_2 by chemosynthesis, using molecular H_2 as the main electron donor, along with sulphide, sulphur and ferrous iron as

other electron donors. The position of these organisms on the phylogenetic tree provides evidence of a chemolithoautotrophic, possibly hyperthermophilic, last common ancestor (Fuchs, 1989; Stetter, 2006; Buckel and Thauer, 2013).

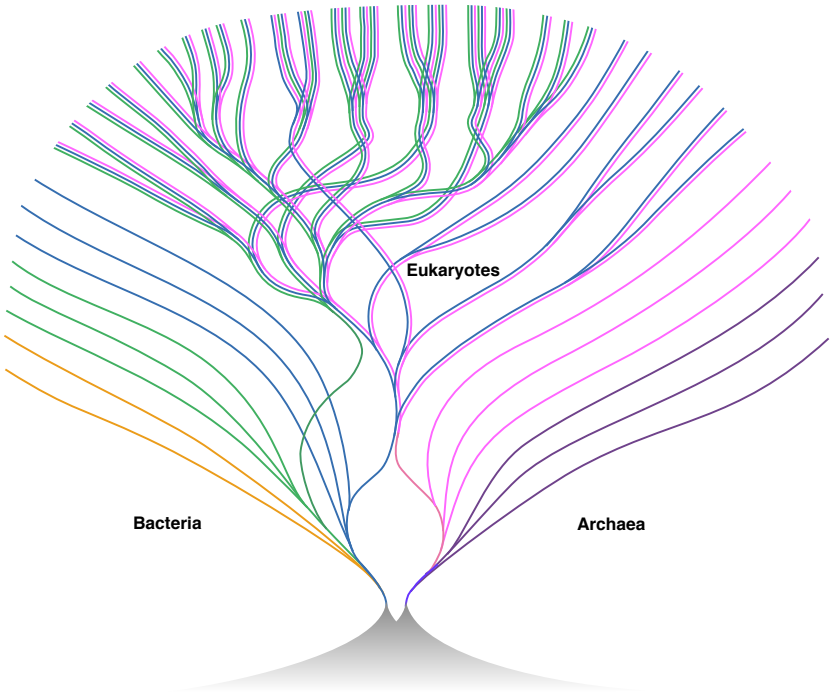

Figure 1.2. A tree of genomes. A working hypothesis for the origin of eukaryotes. It is proposed they descended from both bacteria and archaea, unlike the traditional view that they bifurcated, or were a distinct branch themselves. Different colours represent different groups of prokaryotes. At the base of the tree is the divergence of the archaea and bacteria, the location of LUCA. Note here that there are two separate emergences from vents, indicating that LUCA is thought to have been vent-bound rather than free-living in the oceans. The justification for this deep split is the deep divergence in fundamental properties, such as the cell membrane. Image taken from Martin (1999).

Methanogens reduce CO_2 to methane, using energy released during the synthesis of acetyl-coenzyme-A (acetyl-CoA), using iron-sulphur clusters within enzyme active sites (Thauer, 1998; Martin and Russell, 2007). The process of transferring electrons from H_2 to CO_2 to generate a methyl group involves an ion gradient across a membrane by electron bifurcation, which drives the direct reduction of ferredoxin via another Fe(Ni)S protein in the membrane, the energy-converting hydrogenase (Ech), to then drive ATP synthesis via the ATPase (Martin and Russell, 2007). The overall reaction for methanogenesis conserves

energy in the form of a proton gradient, and is used to drive both carbon and energy metabolism:

$$4\,H_2 + CO_2 \rightarrow CH_4 + 2\,H_2O \tag{1.3.1}$$

Acetogens metabolise in a similar way, but instead of methane they produce acetate as a waste product when they synthesise acetyl-CoA (Thauer, 1998; Martin and Russell, 2007). The production of the acetyl-CoA in this reaction is chemically similar to that of methanogenesis, however the enzymes involved in the methyl synthesis pathway, which is involved in generating the ion gradient, share no similarity with those involved in methanogenesis, which indicates that this part of the pathway has not been conserved (Martin and Russell, 2007). However, the overall use of proton gradients and carbon reduction is conserved between the two groups, as is the use of flavin-based electron bifurcation and multiple FeS proteins. The reaction for acetogenesis can be summarised:

$$4\,H_2 + 2\,CO_2 \rightarrow CH_3COOH + 2\,H_2O \tag{1.3.2}$$

These autotrophs depend on chemiosmotic coupling to drive carbon reduction via FeS proteins. These proteins, most importantly the ATPase, but also the Ech, are very complex structures that depend on membranes which are impermeable to protons (Sojo et al., 2014). In this way autotrophs use proton pumps to create a chemical potential between the inside and outside of the membrane, thereby creating a constant disequilibrium in the system. Unlike the ATPase, membrane proton pumps are not conserved in both bacteria and archaea, along with the lipid membranes as mentioned earlier (Sousa et al., 2013). From this evidence one interpretation, and the most persuasive, is that LUCA must have had some sort of ATPase across a membrane of some kind, yet did not have a modern phospholipid membrane or active ion pumps (Sojo et al., 2014). Consequently, how do we overcome the paradox that there are these huge differences in membranes and proton pumps, but a universality in the protein that utilises the proton gradient that the pumps are needed to create? In effect,

methanogens and acetogens are both chemiosmotic, both use ATPase, both use flavin-based electron bifurcation, both use multiple FeS proteins and many use Ech. But the actual mechanism of electron bifurcation differs, which is the process used to generate the proton gradient. One possible solution is that the first cells could have exploited a natural proton gradient within a vent, sustained by geochemical processes, with the reduction of CO_2 occurring directly by H_2, driven by Fe(Ni)S mineral catalysts, a process which is exactly analogous to acetyl-CoA synthesis in modern methanogens (Russell et al., 1994; Martin and Russell, 2003; Lane, 2014; Herschy et al., 2014; Sojo et al., 2016).

1.3.2 Early metabolic processes

It has been argued that an ancient CO_2-fixation pathway, perhaps similar to the acetyl-CoA pathway, could have driven a chemolithoautotrophic origin of life (Fuchs, 1989; Russell and Martin, 2004; Martin and Russell, 2007; Peretó et al., 2010). The acetyl-CoA pathway is key because it has a few biochemical features that point to a possible antiquity, and therefore possible early evolution. It is a simple, linear pathway which uses simple inorganic starting compounds; CO_2 and H_2, it is exergonic (low energy requirements and releases energy overall), and uses transition metal (Fe and Ni) sulphide clusters as catalysts (Russell and Martin, 2004). This geochemical and biochemical evidence is also supported by phylogenetic evidence from the pathway's occurrence in anaerobic and thermophilic bacteria and archaea, and the positions of the acetogens and methanogens deep in the tree of life (Stetter, 2006; Amend and McCollom, 2009). There are only six known pathways of carbon fixation across life, and acetyl-CoA is the hub of metabolism in all of them (Fuchs, 2011).

Life has the ability to generate complexity from randomness due to the availability of a continuous flux, so there needs to be a constant environmental source of energy to maintain this 'far from equilibrium' state (Schoepp-Cothenet et al., 2013; Lane et al., 2010). Today life uses proton pumps to maintain a proton gradient across a membrane, but how could early, simple molecular systems, probably without an ion tight membrane, have generated this disequilibrium? This

is one of the fundamental problems with the 'prebiotic soup' theory. Nucleotides and other organics are reluctant to react in a soup that is at thermodynamic equilibrium as there is no internal free energy to drive them to react further. All forms of life, and therefore LUCA too, uses the energy flux created by breaking 'high-energy' bonds, such as the thioester bond in acetyl-CoA or anhydride bonds in acetyl phosphate and ATP. The resultant release of energy stored in these bonds enables the synthesis of more complex organics, and the polymerisation of monomers to biopolymers. This system is said to be out of chemical equilibrium (Martin and Russell, 2007; Russell and Martin, 2004; Lane et al., 2010; Whicher et al., 2016).

The mechanism of chemiosmotic coupling, first described by Peter Mitchell, remained controversial for many years due to the counter-intuitive mechanism that it employes. Mitchell (1961) proposed the idea that a proton gradient across a membrane, generated by the oxidation of NADH, drives the synthesis of ATP via complex proteins, known as ATPases today. The idea was not believed by many, and created dispute among biochemists for more than 20 years, consequently it is still not thought by some to play a role in early metabolism (Orgel, 1999; Lane et al., 2010; Lane and Martin, 2012; Lane, 2014). Nonetheless, it is the only form of energy transduction fundamental to all life. Both archaea and bacteria generate proton gradients across plasma membranes using electron bifurcation, even though the actual pathway is different. Electron bifurcation is in fact used to to generate a proton (or sodium) gradient, so in this context of natural gradients this may not matter (Lane et al., 2010).

The biggest question here is how did modern metabolism replace protometabolism? There is a suggestion that the "only scientifically plausible" explanation for the emergence of biological catalysts, such as enzymes or ribozymes, and metabolism as we know it, is selection (de Duve, 2005). The first biological catalysts would have been selected because they enhanced a process that presumably already occurred naturally, being catalysed by inorganic minerals and driven by the disequilibria of geochemistry. If this is the case, then this selection implies a link between metabolism and geochemical flux, enabling continuity; each

intermediate step must be modified from the previous step (Sojo et al., 2016). de Duve (1994) suggests a thioester-based protometabolism, which follows pathways not that dissimilar from today, due to the centrality of thioesters to modern metabolism.

The acetyl-CoA pathway reduces CO_2 with H_2 to form an energy-rich thioester in the presence of a thiol. It does this with the help of electrons supplied by H_2, releasing energy which is then used by chemiosmosis to make ATP. Thioesters are energy-rich, highly reactive compounds and can be used as an energy currency themselves, like ATP, due to their ability to store chemical energy and release it when the thioester bond is hydrolysed or phosphorolysed (de Duve, 1991; Russell and Martin, 2004). The overall reaction of the acetyl-CoA pathway can be summarised, as it occurs in autotrophic bacteria and archaea (Fuchs, 1994):

$$4\,H_2 + 2\,CO_2 + HSCoA \rightarrow CH_3COSCoA + 3\,H_2O \tag{1.3.3}$$

The pathway reduces inorganic carbon, CO_2, to organic carbon, a process which is vital to all life, and at the same time thermodynamically favourable. This reaction is highly exergonic, however, it does not occur without catalysts, which today are enzymes containing metal-sulphide clusters. Interestingly, these clusters are very similar in structure to the mineral forms of (Fe,Ni)S, such as greigite (Figure 1.3). The cubic unit in greigite (Fe_4S_4) is found in clusters in other proteins of relevance to the acetyl-CoA pathway, such as ferredoxin, the [Fe-Ni]-hydrogenase and [Fe]-hydrogenase (Russell and Martin, 2004). It is therefore suggested that these clusters are not inventions of the biological world, but are remnants of the catalytic minerals that occurred before the presence of proteins, leading us to a possible location for the origin of life (Heinen and Lauwers, 1996; Huber and Wächtershäuser, 1997).

At the core of the modern metabolic chart is the Krebs cycle (also known as the tricarboxylic acid or citric acid cycle), which is central to autotrophs for all their biosynthesis. The reverse or reductive Krebs cycle is the Krebs cycle or

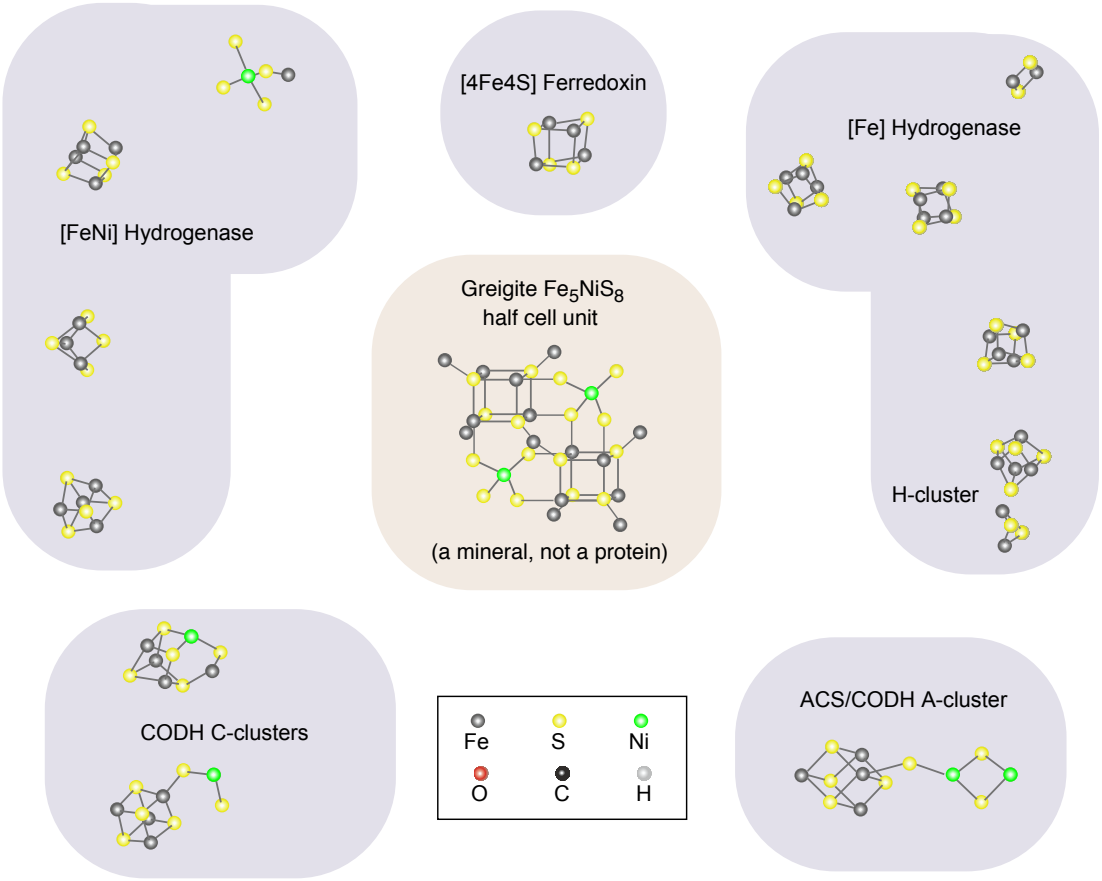

Figure 1.3. Structural similarities between (Fe,Ni)S clusters in enzymes and minerals. The protein structure is represented by shading and shows where the FeS clusters are embedded, either with or without nickel. The central panel shows a repeating crystalline unit of the mineral greigite, where the structure is repeated to make up a lattice of multiple units. The surrounding panels show FeS clusters embedded in proteins, with structures similar to greigite and related minerals, such as mackinawite. The Fe_4S_4 thiocubane units in these proteins, specifically ferredoxin and Fe- and FeNi-hydrogenase, catalyse reactions which have relevance to the acetyl-CoA pathway. Image taken from Lane (2015), adapted from Russell and Martin (2004).

oxidative Krebs cycle run in reverse; where it reduces CO_2 to generate acetyl-CoA and longer chain carbons, rather than oxidising acetyl-CoA and complex carbon molecules to CO_2 and water (Fuchs, 2011). The acetyl-CoA pathway produces acetyl-CoA which is fed into the Krebs cycle by the formation of pyruvate (Lane et al., 2010). This link indicates a possibility that the reverse Krebs cycle is also of ancient origin, supplying precursors for amino acid and nucleoside synthesis, and is consistent with the relationship between the incomplete reverse Krebs cycle and the acetyl-CoA pathway in methanogens and acetogens (Fuchs, 1989; Martin

and Russell, 2007). The reverse Krebs cycle generates acetyl-CoA, whereas the incomplete reverse Krebs cycle converts acetyl-CoA into longer carbon chains, via pyruvate (Martin and Russell, 2007), similar to what might have happened abiotically using thiols as acetyl-CoA precursors, and AcP as an energy currency to drive each stage of the cycle, as ATP does today. Although this pathway is important in the synthesis of amino acids today, the fact that it is a cycle and needs ATP to progress, means it is less likely as a primordial pathway of CO_2 fixation. The complete pathway is also not found in both bacteria and archaea, this suggests that the acetyl-CoA pathway must have come first, then the reverse incomplete Krebs cycle for longer carbon chains, and finally the full Krebs cycle replaced the acetyl-CoA pathway in bacteria and archaea independently. The products of a primordial acetyl-CoA pathway, methyl thioacetate or thioacetic acid and acetyl phosphate could have driven the production of pyruvate and therefore a primitive form of the incomplete reverse Krebs cycle (Martin and Russell, 2007).

Today ATP plays the vital role of energy currency in the majority of core metabolic processes, via phosphorylation and condensation reactions. It is a complex molecule which depends on sophisticated proteins for its synthesis, consequently it is not likely to have played a role in early protometabolic reactions. However, it is important to note that methanogens convert CO_2 to acetyl-CoA without the need for ATP, instead they use transition metal sulphides and thioesters like acetyl-CoA, which are central to primitive bioenergetic pathways (Russell and Martin, 2004; Lane et al., 2010). Analogues of acetyl-CoA could feasibly react with inorganic phosphate to synthesise acetyl phosphate, an energy-rich analogue of ATP, which is still used as a phosphorylating agent by some bacteria today (Thauer et al., 1977; de Zwart et al., 2004; Klein et al., 2007; Whicher et al., 2016).

The key to these pathways is the simple reduction of CO_2 with H_2 that we see occurring in ancient prokaryotes today and therefore the key to understanding how intermediary metabolism might have arisen. This mechanism has been overlooked in other research areas due to the complexity of the membrane

pumping protons (Sojo et al., 2014). However, it might not be such a complex idea if there were such an environment on Earth that could have provided all of these conditions. Deep sea alkaline hydrothermal vents are one such environment, predicted by Russell et al. (1989), and eventually discovered in the year 2000 (Kelley et al., 2001, 2005).

1.4 Alkaline Hydrothermal Vents

1.4.1 Location and chemical conditions

Alkaline hydrothermal vents are not volcanic systems, and are not driven by magma, but are formed by water chemically reacting with ultramafic rocks in the upper mantle, a process called serpentinisation (Russell et al., 1988; Martin et al., 2008). These cool, 'off-ridge', vents today are located a few kilometers away from sea-floor spreading zones, but could have occurred across the whole seafloor 4 Ga. These ultramafic rocks are composed of the mineral olivine [(Fe,Mg)2SiO_4], containing magnesium, iron, and low silica concentrations. Serpentinisation occurs as water percolates through the ultramafic rocks, which hydroxylates the mineral olivine, oxidising Fe^{2+} to Fe^{3+}, fomring serpentinite [$Mg_3Si_2O_5(OH)_4$] (Sleep et al., 2004; Kelley et al., 2005; Russell et al., 2010). The resulting hydrothermal vent fluids are cool in temperature, around 70 - 90 °C, and alkaline in pH (9 - 11). As these fluids percolate up into the ocean from the crust they precipitate out minerals (dependant on hydrothermal fluid and ocean chemistry) that form vent fields over square kilometres, with individual spires attaining 60m in height, on the seafloor. Serpentinisation produces H_2 in the hydrothermal fluids, which along with CO_2 in the acidic ocean, are key to the hypothesis suggesting that life emerged at alkaline hydrothermal vents (Russell et al., 1989, 1994; Früh-Green et al., 2004; Holm et al., 2006; Russell et al., 2010).

On the early Earth, 4 Ga, it is thought serpentinisation would have been much more prevalent than today, due to the crust and mantle being less differentiated (Zahnle et al., 2007), as attested by the relative widespread abundance of komatiite lavas (Sleep et al., 2004; Russell and Arndt, 2005; Jaffrés et al., 2007;

Arndt and Nisbet, 2012). Oxygen isotopes ($\delta^{18}O$) in seawater are fractionated by low temperature weathering in seawater, of which a major component is serpentinisation (Jaffrés et al., 2007; Shields and Kasting, 2007). These high submarine weathering rates are thought to have been caused by a combination of higher atmospheric CO_2 and a greater abundance of relatively easily weathered volcanic rocks, such as komatiites (Jaffrés et al., 2007), along with less continental weathering. The weathering sink for CO_2 was thought to be almost entirely submarine. If serpentinisation was more widespread in the Hadean and Archaean, as the $\delta^{18}O$ fractionation suggests, alkaline hydrothermal systems could potentially have been nearly continuous in distribution (Nisbet et al., 1993).

Lost City is an alkaline hydrothermal vent discovered in the year 2000 by Deborah Kelley, located 15 km from the Mid-Atlantic Ridge (Figure 1.4) (Kelley et al., 2001, 2005). It is mainly composed of a mixture of aragonite ($CaCO_3$) and brucite ($Mg(OH)_2$), forming tall spires as the carbonates are precipitated. High pH and calcium concentrations are typical of fluids percolating through serpentinised ultramafic rocks, and promote carbonate precipitation when they mix with seawater in the modern ocean (Kelley et al., 2005). The active venting parts of Lost City are highly porous and friable structures made of aragonite, out of which the fluids emerge from complex networks of small channels. Cross sections of Lost City show an intricate network of fine carbonate channels lined with brucite, indicating a mixing of seawater and hydrothermal fluids within the interior walls of the vent (Figure 1.5) (Kelley et al., 2001).

While Lost City is a good system to study how alkaline hydrothermal vents form, it is not equivalent in its chemistry to a system that would have occurred 4 Ga (Russell et al., 2010). The key to this difference is that the ocean chemistry would have been very different in the Hadean (Pinti, 2005). The Hadean ocean would have been in equilibrium with a CO_2 rich atmosphere, making it acidic (pH 5 - 7), it would also have been oxygen-free (anoxic) and rich in dissolved metals (Kasting, 1993). Phosphate and silica could have been added to the Hadean oceans by volcanic degassing (although there is much contention over where phosphate came from on the early Earth, this will be discussed further in Section

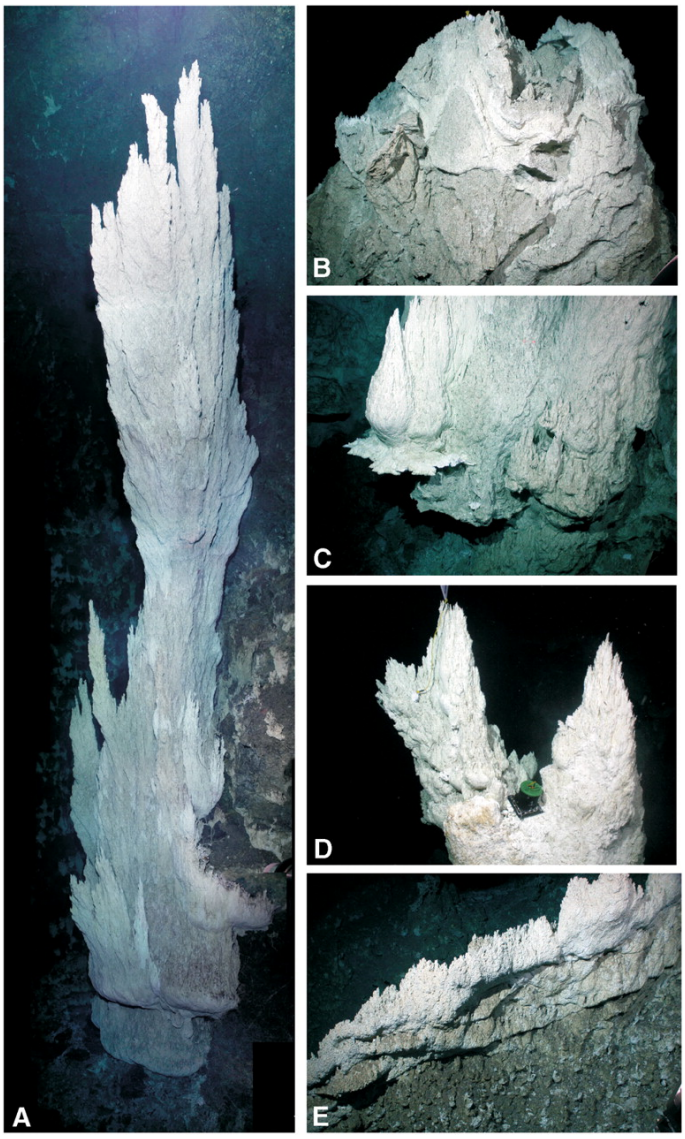

Figure 1.4. Alkaline hydrothermal deposits at Lost City. **(A)** 10 m tall actively venting carbonate chimney growing from the serpentinite cliff on eastern side of the field. **(B - E)** Actively venting sections of Lost City**,** taken from areas located at around 50 °C. Image taken from Kelley (2005).

1.4.2), and black smoker vents would have supplied transition metal ions, mainly ferrous iron but also nickel and cobalt. High levels of bisulphide (HS^-) could have been present in alkaline hydrothermal fluids, as they passed through ridge-crest komatiites saturated in sulphides, due to subsurface interactions (Lambert et al., 1998; Charlou et al., 2002; Russell et al., 2010). At the interface between the warm alkaline fluids and the acidic ocean there should have been precipitation of a compartmentalised system of micropores, with semi-conducting, semi-permeable, catalytic inorganic walls composed of phosphate, silicate, iron sulphide and other

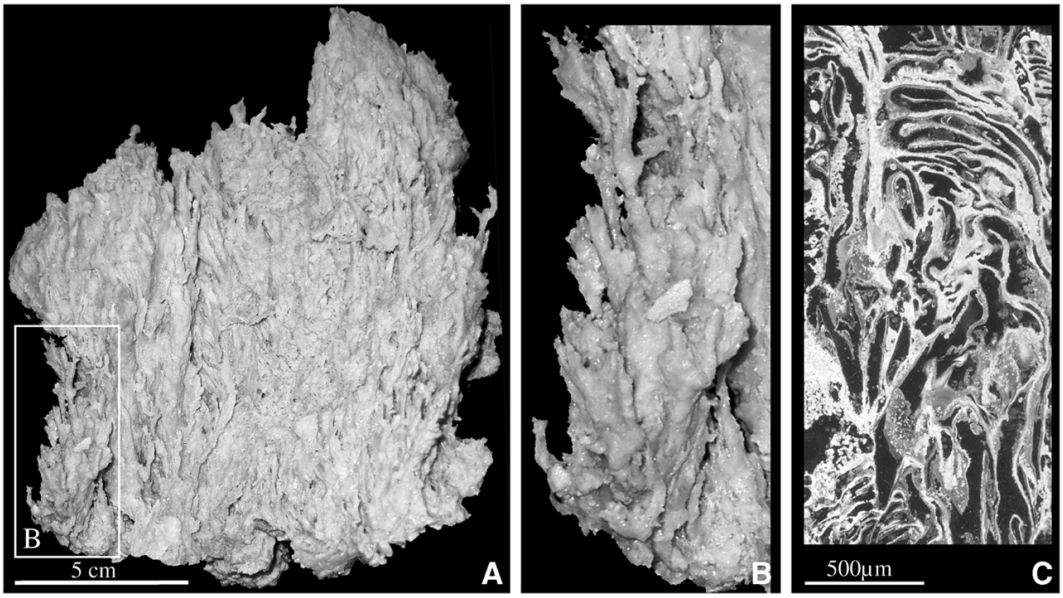

Figure 1.5. Active vent deposits from Lost City. **(A)** Aragonite-rich sample from an area at 50 °C. **(B)** Closeup of sample (A), which highlights the inter-growths of aragonite and brucite. **(C)** Cross-section of the sample, showing the fine network of micropores which is characteristic of these alkaline hydrothermal vent systems, making their structure so different from the black smoker systems. Image taken from Kelley et al. (2001).

transition metals (Russell and Hall, 1997; Russell et al., 2010). The structure should have been similar to that of Lost City, but with a different structural and internal fluid composition.

Another hydrothermal vent system discovered in Eyjafjördur, Iceland, was found to have a complex microporous structure, with a filamentous structure of pores on the scale of 4 μm diameter (Marteinsson et al., 2001; Geptner et al., 2002). This system is composed of saponite clay $[Ca_{0.25}(Mg_{F}e)_3((Si_{A}l)_4O_{10})]$, nonetheless, even though it has a different chemistry to that of a Hadean vent, it could be an equivalent system with a similar structure to that found within early alkaline hydrothermal vents. Carbonates within the ancient vents would have been dissolved in the acidic ocean at depth and high pressure, meaning the vents may have been poorer in carbonates than today, however, given the alkalinity of the hydrothermal fluids in the vents there could have been some carbonate precipitation too. This would leave predominantly serpentinite minerals as the composite, such as brucite and sepiolite, with nickel, iron and other transition metal sulphides forming clusters within the precipitated walls (Russell et al., 2005,

2010).

1.4.2 Hatcheries for the origin of life

Autotrophic cells today use proton gradients to reduce CO_2 and synthesise ATP. The alkaline vent hypothesis suggests that natural proton gradients are created by alkaline fluids permeating through the vent, coming into close contact with mildly acidic ocean fluids, which percolate into the vent. These two fluids would be separated by thin inorganic catalytic, FeS, barriers, which could catalyse the synthesis of organic molecules within the vent's microporous system (Russell and Hall, 1997; Nitschke and Russell, 2009). The pH difference between the alkaline fluids and acid ocean could have produced pH gradients of 3 - 6 pH units. While mixing would have prevented these steep gradients occurring next to each other, laminar flow within the vent pores could have allowed for sharp gradients to exist across thin barriers, creating the opportunity for H_2 in the alkaline fluid to reduce CO_2 (as bicarbonate) in the acid fluid. This situation means that the reduction potential of the $H_2/2H^+$ couple is lowered, allowing for the reduction of CO_2 to CO, formate ($HCOO^-$), formaldehyde (CH_2O) or similar organics, by lowering the energetic barrier that is present when both species are at the same pH (Lane and Martin, 2012; Lane, 2014; Yamaguchi et al., 2014). This situation supports the idea of protometabolism, where hydrothermal H_2 was the first electron donor, and oceanic CO_2 the main electron acceptor (Simoncini et al., 2010). Reduction potentials and subsequent organic synthesis will be discussed in more detail in Chapter 3.

The Fe(Ni)S minerals in the vent walls, such as greigite, are known to catalyse redox reactions (Heinen and Lauwers, 1996; Huber and Wächtershäuser, 1997) and are similar in structure to many clusters found in enzymes required for carbon fixation and energy transduction (as mentioned earlier in Figure 1.3). These clusters are especially found in membrane proteins involved in ancient pathways such as the acetyl-CoA pathway and the reverse citric acid cycle (Eck and Dayhoff, 1966; Russell and Martin, 2004; Sousa et al., 2013).

Volcanic gases would have also supplied sulphur (probably as SO_2 rather than H_2S), in millimolar quantities in the acidic ocean, which would then have been precipitated around the hydrothermal vents, along with ferrous iron minerals, supplied by volcanic hydrothermal fluids (Yamagata et al., 1991; Nitschke and Russell, 2009).

Anoxia is also key to this process for thermodynamic and kinetic reasons. Thermodynamically, because the reaction between H_2 and CO_2 is only favoured under anoxic conditions (Amend et al., 2013), and kinetically because the solubility of Fe^{2+} and Ni^{2+} minerals is much higher in anoxic conditions (Russell and Arndt, 2005; Arndt and Nisbet, 2012). It has been proposed from theoretical modelling that alkaline hydrothermal conditions (anoxic, alkaline (pH 9) and a temperature range of 25 - 125 °C) are thermodynamically conducive to the redox reactions discussed here (Amend and McCollom, 2009). Amend and McCollom (2009) demonstrate that total cell biomass synthesis is most favourable at mild hydrothermal conditions (50 °C). Over the entire temperature range investigated (25 - 125 °C), the synthesis of nucleotides is endergonic, but that of fatty acids and, specifically amino acids, is highly exergonic (Figure 1.6). Therefore the energetics of synthesising total cell biomass (the sum of all monomers) is highly exergonic. This is significant because it shows that in the transition from the prebiotic world to the biotic world, the energetics for monomer synthesis are most favourable in moderate temperatures, where seawater and hydrothermal fluids mix. These results also imply that once life got started in these environments, the input of energy needed for the proliferation of biomass would have been relatively small. There just needed to be coupling between the exergonic reactions, those forming energy-rich thioesters and acetyl phosphate, and endergonic reactions, those synthesising nucleotides (Amend, 1998; Shock and Schulte, 1998; Amend and McCollom, 2009).

These properties of the Hadean ocean chemistry mean that alkaline hydrothermal vents could have operated as electrochemical reactors, where warm, alkaline, H_2-rich fluids come into contact with cool, acidic, CO_2-rich ocean waters, within a labyrinth of micropores containing catalytic Fe(Ni)S minerals (Russell

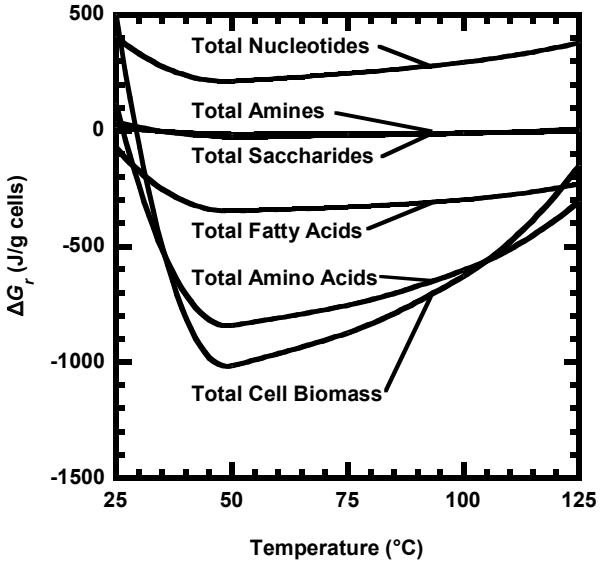

Figure 1.6. Calculated Gibbs energies for molecular building blocks of cells and total cell biomass. Energies of reaction as a function of temperature. Image taken from Amend and McCollom (2009).

and Hall, 1997; Russell et al., 2010). The important chemical disequilibrium which is caused by these steep pH and redox gradients, across catalytic barriers, has a striking similarity to the process of carbon and energy metabolism, chemiosmosis, in autotrophic cells (Figure 1.7), and specifically the chemistry of the acetyl-CoA pathway (Martin and Russell, 2007; Lane and Martin, 2012; Sousa et al., 2013). As noted earlier, the acetyl-CoA pathway involves the reduction of CO_2 by H_2 using the proton motive force to drive redox reactions, along with FeS membrane proteins such as ferredoxin (Fuchs, 2011; Buckel and Thauer, 2013).

Once the endergonic barrier to CO_2 reduction has been overcome, then the next steps of the acetyl-CoA pathway can proceed, and are exergonic. In methanogens and acetogens the acetyl-CoA pathway drives carbon and energy metabolism via acetyl-CoA and ATP (Fuchs, 2011). An abiotic equivalent of this pathway could theoretically occur by producing a simple analogue to acetyl-CoA; methyl thioacetate. This has already been synthesised from CO and CH_3SH by Huber and Wächtershäuser (1997) using Fe(Ni)S catalysts, all ingredients that could have been supplied within the vent system. A CO_2-pathway equivalent has thus been suggested as an ancient form of carbon reduction at the origin of life.

The evolution of mechanisms for phosphorylating organic and inorganic

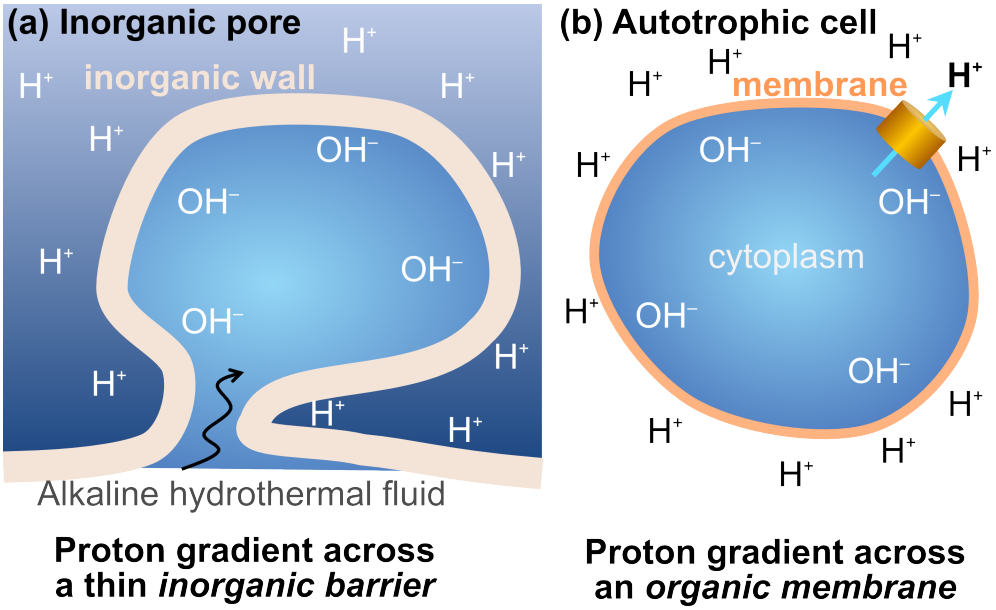

Figure 1.7. Chemiosmotic properties of autotrophic cells as compared to alkaline vent pore. **(a)** A proton gradient is produced by the difference in pH between the alkaline hydrothermal fluids in the vent vesicle and the acidic Hadean ocean, which would percolate into the vent system. This creates a gradient of high H^+ concentration on one side of a thin inorganic barrier and a chemical potential that stores energy, making it available for synthesis and transport. Continuous hydrothermal flow and ocean convection maintain the steep pH gradients. **(b)** The proton-motive force as seen in all autotrophic cells, produced by active membrane pumps which extrude protons to maintain the pH difference. The thickness of the barrier in the inorganic vesicle and the cell would be orders of magnitude different (1 μm vs. 5 nm), however the difference in pH is equivalent in both magnitude and polarity (3 pH units with acid fluid outside). Image taken from Sojo et al. (2016).

molecules is a key step for the origin of life and its subsequent evolution to living systems. Phosphorus is at the heart of all modern biochemical systems, this is due to it having a number of characteristics that are key to it remaining in the membrane; it is soluble in water in the absence of divalent cations (Pasek and Kee, 2011), it should always be charged, and therefore the third linking group needs to be ionisable, and in order for the linking ester bonds to be hydrolytically stable the charge needs to be negative and physically close to the ester group. These characteristics are unique to phosphoric acid (Westheimer, 1987). Reactive phosphorus molecules, such as ATP, act as energy currency molecules to drive endergonic metabolism. As mentioned previously, acetyl phosphate could have acted as an abiotic equivalent to ATP, providing a source of energy for metabolic processes, such as phosphorylation and condensation. Extant cells can

phosphorylate acetyl-CoA to form acetyl phosphate without the need of enzymes. This could point to the possibility for an equivalent prebiotic synthesis. The high phosphorylating potential of acetyl phosphate would then enable the formation of polymers such as polypeptides and nucleotides for further synthesis to nucleic acids from simple precursors (de Duve, 1988, 1995; Martin and Russell, 2007; Lane and Martin, 2012). These key molecules are shown in Figure 1.8. Prebiotic pathways and protometabolic reactions will be discussed in more detail in Chapter 5.

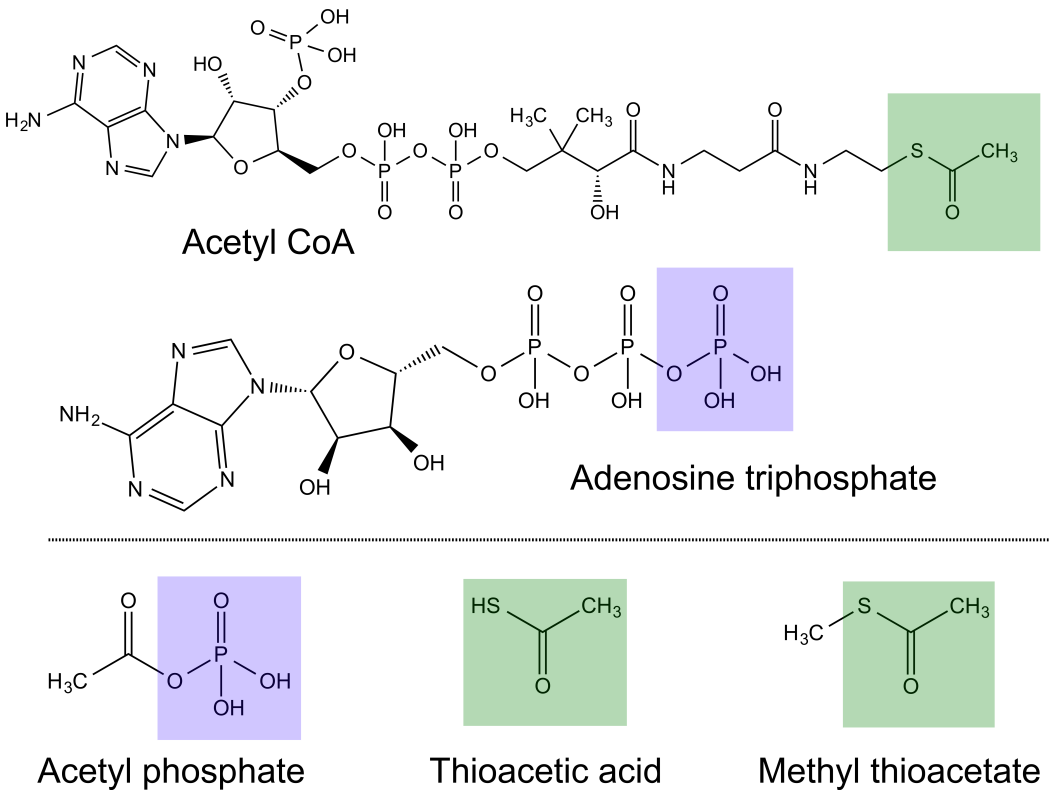

Figure 1.8. Molecular structures of key biotic and prebiotic molecules. Acetyl-CoA is the hub of metabolism in all six known pathways of carbon fixation. The important part of the molecule is the reactive thioester or thiol group (green shaded section) which has prebiotic analogues in methyl thioacetate and thioacetic acid. Adenosine triphosphate (ATP) is the universally conserved energy currency in modern metabolism; acetyl phosphate (AcP) could have been a simple precursor, driving similar reactions. The blue shading highlights equivalent phosphoanhydride bonds in both molecules.

Phosphate is an essential element for prebiotic evolution, however, there is still much contention over what the first source of phosphate was on the early Earth. The prevalent opinion is that the chemistry of phosphorus in geological environments is restricted to the water-insoluble mineral apatite, where it would

not be available for prebiotic chemistry (Keefe and Miller, 1995), however this is not necessarily the case. The concentration of ions such as Mg^{2+}, Ca^{2+} and $PO_4{}^{3-}$ that would have occurred in hydrothermal vents is uncertain. Ca^{2+} rapidly precipitates as carbonates in alkaline pH, and Mg^{2+} precipitates as hydroxides, notably brucite ($Mg(OH)_2$). This precipitation in modern vent systems reduces their concentrations to very low levels (Ludwig et al., 2006). Early oceans would have been mildly acidic, however, due to the high concentration of CO_2, meaning the availability of these ions may have been higher in the oceans. The vents would still have been alkaline, and Mg^{2+} ions could have been supplied within the vent fluid by serpentinisation, and with a lack of oxygen they may not have precipitated as hydroxides (Russell et al., 2010). Brucite scavenges phosphate, and is metastable, breaking down to release phosphate in alkaline hydrothermal systems (Holm, 2012). Similarly, the mineral whitlockite [$Ca_{18}Mg_2H_2(PO_4)_{14}$], also commonly found in modern alkaline systems, is thermally unstable, and breaks down to release phosphate (Holm, 2012; Holm and Baltscheffsky, 2011). It is therefore possible that the breakdown of metastable minerals could increase the concentration of Mg^{2+} and $PO_4{}^{-3}$ (Nitschke and Russell, 2009). Holm (2014) suggests that phosphate could have been contained within glasses and gels, with the content of Al_2O_3 having an important effect on silicate polymerisation. The suggestion that condensed phosphates are dissolved in glasses is also supported by experiments by Cody et al. (2001); Mysen and Cody (2001). Yamagata et al. (1991) alternatively suggest that inorganic phosphate, in the form P_4O_{10}, could have formed through the reoxidation by CO_2 of phosphorus volatilised from a non-reducing magma at high temperatures. If the volcanic gas containing P_4O_{10} was suddenly cooled, condensed phosphates might be produced by its partial hydrolysis, which would sink to the sea bed as insoluble salts. These precipitates could then be cycled back into polyphosphates if they came into contact with volcanic areas, thus cycling phosphate continuously throughout Earth's history (Yamagata et al., 1991). Another solution is from extraterrestrial sources, such as meteorites whose abundance would have been significant during the Hadean accretion event and beyond in the possible heavy bombardment. In this case

phosphorus could have occurred in the form of schreibersite [$(Fe,Ni)_3P$] (which is also now known to be endogenous to Earth, making it an even more plausible prebiotic source), which reacts in water, releasing soluble and reactive reduced phosphorus species, such as phosphite (Pasek and Lauretta, 2008; Kee et al., 2013; Pasek et al., 2013). The potential of these different hypotheses means phosphate may have actually been around and available for prebiotic chemistry on the early Earth, and throughout Earth's history.

Phosphorylation and condensation reactions are only favoured if the concentration of initial products is high enough. The yields of initial monomers are expected to be low, however the hydrothermal vents provide a dynamic concentration mechanism, known as thermophoresis, which circumvents this problem (Braun and Libchaber, 2002; Baaske et al., 2007). Geologically speaking, thermal gradients would have been the most abundant dissipative systems on early Earth, and within the hydrothermal vents these are even more extreme. The process of thermophoresis repels molecules along temperature gradients, which would have existed across the pore structures in the vents, and could easily have accumulated even small organic molecules in the cooler regions. Baaske et al. (2007) show that they can accumulate single nucleotides, $>10^8$ fold, at the bottom of a plugged pore system in a theoretical simulation study. In closed systems it has been shown that larger molecules can be concentrated, even in relatively small thermal gradients (2.3 - 4.4 °C), for example RNA (Mast and Braun, 2010), DNA (Reineck et al., 2010), and fatty acids, which form vesicles (Budin et al., 2009). This process of thermophoresis has also been found to concentrate organics in open systems, such as alkaline hydrothermal vents, enabling the concentration of small organics (Herschy et al., 2014). Herschy et al. (2014) show that temperature gradients of ∼50 °C across a microporous ceramic foam can concentrate fluorescein by 2,500-fold to 5,000-fold, and quinine possibly greater than 30 million fold, by thermophoresis (Figure 1.9). Fluorescein and quinine are of similar sizes to amino acids and nucleotides, suggesting that thermophoresis could very effectively concentrate biopolymers within the vent setting.

The confinement of unstable compounds and the ability to sustain a far from

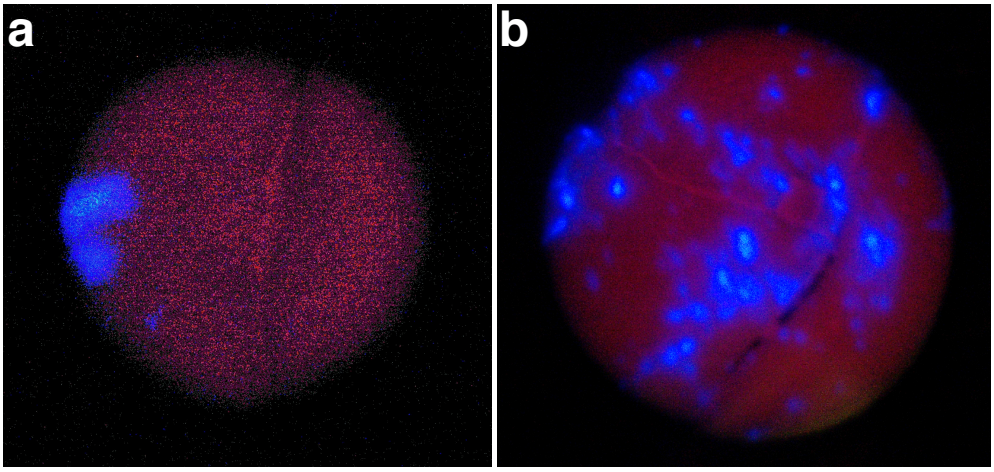

Figure 1.9. Concentration by thermophoresis of fluorescein and quinine in a microporous ceramic foam. Sections of ceramic foam (diameter: 9 cm) exposed to UV light, after being infused with 0.1 µM fluorescein and quinine solution for a period of 4 hours under alkaline vent conditions. The bright blue areas are the areas of molecular concentration. **(a)** Fluorescein concentration, estimated to be between 2,500-fold and 5,000-fold concentration of inflow fluids. **(b)** Quinine concentration, much greater and more widespread over the foam section than fluorescein, estimated to be at least 30 million fold concentration of inflow fluids. Image adapted from Herschy et al. (2014) and unpublished data.

equilibrium system to store energy are essential. If key energy intermediates can be synthesised via proton gradients, how can these molecules then react together further if they are lost and diluted in the hydrothermal flow? Russell et al. (1988) suggest that the micropores in the vents could have acted as compartments to enable complexity to evolve. As seen in a Lost City sample cross-section (Figure 1.5), alkaline hydrothermal vents are made up of a labyrinth of interconnected micropores, providing an environment where larger organic molecules could have accumulated by thermophoresis and become trapped, along with interactions of phosphorylated molecules with mineral surfaces which could have retained molecules in the vent. This could have enabled the beginnings of protometabolism, such as the abiotic analogues of the acetyl-CoA pathway and ATP synthesis (Koonin and Martin, 2005; Herschy et al., 2014). This investigation involves linking the bottom-up approach, looking at what conditions would have been like on the early Earth, to the top-down approach, using phylogenetic data to indicate which metabolic processes and pathways are deeply diverged in extant life, so there is a congruent progression from prebiotic chemical reactions to modern

biochemical processes.

1.5 Project prospective

Whilst the role of alkaline hydrothermal vents as a potential location for the origin of life has been discussed at length (Russell et al., 1988, 1989, 1993; McCollom and Seewald, 2007; Russell et al., 2010; Martin and Russell, 2007; Lane et al., 2010), little experimental data has been provided in support of this theory. The aim of this study was to investigate whether the conditions and ingredients within alkaline hydrothermal vents could have enabled carbon and energy metabolism at the origin of life. Experiments have focused on individual aspects of the vent's chemistry and thermodynamics which could have facilitated this protometabolism, such as pH gradients, temperature and catalytic Fe(Ni)S clusters, along with attempting to synthesise abiotic equivalents of acetyl-CoA and ATP. Specific objectives of the research were:

1. To simulate the formation of iron sulphur precipitates at the interface between warm alkaline fluid flowing into a cool acidic reservoir. The aim was to produce thin tubular, FeS or Fe(Ni)S containing precipitates, with alkaline fluid in the middle of the tubes, surrounded by an acidic reservoir. The precipitates would be synthesised within a bespoke designed bench-top reactor, enabling the pumping of heated alkaline fluid up through a distributor into a reservoir of acidic fluid, within an anaerobic chamber. Previous research by Mielke et al. (2010) and Barge et al. (2012) have shown that it is possible to produce FeS structures in a similar way to that proposed here, but within smaller more contained systems. Barge et al. (2012) showed this only in a static system, not a continuous flow as was attempted here. By producing thin tubular precipitates in a continuous flow system it was hoped that these precipitates would provide a simple analogue to an internal catalytic inorganic barrier within a hydrothermal vent system. Designing a suitable bench-top reactor, that would enable easy access to the precipitates formed in the anaerobic chamber, was one of the challenges

faced at the very start. Investigation then went into the conditions needed to produce precipitates of the desired consistency and appearance. The characterisation of the precipitates formed and observation of FeS crystals, such as mackinawite, was the primary objective of this early research, along with observations about how the precipitates formed.

2. To undertake the observation and quantification of C_1-organic products formed as a result of the FeS precipitates acting as a catalytic barrier, as described in Section 1.4.2. The aim was to create conditions whereby it might be possible to reduce CO_2 within the acidic fluid, with H_2 from the alkaline fluid, across the thin, inorganic FeS or Fe(Ni)S barriers in a dynamic system. The success of this reduction would then be judged by the analysis of formaldehyde, which was the molecule of choice for detection. One of the challenges here was finding a suitable extraction and detection method that was feasible within the constraints of this experimental setup.

3. To investigate a series of protometabolic reactions, synthesising key energy intermediates (C_2 and C_3-organics) needed in carbon and energy metabolism. The aim was to find intermediates that could have been prebiotic analogues of key molecules in modern metabolism, such as ATP and acetyl-CoA. Previous research by Huber and Wächtershäuser (1997) looked at the synthesis of methyl thioacetate, as a precursor to acetyl-CoA, from CO and methyl sulphide (CH_3SH; also known as methanethiol), in the presence of (Fe,Ni)S catalysts. Using methods from this work the synthesis of methyl thioacetate from formate ($CHOO^-$) and methyl sulphide (CH_3SH), in the presence of FeS clusters was investigated. Following on from this the synthesis of acetyl phosphate (AcP) from methyl thioacetate (CH_3COSCH_3), or thioacetic acid (CH_3COSH), and inorganic phosphate was investigated, as a prebiotic analogue for ATP (Figure 1.8).

4. To establish if AcP might be able to drive prebiotic chemistry in water, acting as a key energy intermediate, under mild hydrothermal conditions. Reactions similar to that which ATP carries out today were investigated.

These included synthesis and phosphorylation of key intermediates; synthesis of adenosine and AMP from adenine and ribose in the presence of AcP, and the phosphorylation of adenosine to AMP by AcP.

Chapter 2

Materials and Methods

2.1 Recreating hydrothermal FeS precipitates

The formation of iron sulphide (FeS or Fe(Ni)S) alkaline hydrothermal precipitates in the laboratory, which transect pH and temperature gradients, was simulated by pumping alkaline fluid into an acidic reservoir, within a bespoke designed flow-reactor.

2.1.1 Flow-reactor design

The flow-reactor was designed to allow modelling of hydrothermal vent activity by enabling the introduction of heated alkaline fluids into a chamber of cool acidic water. The first, larger flow-reactor consisted of a glass cylinder 4.5 L in volume, with four sampling ports located on opposite sides. The second, smaller reactor was 700 mL in volume, with either 4 or 8 sampling ports (Figure 2.1). Two titanium discs formed the top and base endplates of the reactor, sealed with a silicone O-ring to the glass cylinder. The top endplate had a 1 cm wide vertical spout in the centre for outflowing fluid. The baseplate had a 1 cm wide hole, with welded tube attached to serve as an inlet for fluid rising into a flow distributor. The distributor had 2.5 mm (large reactor) or 1.6 mm (small reactor) holes evenly spaced around a circular plate. Titanium alloy metal (Titanium with 6 % Aluminium and 4 % Vanadium) was used for metal work that may have

come into contact with sample fluid due to the combination of strength, chemical inertness and non-corrosive properties it provided. The large reactor had two heating elements connected to the inlet base tube to heat the incoming fluid; the small reactor had a copper jacket around the inlet tube that was heated, providing a more even distribution of heat around the inlet tube. The large reactor was connected to four tripod-like legs to keep it suspended 40 cm off the ground. The small reactor was supported by three legs, which was more robust and practical. Alkaline fluid was pumped into the base of the reactor, and acidic fluid into a side port along lengths of silicone tubing, which were connected through Cole Palmer Masterflex C/L peristaltic pumps (Figure 2.2).

2.1.2 Fluid compositions

The composition of the acidic and alkaline fluids was based on a very simplified version of acidic ocean and alkaline hydrothermal fluid compositions that are believed to have existed on the early Earth, 4 Ga. Initial compositions and concentrations used were based on a combination of two experiments carried out by Barge et al. (2012) and Mielke et al. (2011). The main components, iron, silica and phosphate, would all have been present in the Hadean ocean, however actual concentrations where not considered of importance in this instance, as the aim was to produce stable, thin precipitate structures, rather than model the Hadean conditions exactly. Both acidic and alkaline fluids were made with degassed 18 MΩ Milli-Q water. The concentrations of components in fluids used in the small reactor experiments were then reduced (Table 2.1). This reduction was made for a number of reasons; the flow dynamics were different in the small reactor, enabling a lower concentration of silicate and phosphate to still produce stable precipitates and with lower silicate concentrations the precipitates are more likely to be more semi-conducting, as the FeS minerals are not insulated by a layer of silicate. Acidic 'ocean' water was made up of 50 mM iron(II)chloride tetrahydrate ($FeCl_2 \cdot 4\,H_2O$; Acros Organics), simulating ferrous iron in the early oceans; 10 mM sodium biocarbonate ($NaHCO_3$; Sigma Aldrich), simulating the bicarbonate/CO_2 partition of the early oceans; and 2 M hydrochloric acid (HCl;

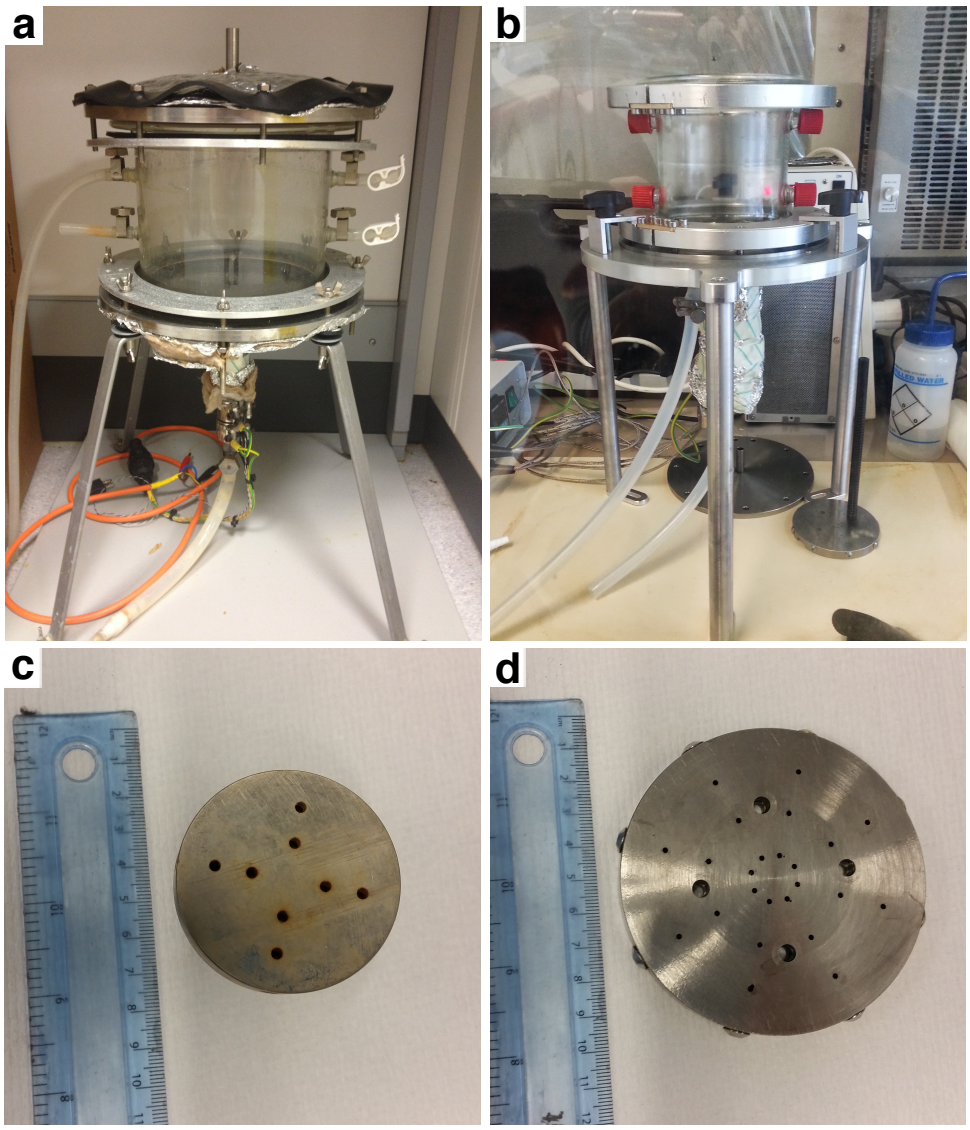

Figure 2.1. Photographs of the large and small bench-top flow-reactors, with their corresponding distributors. The reaction chamber is open-flow, allowing heated alkaline fluids to be pumped into the base through a distributor, into a reservoir of cool acid fluid. The ports on the side of the reactor allow for addition of fluids and sampling while the reactor is in operation. **(a)** Large reactor used at the start of the investigation (4.5 L volume). **(b)** Small, redesigned reactor used for all subsequent precipitate investigations and carbon reduction experiments (700 mL volume). **(c)** Large reactor distributor. Small area with large holes (2.5 mm). **(d)** Small reactor distributor. Large area with smaller holes (1.6 mm).

VWR), used to acidify the solution to between pH 4.7 - 5. The pH was chosen to be this low (the more acidic end of the range estimated for Hadean oceans) due to the Fe^{2+} ions precipitating out into solution, possibly as siderite ($FeCO_3$), at higher pH making the solution go a brown cloudy colour. A pH of less than 6 was needed to facilitate the solubility of CO_2 and bicarbonate (HCO_3^-) in solution

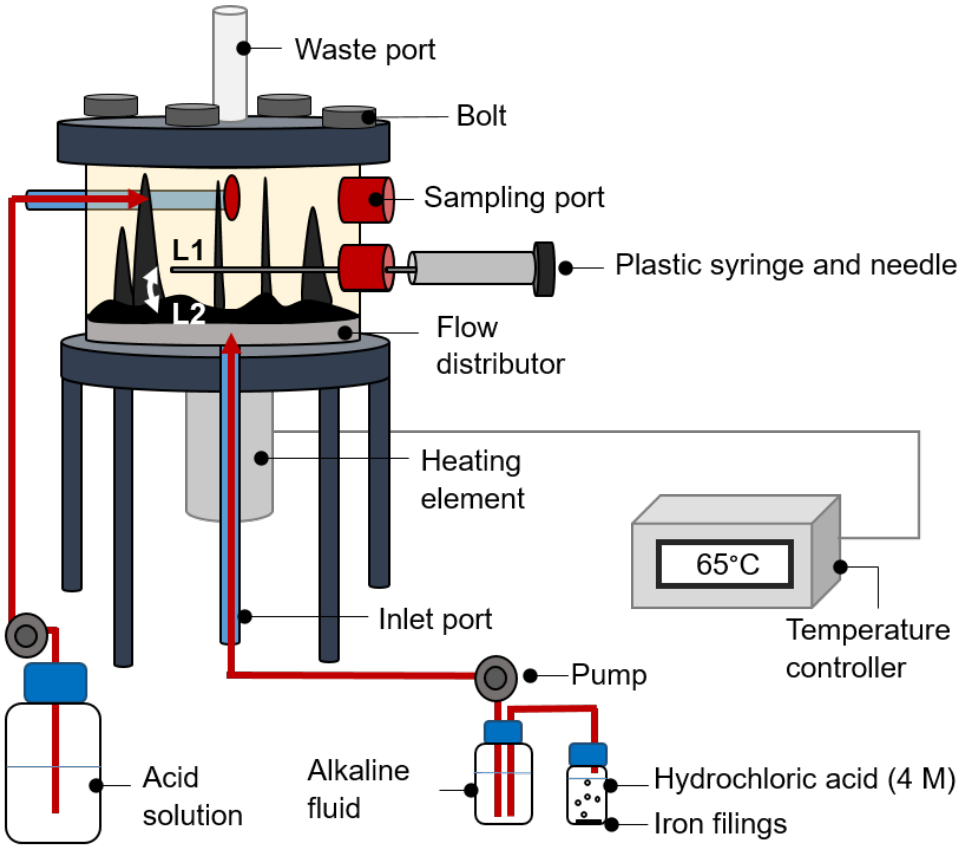

Figure 2.2. Schematic of small reactor setup and sampling procedure. Samples were taken from two locations in the reactor vessel: solution around the precipitates (L1) and from the FeS precipitate itself (L2). Hydrogen is added to the alkaline fluid by way of iron fillings in hydrochloric acid. Drawing adapted from S. Lim, Laboratory Report, 2016.

(Figure 2.3), along with the Hadean ocean expected to be lower in pH than today (mentioned in Chapter 1, section 1.4.1). To some of the experiments in the small reactor 5 mM nickel(II)chloride ($NiCl_2 \cdot 6\,H_2O$; Alfa Aesar) was added, simulating the nickel component in the iron sulphides, which can contain up to 20 % nickel (Russell and Hall, 1997). Alkaline 'hydrothermal' fluid was made up of 10 - 100 mM sodium silicate ($Na_2Si_3O_7$; Sigma Aldrich), 10 - 50 mM potassium phosphate (K_2HPO_4; Sigma Aldrich), both used to increase stability of the structures, and 10 mM sodium sulphide (Na_2S; Alfa Aesar), as the source of sulphur to react with ferrous iron, producing FeS minerals as part of the precipitate structures. The alkaline fluid was pH 11 - 12 and heated to 80 °C in the final experiments. Both of these conditions are similar to that found for

alkaline hydrothermal fluids today at Lost City (Kelley et al., 2001, 2005).

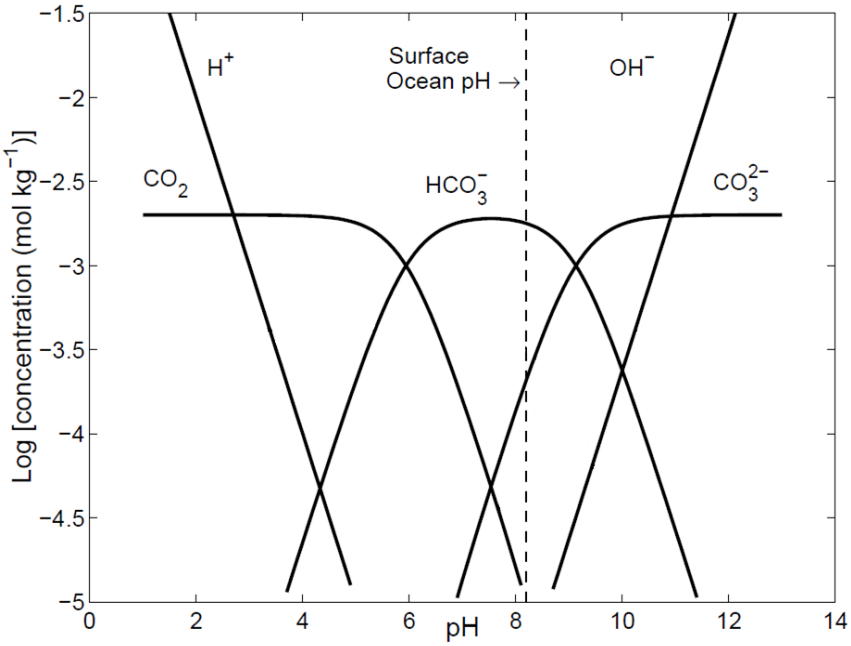

Figure 2.3. Equilibrium relationships between dissolved carbon dioxide (CO_2), bicarbonate (HCO_3^-) and carbonate (CO_3^{2-}) as a function of pH in seawater.

All experiments were run in the flow-reactor within an anaerobic chamber (COY Inc. Grass Lake, MI), with an atmospheric composition of 2.5 % H_2 in N_2. This atmosphere maintains strict anoxia in combination with Stak-Pak catalysts, containing a palladium catalyst, in the chamber. The catalysts react any oxygen in the atmosphere with the H_2 in the atmosphere to form water. They were periodically rejuvenated to remove the water by baking them for 2 hours in a high temperature oven (800 °C). Initially all water used in the experiments was left stirring in the chamber overnight to deoxygenate before experimentation (this was found to be sufficient time to remove all oxygen using a Extech DP700 dissolved oxygen meter). Later evidence indicated that this procedure produced a lot of organic contamination within the water from the atmosphere, which contained organic volatiles from the experiments. Subsequent deoxygenation was conducted outside the chamber by bubbling N_2 into the water for at least 2 hours. Acid and alkali fluids were made up to different volumes depending on the reactor and the run time needed.

Table 2.1: Concentrations of chemicals used in acid and alkali fluids during different reactor experiments.

Chemicals	Concentration (mM)	
Acid	***Large reactor***	***Small reactor***
$FeCl_2$	50	50
$NaHCO_3$	10	10
$NiCl_2$	N/A	5
Alkali		
$Na_2Si_3O_7$	100	10
K_2HPO_4	50	10
Na_2S	10	10

2.1.3 Experimental method

Large reactor

The reservoir was filled with cool (20 °C) acidic fluid. Alkaline fluid was pumped into the base of the reactor at full speed (140 mL/h) to prime the tube. Once primed the alkaline fluid was pumped into the reactor at speeds between 15 - 100 mL/h, with the heating element set to between 70 – 120 °C, comparing the relationships between temperature, speed and fluid composition to precipitate structure and stability. As alkaline fluid was pumped into the reactor pictures were recorded of the precipitates and the pH and conductivity monitored (using Extech PH220-C pH and conductivity probe). Samples of forming precipitates were collected using a cut off disposable pipette and placed into 15 mL falcon tubes for analysis. Precipitate samples were centrifuged for 8 minutes at 4000 r.p.m., the supernatant decanted into a clean falcon tube and the solid precipitate frozen on dry ice and freeze-dried for 2 hours.

Small reactor

Alkaline fluid was pumped into the reactor in a similar way to the large reactor, however speeds were optimised to produce the best vent-like structures (thin-walled to enable potential electron transfer from H_2 to CO_2, but stable enough not to collapse). The speed was set to 70 mL/h for the first 10 minutes and then

decreased to 50 mL/h for the remainder of the experiment. The temperature was set at 80 °C. Samples of precipitate were collected in the same way as for the large reactor.

2.1.4 Qualitative analysis

Analysis of the precipitate was conducted by electron microscopy and elemental mapping by energy-dispersive X-ray (EDX) on a Jeol JSM-6480LV high-performance, Variable Pressure Analytical Scanning Electron Microscope (SEM) and a Jeol JEM-2100, LaB6 electron source Transmission Electron Microscope (TEM). TEM images were analysed for atomic spacings using the program Gatan Digital Micrograph. Light intensity cross sections were used to measure the atomic spacing within individual crystals, in which a spectrum is drawn perpendicular to the space group orientation, to gain information about the spacing between the atomic planes. Fast Fourier transform (FFT) images were used to get an average atomic spacing for the whole image (many crystals within one image). In this method distances between different points in the outer rings on the image to the centre point give the spacing for individual crystals. The precipitate was also analysed for crystalline structures using powder x-ray diffraction (PXRD) on a Stoe Stadi-P Diffractometer. Two types of radiation were used, with different sampling methods; Copper (Cu Kα1, 50 kV and 30 mA) radiation source was used with a dry sample in a capillary tube, and molybdenum (Mo Kα1, 50 kV and 30 mA) radiation source was used with a wet sample placed between two thin plastic foils. Two different radiation sources were used to see if the fluorescence produced in the output from the iron was reduced in the molybdenum source compared to the copper.

2.2 CO_2 (as bicarbonate) reduction by hydrogen

Experiments were carried out to discover if the hydrothermal precipitates were of a suitable composition and structure to enable the reduction of CO_2 by H_2. Hydrothermal precipitates were produced by the method in 2.1, and samples of

fluid surrounding the hydrothermal precipitates, plus some of the precipitates, were collected with a syringe (10 mL), through the sampling ports of the reactor every 20 minutes for periods of up to 4 hours. Later experiments separated the collection of samples from the surrounding solution and the precipitates. Experiments were carried out with FeS or Fe(Ni)S mineral precipitates, and with or without H_2 (in principle, the excess Fe^{2+} ions present in the ocean solution, and the continuously forming precipitate means it is plausible that CO_2 reduction could take place even in the absence of H_2, with Fe^{2+} as the electron donor rather than the catalyst).

In the initial experiments to add hydrogen to the system, iron filings (0.5 g) were added to 100 mL 1 M HCl in a 100 mL glass bottle. A tube from the lid was connected through a peristaltic pump to a hypodermic needle, which was inserted into the silicone tube near the base of the reactor's heating element. Hydrogen was bubbled into the reactor at 16 mL/h. This rate would have started to decrease as the iron filings were dissolved in the acid, producing less and less H_2 over time; good bubbles were produced for around 2 hours with this volume of acid and amount of iron. The problem with this method was it disrupted the precipitates every time a bubble passed through the distributor. Later experiments produced H_2 in the same way, but added it to the atmosphere above the alkaline fluid, enabling H_2 to dissolve into the alkaline fluid, rather than bubbling it straight into the reactor. The problem with this method was that only a very low concentration of H_2 dissolves into solution at atmospheric pressure ($<$1 mM), however it did seem to work much better than the bubbling directly into the reactor.

All reduction products were of interest; however, due to their instability and volatility they were not easy to detect, therefore derivatisation of specific molecules was needed. Samples were analysed for formaldehyde (CH_2O), due to it being the hardest reduction step to reach when CO_2 is reduced by H_2, posing a symbolic state which has overcome the thermodynamic barrier to its synthesis. It was detected using two methods. Formaldehyde is a small molecule, relatively polar and it does not fluoresce, therefore it can be detected only by derivatisation or by GC-MS using a specific column for small volatile organics (this was difficult

to use in this project as the GC-MS being used was a core facility machine, making using a dedicated column too time consuming and inconvenient). Two derivatisation methods were modified and developed from previously described procedures. The method using 2,4-dinitrophenylhydrazine (DNPH) derivatisation was detected by High Performance Liquid Chromatography (HPLC), and was modified from Kieber and Mopper (1990) (see section 2.2.1). The second method involved derivatisation with o-(2,3,4,5,6-pentafluorobenzyl)-hydroxylamine (PFBOA) and detected by Gas Chromatography-Mass Spectroscopy (GC-MS), and was modified from Sugaya et al. (2001) (see section 2.2.2). For each run a sample of the initial acid solution was taken, to act as a control for compounds within the initial acid solution.

The total organic content was measured using Total organic carbon (TOC) method (see section 2.2.3); in this way the total amount of organic material being produced could be assessed, even if individual compounds were not detected in this method.

The results from individual experiments were averaged and the standard deviation of the mean (SD) was calculated to determine the variability in the results. A one-way analysis of variance (ANOVA) with a Brown-Forsythe test, followed by Bonferroni's multiple comparison test, to compare each group to one another, was carried out to test the statistical significance of the results.

2.2.1 DNPH derivatisation

DNPH reagent preparation was done according to Kieber and Mopper (1990) to improve the quality of the reagent. This recrystallised reagent was then prepared weekly by dissolving 20 mg recrystallised DNPH in 4 mL of 12 M hydrochloric acid (HCL; Fisher), 10 mL Milli-Q-water (18 MΩ) and 2 mL acetonitrile (ACN; Sigma Aldrich). The reagent was then shaken and left for 1 hour. To reduce the background aldehyde signal the reagent was extracted with 2 mL dichloromethane (DCM; Sigma Aldrich) and shaken for 10 minutes. The organic layer was removed with a separating funnel and the extraction process repeated. DNPH reagent extraction was done twice on the first day of use and once each subsequent day,

for up to one week. Potassium phosphate buffer (KPB, 0.1M) at pH 9 was prepared by adding 0.11 g of potassium dihydrogen phosphate (KH_2PO_4; Sigma Aldrich) and 8.5 g of potassium phosphate dibasic (K_2HPO_4; Sigma Aldrich) and diluted to 500 mL Milli-Q water. Samples or standards were prepared by adding 1 mL of sample or standard to a chromatography vial, adding 10 μL of KPB and 10 μL DNPH. The vial was shaken and left to react for 1 hour at room temperature. Samples were filtered to 0.22 μm if precipitate was present. The samples were then run on a Dionex HPLC (LC Packing FAMOS Autosampler, Dionex P680HPLC Pump, Dionex TCC-100 Column oven and Dionex UVD170U Ultraviolet detector), using a HiChrom ACE C18-5 (150 x 4.6 mm) column. Injection volumes were 20 μL with a 16.6 μL/s, 50:50 isocratic run of HPLC grade water (0.1 % trifluoroacetic acid) and acetonitrile. The column temperature was set at 30 °C and UV detection set at 360 nm (primary) and 370 nm wavelengths.

2.2.2 PFBOA derivatisation

Standards of formaldehyde were prepared by diluting 10 μL of each standard stock solution into 10 mL HPLC grade water (Fisher) in a 20 mL headspace vial. For the later experiments (once the GC-MS had been cleaned and detectors replaced to increase sensitivity) the samples had to be diluted 10x, and even better when diluted 100x, due to the high levels of formaldehyde detected with the new sensitivity, which saturated the GC-MS detector (an upper limit of 0.5 mM for accurate detection). To each standard in a 20 mL headspace vial 0.6 mL PFBOA (Sigma Aldrich) solution and 3 g sodium chloride (NaCl; Fisher) was added, and immediately sealed with a PTFE-lined septum and aluminium cap. Later experiments used an internal standard of 1-bromo-4-fluorobenzene; 13.14 μM placed into each sample vial, to act as a standard so variations in the machine could be discounted. The final peak areas for the PFBOA formaldehyde adduct were integrated against the internal standard. The samples were left for 5 hours at 20 °C to allow the derivatising reagent to react. For the experimental samples the same volumes of PFBOA and NaCl were added to headspace vials with 10 mL of liquid sample inside the anaerobic chamber. The samples were run

on a Thermo Scientific GC-MS (Trace 1310 Gas GC, connected to ISQ quadropole MS, with RSH autosampler) using an Rxi-5Sil MS fused silica column (15 m x 0.25 mm x 0.25 μm). Full scan and selected ion monitoring (SIM) was used; analytical conditions are summarised in Table 2.2. SIM was used as selective masses could be chosen to only detect the masses of the PFBOA formaldehyde derivative, thereby increasing the sensitivity for detecting the molecule of interest. Formaldehyde PFBOA adduct was detected at 3.8 minutes, PFBOA was detected at 4.8 minutes (Figure 2.4).

Standard stock solutions of formaldehyde (37 wt% with 10-15 % methanol; Sigma Aldrich) were prepared using various stepwise dilutions ranging from 1 nM to 10 mM. Various concentrations were tested for each method to obtain calibration curves. Figure 2.5 shows an example of a calibration curve from different dilution methods; **(a)** is from the original method, with no dilution of samples, **(b)** is from the newer experiments using a 1 in 10 (sample to HPLC water) dilution method, and **(c)** is from the newer experiments using a 1 in 100 (sample to HPLC water) dilution method. In later experiments after the GC-MS had been cleaned and the sensitivity increased, concentrations greater than 0.5 mM saturated the detector (Figure 2.6). This meant the samples had to be diluted 100x to get the most accurate relationship between area under the formaldehyde detection peak and concentration.

Table 2.2: Operational conditions of GC-MS and headspace autosampler for formaldehyde detection, using PFBOA derivatisation.

Headspace autosampler	
Needle temperature	120 °C
Agitator temperature	60 °C
Agitator time	10 mins
Injection depth	40 mm
GC-MS	
Column	Rxi-5Sil MS (Thames Restek) Fused silica capillary column; 15 m x 0.25 mm x 0.25 μm
Oven temperature	40 °C (1 min) $\rightarrow$ 15 °C/min $\rightarrow$ 220 °C
Carrier gas	Helium
Injection temperature	200 °C
Ion source	NCI or EI
CI gas	Isobutane, 1.5 mL/min
Ion source temperature	200 °C
Transfer line temperature	220 °C
Injection mode	Split 10:1, 15 mL/min
SIM for formaldehyde	175, 181, 205, 225

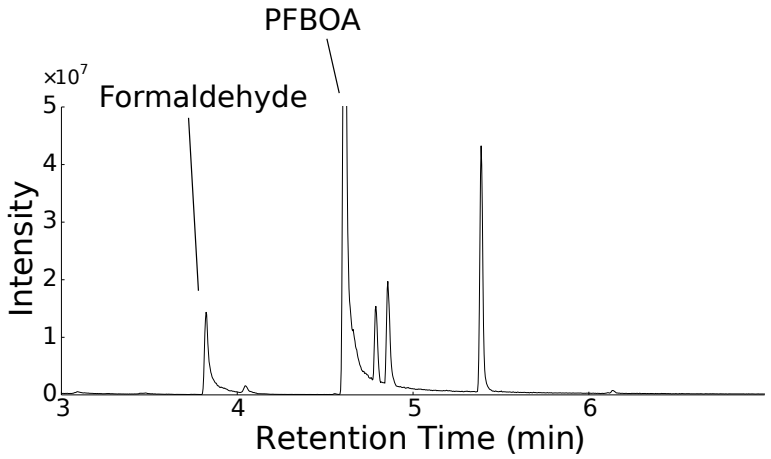

Figure 2.4. GC-MS trace showing analysis for formaldehyde derivatised with PFBOA. The formaldehyde PFBOA adduct peak is detected at 3.8 minutes and the PFBOA is detected at 4.8 minutes. Estimated concentration is 100 nM here, based on extrapolation from calibration curve data (calibration curves shown in Figure 2.5).

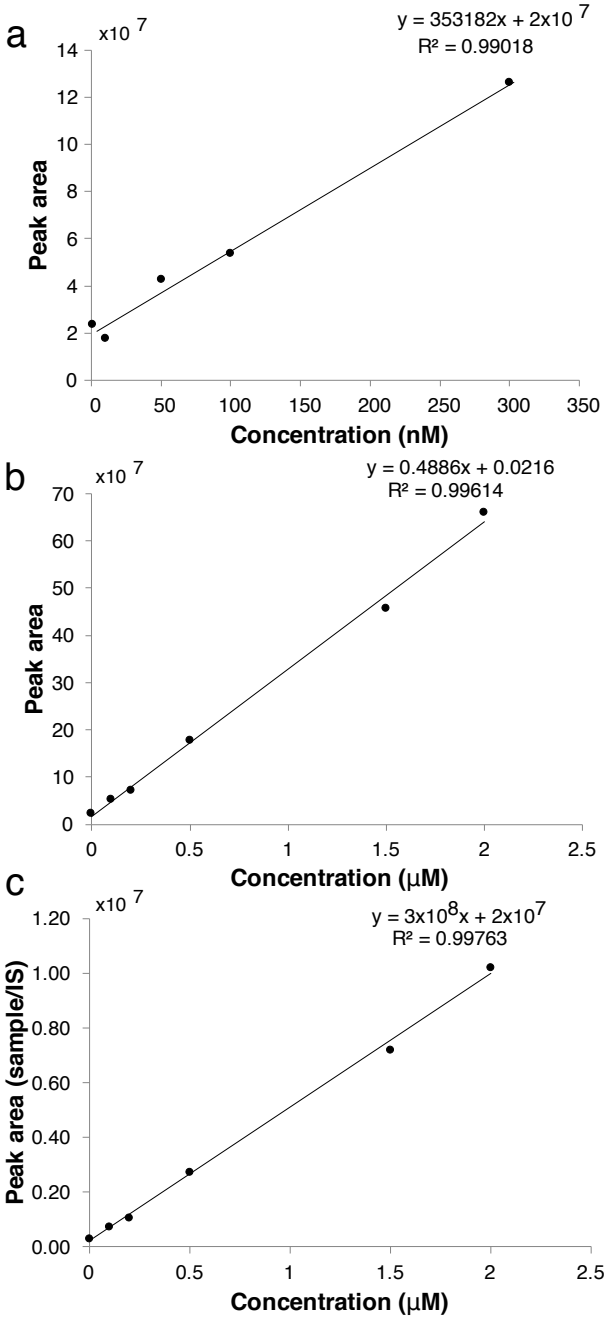

Figure 2.5. Calibration curves for GC-MS for formaldehyde detection, for older and newer GC-MS and flow reactor methods. **(a)** Calibration curve for old experiments using GC-MS and flow reactor without contamination prevention methods. Standards in nM concentrations. **(b)** Calibration curve for newer experiments, using diluted samples at a ratio of 1:10 in HPLC water. Standards in μM concentrations. **(c)** Calibration curve for newer experiments using a dilution ration of 1:10 in HPLC water, y-axis is the peak area in the GC-MS chromatogram with formaldehyde integrated to the internal standard, giving a more accurate standard curve. Standards in μM concentrations. Detection is an order of magnitude more sensitive in the newer experiments, indicating the recalibrated GC-MS, and reduced contamination in the chamber, has increased level of formaldehyde detection.

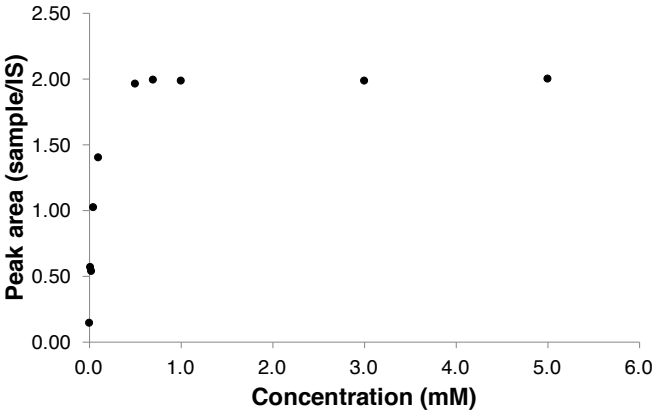

Figure 2.6. Saturated calibration curve for formaldehyde detection by the new GC-MS detector. High concentrations of formaldehyde (>0.5 mM) saturates the detector, so that the calibration curve is no longer linear, and therefore no longer an accurate prediction of concentration vs area under the formaldehyde peak.

2.2.3 Total Organic Carbon

Three or four 20 mL samples were taken from the experimental run (30, 60, 90 and 120 minutes), along with a sample of the acid fluid and an HPLC water blank, and placed in headspace vials. Total organic carbon (TOC) was measured using a Shimadzu TOC-L with ASI-L auto sampler. Initially the purgeable organic carbon (POC) method was used, where the sample was vaporised and both purged and non-purged carbon measured. In this method both total carbon (TC) and inorganic carbon (IC) can be determined and TOC is calculated as IC is subtracted from TC (Figure 2.7). A non-purgeable organic carbon (NPOC) method (temperature 680 °C, carrier gas flow 150 mL/min, gas pressure 200 KPa) was subsequently developed due to the high levels of IC (bicarbonate) in the samples interfering with the detector and producing false negative results. This method first removed the inorganic carbon by purging with purified air and diverting it from the detector, and then the TOC was determined by measuring TC, where TC equals TOC (Figure 2.8). Samples of HPLC grade water, Milli-Q water, CH_2O (6 mg/L), CHOONa (6 mg/L) and the acidic fluid, prepared in the anaerobic chamber, from both water that had been a) left to deoxygenate within the chamber (anaerobic), and b) left to deoxygenate outside the chamber by bubbling through with N_2 (aerobic), were analysed with the NPOC method.

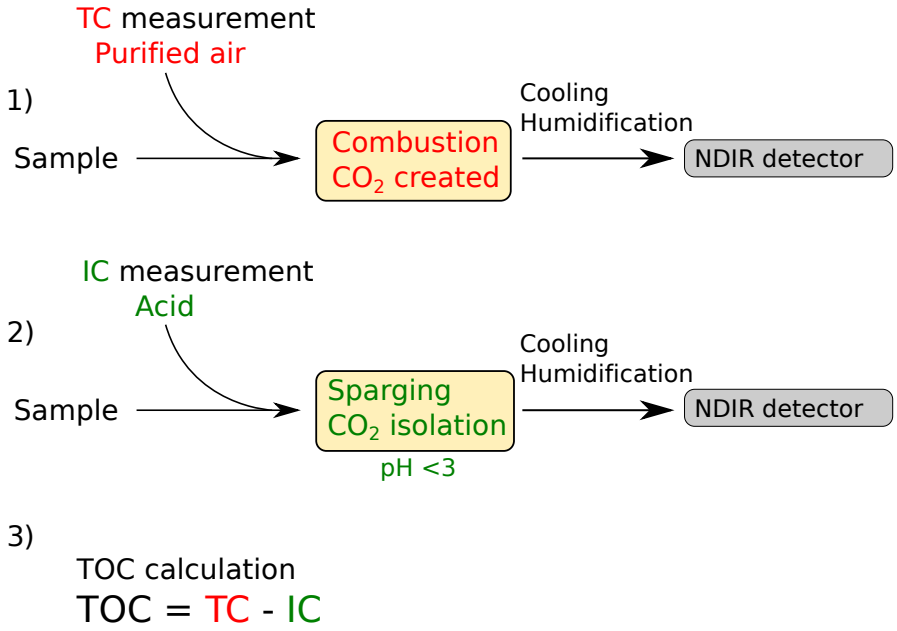

Figure 2.7. Total organic carbon TOC measurement using the 680 °C combustion catalytic oxidation method and the infrared gas analyser (NDIR) method. The sample is delivered to the combustion furnace, which is supplied with purified air. There, it undergoes combustion through heating to 680 °C with a platinum catalyst. It decomposes and is converted to carbon dioxide. The carbon dioxide generated is cooled and dehumidified, and then detected by the NDIR. (1) The concentration of TC (total carbon) in the sample is obtained through comparison with a calibration curve formula. (2) By subjecting the oxidised sample to the sparging process, the IC (inorganic carbon) in the sample is converted to carbon dioxide, and the IC concentration is obtained by detecting this with the NDIR. (3) The TOC concentration is then calculated by subtracting the IC concentration from the obtained TC concentration. Images modified from Schimadzu (2016)

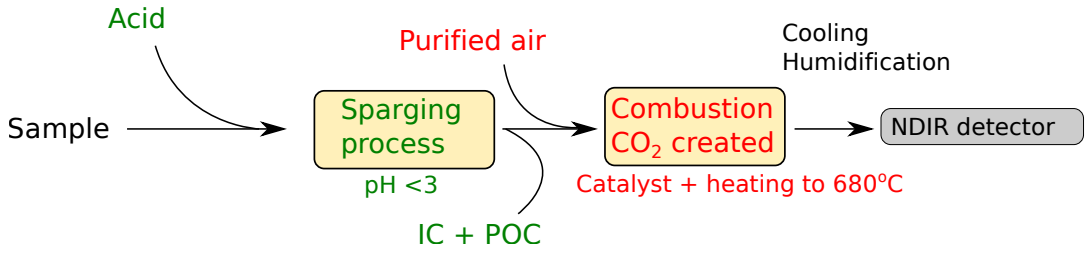

Figure 2.8. Non-purgeable organic carbon (NPOC) measurement using the 680 °C combustion catalytic oxidation method and the infrared gas analyser (NDIR) method. By sparging samples to which a small amount of acid has been added, the IC in the sample is converted to carbon dioxide. This carbon dioxide is removed, and the TOC is obtained by measuring the TC in the treated sample. When the carbon dioxide from the IC is removed, POC (purgeable organic carbon) may also be lost. Accordingly, the TOC obtained with this method may be referred to as NPOC. Images modified from Schimadzu (2016)

2.3 Thioester synthesis

To investigate the synthesis of key energy intermediates needed for carbon and energy metabolism, methyl sulphide (CH_3SH; also known as methanethiol) was reacted with formate (CHOOH) in the presence of FeS and/or NiS catalysts. For a typical experiment, 20 mM nickel chloride hexahydrate ($NiCl_2{\cdot}_6H_2O$; Alfa Aesar) and sodium sulphide (Na_2S; Alfa Aesar) were added to deoxygenated 12 MΩ Milli-Q water in 20 mL screw capped sample vials. To this was added 5 mM sodium formate (CHOONa; Sigma Aldrich) and 1 mM sodium methanethiolate (CH_3SNa; Sigma Aldrich). For analysis by HPLC (make and model as mentioned previously), 20 mM aniline (Sigma Aldrich) was added as a trapping agent for acetic acid, where acetanilide is produced when methyl thioacetate hydrolyses (method used by Huber and Wächtershäuser, 1997). The pH of the mixture was adjusted to pH 5 using 2 M HCl (Fisher). The vials were then sealed and placed in a water bath at 80 °C. Each vial constituted a sample for a different time point; one sample was removed every 30 minutes over a 6 hour period, and filtered to 0.22 μm. Samples were quantified by HPLC (injection volume of 20 μL, at a speed of 16.6 μL/s; 90 - 10 % gradient HPLC grade water (0.1 % trifluoroacetic acid) to acetonitrile over 6 minutes, detection wavelength 240 nm). Aniline eluted at 3 minutes and acetanilide eluted between 6.0 - 6.1 minutes.

To separate formanilide from acetanilide, a new HPLC method was developed, using a shallower gradient; 70 – 30 % gradient HPLC grade water (0.1 % trifluoroacetic acid) to acetonitrile, over 10 minutes, detection wavelength 240 nm. Formanilide was eluted at 3.5 minutes and acetanilide at 3.6 minutes. Methyl thioacetate standards were also detected by this method, when no aniline was added, and eluted at 4.7 minutes. Experiments were carried out with and without aniline, to try and monitor acetic acid and methyl thioacetate production.

The experiment was repeated in the presence of 20 mM iron(II) chloride tetrahydrate ($FeCl_2{\cdot}_6H_2O$; Acros Organics) instead of nickel chloride, in the presence of both catalysts together and without any catalysts (no metals or sulphide), as a control. The experiment was repeated at pH 10 and pH 2,

with samples measured at 0 minutes and 300 minutes, to create a pH profile for the reaction. Acetanilide standards were synthesised from aniline and acetic anhydride (Sigma Aldrich) as described by Bell et al. (2000).

Samples were also tested in headspace and liquid injection GC-MS (make and model as mentioned previously), to see if non-derivatised products could be detected. For headspace GC-MS NaCl was added to force the products into the gas phase (method termed 'salting-out effect' by Sugaya et al., 2001). For liquid injection GC-MS samples were extracted from the aqueous phase into an organic phase using dichloromethane (DCM; Sigma Aldrich) or ethyl acetate (Sigma Aldrich). This method did not detect enough of the product to be precise.

Formanilide and acetanilide standards were verified by Mass Spectrometry (Figure 2.9), (electrospray ionisation (ESI), time-of-flight detection (TOF), single hexapole MS with a solvent ratio of 50:50 methanol (0.5 % formic acid) to aqueous sample).

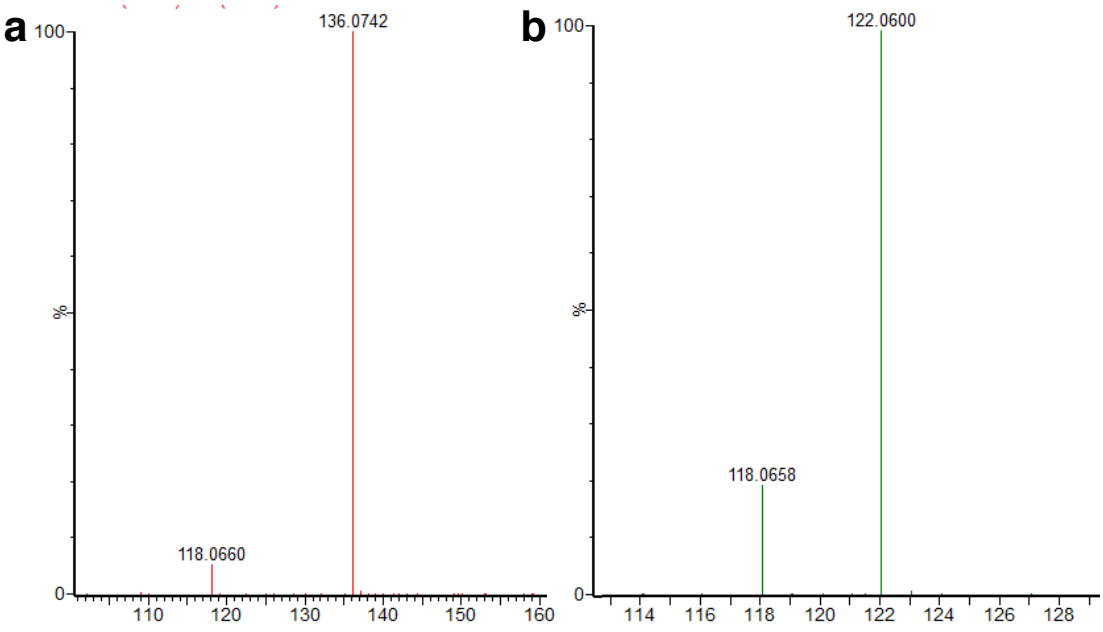

Figure 2.9. MS positive electrospray analysis, showing the molecular ion (M+) for each compound **(a)** Acetanilide M+ = 136. **(b)** Formanilide M+ = 122.

2.4 Synthesis of acetyl phosphate

2.4.1 Synthesis of abiotic acetyl phosphate

Solutions of inorganic phosphate, 20 mM, (Na_2HPO_4; Sigma Aldrich) in 10 % D_2O and Milli-Q water (18 MΩ) were prepared with different concentrations (0, 2, 10, 20 mM) of either magnesium or calcium ions ($MgCl_2$, $CaCl_2$; Sigma Aldrich) or an equimolar mix of both. Experiments used methyl thioacetate, 40 mM, (CH_3COSCH_3; Sigma Aldrich), initially, and then thioacetic acid, 40 mM, (CH_3COSH; Sigma Aldrich), as the activated thiol. The thiol was added to the vials and the pH adjusted to 6, 7, 8 and 11 with aqueous HCl or NaOH (1 M). Samples (600 μL) were taken at time points (2, 10, 20, 30, 40, 50, 60, 120 and 180 minutes) and immediately frozen at –80 °C. Controls were carried out using the same conditions without the addition of thioacetic acid. To every time point 15 minutes was added to the time to take into account time taken from defrosting to start of analysis. Experiments were carried out at 20 °C and 50 °C. Samples were defrosted and analysed using proton nuclear magnetic resonance (^{1}H−NMR; Bruker Avance 600 Hz; 10 % D_2O, 16 scans, water suppression) with potassium hydrogen phthalate (KHP, 1 mM) as an internal standard. Concentrations were calculated using the integrated ratio of protons in the internal standard compared to acetyl phosphate (AcP). Standards of AcP were measured with ^{1}H−NMR to confirm the shift of the detected peak within the experiments. KHP was detected between 7.4 – 7.6 ppm and AcP at 2.1 ppm. All peaks in NMR were identified by analysis of both pure standards (lithium potassium acetyl phosphate salt; Sigma Aldrich) and spiking of experimental samples. Figure 2.10 and 2.11 show ^{1}H−NMR traces for standards of methyl thioacetate alone and spiked with AcP (100 μM) (Figure 2.10), or thioacetic acid and AcP (100 μM) alone (Figure 2.11). Both samples were analysed in the presence of inorganic phosphate (20 mM), Mg^{2+} and Ca^{2+} ions (20 mM), and KHP (1 mM) internal standard. It can be observed that AcP has a large peak at ∼2.11 ppm, methyl thioacetate has peaks at 2.04 and 2.19 ppm, and thioacetic acid has peaks at 1.98, 2.33 and 2.35 ppm (peaks can shift slightly with differences in pH).

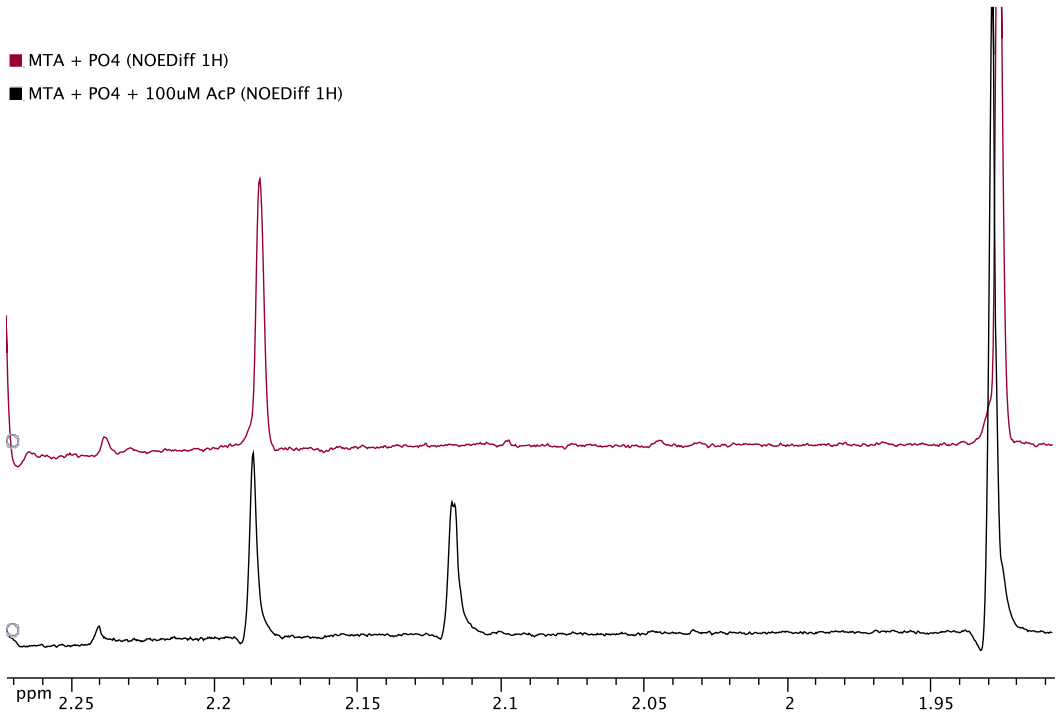

Figure 2.10. ^{1}H−NMR trace (600 Hz) for standard of methyl thioacetate, 20 mM (red line) alone and then with 100 μM AcP added (black line). Both in the presence of inorganic phosphate (20 mM), Mg^{2+} and Ca^{2+} ions (20 mM) and KHP (1 mM) internal standard (double peak at 7.4 - 7.6 ppm). AcP has a distinctive peak at 2.11 ppm

Subsequent experiments were carried out using the same method but with Fe^{2+} ions at differing concentrations; 200, 400 and 100 µM ($FeCL_2$; Sigma Aldrich) in anaerobic conditions at pH 7, to see how Fe^{2+} ions affected the synthesis. A control to investigate how oxic and anoxic conditions affected thioacetic acid reactivity was also carried out with no ions at pH 7.

2.4.2 Production of acetyl phosphate stock

Disodium acetyl phosphate (procedure in dilute solution)

Following a method developed by Crans and Whitesides (1983) AcP was synthesised to produce a stock solution to use for further experiments. Phosphoric acid (22.5 mL; Sigma-Aldrich, 85 wt. %) was dissolved in ethyl acetate (200 mL; Sigma-Aldrich, ≥99.7 %) and cooled to 0 °C using an ice bath. Pre-cooled (0 °C) acetic anhydride (62.5 mL; Sigma-Aldrich) was slowly added slowly over 15 minutes.

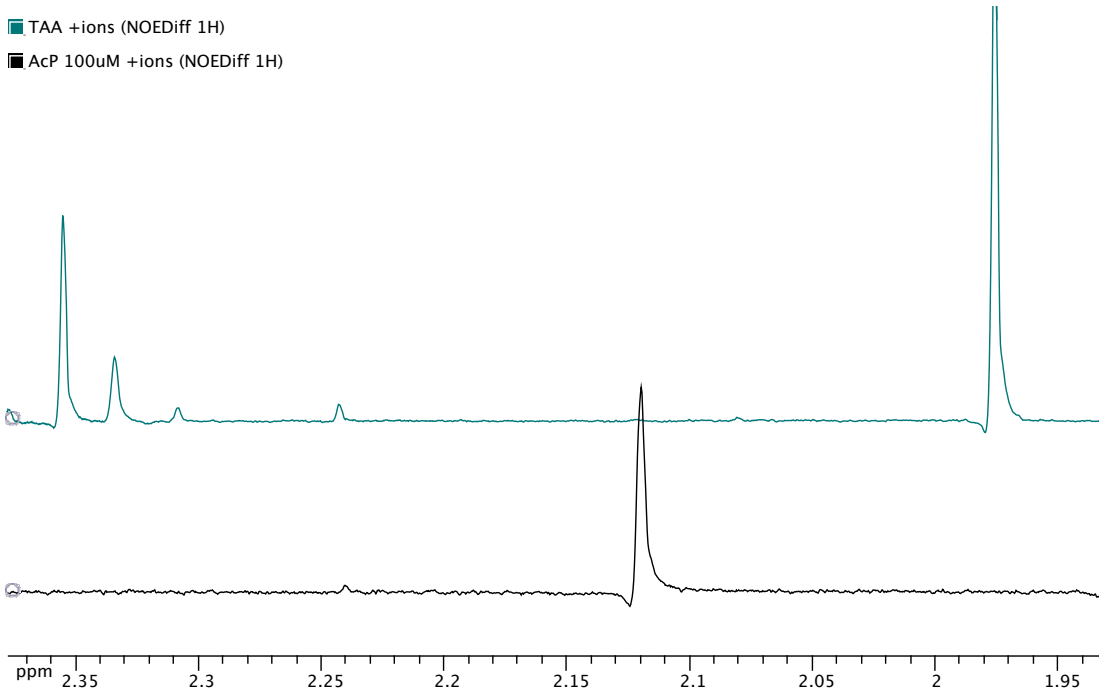

Figure 2.11. ^{1}H−NMR trace (600 Hz) for standard of thioacetic acid, 20 mM (green line) alone and then 100 μM AcP alone (black line). Both in the presence of inorganic phosphate (20 mM), Mg^{2+} and Ca^{2+} ions (20 mM) and KHP (1 mM) internal standard. AcP has a distinctive peak at 2.11 ppm

The mixture was stirred for 6 hours at 0 °C and added to a suspension of 165 mL milli-Q water, 85 g ice and 28 g sodium bicarbonate (Sigma-Aldrich, 99.5 - 100.5 %). The mixture was stirred at 0 °C until no more CO_2 evolved, and then transferred to a separation funnel and mixed vigorously. The organic layer was separated and discarded. The resulting acetyl phosphate was washed with ethyl acetate, to extract the acetic acid from the aqueous solution (300 mL followed by 165 mL) and the organic layer removed after each wash. The resulting volume was neutralised with 10 M NaOH, which caused the appearance of a thin ethyl acetate layer that was also discarded. As much acetic acid was removed as possible by the ethyl acetate washes, however, there was always a residual concentration left over. With at least three extraction washes acetic acid can be reduced to less than 0.4 M in the acetyl phosphate solution (Crans and Whitesides, 1983). The concentration of acetyl phosphate in the final solution was around 1.1 M, as verified by the hydroxylamine method, adapted from Lipmann and Tuttle (1944), described below. The final product was divided into 9 mL aliquots and stored at -80 °C.

Hydroxylamine method to confirm concentration of acetyl phosphate in solution

The concentration of AcP in the stock solution was verified using a method adapted from Lipmann and Tuttle (1944), performed to ensure accurate quantities of phosphorylating agent could be used in further experiments. A set of dilutions were prepared from a pure AcP solution (0.1 M lithium potassium acetyl phosphate; Sigma-Aldrich, ≥85%) in Milli-Q water, at a concentration range from 100 μM to 5 mM. This created a calibration curve for pure AcP.

A 2 M hydroxylamine hydrochloride solution ($NH_2OH{\cdot}HCl$, Sigma-Aldrich, 99 %) was prepared, and the pH adjusted to 7 using 10 M NaOH. A 0.5 M ferric chloride solution ($FeCl_3$, Sigma-Aldrich, ≥99.99%) was prepared in Milli-Q water and 12 M HCl. To conduct the assay a development solution was prepared freshly by mixing equal volumes of the ferric chloride solution and Milli-Q water. AcP stock solution or pure standard solution (600 μL) were added to 1.5 mL Eppendorf tubes, and 100 μL of hydroxylamine hydrochloride solution was added and left for 5 min at 60 °C, after which 200 μL of development solution was added. Each vial was transferred to 1.5 mL polystyrene cuvettes and measured on a spectrophotometer at 500 nm. An aliquot of Milli-Q water was analysed in the same way to act as a spectrophotometry blank. The spectrophotometer used was a NanoDrop 2000c (Thermo Scientific) in cuvette mode with NanoDrop 2000/2000c (1.4.2) software. The UV absorption of the stock solution samples was compared to the absorption of the pure standard calibration curve and the concentration of AcP within the stock was confirmed as between 1.1 - 1.2 M each time the stock was made up.

2.4.3 Stability of acetyl phosphate

Solutions of AcP (300 mM) were prepared as in section 2.4.2 with either 20 mM magnesium or calcium ions ($MgCl_2$, $CaCl_2$) or no ions, and the pH adjusted to 7, 9 and 11 at 20 °C and 50 °C. Samples (500 μL) were taken at 2, 30, 60, 120 and 300 minutes and frozen at -80 °C. Samples were defrosted, centrifuged to remove

precipitated phosphates, 50 μL D_2O and 5.5 μL KHP (1 mM internal standard) were added and analysed using ^{1}H−NMR (Bruker Avance 300 Hz; 10 % D_2O, 8 scans, water suppression). Concentrations were calculated as in section 2.4.1. Later experiments were carried out adjusting the pH every 30 minutes to keep it constant. This did not make a significant difference to the concentration of AcP detected.

2.5 Protometabolic reactions with acetyl phosphate

2.5.1 Synthesis of adenosine

Solutions of adenine (2 mM) and AcP (780 mM) were prepared as in section 2.4.2 and the pH adjusted to 5, 7, 9 and 11 at 20 °C. D-ribose (used initially) or ribose-5-phosphate (2 mM; Sigma Aldrich) was added and samples (300 μL), taken at 0, 30, 60, 48 and 300 minutes and frozen at −80 °C. Controls were carried out parallel to experiments: R5P and adenine with AcP, and R5P with adenine (without AcP). The experiment was also run with the adenine at pH 11 and the ribose (10 μL) added drop-wise every 30 seconds.

Samples using ribose were analysed on Dionex HPLC, using a TELOS AT dC18 (100 x 4.6 mm) column, with mobile phases; A: 150 mM KH_2PO_4 and 150 mM KCl, B: 15 % v/v acetonitrile in phase A. Peaks for the desired products, adenosine and AMP, were identified by comparing to standards (Figure 2.12).

Quantification of samples using ribose-5-phosphate were performed using LC-MS (Waters Acquity LC with UV detector; Single Quad Waters MS in ESI mode; mobile phase gradient from HPLC water/0.1 % formic acid to acetonitrile over 5 minutes). Adenosine or adenosine monophosphate (AMP) were identified using retention time and fragmentation pattern of standards, and quantified using calibration curves. Electron ionisation mass spectrometry showed the molecular fragment 268.2 m/z for adenosine and 348.1 m/z for AMP. Uridine (245.2 m/z) was used as an external standard, and run at the same time as each repeat to account for variations in the machine.

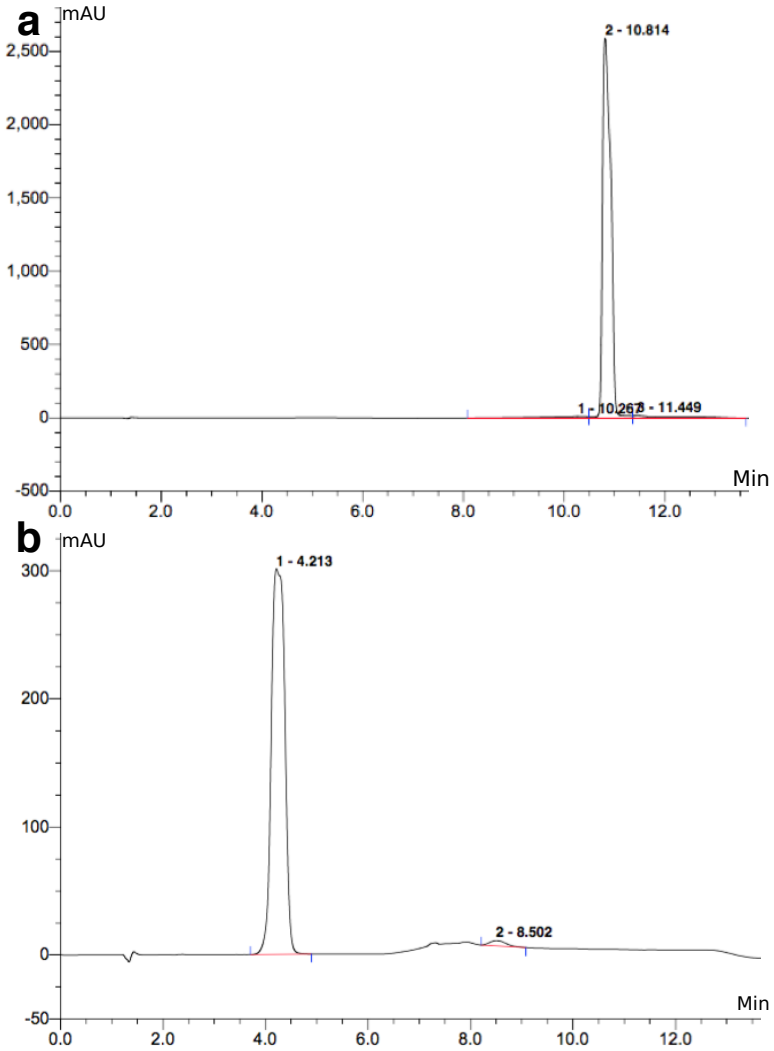

Figure 2.12. HPLC trace for standards of adenosine (2 mM) and AMP (500 μM) at pH 7. **(a)** Peak for adenosine seen at 10.8 minutes. **(b)** Peak for AMP seen at 4.2 minutes.

To see if AcP was breaking down to pyrophosphate, the results were analysed by phosphorous nuclear magnetic resonance (^{31}P−NMR). pH was also adjusted to ensure that it stayed stable throughout the duration of the reaction. A standard of potassium pyrophosphate, 1 mM and 0.1 mM (Sigma Aldrich), were used to test sensitivity of the NMR (Bruker Avance 400 Hz; 10 % D_2O, 24 scans, water suppression), methylphosphonic acid, 100 μM (Sigmas Aldrich) was used as an internal standard.

2.5.2 Phosphorylation of adenosine to AMP

Solutions of adenosine (2 mM; Sigma Aldrich) and AcP (800 mM) were prepared as in section 2.4.1 and the pH adjusted to 7, 9 and 11 at 20 °C. Samples (500 μL) were taken at 0, 1, 5, 24, 48 and 144 hours, diluted to 1 mL with Milli-Q water and frozen at −80 °C. Samples were analysed on a Dionex HPLC, using a TELOS AT dC18 (100 x 4.6 mm) column, with mobile phases; A: 150 mM KH_2PO_4 and 150 mM KCl, B: 15 % v/v acetonitrile in phase A. Peaks were identified using pure standards and spiked samples (Figure 2.13), and quantified using standard calibration curves (Figure 2.14).

This phosphorylation was also conducted under anaerobic conditions (COY Inc. Grass Lake, MI), using low concentrations of Fe^{2+} or Mg^{2+}, as might be predicted in Hadean ocean concentrations (Keller et al., 2014), to see if they might act as catalysts for the reaction. To mixtures of the same concentrations of adenosine and AcP used in the previous experiments, 200 μM $FeCl_2$ or 2, 20, 100 and 200 mM $MgCl_2$ were added to the reaction. Samples were taken at the same time points as in the aerobic experiments, at pH 7 and 20 °C .

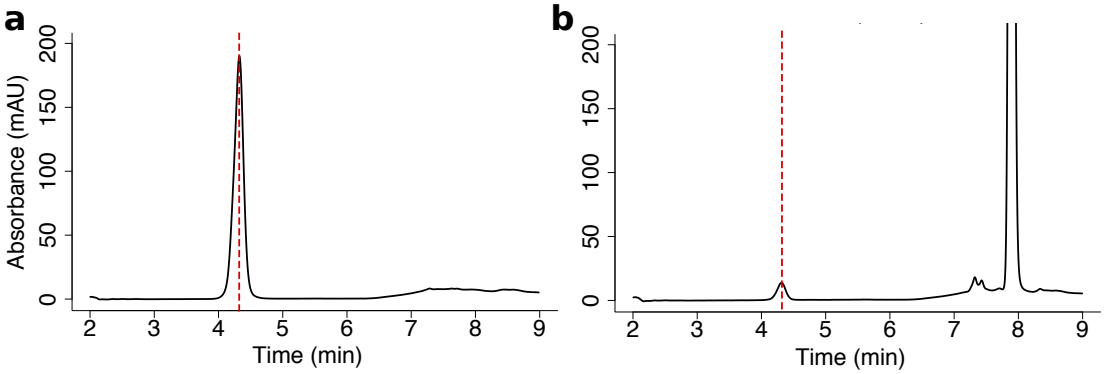

Figure 2.13. HPLC trace for detection of AMP at 4.3 minutes at 254 nm UV wavelength; **(a)** standard and **(b)** experimental sample. The red line shows the peak for AMP, and the large peak at 7.9 min is adenosine.

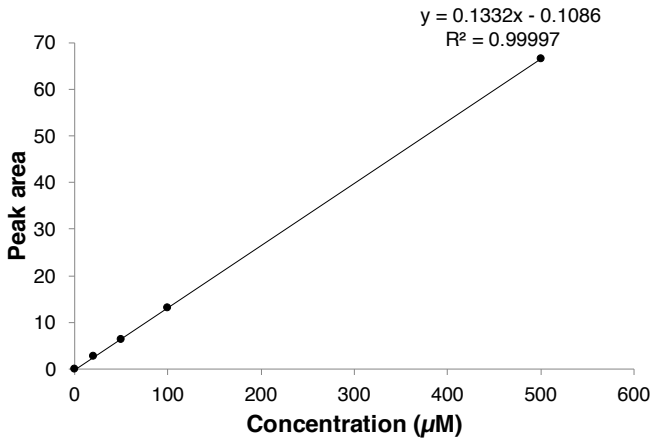

Figure 2.14. Calibration curve for AMP by HPLC.

Chapter 3

Alkaline hydrothermal Fe(Ni)S precipitate simulations

3.1 Introduction

The ocean and its composition plays a key role in the evolution of life. The first organic chemicals are likely to have been synthesised in aqueous solutions, as can be inferred from metabolism in extant life always occurring in aqueous environments. Nonetheless, the level of knowledge about the origin and evolution of the oceans, and what the conditions might have been like in the Hadean is poor. This is due to a sparse geological record for the Hadean period (4.6 - 4 Ga), resulting from intense tectonic activity and/or meteorite bombardment on the young Earth (Pinti, 2005).

Due to the tectonic activity on the young Earth (Pinti, 2005) there is a difficulty in interpreting geochemical proxies. For example there have been attempts to estimate the temperature of the early oceans using the ratio of stable isotopes of oxygen-18 (^{18}O) and oxygen-16 (^{16}O), which is expressed as δ^{18}O, measured in ancient cherts. The $\delta^{18}O_{rock-water}$ in cherts decreases as the temperature of the oceans increases, due to isotopic fractionation during precipitation of silica in the ocean. This means that isotopic values recorded from cherts of different ages can give an estimated measure of oceanic temperature at any given time. In the Archaean (4 - 2.5 Ga) this has been estimated at $\sim$50 °C warmer

than today by some authors (Knauth and Lowe, 2003). However, there is much contention over these high temperatures and the use of these isotopes. It seems that most of the silica gel precipitated was from hydrothermal fluids, therefore the temperature curve produced for the early oceans may reflect the temperature of hot hydrothermal flows rather than ambient seawater (Pinti, 2005). Blake et al. (2010) and Jaffrés et al. (2007) predict much lower temperatures, between 10 °C to 30 °C, after combining oxygen and hydrogen isotope ratios of cherts, along with oxygen isotope ratios of dissolved inorganic phosphate, as mentioned in Chapter 1.2.2.

The primitive oceans, just like modern oceans, would have been in equilibrium with the atmosphere, which, as the low temperature weathering rates attest, had high levels of CO_2 (Sleep et al., 2001; Jaffrés et al., 2007; Trail et al., 2011). Therefore the pH of the oceans would have been relatively acidic (pH 5 - 7), as high levels of dissolved CO_2 increase ocean acidity (Nisbet and Sleep, 2001). Due to this acidity of the oceans high concentrations of dissolved ferrous iron would have been available, derived from the black smokers (Cairns-Smith et al., 1992), as evidenced by the precipitation of banded iron formations (BIF) at the start of the Proterozoic Era (Holland, 2002; Pinti, 2005; Holland, 2009; Sleep et al., 2011). In an alkaline, oxygenated ocean, as we see today, Fe^{3+} is precipitated as iron hydroxides, $Fe(OH)_3$. In anoxic and acidic oceans Fe^{2+} is soluble in water. The BIF show that once the iron is oxidised, such as by organisms in oxidative phosphorylation and during the Great Oxidation Event (which occurred between 2.2 -2.4 Ga), it precipitates out as $Fe(OH)_3$. Therefore the BIF in the Archaean and Proterozoic clearly indicate a high level of dissolved iron on the early Earth, with a more acidic and anoxic ocean (Holland, 2002; Pinti, 2005).

de Ronde et al. (1997) found that by looking at fluid inclusions from 3.2 billion year old ironstone pods from South Africa, a prediction of Archaean ocean composition could be made. They found that the Archaean seawater chemistry may not have differed that much from today, except for ratios of calcium, strontium and ammonia, which were likely to be higher in concentration, along with higher salinity and lower sulphate (de Ronde et al., 1997). There is,

however, much debate around whether using inclusions to infer water chemistry is plausible on the basis that they may not be water or gas tight.

There is some debate over the supply of fixed nitrogen for the first life. Nitrogen is an essential element for all life, but it is locked in the kinetically stable form, N_2, in the Earth's atmosphere. Today there are nitrogen fixing organisms, however, how was it fixed on the early Earth before these nitrogen fixing organisms evolved? Some suggest the vents could have supplied fixed nitrogen in the form of ammonia, NH_3, (Martin and Russell, 2007), in the absence of O_2 in the oceans, NH_3 could have been the dominant fixed nitrogen species (Boyd, 2001). Others suggest nitrogen could have been fixed abiotically during lightning discharge, volcanism and meteorite impacts, as nitric oxide, and then subsequently photochemically converted to nitrate and nitrite in the atmosphere and rained into the oceans (Navarro-Gonzalez et al., 2001; Ducluzeau et al., 2009).

As mentioned in Chapter 1.4.1, high concentrations of bisulphide ions would have reacted with the dissolved iron in the oceans and precipitated out FeS within the vent, forming minerals such as mackinawite, and possibly greigite. Greigite may also have been produced by the oxidation of FeS in the presence of organics. Wang et al. (2015) show that freshly precipitated FeS can be selectively oxidised to form greigite in the presence of α-oxo acids, providing a possible pathway for the abiotic formation of greigite in nature. In the context of prebiotic evolution, greigite might have been sequestered by primordial peptides, and the whole finally evolved into the first iron-sulphur proteins with relevance to the acetyl-CoA pathway (discussed previously in Chapter 1.3.2).

Alkaline hydrothermal fluids would have been warm (25 - 125 °C), and have been predicted to be thermodynamically conducive to the synthesis of monomers and polymers needed for total cell biomass from H_2 and CO_2 (Amend and McCollom, 2009; Amend et al., 2013; Herschy et al., 2014). However, the reality is that H_2 and CO_2 do not react spontaneously, despite the favourable thermodynamics, because of a kinetic barrier to the first steps, due to a problem with the reduction potentials. Natural proton gradients across thin catalytic Fe(Ni)S barriers could theoretically lower the energetic barrier for the reduction of CO_2, promoting

organic synthesis (Lane, 2014; Yamaguchi et al., 2014). The problem is getting the reduction potential of the $H_2/2H^+$ couple to be lower than the CO_2/CH_2O couple, to enable the reduction of CO_2 (Lane and Martin, 2012; Lane, 2014). A pH dependance for redox reactions is true of both H_2 and CO_2, and at any particular pH the reduction remains difficult. Alkaline hydrothermal vents offer a structural solution to this problem; H_2 is dissolved in the hydrothermal fluids, at pH 10, whereas CO_2 is dissolved in the oceans, at pH 6. This sharp difference should mean that the reduction potential of both species is sufficient to drive the reduction of CO_2 (Figure 3.1a-b). This unique situation, where we have fluids at very different pH across a thin semi-conducting, catalytic Fe(Ni)S barrier, should theoretically enable the reduction of CO_2 to CO, $CHOO^-$ and CH_2O by H_2 (Figure 3.1c) (Herschy et al., 2014).

Iron is very important in this system; if ferrous iron in iron sulphide (FeS) minerals pass electrons onto CO_2, ferric iron is produced. The H_2 then reduces the ferric iron back to ferrous iron, resulting in the FeS cluster remaining ultimately unchanged, acting as a catalyst (Equation 3.1.1, where the arrows refer to the flow of electrons from to and from the different Fe ions):

$$H_2 \rightarrow Fe^{3+} \rightleftarrows Fe^{2+} \rightarrow CO_2 \tag{3.1.1}$$

This is analogous to ferredoxin or the energy reducing hydrogenase (Ech) in methanogens and acetogens today. Another key point is the reduction potential of the FeS minerals, such as mackinawite, which is dependant on pH. Mackinawite will protonate with a pKa $\sim$7, therefore there should be a tendency to transfer electrons across the mineral wall from the alkaline to the acid (protonated) side, making this an even better catalyst in these conditions (Figure 3.1c) (Lane, 2014; Herschy et al., 2014).

The important structure in this situation is the thin barrier, containing Fe(Ni)S semi-conducting clusters, which forms as part of the microporous vent structure. The aim of this study was to model the internal catalytic barriers within this microporous structure, recreate the redox gradients and experiment-

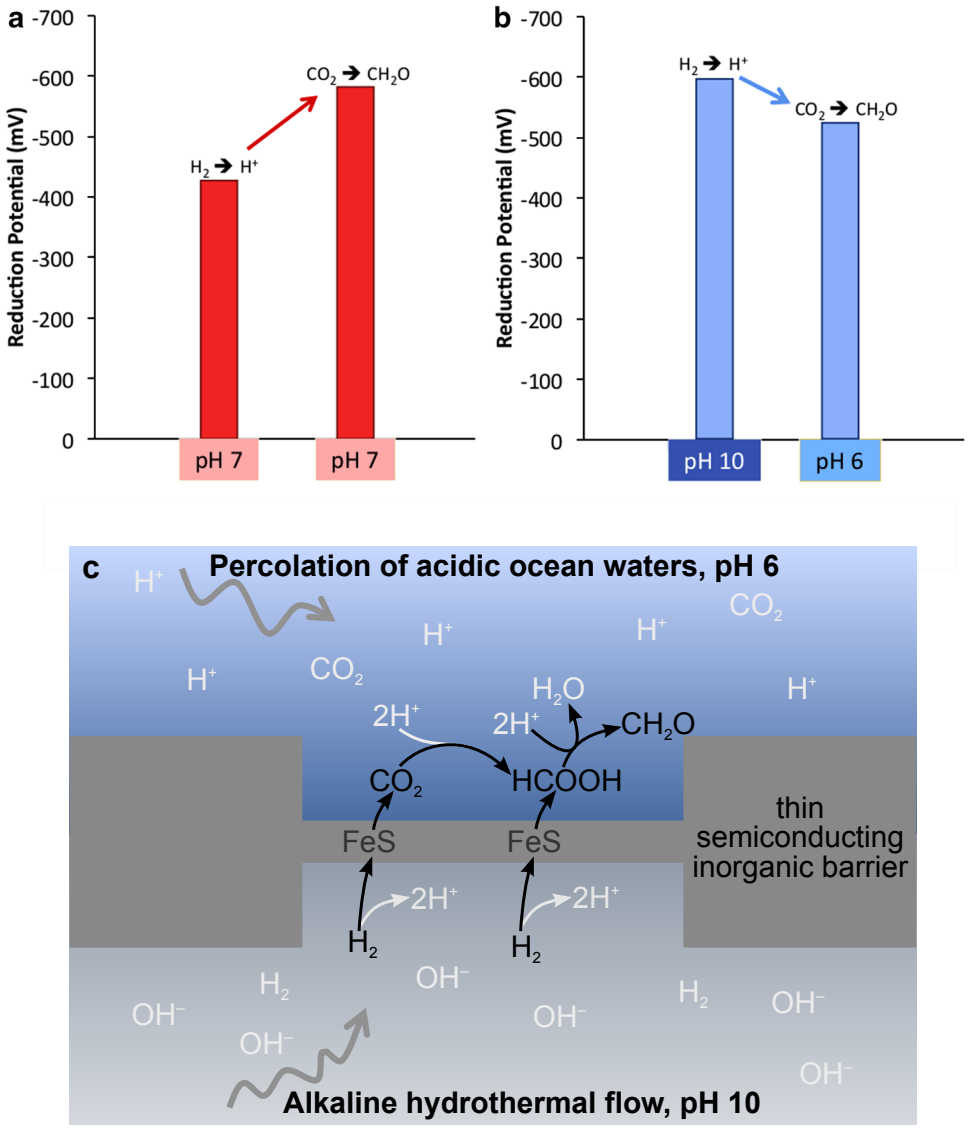

Figure 3.1. Reduction potentials in different pH and geochemical settings. **(a)** Standard reduction potentials of H_2 and CO_2 couples at pH 7. In this situation the transfer of electrons is unfavourable as the reduction potential for the CO_2/CH_2O at this pH is lower (more negative) than H_2/H^+. **(b)** In a situation where H_2 is dissolved in fluids at pH 10, and CO_2 dissolved in fluids at pH 6, the reduction potential for CO_2 becomes higher (more positive) than H_2, making the reduction of CO_2 favourable. **(c)** A simple depiction of how acid and alkaline fluids could be in such close contact inside an alkaline hydrothermal vent, with a thin semi-conducting FeS barrier transecting the pH gradient, leading to the reduction potentials in (b), and the subsequent reduction of CO_2 to formaldehyde via formate. Modified from from Herschy et al. (2014) and Sojo et al. (2016).

ally investigate the reduction of CO_2 by H_2. A simple bench-top reactor was designed, built and operated in an anaerobic hood, in order to simulate conditions in alkaline hydrothermal vents and test if these conditions could drive the

origins of biochemistry. Previous experiments have looked at simulating alkaline hydrothermal precipitates (Mielke et al., 2010, 2011; Barge et al., 2012), however, not for the investigation of CO_2 reduction. The majority of these studies were focused on the electrical properties of the FeS barriers they were producing, using the pH gradient to synthesise pyrophosphate and not for the reduction of CO_2 by H_2, as an electron donor for the synthesis of organics. The FeS walls in these earlier studies were therefore robust structures capable of holding a charge over periods of hours. In contrast, in this study the interest was in dissipating the charge, by transferring it across the barrier onto CO_2, so deliberately aiming to make dynamic structures and facilitate mixing, a very different objective to the previous work. That meant earlier studies were used as a starting point for the experiments, but not as the basis for the work. Many of these experiments also lacked H_2 altogether, using Fe^{2+} as an electron donor rather than a catalyst. In this investigation Fe^{2+} acts as a catalyst; being oxidised to Fe^{3+} but then reduced back to Fe^{2+} by H_2 (equation 3.1.1).

Concentrations used were thought to be plausible in the Hadean ocean, all be it at higher concentrations in these experiments to take into account the high pressure that is present at ocean depths of around 800 m. These high pressures at depth would have increased the concentrations of H_2, CO_2 and other gases dissolved within the alkaline and acid fluids, to a greater level than can be replicated in the laboratory at atmospheric pressure. For this reason concentrations of reactants were increased and yields were predicted to be low.

3.2 Iron sulphide precipitate formation

3.2.1 Structural considerations

When considering what structure the precipitate should form within the reactor, what was to be gained by forming them in the first place had to be considered; what was the experimental purpose of the precipitate structures? Overall, the aim was to achieve simulations of thin, semi-conducting barriers within the vent's microporous system, not the vent as a whole. The key property was to ensure

the walls of the tubes were thin enough to separate an alkaline compartment from an acidic compartment, with a thin semiconducting barrier that could hold an electrochemical potential between, but at the same time dissipate the build up of electrical potential to enable the continued transfer of electrons. The aim was the keep the situation in disequilibrium, hence the need for continuous flow of fluids on either side of the semi-conducting barrier, simulating the barriers explained in Figure 3.1c. Mixing is essential otherwise the transfer of electrons across the barrier would produce a charge on the barrier, which would oppose further transfer of electrons to CO_2. The method was not trying to replicate internal vent conditions exactly, but more to be a proof of concept that sharp pH gradients across semi-conducting barriers within alkaline vents could lend themselves to the abiotic reduction of CO_2 via the mediation of effective electron transfer.

Differing combinations of chemicals and their concentrations were tested in 50 mL falcon tubes to discover which combinations produced thin-walled tubular structures that were still stable enough to stand, which was considered an ideal precipitate (Figure 3.2). Alkaline fluid was injected at differing speeds into the base of the falcon tubes filled with acid fluid. The components chosen were used in previous literature on hydrothermal vent precipitate formation in laboratory conditions (Mielke et al., 2011; Barge et al., 2012). The concentration of those components was then chosen based on trial and error in producing stable but also thin and dynamic precipitate structures. The main components, iron, silica and phosphate, would all have been present in the Hadean ocean, however actual concentrations where not considered of importance in this instance, as the aim was to produce stable, thin precipitate structures, rather than model the Hadean conditions exactly. Concentrations used had to be high enough in order to form detectable quantities of products, without the effect of high pressure, and on timescales sufficient for laboratory experimentation. Temperature and pH of the alkaline fluid was based on conditions found in alkaline hydrothermal fluids today at Lost City (Kelley et al., 2001, 2005), and the acid fluid was based on conditions thought to be present in the oceans in the Hadean (Henderson-

Sellers and Henderson-Sellers, 1988; Russell et al., 1989; Martin and Russell, 2007; Russell et al., 2010).

These trials showed that with insufficient concentrations of silicate or phosphate the structures were not stable enough to withstand higher inflow rates, and the FeS would break up into a fine suspension as it precipitated. On the other hand, if the silicate or phosphate concentrations were too high, the precipitates would be too thick and solid. If there was insufficient sulphide concentration FeS would not precipitate at all, and the structures would be white or colourless.

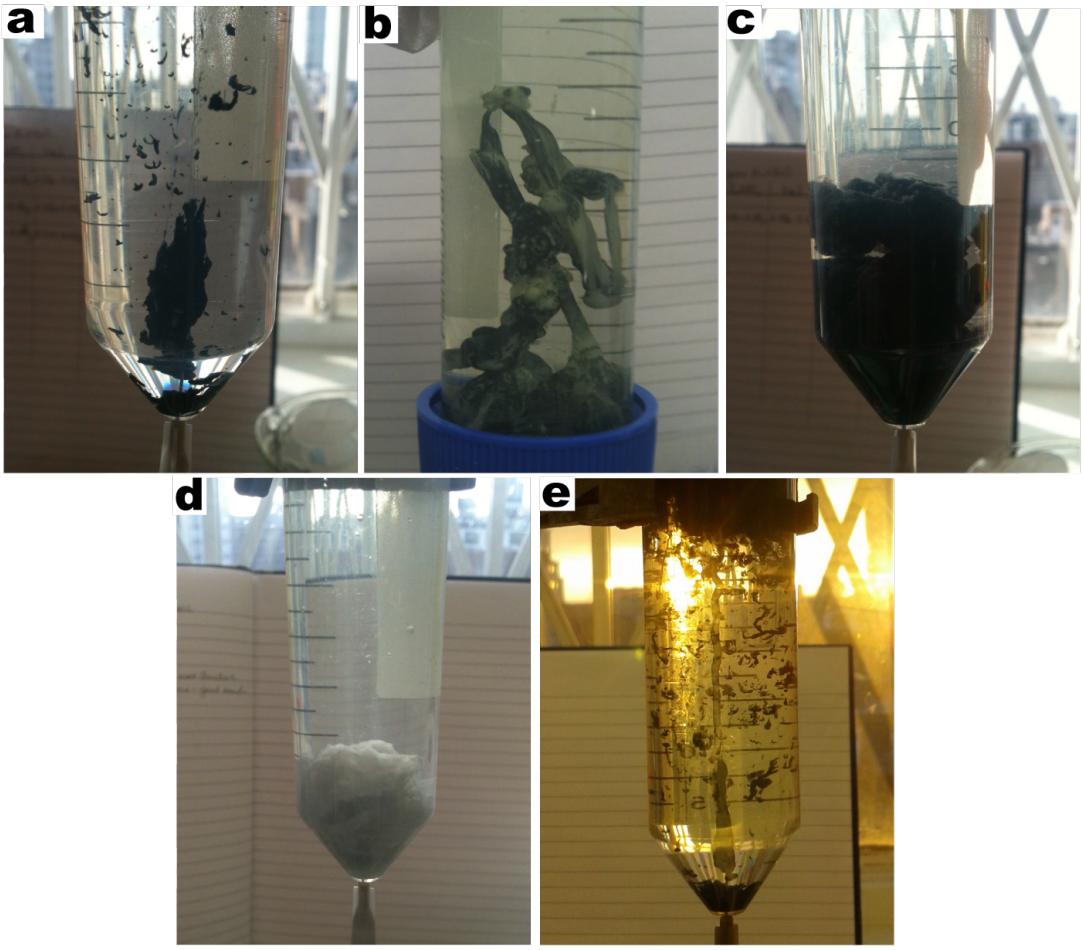

Figure 3.2. FeS precipitate trials in falcon tubes. **(a)** Good vent structure, however too thick so therefore the precipitate remains in the bottom of the tube. **(b)** Very thick and solid precipitate formed when concentrations of silicate and phosphate are too high. **(c)** High concentration of silicate inhibits the precipitate from rising to the surface. **(d)** White precipitate, insufficient concentration of sulphide, therefore no FeS is produced. **(e)** Ideal precipitate, very thin and membranous, but stable enough for a tube to rise upwards.

3.2.2 Large reactor experiments

Once a suitable precipitate was formed within the Falcon tubes, the same concentrations were investigated within the large bench-top reactor. Vertical tube-like structures formed as FeS and iron silicate (FeSi) started to precipitate around the alkaline fluid rising out of the flow distributor. A number of different conditions and concentrations within the acid and alkaline fluid were tested within the reactor, as the change in flow dynamics altered the structures of the precipitates from the falcon tube experiments. Structures varied hugely depending on the composition, concentration, speed and inflow temperature of the alkaline fluids. Even with similar composition and concentration, structures varied considerably. Ideal precipitates were stable enough to rise and sustain a vertical tubular structure, at the same time maintaining very thin membranous walls (Figure 3.3). Precipitates that did not form as required were due to either silicate levels being insufficient to sustain a good structure (less than 100 mM does not gel the iron sulphides together and they form as separate globules), inflow temperature too high (over 80 °C), flow rate too fast (over 50 mL/h), or insufficient sulphide (10 mM) to form FeS minerals within the precipitate (Figure 3.4). If the temperature was too high the silicate becomes less viscous and so the precipitates do not form as solid formations. If the flow rate was too fast then the formations start to break up and do not form a continuous structure. After around 30 minutes all precipitates stopped rising, collapsed and started to flow out of the side ports in the distributor (Figure 3.5), which could have been due to the precipitate blocking the holes in the top of the flow distributor where the precipitates originally formed, leaving the side ports as the only exit points for the precipitate. There were no detectable differences in conductivity, pH or temperature after the precipitates had collapsed, therefore it can be deduced that this collapse in formation was related to the flow dynamics within the flow distributor, not the surrounding fluid conditions. Samples of the precipitate once it had stopped rising were collected for structural analysis.

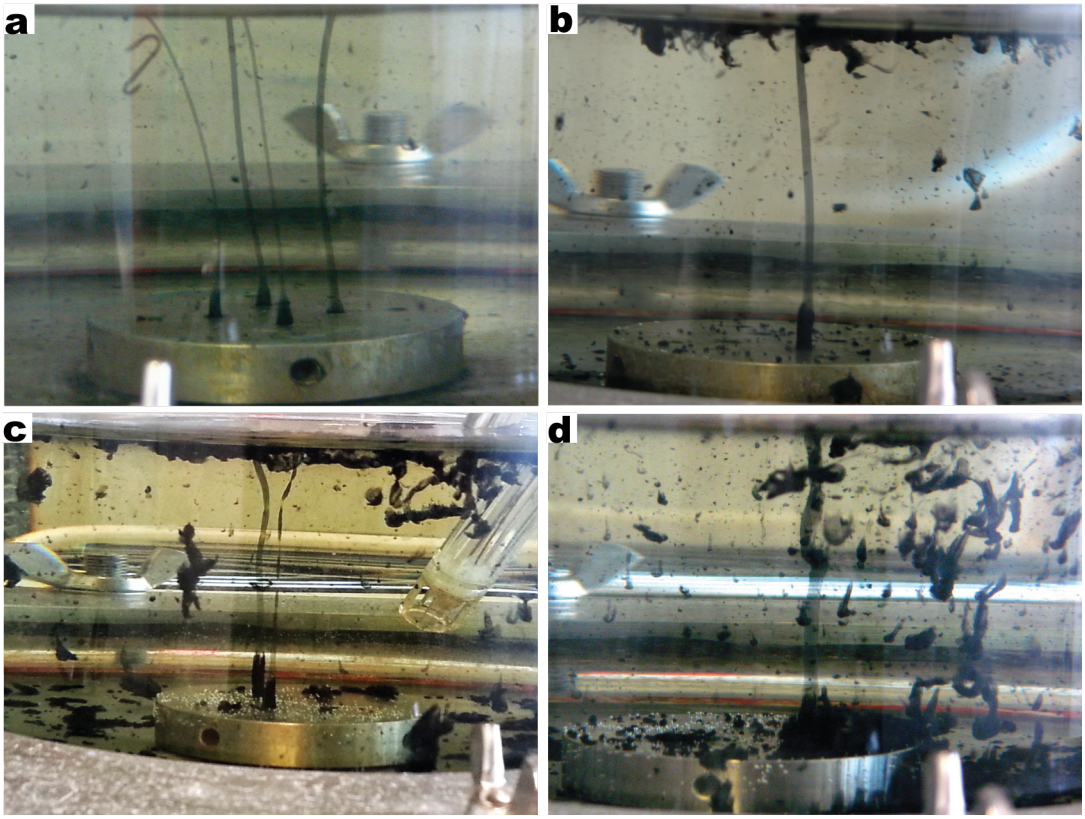

Figure 3.3. Photographs of examples of good precipitate formation in the large reactor. Formed as alkaline fluid was pumped up into the acidic reservoir, through a distributor with 2 mm holes. Conditions and composition were perfected to allow stable, thin tubular structures. **(a)** Thin, tubular structures forming, slight thickening at the base. **(b)** Only one tube precipitated, possibly other holes were blocked and prevented more tubes forming. **(c)** Thin, tubular structure but less smooth in precipitation (globular). **(d)** Again more globular precipitate, but still thin and tubular.

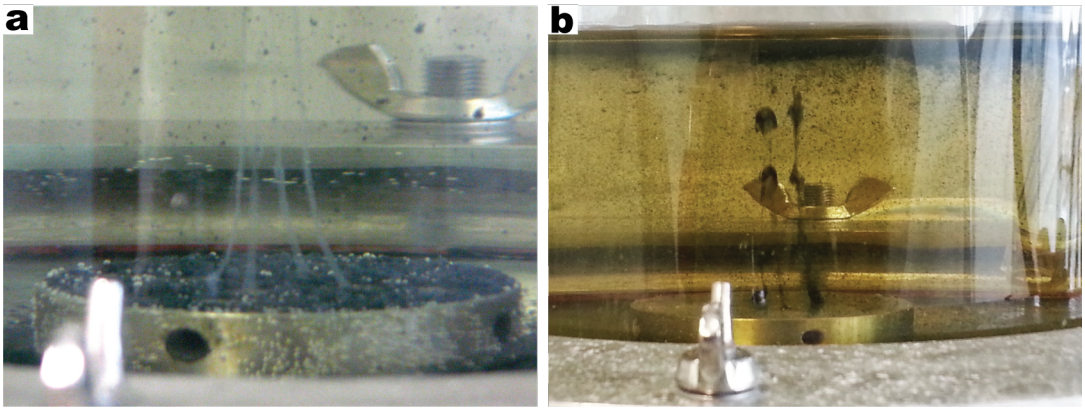

Figure 3.4. Photographs of unstable or unsuitable precipitate formation in the large reactor. **(a)** Insufficient concentrations of Na_2S to create FeS minerals in the precipitate (less than 10 mM). **(b)** Too fast a flow rate (over 50 mL/h), structures were disrupted and became globular instead of a smooth tube.

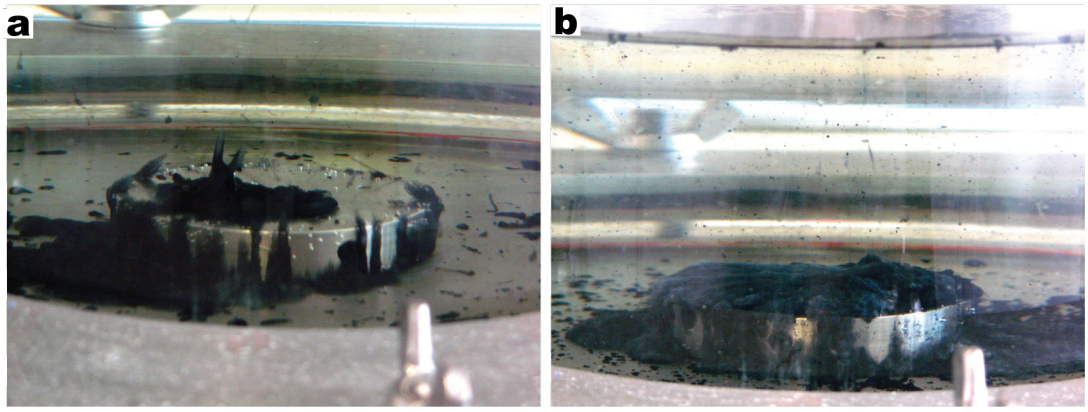

Figure 3.5. Photographs of collapsed precipitate formation in the large reactor. After around 30 minutes the precipitate stopped rising, sank and started to flow along the bottom of the reactor and out of the side ports in the distributor. This only happened in the large reactor, due to there being no side holes in the small distributor and the flow dynamics being different (larger area with more frequent, smaller holes).

3.2.3 Small reactor experiments

After the design of the small reactor, experiments were continued with this setup, following the same method and procedures as the large reactor. Initially precipitates did not form satisfactory tubular structures as in the larger reactor, due to changes in the flow dynamics. To overcome this, a 10-fold decrease in the silicate concentration was used, which meant that the concentrations of silicate, phosphate and sulphate were equal (10 mM). This enabled very stable precipitates to build up over time, producing thick tubular structures after a few hours. The differences between the large and small reactor are likely to be due to the different flow dynamics between the reactors, and the narrower holes in the distributor (1.6 mm) in the small reactor. The precipitates continued to form, over much longer periods than in the large reactor. They built up over a number of hours, up to 6 hours in some cases (Figure 3.6), however after 4 hours the precipitates started to thicken considerably, which probably inhibited any reduction across the barrier. If the precipitate is too thick then the pH gradient might not be maintained within such close proximity, which might stop the flow of electrons across the semi-conducting barrier. However, this was not fully understood as was discovered after later experiments discussed in Chapter 4. The ideal alkaline flow rate required to produce suitably thin, but also stable, structures was 50 mL/h,

allowing dynamic structures to form over several hours.

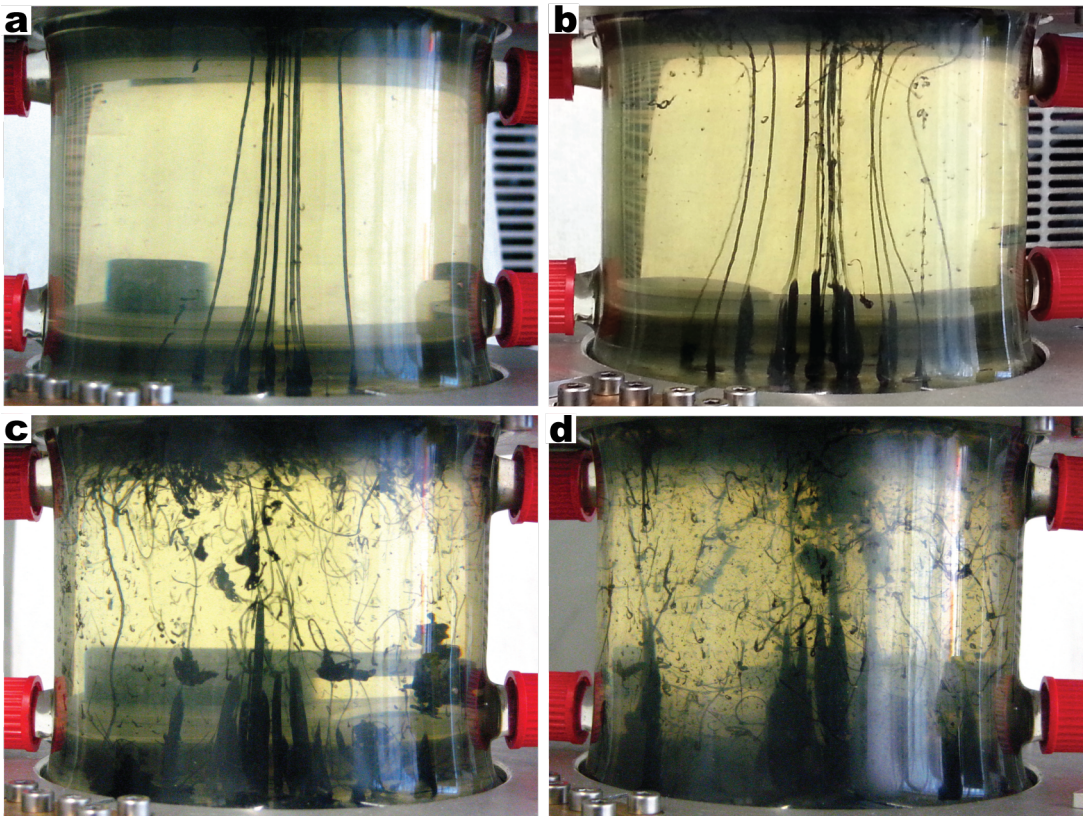

Figure 3.6. Series of photographs take of the precipitates formed inside the small reactor over 4 hours. (**a**) Initial formation of the precipitate structures 10 minutes after start. (**b**) After 30 minutes the structures continue to form, initiating from more holes in the distributor. (**c**) After 50 minutes precipitates are starting to thicken at the base and they start to sink as they hit the top of the reactor. They may also start to cool, which would make them less buoyant and consequently sink. (**d**) After 4 hours the precipitates are very thick, possibly inhibiting reduction across the barrier. However, Chapter 4 has data that may disprove this theory.

3.3 Compositional characterisation

3.3.1 Elemental analysis

Scanning electron microscopy (SEM) with energy-dispersive X-ray (EDX) elemental analysis of the precipitates from the large reactor showed structures consisting largely of iron, phosphate, silicon and oxygen, which were not homogeneous in composition (Figure 3.7 and 3.8). The large percentage of oxygen present is due to the oxidation states of the compounds, this is atomic oxygen, so there could have been hydroxides formed even if conditions kept strictly anoxic, green rust ($Fe(OH)_2$). The amount of atmospheric oxygen contact was kept to a minimum, but once they were placed on the plate for SEM analysis they were exposed to the atmosphere for at least 10 minutes. Regardless of their oxidation state there was only a small percentage of sulphur in these samples, even though the same concentration of NaS was added to the alkaline fluid as silicate and phosphate. This could be due to the sulphide oxidising to sulphate, which would then dissolve into solution. It was hoped the precipitate would be composed of FeS crystals, however the SEM data showed the majority of the precipitate was composed of iron oxides, silicates and phosphates, no sulphur was present.

Elemental analysis was conducted with transmission electron microscopy (TEM) on samples from the large and small reactors (Figure 3.9). Similar results were seen as in the SEM elemental analysis for the large reactor precipitate, with iron, silica and phosphate dominating the composition. No sulphur was seen in the sample from the large reactor; this was unexpected considering the precipitate was black, which implies the presence of FeS, but it is in agreement with the SEM results (which showed low S concentrations). The composition of the precipitate from the small reactor was slightly different, but more in line with what was anticipated; sulphur and iron dominated the composition, with less silica and phosphate. Elemental mapping confirmed that the iron and sulphur were located within the precipitate only, not in the surrounding space, showing that the Fe and S are definitely from the precipitate (Figure 3.10). TEM was found to be a more informative and accurate qualitative analysis than SEM for these precipitates.

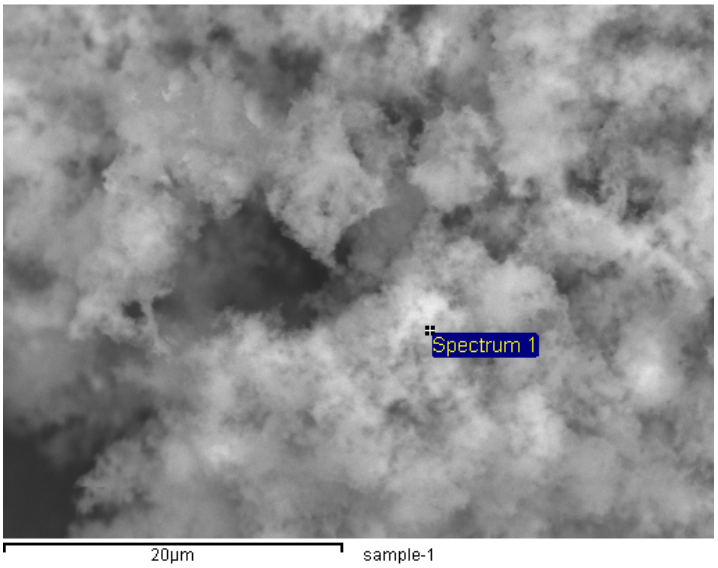

Element	Weight%	Atomic%
O	39.11	63.21
Si	2.71	2.49
P	17.34	14.47
S	1.00	0.81
Cl	1.72	1.25
K	0.56	0.37
Fe	37.56	17.39
Totals	100.00	

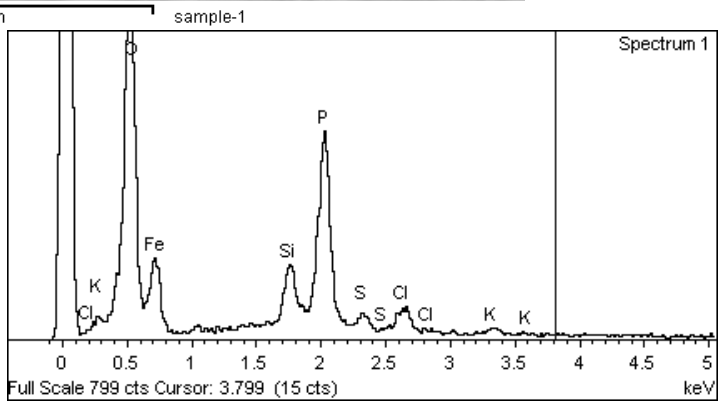

Figure 3.7. SEM-EDX elemental analysis; sample 1. Spectrum and percentage of elements and their percentage composition present in the precipitate from the large reactor. The spectrum shows the EDX analysis at the point shown on the image. A quantitative analysis was then performed by taking the area under the element curves to calculate atomic and weight percent for each element, this can also be converted into weight and atomic percentage. This section of the precipitate was composed mainly of Fe, P and Si, and a small amount of S (a much smaller percentage than the other elements).

3.3.2 Crystal identification

SEM images were taken of the precipitate powder (Figure 3.11). It was hard to tell if the precipitate was crystalline from SEM as the magnification and detail were not sufficient. Crystals of phosphate were seen in samples (Figure 3.11b) that had been left in the chamber for a few days before analysis, suggesting they crystallised out after precipitation as they were not seen in freshly analysed samples. For this reason, and the risk of oxidised ferrous sulfides, only freshly

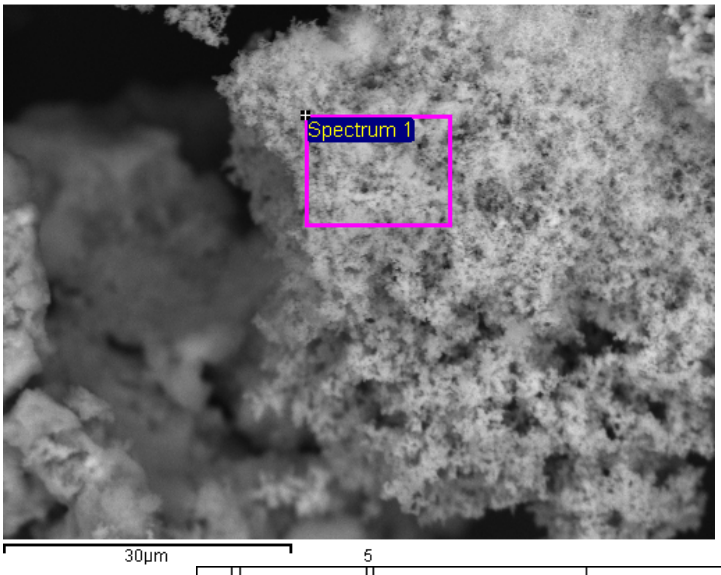

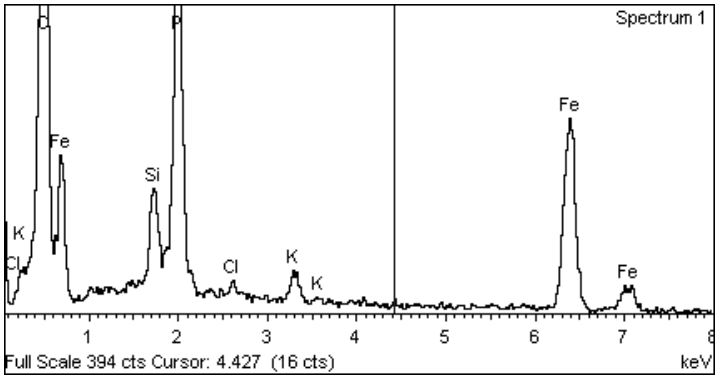

Element	Weight%	Atomic%
O	39.76	63.85
Si	2.51	2.30
P	18.74	15.54
Cl	0.38	0.28
K	1.35	0.89
Fe	37.26	17.14
Totals	100.00	

Figure 3.8. SEM-EDX elemental analysis; sample 2. Spectrum and percentage of elements and their percentage composition present in the precipitate from the large reactor. The spectrum shows the EDX analysis of the area in the box shown on the image. A quantitative analysis was then performed by taking the area under the element curves to calculate atomic and weight percent for each element, this can also be converted into compositional percentage. This section of the precipitate was composed mainly of Fe and P, less Si, and no S.

precipitated samples were analysed.

Samples from each reactor were analysed using powder X-ray diffraction (PXRD). Both were found to be amorphous, due to the absence of peaks in the spectra (Figure 3.12). The PXRD pattern for samples from the molybdenum source (Figure 3.12b) could have some similarity to results found by Bourdoiseau et al. (2008), where the spectrum was made of broad humps, characteristic of a nanocrystalline compound, however it was hard to tell if there are any peaks due to the noise in the spectra. According to recent studies this could

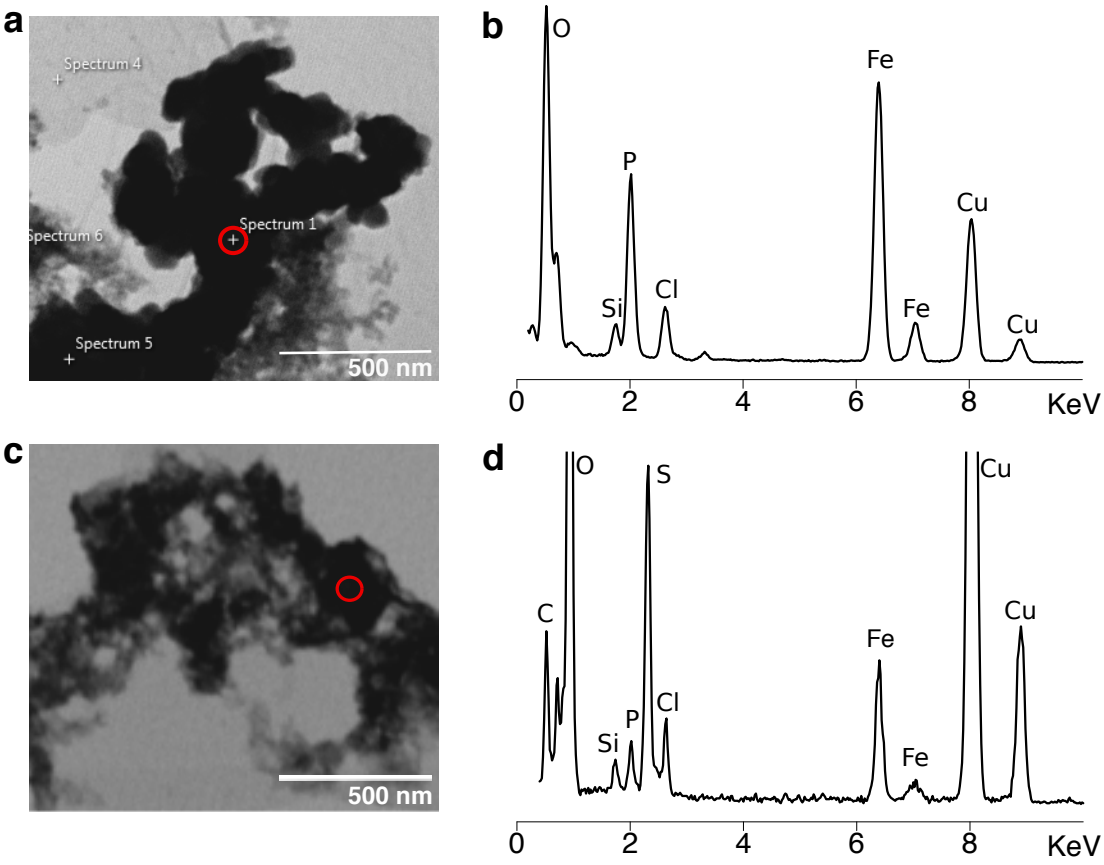

Figure 3.9. Differences in TEM-EDX for precipitates from the large and small reactor. **(a)** TEM image for precipitate from the large reactor, red circle indicates where EDX was taken from. **(b)** EDX spectra for precipitate in (a), no sulphur present. **(c)** TEM image for precipitate from small reactor, red circle indicates where EDX was taken from. **(d)** EDX spectra for precipitate in (c), sulphur present here, other elements in similar ratio as for (b), specifically Fe. Cu is detected from the grid used for supporting the precipitate. There could have been more of the grid showing in (d), hence the higher Cu signal.

indicate nanocrystalline, or disordered, mackinawite (Wolthers et al., 2005; Jeong et al., 2008; Bourdoiseau et al., 2008). This method of crystal detection was not adequate for the sample, due to the interaction between the iron and the radiation source producing flourescence, disguising any peaks that could be identified, even when the radiation source type was changed. Therefore this method for crystal detection was discarded.

TEM allowed a more in-depth investigation of the crystallinity of the precipitate. On examination of the early precipitates, the majority of the samples collected from the large reactor were composed of an iron silicate amorphous gel (Figure 3.13a - b), as confirmed by the EDX and PXRD analysis. In one section

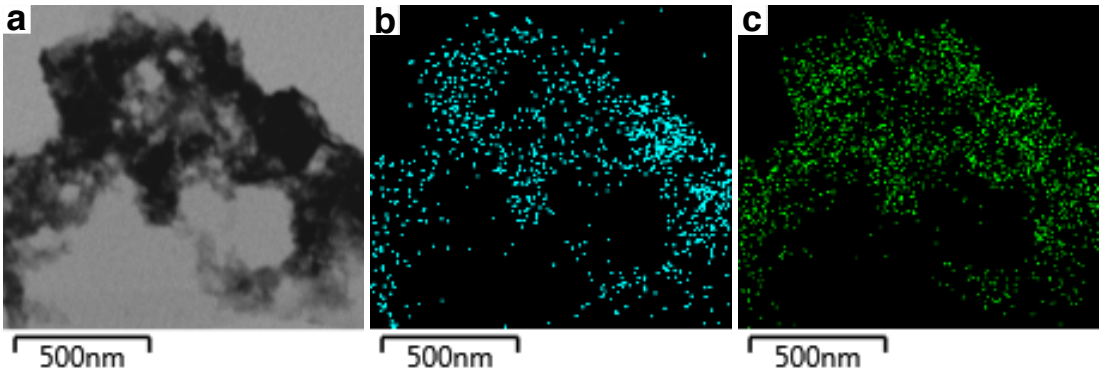

Figure 3.10. TEM elemental mapping of precipitate sample from the small reactor, showing that iron (Fe) and sulphur (S) were detected within the precipitate sample and not in the surrounding area. **(a)** TEM image of sample. **(b)** TEM elemental map for Fe. **(c)** TEM elemental map for S.

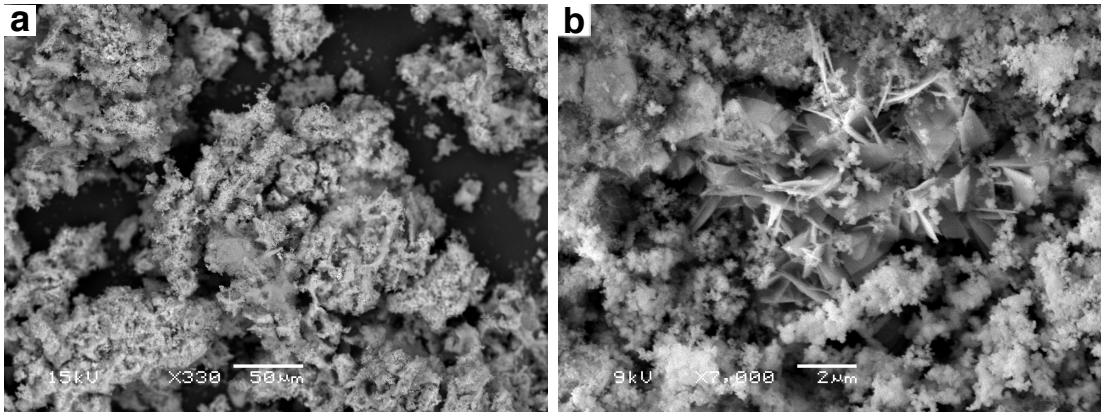

Figure 3.11. Scanning electron microscopy (SEM) images of the precipitate formed in the large reactor. **(a)** Iron sulphur or silicate structure; it is unclear whether it is crystalline or nanocrystalline. **(b)** A section of phosphate crystal crystallised after drying, while left in the anaerobic chamber, not during precipitation; not seen in freshly precipitated samples.

of the sample, small, individual nanocrystals were identified (Figure 3.13c - d). In the samples from the large reactor these crystalline sections were quite rare (only one section found within 6 sample plates). In later samples from the small reactor, however, all samples analysed had 100 % crystalline precipitate (Figure 3.14a-b), and individual atomic planes can be identified (Figure 3.14c-d), however, it can be observed that the overall structure is disordered and amorphous.

TEM allows the identification of atomic planes within individual crystals. These planes were identified within the nanocrystals of the precipitate. Single crystal atomic spacing was measured using a light intensity spectrum drawn

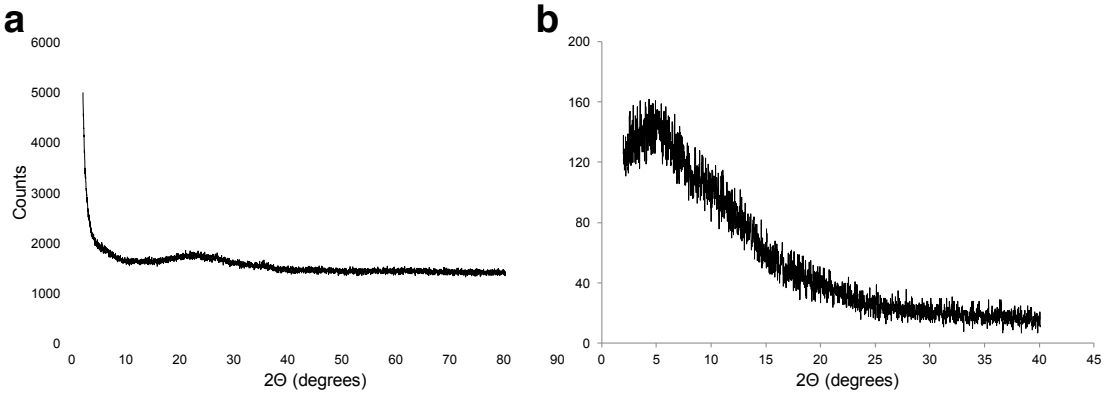

Figure 3.12. Powder x-ray diffraction (PXRD) scan of precipitate from the large and small reactors. The absence of peaks indicates that the both samples were amorphous, or possibly nanocrystalline, in composition. **(a)** Sample from the large reactor analysed by copper radiation source (50 kV and 30 mA). **(b)** Sample from the small reactor analysed by molybdenum radiation source (50 kV and 30 mA).

perpendicular to the space group orientation (Figure 3.15). To gain an average spacing for all the crystals observed in a single image a fast Fourier transform (FFT) spectrum was used to identify different spacings. Distances between different points on the image to the centre give the spacing for individual nanocrystals (Figure 3.16). In the three samples analysed 46 images were analysed by FFT, and spacings of 0.16, 0.2, 0.3, 0.5, and 0.7 nm, were found. The majority of the spacings measured were 0.3 nm and 0.5 nm. It was therefore inferred that the nanocrystals were likely to be disordered mackinawite, which has a tetragonal lattice system with cell unit parameters c = 0.5 nm and a = b = 0.3 nm (Figure 3.17), amorphous in overall structure, and is the first FeS mineral to be precipitated (Jeong et al., 2008). The measured spacing does not always represent the cell unit spacing of the crystal, due to differing orientations of the crystal and its angle to the beam, however, due to the high number of 0.3 and 0.5 nm spacings it can be inferred that the mineral being detected was most likely mackinawite. The 0.16, 0.2 and 0.7 nm observed spacings are most likely examples of the differing orientations of the crystals to the TEM electron beam, creating an artificially larger or smaller spacing.

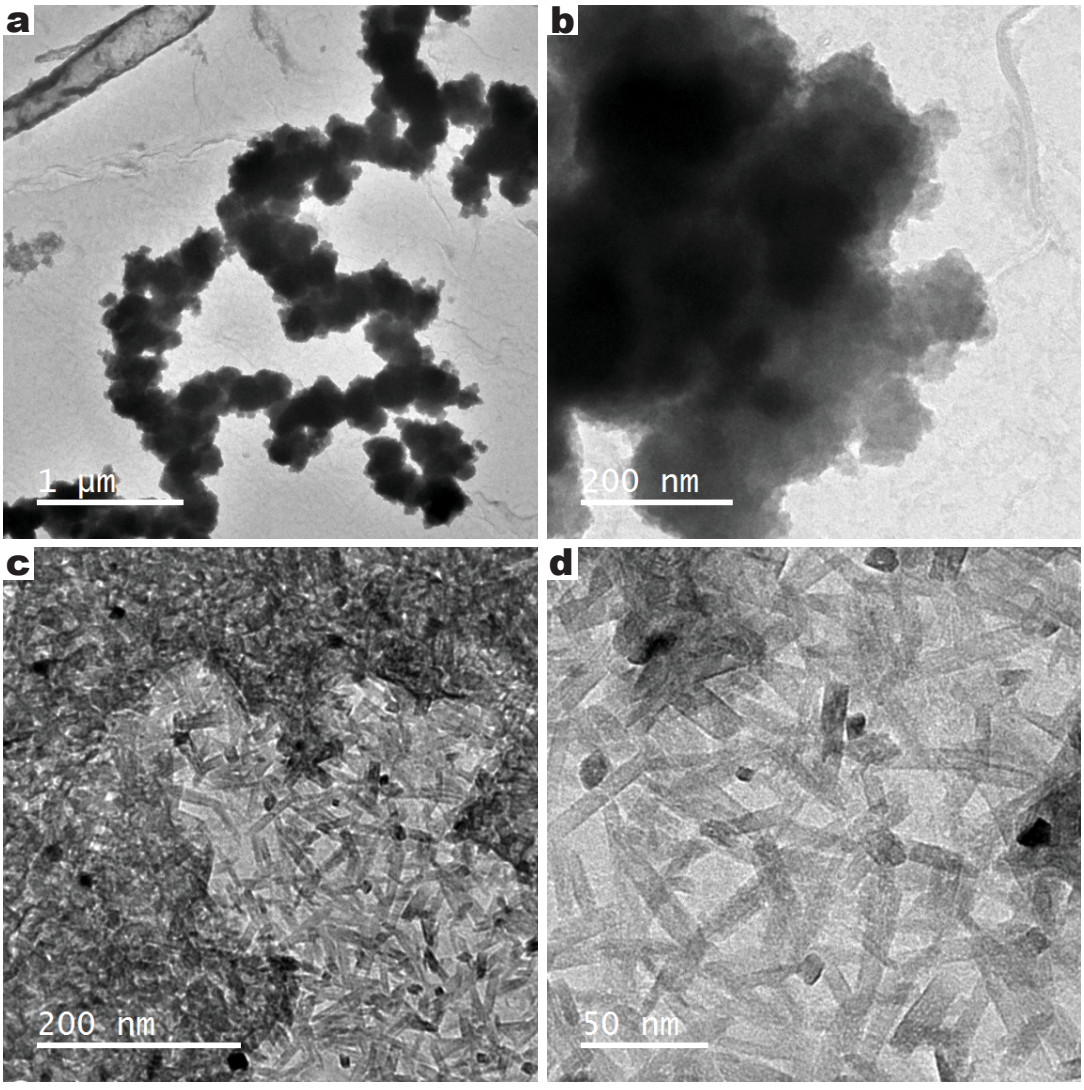

Figure 3.13. TEM images of precipitate from the large reactor. **(a)** Amorphous iron silicates. **(b)** 5x magnified section of (a). **(c)** Long, thin tetragonal FeS nanocrystals found in a portion of the precipitate. **(d)** 4x magnified section of (c).

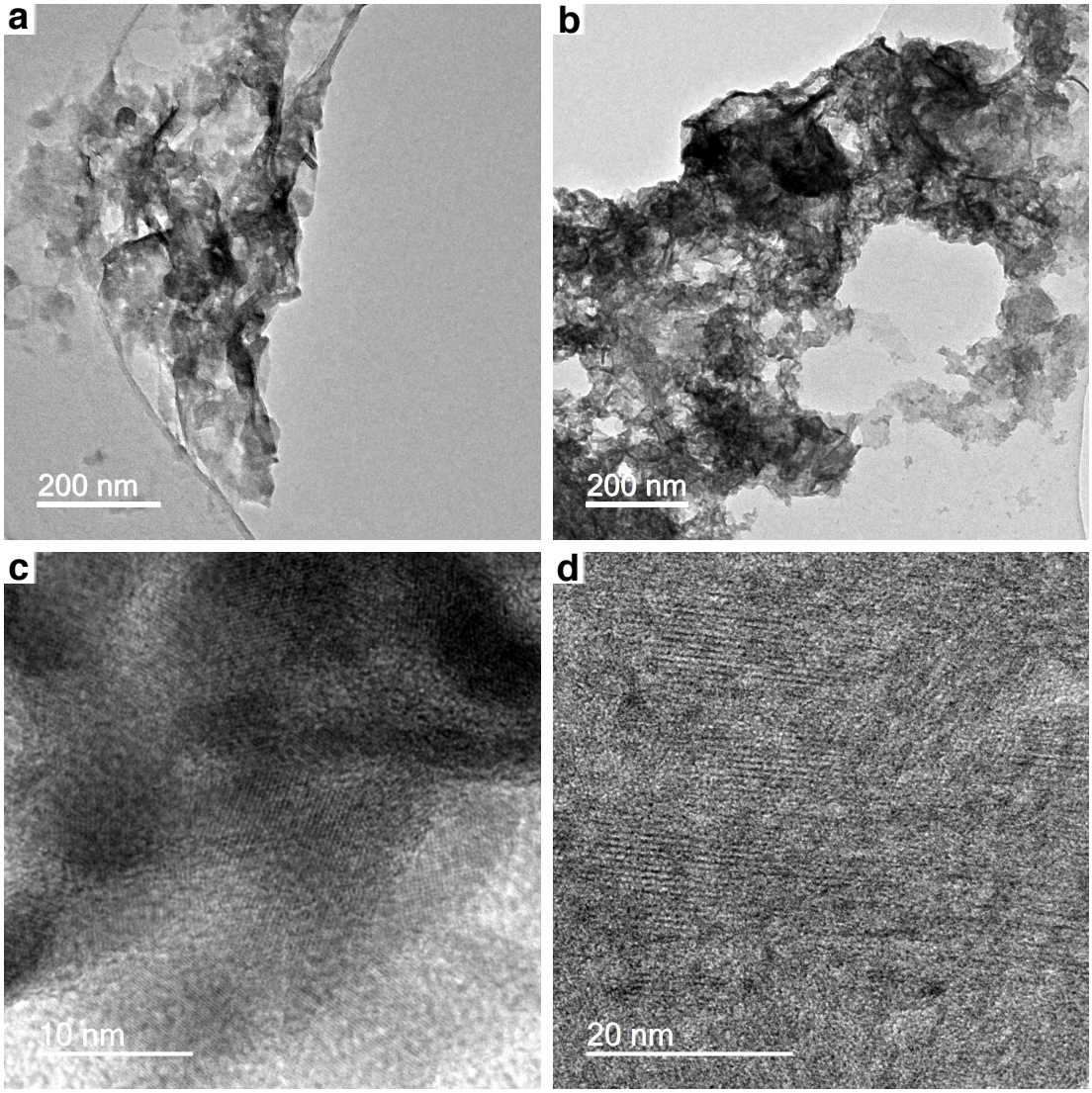

Figure 3.14. TEM images of precipitate from the small reactor. **(a - b)** Sections of nanocrystalline FeS precipitate. **(c - d)** Magnified section of precipitate. The atomic planes of the nanocrystals are visible in the overall disordered, amorphous structure.

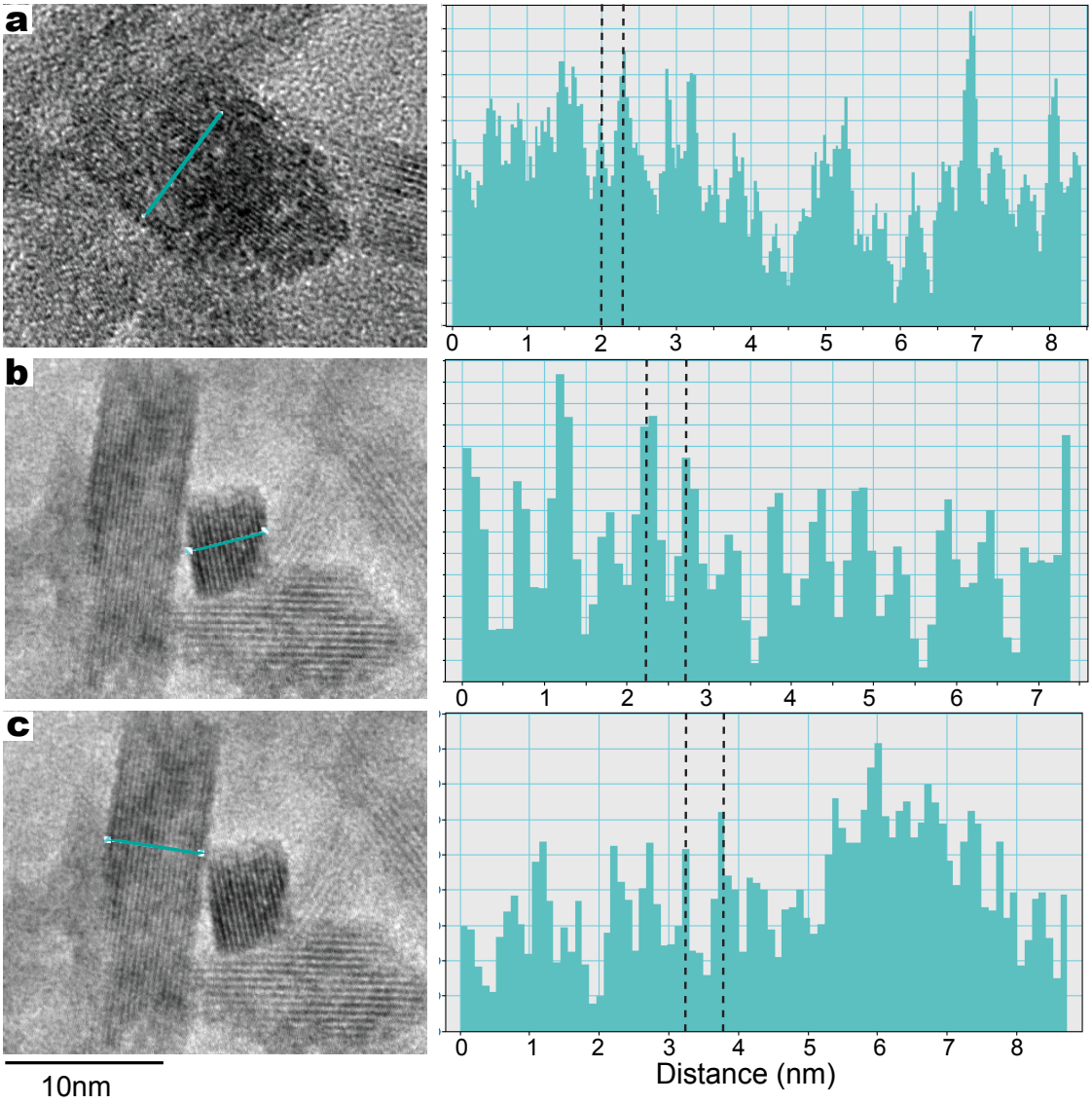

Figure 3.15. TEM images of disordered mackinawite nanocrystals. Atomic planes visible, measured using Gatan Digital Micrograph. The spectra show light intensity at a specific cross section of an individual nanocrystal (shown by line on the respective image), indicating the spacing between atomic planes. **(a)** An average atomic spacing of 0.3 nm was observed for this crystal **(b - c)** Nanocrystals with an average atomic spacing of 0.5 nm were observed in these samples.

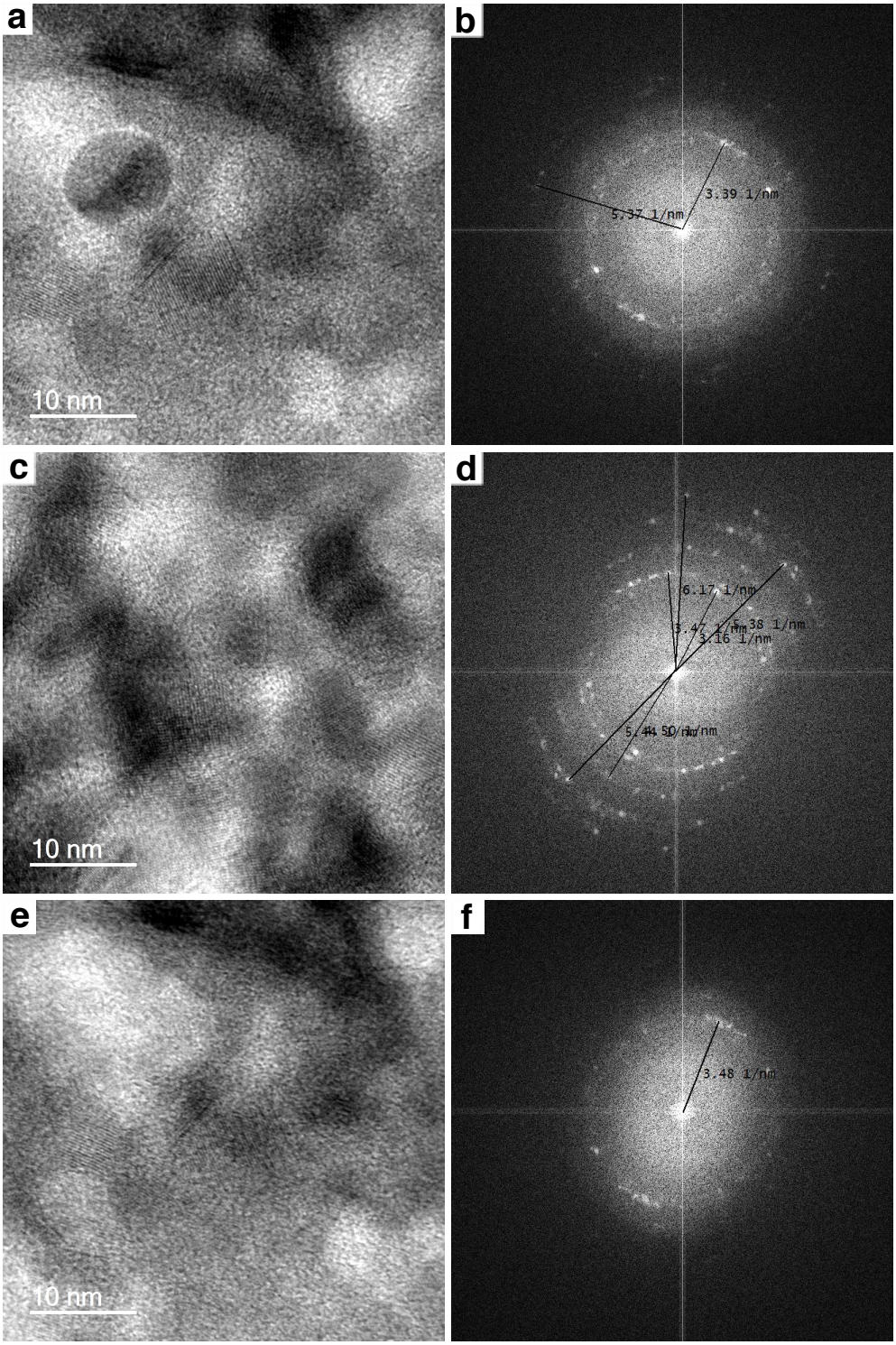

Figure 3.16. TEM images of disordered mackinawite nanocrystals, where atomic planes were measured using fast Fourier transform (FFT) for the average spacings of the whole image. Distances to points on the FFT image give the atomic spacing for individual nanocrystals; a point for each spacing measured which creates multiple rings for all the different atomic spacings in the section. **(a, c, e)** Images of nanocrystalline sections with atomic planes clearly visible in sections of the images. **(b, d, f)** Corresponding FFT images for the average spacings in the adjacent image. Distances of 0.5 and 0.3 nm were most commonly measured from the centre to different distance points in the FFT circles.

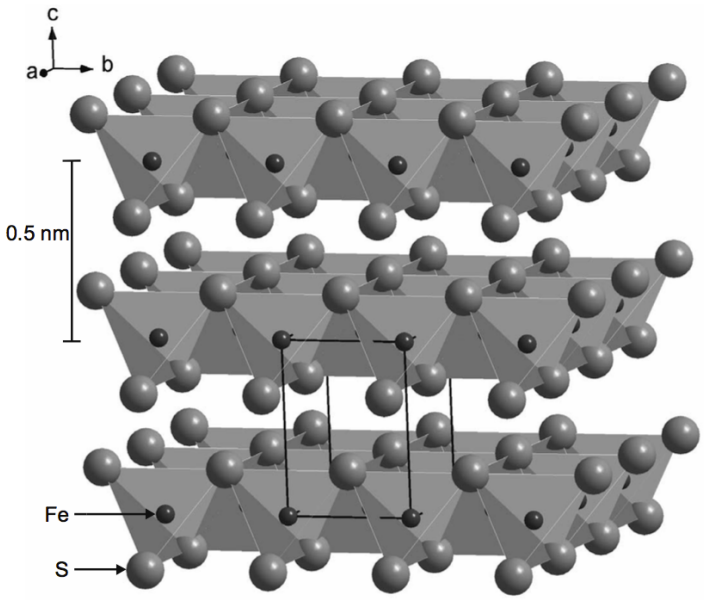

Figure 3.17. Schematic diagram of mackinawite structure. Viewed from ∼30 ° above the (001) plane, with the tetragonal unit cell indicated (Wolthers et al., 2005). The sheets of Fe atoms are separated by 0.5 nm, and are held together by weak Van der Waals bonding with the S atoms. Distance between Fe atoms within each sheet is 0.3 nm (c = 0.5 nm and a = b = 0.3 nm). Image taken from Wolthers et al. (2005) and Jeong et al. (2008).

3.4 Discussion

The alkaline precipitate structures in this investigation were developed and optimised to try and create the thinnest walled tubes possible, while at the same time maintaining vertical stability. Synthesis of these precipitates was accomplished after a sequence of trial experiments varying different chemical concentrations of the acid and alkali fluids and physical parameters in the large reactor. The sinking of the precipitates after 30 minutes was assumed to be due to the flow distributor having holes in the side, and when the holes in the top became blocked with precipitate the fluid started to flow out of the sides (path of least resistance). The faults in the large reactor, including the low surface area to volume of the tubes, were all taken into consideration to improve the design of the small reactor. The experiment was significantly improved within the small reactor, where the precipitate structures remained intact and stable, but at the same time dynamic (fluid remained flowing within the chimneys) for a number of hours. The flow distributor in the small reactor did not have holes in the side so the alkaline fluid could only flow out of the top. Overall, the small reactor was an improved design, overcoming many of the disadvantages of the larger reactor, and therefore produced precipitate structures with thinner walls (the distributor had smaller, and more frequent holes), while still stable enough to remain intact for a number of hours. The small reactor was also easier to sample from and had a reduced reservoir volume, decreasing the dilution effect a large reservoir would have on potential synthesised organics.

It was observed by elemental analysis that the precipitate composition from the large reactor contained almost undetectable levels of the element sulphur; this could be due to the sulphide oxidising to sulphate, which would then dissolve into solution. When the precipitates from the small reactor were analysed, a much higher concentration of sulphur was detected. This could be due to the improved methodology for the small reactor, which involved a reduction in the concentration of silicate and phosphate in the alkaline fluid, thereby increasing the sulphide ratio. Smaller holes allowed lower silicate and phosphate concentra-

tions which could have been more realistic to the natural environment (previous concentrations were extremely high) and also allowed more sulphur to be present in the ratio of elements, leading to more conductance. The differences between the precipitate formed in the large and small reactor could also be due to the sampling method. When using the large reactor the lid was usually left off and the amount of air (even though this was still anoxic conditions within the chamber) in contact with the experiment while it was in progress was significant. When using the small reactor the lid was always kept on, reducing the amount of anoxic air in contact with the fluids. Even though the levels of oxygen within the chamber should have been zero, there was a period when levels of H_2S were very high in the chamber, which started to corrode the electronics, and the oxygen detector became faulty. The monitor was replaced once this was discovered.

The nanocrystalline structure of the two different precipitates supports the idea that the sulphide might have oxidised to sulphate in the large reactor experiments. Most of the samples taken from the large reactor were seen to be amorphous which is likely to be iron silicate, only small sections were found to be nanocrystalline. On the other hand, in the small reactor all the samples analysed by TEM were nanocrystalline. This suggests that the conditions used in the small reactor and the concentrations of compounds in the alkaline fluid was conducive to the formation of iron sulphides as hoped.

The images for crystal sections and atomic spacing from the small reactor are not as high quality as the images from the large reactor; this could be due to the larger volume of crystals in the small reactor precipitate. The large reactor crystalline section was very small and not very thick, resulting in very high quality images of the crystals, not necessarily indicating a better quality crystalline precipitate.

The crystalline sections, identified by TEM atomic plane spacing measurements, were considered to be nanocrystalline mackinawite, which has a tetragonal lattice structure with cell unit parameters c = 0.5 nm, and a = b = 0.3 nm (Figure 3.17). At ambient temperatures, the most common phase for FeS is an amorphous or disordered, poorly crystalline precipitate (Wolthers et al., 2005).

This corresponds to the lack of highly crystalline material found with the X-ray diffraction, and the amorphous structures observed with TEM. Disordered mackinawite is the first FeS mineral to precipitate from sulphide and Fe^{2+} ions (Mullet et al., 2002), and nanocrystalline mackinawite is defined as the initial, less crystalline phase of mackinawite, which then develops into a crystalline form with ageing (Bourdoiseau et al., 2008). Greigite (Fe_3S_4) or pyrite (FeS_2) are then formed by the partial oxidation or heating of mackinawite (Lennie et al., 1997). If the time and availability had been present then Raman spectroscopy could also be used to look for precipitate composition.

The cubit cell unit of greigite (Fe_4S_4) has a very similar structure to the Fe(Ni)S centres found in thiocubane units of many enzymes and proteins today (see figure 1.2 in Chapter 1) (Russell and Hall, 1997). Ferredoxins are thought to be the most ancient of all biological catalysts, which store and transfer electrons (however, hard to prove), implicating mackinawite and greigite as possible catalysts in early non-biological systems (Eck and Dayhoff, 1966; Sousa et al., 2013; Wang et al., 2015). It was therefore anticipated that if thin enough precipitate walls could be formed within the reactor, they might be able to act like semiconducting barriers, containing catalytic FeS or Fe(Ni)S minerals. This should enable redox reactions to occur across the barrier, enabling the transfer of electrons from H_2, or Fe^{2+} alone, to CO_2 at higher redox potential (equation 3.1.1). H_2 maintains iron in the same oxidation state after it has reduced CO_2, thereby enabling the iron to act as a catalyst. If there were no H_2 the reaction could still take place with Fe^{2+} reducing CO_2, however, the mineral would become oxidised, thereby acting as the electron donor rather than a catalyst.

The precipitates formed within the small reactor looked, from the characterisations of structure, crystallinity and composition, to be ideal for the purpose intended; to investigate the ability of semi-conducting, FeS containing, inorganic barriers to facilitate the reduction of CO_2 by H_2 in a laboratory setting. The simplest way to test if these precipitates could accomplish these reductions was to analyse samples for small organics that might be produced around and within the precipitates. These experiments were carried out with the method for precipitates

formed here and the results shown in Chapter 4.

Chapter 4

Redox gradients and carbon reduction

4.1 Introduction

Adenosine triphosphate (ATP) drives energy metabolism in all extant life, and there are only two fundamental processes to its synthesis; substrate-level phosphorylation, via reactive acyl phosphates, and chemiosmotic coupling. The simplest, and arguably most ancient forms of both processes are found in methanogens (archaea) and acetogens (bacteria) (Lane and Martin, 2012; Martin et al., 2014). Both drive carbon and energy metabolism by reducing CO_2 with electrons from H_2, to form methane or acetate, via the acetyl-CoA pathway (Buckel and Thauer, 2013).

The most common form of substrate-level phosphorylation is glycolysis (Embden-Meyerhof-Parnas pathway), the metabolic pathway that converts glucose into pyruvate, and the energy that is released in this process is then used to synthesise high-energy compounds such as ATP and NADH (reduced nicotinamide adenine dinucleotide) (Ferry, 2006; Buckel and Thauer, 2013). Interestingly the glycolytic pathway is not universal among prokaryotes; archaeal glycolysis is similar in chemical steps to bacteria, but the enzymes responsible, especially in the upper C_6 steps (as opposed to the lower C_3 steps shared with gluconeogenesis) are phylogenetically distinct in bacteria and archaea. (Martin and Russell, 2003).

Chemiosmotic coupling on the other hand is universal across life. This mechanism is used by cells to harness energy using ion gradients; protons are pumped across a membrane to build up a proton concentration gradient, which in turn drives the synthesis of ATP, via the ATP synthase (Mitchell, 1961). As discussed in the introduction, not only does chemiosmotic coupling drive the synthesis of ATP, it also drives the reduction of CO_2 via the energy-converting hydrogenase (Ech). ATP synthase is universal and was likely present in LUCA, as was chemiosmotic coupling, but it is so complex it is hard to see how it could have arisen. Ech is not completely universal, especially in its carbon fixation role, however, it gives an insight into the origins of chemiosmotic coupling because it is fundamentally simple in comparison with the molecular complexity of the ATPase. Ech itself is relatively complex, but it is reducible conceptually to a membrane-bound FeS protein powered by the proton-motive force, which is again conceptually reduced to differences in redox potential across a membrane, as discussed in the previous chapter. Despite this evidence, the argument posed against chemiosmosis is still due to its use of complex proteins and enzymes; the ATP synthase and Ech. However, if we look at the simplest form of chemiosmotic coupling, the acetyl-CoA pathway, it has several properties that make it attractive as an ancient form of metabolism (Martin, 2012). It is a short, linear pathway, and is the only carbon-fixation pathway universal to both bacteria and archaea. It is deeply diverged in these two groups today (Fuchs, 2011), indicating that it evolved early in life's history. The acetyl-CoA pathway also has many properties that indicate it could have occurred abiotically, without the need for very complex proteins and enzymes. The chemistry that links acetogens and methanogens to each other, also links them to alkaline hydrothermal vents (Martin et al., 2014). Methanogens have the membrane-integral Ech which uses proton gradients to drive reduction of the FeS protein, ferredoxin, with H_2 to produce a methyl group (Buckel and Thauer, 2013). Proton gradients transected by thin inorganic catalytic barriers are also found naturally in hydrothermal vents, along with key ingredients for abiotic CO_2 reduction; H_2 and FeS clusters (Lane et al., 2010). Chemiosmotic coupling and the conditions needed for the acetyl-CoA pathway

are remarkably analogous, and arguably homologous, with these vent conditions.

For CO_2 reduction to take place conditions have to be thermodynamically favourable (Martin and Russell, 2007). The overall reduction of CO_2 by H_2 to CH_4, or even organics such as CH_3OH or CH_3COO^-, is exergonic, however, the initial steps present a kinetic barrier to the reaction. Methanogens use proton gradients with the help of FeS cofactors in the acetyl-CoA pathway to drive the reaction. In the geochemical pathway this reaction has a large thermodynamic barrier to overcome before any CO_2 can be reduced (Figure 4.1) (Maden, 2000). At neutral pH the reduction potential of CO_2 is not low enough compared to H_2 to allow its reduction to take place. Alkaline hydrothermal vents provide a potential solution to this problem by having a difference in pH on different sides of catalytic FeS barriers; acid on the side of CO_2 and alkaline on the side of H_2. This situation modulates the reduction potentials for each species to enable the reduction of CO_2, potentially an abiotic equivalent to the process in methanogens (Figure 3.1a-b, previously discussed in Chapter 3.1) (Lane, 2014). The Fe(Ni)S minerals within the barrier separating these two species act as a catalyst, transferring electrons from H_2 onto CO_2, via the oxidation of Fe^{2+} to Fe^{3+}, but remaining ultimately unchanged in the process due to the continued presence of H_2 returning the Fe^{3+} back to Fe^{2+} (Figure 3.1c). This combination of catalytic Fe(Ni)S minerals with natural proton gradients could have provided the crucial redox chemistry needed to drive primordial carbon and energy metabolism (Cody, 2004; Lane and Martin, 2012).

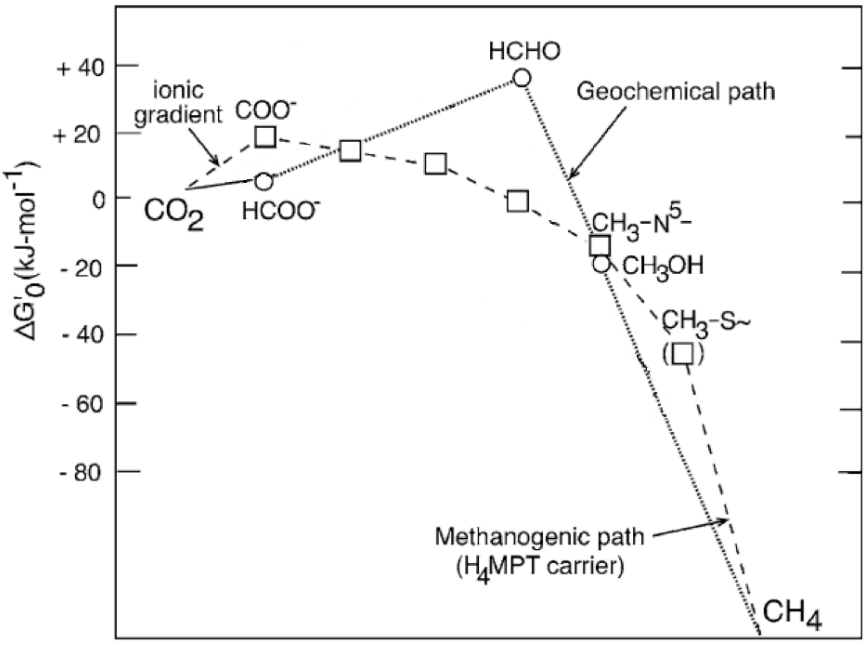

Figure 4.1. Free-energy profiles of C_1 reduction pathways; reduction is from left to right. The methanogenic reduction pathway compared to the geochemical pathway. Methanogens utilise an ionic gradient to drive the early stages of CO_2 reduction; without this energy input the geochemical reduction of CO_2 to formaldehyde barely occurs, if at all. Proton gradients within the vent are anticipated to lower the energetic barrier to the first steps of CO_2 reduction to formaldehyde, driving the geochemical pathway. Image adapted from Maden (2000) and Nitschke and Russell (2009).

These hypotheses suggest that the reaction between CO_2 and H_2 to make small organics, such as formaldehyde, should occur spontaneously in the vents with the conditions mentioned (Lane and Martin, 2012). It is therefore predicted that these redox reactions can be simulated in the laboratory, via the precipitates formed in the flow-reactor (formation described in Chapter 3).

The reactions that were anticipated to occur across the Fe(Ni)S, semi-conducting barriers were:

$$CO_2 + H_2 \rightarrow HCOOH (\Delta G'_o = {}^{+}3.5 \text{ kJ mol}^{-1}) \tag{4.1.1}$$

$$CHOOH + H_2 \rightarrow CH_2O + H_2O (\Delta G'_o = {}^{+}32.3 \text{ kJ mol}^{-1}) \tag{4.1.2}$$

All reduction products were of interest, however, they were not easy to detect, therefore derivatisation of specific molecules was developed. Formaldehyde (CH_2O) was chosen as the key molecule of interest for the key reason that it is symbolically the most difficult product to form from H_2 and CO_2 (equations 4.1.1 and 4.1.2 combined; $\Delta G'_o = +35.8\,\mathrm{kJ\,mol^{-1}}$). Being an endergonic reaction there is a thermodynamic barrier to its forward progression, as seen in Figure 4.1, and different pH conditions are needed for each gas species to enable the correct reduction potentials for CO_2 to be reduced to formaldehyde, as seen in Figure 3.1 in Chapter 3. The detection of formaldehyde would be proof of principle that the reaction can take place, however, formaldehyde is reactive and we would anticipate that it should form other organic products, including by simple disproportionation to form $HCOO^-$ and CH_3OH. Additionally it is also the basis for the formose reaction to produce sugars, such as ribose, which is a building block for nucleotides.

A potential problem for the progression of the reaction from formate to formaldehyde is that it is a condensation reaction. Having water as a product in an aqueous environment is a potential barrier to the forward progression of the reaction. Is it possible to force this reaction to occur in an aqueous environment without pressure, with reduction potentials alone?

Once formaldehyde has been synthesised its further reduction to methanol is likely to take place (Equation 4.1.3), in part because it is not a condensation, just a reduction. It could also form by disproportionation (Equation 4.1.4). Once methanol is formed it could react with hydrogen sulphide to produce methyl sulphide, however, again water is a product, potentially making the reaction unlikely (Equation 4.1.5). This reaction has reportedly been carried out by Heinen and Lauwers (1996) from HS^- and CO_2. Hydrogen sulphide could be important in early protometabolic reactions as a source of sulphur to early biochemistry, and precursors of the acetyl-CoA pathway (discussed in more detail in Chapter 5). Pressure could be the driving force for these reactions, shifting the equilibrium towards the products, away from the gas phase, and potentially overcoming the barrier created by condensation reactions in aqueous conditions. Therefore, even

if these reactions are not possible in the laboratory, they may still be feasible in the alkaline hydrothermal vent environment, which would have been subjected to high pressure.

$$CH_2O + H_2 \rightarrow CH_3OH \tag{4.1.3}$$

$$2\,CH_2O + OH \rightarrow HCOO^- + CH_3OH \tag{4.1.4}$$

$$CH_3OH + H_2S \rightarrow CH_3SH + H_2O \tag{4.1.5}$$

4.2 Reduction of CO_2 to formaldehyde

Much of the initial experimentation analysing for formaldehyde involved extensive method design and development. Formaldehyde is a very small organic molecule and the product concentration was expected to be very low due to the lack of pressure in the system. Finding a method to detect such low concentrations over the background levels in water was a significant challenge. The lowest limit of detection for formaldehyde using the DNPH derivative with HPLC (described in Chapter 2.2.1) was 100 μM. After a few trial runs with FeS precipitates in the small reactor it was evident that this level of detection was not sensitive enough for the concentrations of formaldehyde that would potentially be produced; peak areas for formaldehyde were sometimes too small to accurately measure, and detection was very variable, suggesting the formaldehyde that might have been present could have been lower than the detection limit for this method. The method from Sugaya et al. (2001) using PFBOA (described in Chapter 2.2.2), was eventually used due to its sensitivity and the fact that it used a column that was available on the GC-MS (Figure 4.2). Sugaya et al. (2001) found background levels of between 20 - 110 nM in tap water, with their very sensitive method. The lowest limit of detection for formaldehyde using this method was between 1-10 nM. Many different operational conditions were tested on the GC-MS with

formaldehyde standards; the method that produced the lowest detection and best separation of peaks was used for all samples analysed (Chapter 2.2.2). This was a very sensitive method for formaldehyde detection, however, due to this sensitivity a background concentration of ∼10 nM formaldehyde was detected in the distilled water used in the experiments. As a result 18 MΩ Milli-Q water was used thereafter, in which the level of formaldehyde was below 10 nM.

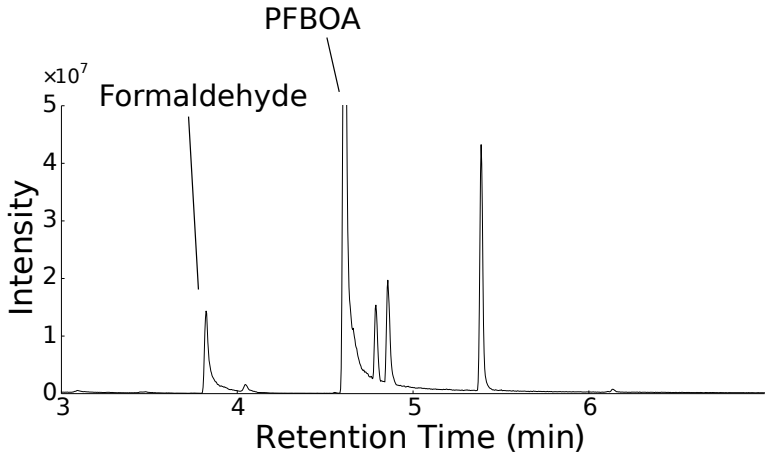

Figure 4.2. GC-MS trace showing analysis for formaldehyde derivatised with PFBOA. The formaldehyde PFBOA adduct peak is detected at 3.8 minutes and the PFBOA is detected at 4.8 minutes. Concentration is 100 nM here, based on extrapolation from calibration curve data (calibration curves shown in Chapter 2.2.2).

The original experiments to detect formaldehyde were carried out with no H_2, as the method of infusing it into the inlet tube disrupted the precipitates to an extent that their whole structure was destroyed every time a bubble entered the reactor. In principal, the excess Fe^{2+} ions present in the acid ocean, and the continuously forming precipitate meant it is plausible that CO_2 reduction could take place even in the absence of H_2. In the FeS precipitate the Fe^{2+} should pass electrons directly to CO_2 without the need for H_2 to reduce the resulting Fe^{3+} ions back to Fe^{2+}, and the difference in reduction potentials across the barrier could mean that Fe^{2+} is more reducing, as electrons pass from Fe^{2+} on the alkaline side to Fe^{3+} on the acidic side, where CO_2 is more easily reduced. This was the reason for its omission until a more effective method of addition to the setup was investigated.

Many experimental trials were conducted within the small reactor, using

both Fe(Ni)S and FeS precipitates. Fe^{2+} is able to reduce CO_2, but with only one electron reduction each time, therefore there need to be two Fe^{2+} ions coordinated at the same time to enable this reduction to take place (Equation 4.2.1). If Ni^{2+} is added to the catalyst, it is capable of two electron reductions directly, increasing the efficiency of the catalyst; first two Fe^{2+} ions reduce the Ni^{2+} ion to Ni (Equation 4.2.2), which can then go on to carry out the two-electron reductions to reduce CO_2 directly (Equation 4.2.3). This suggests that the reduction of CO_2 is more likely to occur if the catalyst is made up on Fe(Ni)S clusters instead of FeS alone, as is found in many hydrogenase enzymes. However, it must be noted that this reduction is still thermodynamically unfavourable under standard state conditions.

$$2\,Fe^{2+} + CO_2 + H^+ \rightarrow HCOO^- + 2\,Fe^{3+} \tag{4.2.1}$$

$$Ni^{2+} + 2Fe^{2+} \rightarrow Ni + 2Fe^{3+} \tag{4.2.2}$$

$$Ni + CO_2 + H^+ \rightarrow HCOO^- + Ni^{2+} \tag{4.2.3}$$

The PFBOA GC-MS method was repeated multiple times until a complete set of results was collected. This method development took longer than expected due to the variability in the precipitates (sometimes there were five or more precipitate tubes to collect from, and on other occasions only a single tube formed) and the difficulty in the sample collection method (if the precipitate only formed one tube and it was out of reach of the syringe, then no sample could be collected). The GC-MS was also very variable in its sensitivity. The limit of sensitivity of the instrument was close to 100 nM, as the graphs b and c in Figure 4.3 show, the curve is no longer showing a positive correlation between concentration and peak area, as both have concentrations below 120 nM. The R^2 values for the early calibration curves started to decrease dramatically over the period of a week, it was therefore discovered the GC-MS machine was losing sensitivity and needed to be cleaned, and the column trimmed. This was an occupational

hazard of working with a core facility machine with heavy usage. The column becomes contaminated and needs to be changed or trimmed and recalibrated. When this occurred the results from the experiment had to be discarded and the GC-MS inspected. Overall four repeats with good calibration curves were collected (Figure 4.4).

The levels of formaldehyde being detected over the time course of these experiments indicated an overall increase in formaldehyde over time. Samples were taken over 90 minutes for the first two experiments, then increased to 240 minutes as it was predicted there might be an increase in formaldehyde production over a longer period, due to the continuing increase in detected formaldehyde over the time course of the initial experiments. As mentioned in Chapter 3, after 4 hours the precipitates started to thicken considerably, potentially inhibiting any reduction across the barrier. For this reason the experiments were restricted to less than 240 minutes.

These preliminary findings were encouraging, although the synthesis of formaldehyde was variable and inconsistent between experiments. Statistical analysis of the mean results found no significant difference in formaldehyde concentrations between experimental runs, or in concentrations between time points ($p = > 0.05$). This indicates there was no significant increasing trend in the data over time for the mean results (Figure 4.5); the variability in the results between experiments meant there was a loss of the observed increase seen in each experiment. It is arguably more useful to analyse each experiment separately than to look for an increasing trend in the means, due to this variability in detection. The levels of formaldehyde detected in the acid ocean were also found to be relatively high, and varied between experiments. In part this may have reflected catalysis by Fe^{2+} in the acid ocean, but the variation between runs could also indicate contamination within the anaerobic chamber, which was disguising any formaldehyde production that may have been occurring. This contamination was subsequently investigated and will be discussed in section 4.2.1 and 4.3, along with the remediation measures taken to try and reduce the levels of contamination.

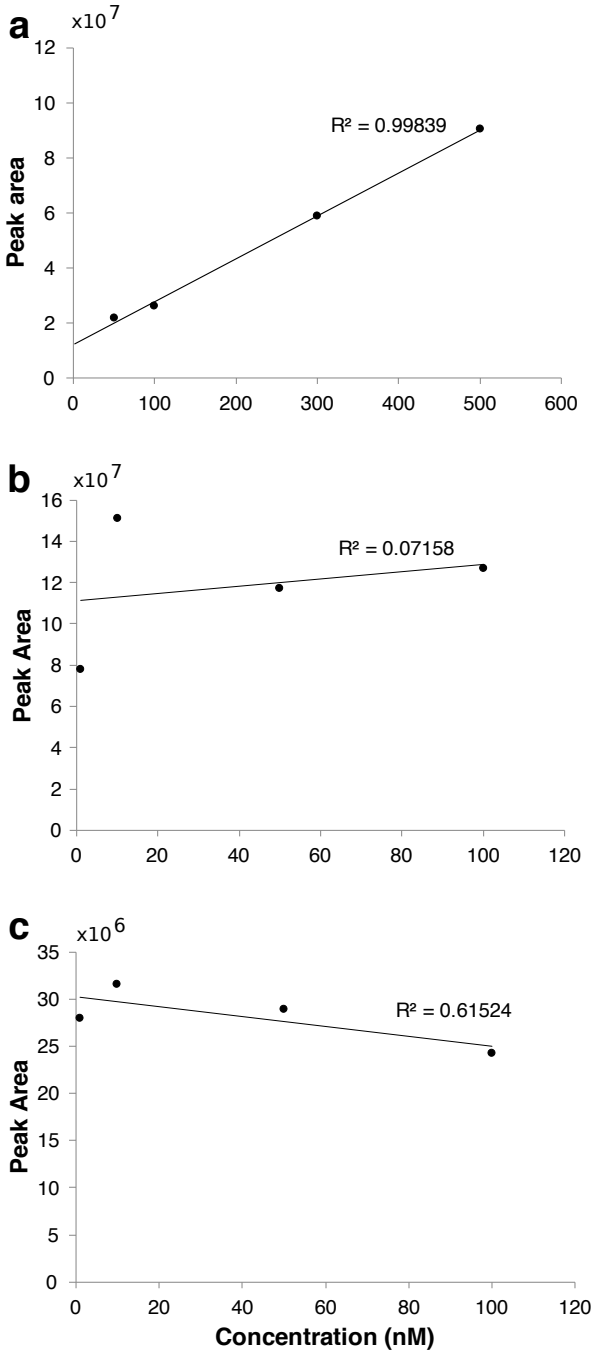

Figure 4.3. GC-MS calibration curves for formaldehyde detection from three different experiments. **(a)** Calibration curve from 9th December, good R^2 value. **(b)** Calibration curve from 12th December, points are not on a line, and the R^2 value is very low. **(c)** Calibration curve from 13th December, points do no correlate with concentration, and the curve seems to be reversed. The method for making the standards was the same each time, therefore it was deduced that the machine was losing sensitivity and becoming contaminated, rather than human error. Any experimental results acquired from the GC-MS with these last two calibration curves had to be discarded.

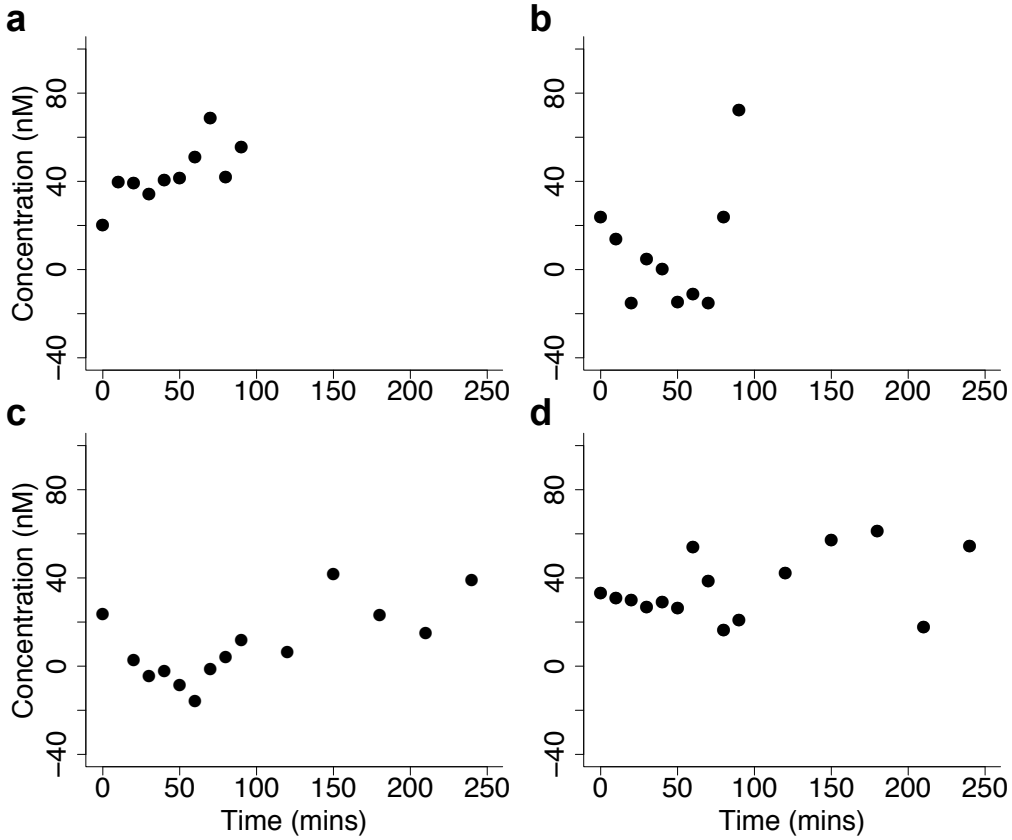

Figure 4.4. Formaldehyde detection within the small flow-reactor over time intervals, in the anaerobic chamber. Four different repeats were conducted using Fe(Ni)S precipitates, over 90 – 240 minutes. Concentrations were calculated using separate calibration curves for each experimental run. **(a)** Increasing formaldehyde concentration from the start can be observed. **(b - d)** An observed drop in formaldehyde detection in the first 50 minutes, with a subsequent slight increase. Initial detection in the acid ocean (time zero) must therefore be from catalysis by Fe^{2+} in the acid ocean or contamination.

4.2.1 Chamber contamination

An issue encountered with these experiments, and which may account for the large variation in the results, was an increase in background levels of formaldehyde in the water after being left in the anaerobic chamber overnight to deoxygenate. Even higher levels of formaldehyde were found in the freshly made up acid ocean. Contaminants other than formaldehyde were found within the different reagents, contributing to an overall background contamination in the acidic and alkaline fluids (Figure 4.6). It was presumed the contaminants were products released from the experiments being carried out in the reactor. Formaldehyde and hydrogen sulphide would have been produced, and due to this being an open

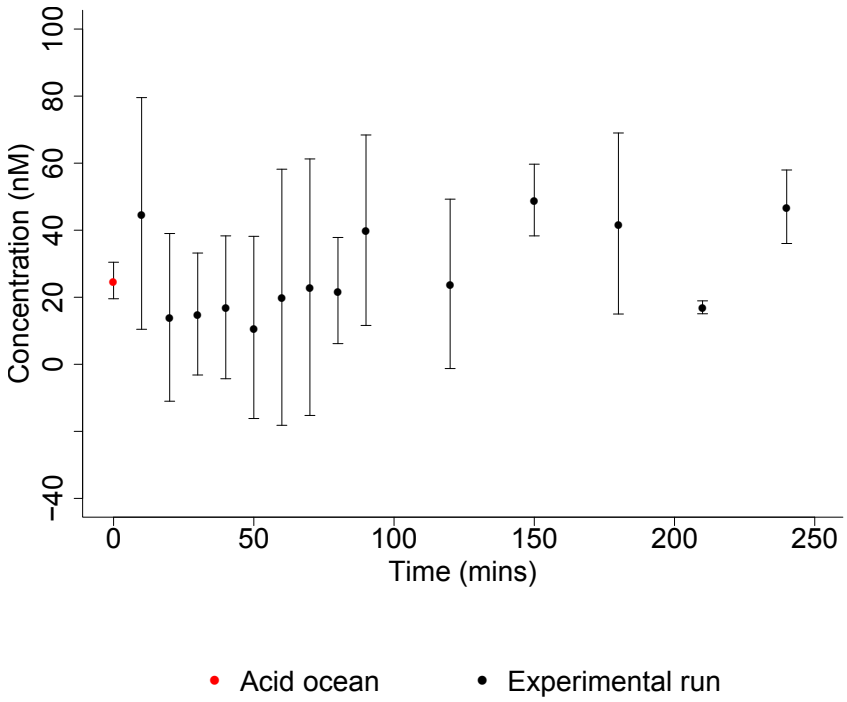

Figure 4.5. Formaldehyde production over time, averaged from four individual experiments, using Fe(Ni)S precipitates, over 4 hours. Concentrations calculated using separate calibration curves for each experimental run, to take into account machine variability. The acid ocean was shown separately to highlight the high levels of formaldehyde in the starting acidic fluid. There is no significant difference between time points ($p > 0.05$), indicating there is no significant increasing trend temporally. N = 4 ± SD.

system they were easily released into the anaerobic chamber atmosphere. Due to a lack of circulation of the atmosphere out of the chamber the levels of gases could have built up.

These contaminants were seen to increase within the acidic ocean, this could have been due to the high levels of Fe^{2+} and Ni^{2+} ions within the solution, acting as catalysts for formation of organics from the CO_2 (as bicarbonate) in solution and the H_2 within the chamber atmosphere (around 2% H_2 atmosphere) directly, without the need for the precipitate structure, and also the continued reduction of formaldehyde to methanol and methane and other organics. The contaminants seen were acetaldehyde, acetone and possibly cyclohexane as seen by mass spectrometry (Figure 4.6).

4.3 Total organic carbon detection

Total organic carbon (TOC) and inorganic carbon (IC) were measured in three different experiments using the initial purged organic carbon (POC) method (described in Chapter 2.2.3), to see what concentration of organics were being formed. Results were extremely variable, with TOC being detected in the acid ocean and not at all in the experimental run on some occasions, and the opposite on others (Figure 4.7). TOC results recorded in the first repeat showed very low concentrations observed in the water control and acid ocean, and very high concentrations in the subsequent time points, however, it was not seen to be increasing with time. TOC results for second repeat showed a large concentration in the acid ocean, and extremely low levels in the subsequent time points (opposite to that found in the first repeat). Results recorded in the third repeat showed high concentrations in the acid ocean, and even higher concentrations (up to 10 mg/L) for 40 minutes, and then a decrease observed for the rest of the time points. The IC recorded in all three repeats was extremely high, an order of magnitude higher than the TOC, with the highest concentrations recorded in the third repeat at $\sim$80 mg/L. All IC recorded in the water controls were very low, and most of the TOC recorded in each water control repeat was also low, with the highest concentration recorded at $<$ 1 mg/L. Due to the extremely high levels of IC compared to TOC within the samples, the POC method can result in significant errors and false positive results can occur (as seen in this study) as it interferes with the detector. Due to the high concentrations of IC this method was not an accurate measure of TOC for this experiment.

A non-purged organic carbon (NPOC) method (described in Chapter 2.2.3) was developed to take into account high IC levels. Water deoxygenated inside and outside the anaerobic chamber was used to make up the acid ocean fluid, and then analysed for contaminants using the NPOC method. Samples of HPLC grade water, Milli-Q water, formaldehyde, CHOONa and the acidic ocean were prepared in the anaerobic chamber, from both water that had been a) left to deoxygenate within the chamber (anaerobic), and b) left to deoxygenate outside the chamber,

by bubbling N_2 through it (aerobic). The levels of TOC in the samples prepared from water left inside the anaerobic chamber were an order of magnitude greater than those prepared with water deoxygenated outside the chamber (Figure 4.8). The acid ocean had much greater TOC levels than the pure water in both cases, but still significantly less when using water deoxygenated outside the chamber. This shows that water left to deoxygenate within the chamber accumulates contaminants that were present in the chamber's atmosphere. The high levels of TOC in the acid ocean could also be due to Fe^{2+} and Ni^{2+} ions catalysing the reaction without the need for the FeS precipitates (as mentioned earlier). If the levels of contaminants can be decreased at the start the final results would be more accurate in indicating how much formaldehyde was synthesised across the precipitates in the flow reactor. Therefore all subsequent experiments looking at formaldehyde synthesis used water deoxygenated with N_2 outside the anaerobic chamber, reducing the background contamination levels.

These contamination results correlated with the GC-MS contamination results that showed high contamination in reagents prepared within the anaerobic chamber (Figure 4.6). It is also interesting to note that the variability in TOC for the solutions prepared in the anaerobic chamber was much greater than those prepared outside, indicating that the level of contamination was highly variable. This could be attributed to the length of time the water was left in the chamber to deoxygenate before it was used; the longer it was left the more contaminants started to accumulate. TOC experiments were abandoned due to the huge variability in results and the high levels of contaminants affecting the overall results The aim was to see if there was a systematic increase in total organic carbon over time, even given the contaminants, there was no observed increase.

The levels of contaminants being released into the anaerobic chamber's atmosphere were reduced by the installation of traps at the outlet tube of the flow reactor. One trap contained a solution of DMSO (dimethyl sulfoxide) to catch any volatile organics, such as formaldehyde, and another contained silver sulphate solution to remove the majority of H_2S produced from the reaction in

the flow reactor. A large hydrogen sulphide removal column (HSRC; COY Inc. Grass Lake, MI) was also installed to remove H_2S within the chamber atmosphere. The HSRC continuously recirculates the chamber atmosphere through the column, removing H_2S by a combination of H_2S optimised activated carbon and permanganate impregnated media in the column. The HSRC has a unique layering of media that acts by a combination of adsorption and chemisorption to remove the H_2S from the atmosphere.

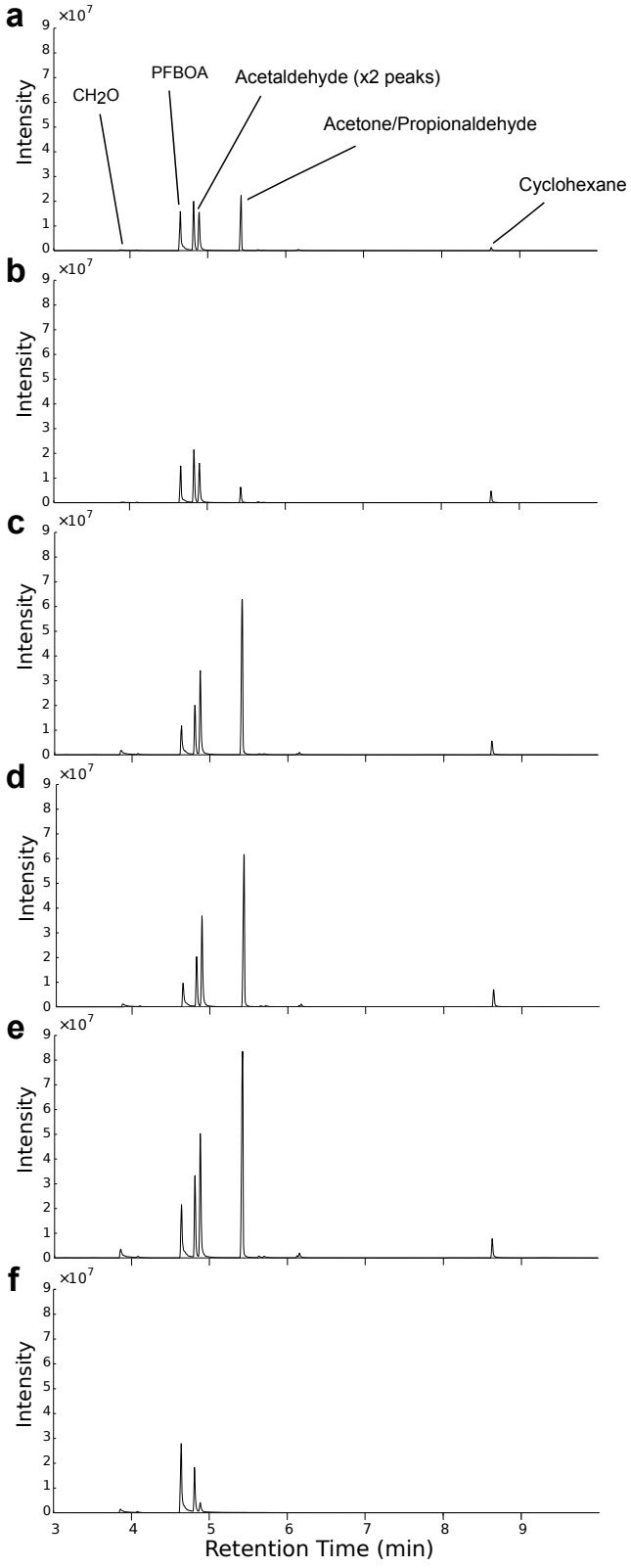

Figure 4.6. Contaminants detected within acidic and alkali starting solutions. GC-MS spectra indicating compounds identified within different reagents of the acidic and the alkali fluids, all made from water deoxygenated within the chamber. **(a)** HPLC water; **(b)** Bicarbonate fluid ($NaCHO_3$); **(c)** $FeCl_2$ fluid; **(d)** $FeCl_2$ and $NiCl_2$ fluid; **(e)** Acid solution ($FeCl_2$, $NiCl_2$, $NaCHO_3$ and HCl); **(f)** Alkali solution ($NaSiO_4$,K_2HPO_4 and Na_2S).

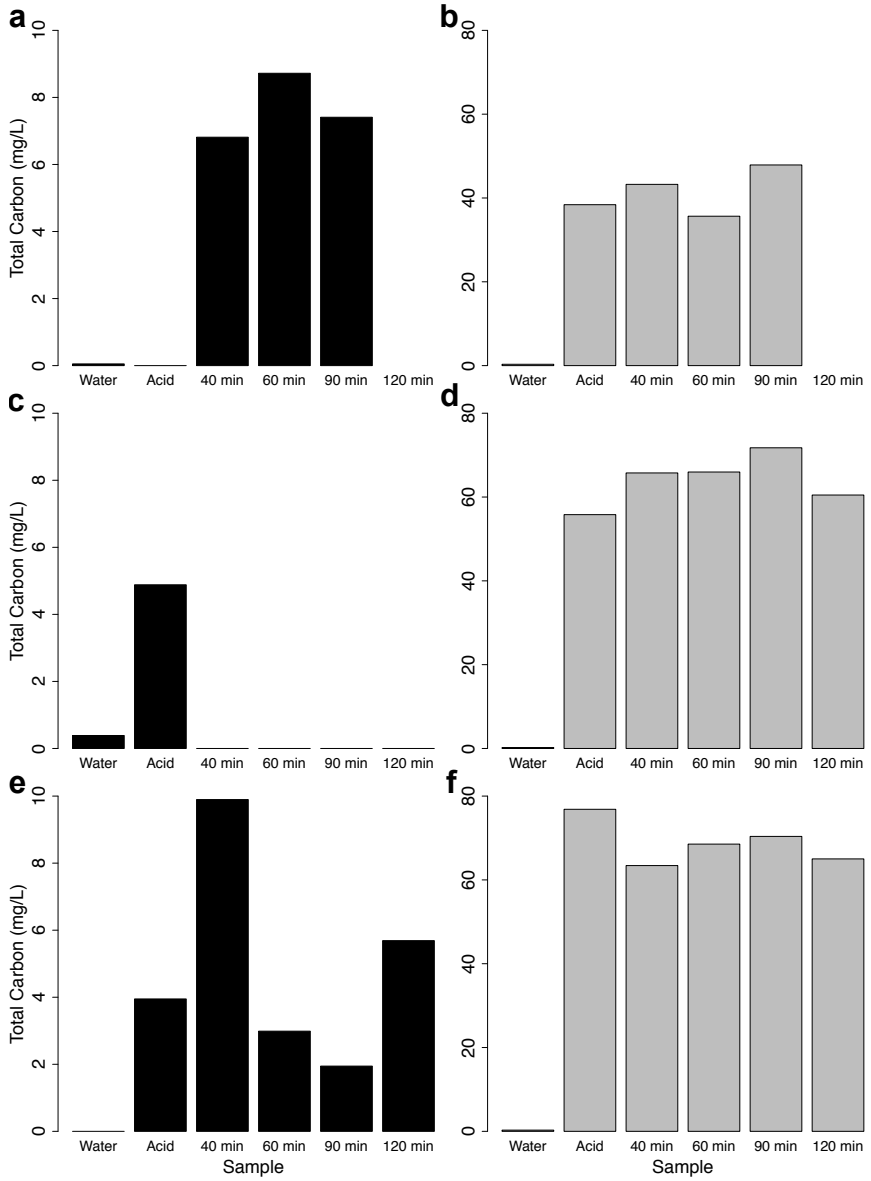

Figure 4.7. Total organic carbon (TOC) and inorganic carbon (IC) results, measured using purged organic carbon (POC) method for three repeats within the small flow reactor. **(a)** TOC recorded in the first repeat; very low concentrations observed in the water control and acid ocean, and very high concentrations in the subsequent time points, however, it is not increasing with time. No sample measured at 120 minutes; **(b)** IC recorded in the first repeat; relatively high concentrations of IC in the acid ocean and different time points; **(c)** TOC for second repeat; a large concentration observed in the acid ocean, and extremely low concentrations in the subsequent time points (opposite to the first repeat); **(d)** IC recorded in the second repeat; extremely high concentrations observed in all samples; **(e)** TOC recorded in the third repeat; high concentrations observed in the acid ocean, and even higher concentrations (up to 10 mg/L) for 40 minutes, and then a decrease observed for the rest of the time points; **(f)** IC recorded in the third repeat; the highest concentrations recorded from the three repeats (up to ∼80 mg/L). All IC recorded in the water controls were very low, and most of the TOC recorded in each water control repeat was relatively low, with the highest concentration recorded at < 1 mg/L.

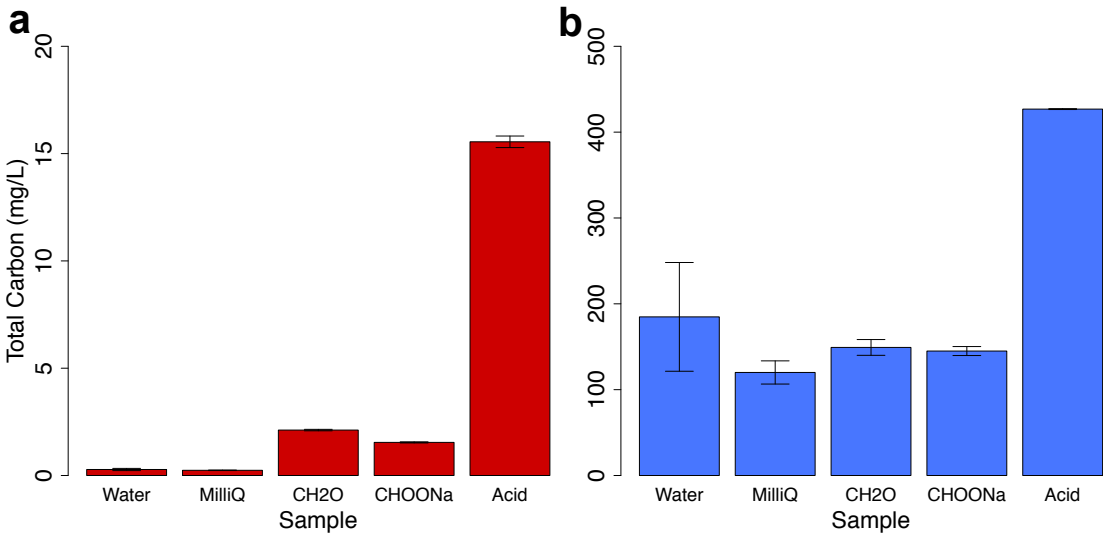

Figure 4.8. Total organic carbon (TOC) measurements using non-purged organic carbon (NPOC) method for distilled water, 18MΩ Milli-Q water, formaldehyde (6 ppm), formate (6 ppm), and the acid ocean ($FeCl_2$, $NiCl_2$, $NaCHO_3$ and HCl). **(a)** Samples prepared from fresh Milli-Q water deoxygenated outside the chamber; **(b)** Solutions prepared from fresh Milli-Q water deoxygenated overnight inside the anaerobic chamber. Note the amount of total carbon in (a) is an order of magnitude smaller than in (b) but there is still considerably more TOC in the acid ocean in both cases, again implying some degree of catalysis rather than simply contamination. N = ±2 SD.

4.4 New method for reduction of CO_2 to formaldehyde

New modified and improved experiments for the reduction of CO_2 to formaldehyde were designed, along with the addition of contamination prevention methods detailed in the previous section. These experiments were conducted by Sylvia Lim, a fourth year undergraduate student under my supervision. The method for FeS precipitate production was the same as previous experiments, although no Ni was used this time, and H_2 was added to the system by creating an atmosphere of H_2 above the alkaline fluid using iron fillings in acid.

The samples for these experiments were taken from the precipitate at the base of the reactor and the solution next to the precipitates separately. Previous experiments had taken samples as a mixture of both environments. The method used for the GC-MS had a slight modification in that the samples were diluted. It was found that the levels of formaldehyde were too high for the detector in the GC-MS once it had been cleaned and recalibrated, this was discovered when the calibration curve started to level off at higher concentrations (over 0.5 mM), indicating a saturation of the detector (Figure 4.9), resulting in the samples having to be diluted by either 10- or 100-fold to enable accurate measurements.

Controls for the deoxygenated 18MΩ Milli-Q water (water control), acid ocean and alkaline fluid were left inside the chamber and samples taken at the same time points as for the experiment, to monitor whether contamination within the original fluids was affecting the concentrations detected. A deoxygenated water control was not used in the original experiments. The water control should have been used to enable a better understanding of the effect of contamination in the chamber and metal ions in the acid ocean. It was not conducted originally as it was thought the water showed low levels of formaldehyde compared with the precipitate samples (highest levels detected were 0.3 μM), however it was found that the levels of formaldehyde detected in the water from the newer experiments were higher than those detected within the samples of the older experiments (detection was around 40 nM for formaldehyde in older experiments).

This suggests the GC-MS method was much more sensitive overall in the newer experiments. This is corroborated by comparing the calibration curves for the previous experiments with these newer experiments, where the sensitivity of the GC-MS was almost an order of magnitude greater than for the previous experiments (Figure 4.10). The newer experiments also used an internal standard (IS), which increased the reliability of the results, due to the IS eliminating the effect of variability from day to day in the GC-MS, making the results much more reliable.

The results of these newer experiments showed a much greater increase in formaldehyde production over time than the previous experiments. The samples were first diluted 10-fold (Figure 4.11), and then subsequently 100-fold (Figure 4.12). The results from the 100-fold dilution produced the highest concentrations of formaldehyde (results were corrected for the dilution), indicating that this was the best dilution ratio to prevent the detector from becoming saturated and giving a false result. When the results from both dilution methods were averaged onto one graph the concentrations of formaldehyde showed a dramatic increase in the precipitate compared to the solution and controls overall, unlike that seen in the older experiments, showing that the variability in the individual experiments was much less that previously (Figure 4.13). There was still a large variation between experiments as seen by the standard deviation error bars, however, it is still possible to see the significant increase in formaldehyde production in the precipitates compared to solution over time.

Concentrations of formaldehyde detected in these newer experiments were $\sim 10^{3}$ times higher than those detected in the original experiments (μM concentrations rather than nM), however only in the samples taken from the precipitates, results for the samples taken from the solution were much lower, more similar to those seen in the original experiments (which were taken as a mixture of solution and precipitate). This indicated that formaldehyde was being produced in much greater concentrations in the precipitate, and may get trapped in the precipitate and accumulate there. This may relate to the dehydration step to form formaldehyde, it occurs more readily on the hydrophobic surfaces of

the FeS mineral, and seems to remain bound. Any formaldehyde that was synthesised across the barrier in the precipitate tubes and ended up in the acid ocean solution would mostly likely be diluted, and therefore was detected in much lower concentrations.

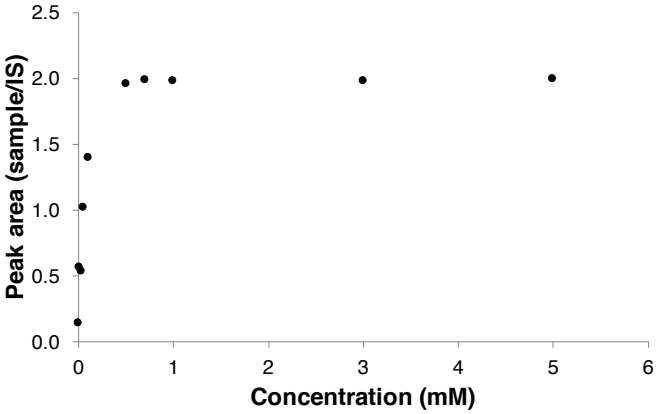

Figure 4.9. Saturated GC-MS calibration curve for mM concentrations of formaldehyde standards. The y-axis is the formaldehyde peak area in the GC-MS chromatogram integrated to the internal standard (IS). Standards over 0.5 mM see a levelling off in the calibration curve, indicating saturation of the GC-MS detector at concentrations higher than this.

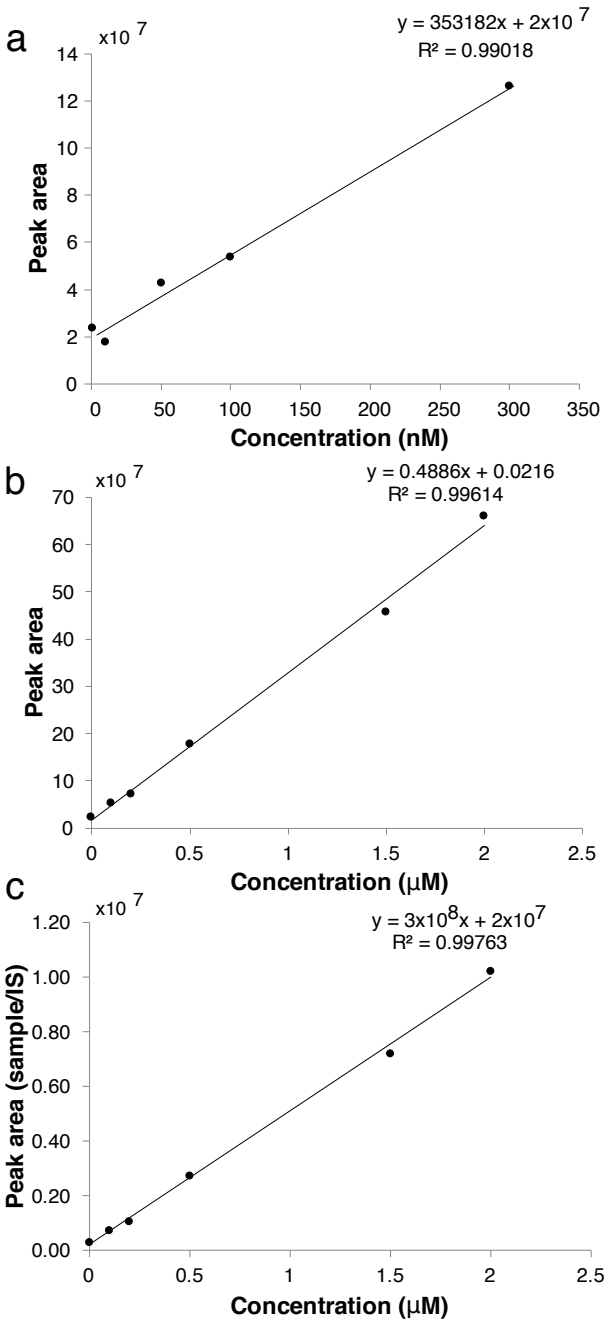

Figure 4.10. Calibration curves for GC-MS for formaldehyde detection, for older and newer GC-MS and flow reactor methods. **(a)** Calibration curve for old experiments using GC-MS and flow reactor without contamination prevention methods. Standards in nM concentrations. **(b)** Calibration curve for newer experiments, using diluted samples at a ratio of 1:10 in HPLC water. Standards in μM concentrations. **(c)** Calibration curve for newer experiments using a dilution ration of 1:10 in HPLC water, y-axis is the peak area in the GC-MS chromatogram with formaldehyde integrated to the internal standard, giving a more accurate standard curve. Standards in μM concentrations. Detection is an order of magnitude more sensitive in the newer experiments, indicating the recalibrated GC-MS, and reduced contamination in the chamber, has increased level of formaldehyde detection.

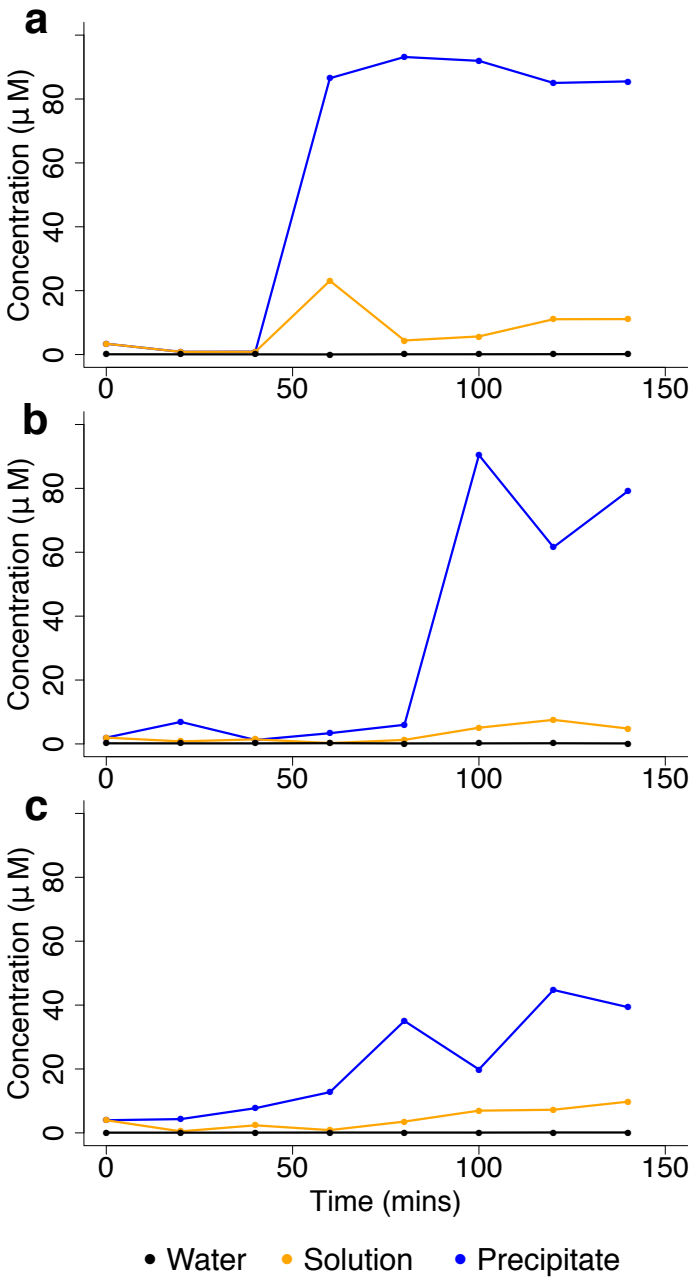

Figure 4.11. Formaldehyde detection within the small flow-reactor over 140 minutes. Samples were diluted 10-fold for GC-MS analysis. Three repeat experiments using FeS precipitates, samples collected from the precipitates themselves, the solution around the precipitates, and water left in the chamber as a control. In all experiments the concentration of formaldehyde in the water is almost negligible compared with the precipitate. **(a)** A large increase in formaldehyde concentration detected in the precipitate after 40 minutes from very low concentrations to 100 μM, where the concentration remained constant for the rest of the experiment. **(b)** A large increase in formaldehyde concentration detected in the precipitate after 80 minutes from very low concentrations to between 80 and 100 μM, **(c)** A more gradual increase in formaldehyde concentration detected in the precipitate over the whole experiment, to a maximum concentration of $\sim$40 μM. Only a small increase seen in the solution samples (maximum concentrations of around 10 μM) in all repeats compared with the water controls. However, the lower concentrations were affected by the sensitivity of the instrument on a day to day basis.

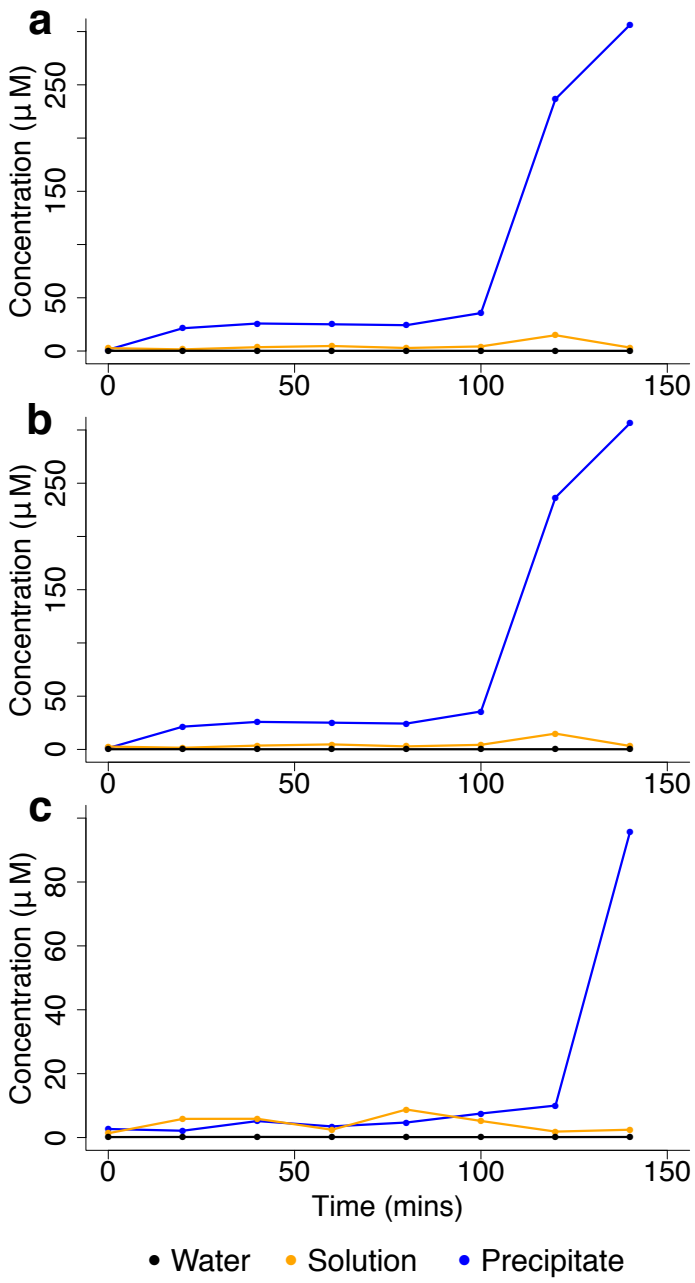

Figure 4.12. Formaldehyde detection within the small flow-reactor over 140 minutes. Samples were diluted 100-fold for GC-MS analysis. Three repeat experiments using FeS precipitates, samples collected from the precipitates themselves, the solution around the precipitates, and water left in the chamber as a control. In all experiments the concentration of formaldehyde in the water is almost negligible compared to the precipitate. **(a and b)** A small increase in formaldehyde concentration detected in the precipitate until 100 minutes, then a large increase from around 40 to 300 μM. Only a small increase seen in the solution compared with the deoxygenated water control. **(c)** A small increase in formaldehyde concentration detected in the precipitate until 120 minutes, then a large increase from around 10 to 100 μM (less than that seen for the previous two repeats). Only a small increase seen in the solution compared with the deoxygenated water control.

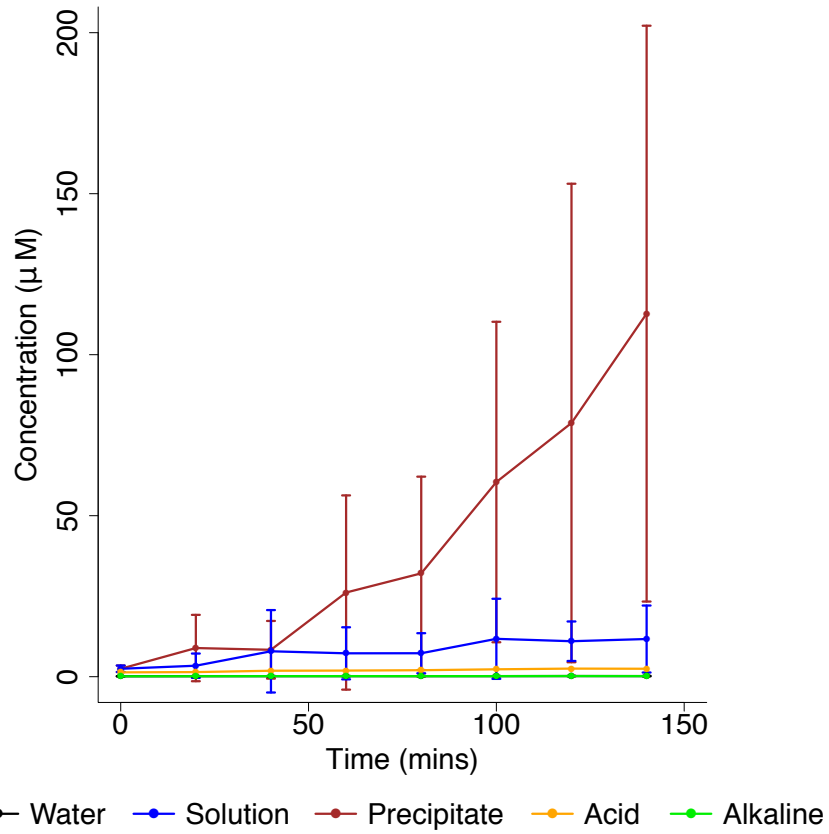

Figure 4.13. Mean formaldehyde detection within the small flow-reactor over 140 minutes. Samples were diluted 10- and 100-fold for GC-MS analysis. Average concentration of formaldehyde detected over 9 reactor runs. Water, acid ocean and alkaline fluids sampled at the same time to act as negative controls for contamination within the chamber. N = 3 ± SD.

4.5 Discussion

Formaldehyde was chosen as a detection product because it is the hardest reduction step to take place, due to there being a significant endergonic barrier to its formation (Figure 4.1). But it is also one of the simplest organic molecules produced by the reduction of CO_2. The original, older, experiments showed a slight increase in formaldehyde over time, but due to the high variability in the results average, statistically significant increases could not be confirmed. One reason for the variability between experiments could be due to the variability in precipitate character and structure between experiments. As mentioned in Chapter 3, the variability in precipitate formation was huge, with different structures and characteristics occurring each time the experiment was run. The large volume of fluid within the reactor, meant there was a low surface area of precipitates to volume of acid ocean, which meant a low concentration of products as they rely on the precipitates to form.

The detection levels of formaldehyde in the older experiments were relatively low, in the nM range, not that much higher than background concentrations found in tap water (20 - 110 nM found by Sugaya et al., 2001). Formaldehyde can decompose to formic acid, CO, and even back to CO_2 and H_2 in the presence of basic catalysts, which would lower detection levels. It could also be further reduced to methanol with the addition of more H_2. The reduction of CO_2 to methanol occurs via a number of sequential steps, that produce formic acid and CO (both of which have the same redox state) as reaction intermediaries in this aqueous reaction (Figure 4.14). Each of the reaction steps is reversible, allowing for the intermediates to attain states of redox-dependant thermodynamic equilibrium on the time scale of a laboratory experiment. The abundance of these intermediaries may vary as a function of CO_2 partial pressure, H_2 partial pressure, pH, redox state, and temperature in the hydrothermal system, due to the relatively rapid reaction kinetics for each reaction. This means that the low concentrations of formaldehyde in CO_2-rich environments may not reflect an absence of a formation mechanism, but the thermodynamic controls on their

abundance under the chemical conditions present (Seewald et al., 2006; McCollom and Seewald, 2007). Increasing the partial pressure of H_2 could stop the reverse reactions taking place, both because the addition of H_2 further reduces the carbon compounds, but also as Le Chatelier's principle states: increasing the pressure or concentration of one or all of the reactants of a system will force the equilibrium of the reaction towards the products, in this case to formaldehyde and methanol (Le Chatelier and Boudouard, 1898).

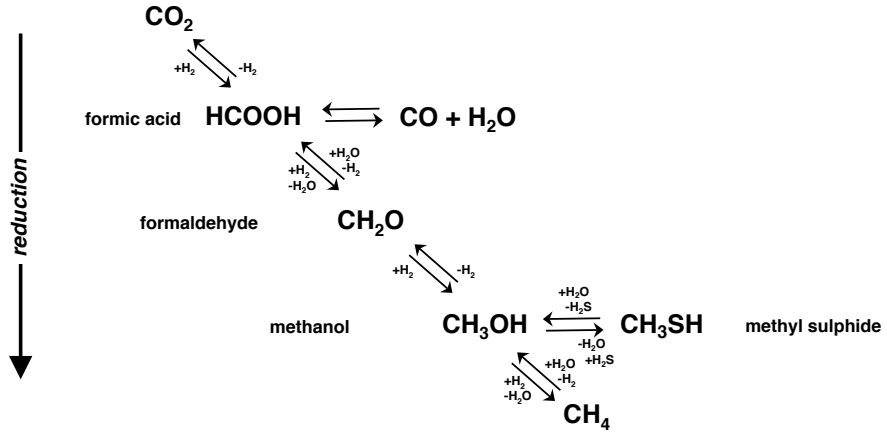

Figure 4.14. Reaction scheme for the reduction of CO_2 to methane. Reversible redox reactions that may regulate the speciation of single carbon compounds in aqueous, hydrothermal conditions. Notice that formate and CO are at the same redox state, as are methanol and methyl sulphide. Increasing the partial pressure of H_2 could also hinder the reverse reactions taking place, forcing the equilibrium of the reaction towards formaldehyde and onto methanol. Image adapted from Seewald et al. (2006).

Total organic carbon (TOC) detection was not accurate or reliable using the initial purged organic carbon (POC) method. The levels of inorganic carbon (IC) were very high compared to the TOC values, which created significant errors in the TOC measurements. If IC is not fully removed by a TOC analyser with normal operations, a false positive result can occur. Consequently a new method was developed using non-purgeable organic carbon (NPOC), which took into account high IC, and low TOC levels within the samples. Reagent solutions analysed using the NPOC method indicated that there were high levels of organics in the anaerobic chamber atmosphere, which were absorbed into the water when left stirring to deoxygenate overnight. It was hoped measuring TOC would give an indication as to whether any organics were being produced in the flow-reactor,

regardless of the composition. If formaldehyde was indeed being produced in the precipitate experiments, but was breaking down within the acid solution, or forming polymers or other organics, these derivatives were hoped to have been detected by TOC. Nonetheless, the concentration of organics being produced might still have been too low to detect using this method. The NPOC method was not used to analyse the formaldehyde synthesis experiments as the formaldehyde concentrations were too low, and contamination was too high, which would have given misleading results.

The contamination within the anaerobic chamber severely disrupted the older experimental results, adding to the variability between experiments. Several methods were developed to reduce the contamination of the chamber atmosphere, which was thought to be mainly formaldehyde escaping as gas from the reactor, and H_2S gas produced as the FeS precipitates decomposed in acid conditions. As mentioned in section 4.3, the levels of contaminants being released into the anaerobic chamber's atmosphere were reduced by the installation of a lid on the reactor reservoir, and traps at the end of the outlet tube of the flow reactor. The traps included a solution of DMSO to catch any volatile organics (such as formaldehyde) and a solution of silver sulphate to remove the majority of H_2S. A large hydrogen sulphide removal column (HSRC; COY Inc. Grass Lake, MI) was also installed to remove high concentrations of H_2S within the chamber atmosphere. The washing of the reactor between runs was more carefully conducted in subsequent experiments, keeping all fluids within the closed system, and making sure there was minimal contact with the atmosphere to reduce the levels of H_2S escaping and becoming trapped in the chamber. It was observed that the level of contamination was substantially greater in the fluids which contained $FeCl_2$ or $NiCl_2$, as seen in the TOC results, indicating that these metal ions can act as catalysts for the direct reduction of CO_2, without the need for FeS precipitates, and possibly even without the need for H_2. To reduce exposure of the water to the chamber's atmosphere, and the catalysis of H_2 by the Fe^{2+} ions in the acid solution, the water used for the experiments was deoxygenated with N_2 gas bubbled through it outside the anaerobic chamber, rather than by leaving

it stirring overnight in the chamber.

The subsequent, newer, formaldehyde experiments incorporated many modifications to the sampling and analysis methods to improve the concentration of formaldehyde collected in each sample and the sensitivity of detection. With these new methods concentrations of formaldehyde were seen to increase over time, and where detected at levels $\sim 10^{3}$ times that of the previous experiments. Samples were taken from the solution around the precipitates and directly from the precipitate at the base of the reactor, whereas in the older experiments the samples were taken at random locations around the reactor as a mixture of both precipitate and solution. This sampling method indicates that formaldehyde has a close association with the FeS precipitates, becoming bound onto the precipitate and consequently detected to a lesser degree in solution, where it could become too dilute or start to breakdown.

The addition of H_2 to the system in the early experiments was not as effective as hoped. Bubbling it into the inlet tube disrupted the FeS precipitate formation, and therefore discounted the whole purpose of specific precipitate characteristics. The original formaldehyde experiments were therefore conducted with no H_2 in the system, as it was hoped that the Fe^{2+} ions within the acid ocean could directly reduce CO_2 (in the form of bicarbonate in the acid ocean), without the need for H_2 gas. The subsequent, newer, experiments used an atmosphere of H_2 above the alkaline fluid, to allow some H_2 to dissolve into solution, albeit at concentrations less than 1 mM at atmospheric pressure and room temperature. Moreover any increase in temperature will then decrease the partial pressure (Kaye and Laby, 1986).

Despite these problems, all the improvements together led to the detection of 10^{3} times more CH_2O, so they worked very well in increasing the formaldehyde detection within the system. To make this experiment more robust and simulate that of hydrothermal vents more accurately, a system conducted at high pressure could be designed. This would increase the concentrations of CO_2 and H_2 dissolved in solution significantly. In the deep ocean there would be a significant pressure; at 900 m (depth of Lost City hydrothermal field) the pressure is 90

atmospheres (90 times that at sea level). Alkaline hydrothermal vents in the Hadean could have been located even deeper, around 2000 - 3000 m, which would have pressures of up to 3000 times that of sea level. This would have an effect on the concentrations of reactants and products, the concentration of dissolved gases in the water, and then the subsequent reaction efficiencies of the products formed. Le Chatelier's principle states that a shift in pressure or volume will shift the equilibrium of the system. If there in an increase in pressure the equilibrium shifts to the right, where there are fewer moles of gas (Le Chatelier and Boudouard, 1898). Using this principle we can assume that any reactions involving CO_2 and H_2 will shift to the right, in favour of the products, such as the formation of organics and for the same reasons, should also tend to promote condensation reactions where water is produced in an aqueous environment. Overall, pressure should increase reaction rates and the potential for CO_2 reduction to take place. A high partial pressure of H_2 might not only increase the reduction of CO_2 by electron donation, but as mentioned earlier, it might also inhibit the breakdown of formaldehyde back to CO_2 and H_2, halting the reverse reactions (Figure 4.14) as the equilibrium is shifted to the side of the products and away from the gas phase (Le Chatelier and Boudouard, 1898). In this way the concentration of formaldehyde detected, particularly in the solution, could be increased.

In conclusion, the levels of formaldehyde detected in the original experiments were very low, but once the contamination had been reduced in the anaerobic chamber, the sampling method, and sensitivity of the GC-MS improved, then the concentrations of formaldehyde detected were relatively high (μM range as opposed to nM range, well above background levels detected in water). The high concentrations of formaldehyde detected on the precipitates, as opposed to the surrounding solution, indicates that CO_2 is being reduced to formaldehyde on the surface of the FeS precipitates. One question this brings up is whether pH is driving this reduction (as shown in figure 3.1, shown in Chapter 3), or if the reduction can take place by FeS catalytic minerals alone. If the transfer of electrons can occur over relatively long distances, could the transfer of electrons occur in the FeS precipitate mound, with alkaline fluid at

the base of the reactor and the acid ocean remaining on the outer surface over relatively thick precipitates, rather than the thin tubular structures originally though to be necessary? The experiments here seem to indicate this to be the case, as the largest increases in CH_2O were from the precipitate formed at the base of the reactor, with alkaline fluids beneath the precipitate, and acidic ocean above. This question could also be addressed by the use of microfluidics, where the precipitate can be formed in a contained environment, with very controlled pH and temperature conditions on either side, creating an increased surface area to volume system, which would ultimately increase product concentrations. This system could investigate the thickness of precipitate able to transfer electrons, and whether electrons could flow through a semi-permeable membrane, thereby modelling a 'leaky' membranous primordial cell in an alkaline hydrothermal vent environment.

Future methods should be developed to search for other carbon species, such as formate (which was investigated briefly by Barry Herschy another member of the group, but was never detected within the flow reactor system) and methanol, as these compounds could also be formed in the reactor. It was a significant challenge to trap the volatile organics within the reactor in a way that made them detectable by any analytical methods available here. A future method to trap all the organics produced might be developed to accurately measure total organic synthesis within the system. Overall, the results from this investigation act as groundwork to drive more focused experiments, such as a high pressure system, which might increase gas partial pressures, decreasing the reverse reactions and formaldehyde breakdown, or microfluidics which increases the surface area of precipitates to volume of fluids.

Chapter 5

Protometabolism in hydrothermal vents

5.1 Introduction

At the core of all living processes on Earth today are energy-releasing chemical reactions, and their main by-product is adenosine triphosphate (ATP). ATP is universally conserved across all life and drives core metabolic processes via phosphorylation and condensation reactions, it is therefore known as life's primary energy currency (Martin et al., 2014). It is, however, unlikely that ATP would have been present to carry out this role at the very origin of life, due to its complexity. Its synthesis and metabolic reactions depend on highly evolved enzymes. Therefore what molecules could have preceded ATP, and under what conditions did these first bioenergetic processes evolve?

Previous studies have tried to recreate phosphorylation and condensation reactions under prebiotic conditions to form polymers, such as polypeptides. In these previous studies reactions are driven by physical processes that bear little resemblance to modern cell processes. Some of these processes include high temperatures (Yamagata et al., 1991), low water activity (Morasch et al., 2014; Burcar et al., 2015), wet-dry cycles (DeGuzman et al., 2014), alternative solvents such as formamide (Costanzo et al., 2007), or highly reactive and geologically implausible abiological dehydrating agents such as cyanamide (Lohrmann and

Orgel, 1968; Liu and Orgel, 1997), carbonyl sulphide (Leman et al., 2004), or CO (Huber et al., 2003). The difficulty of getting condensation reactions to occur in water is such a big problem that some have made a suggestion for an origin of life on Mars, where there was less water (Benner, 2013).

The problem with these processes is they do not bear any resemblance to metabolic pathways used in cells today, in terms of substrates, catalysts, metabolic pathways or energy coupling (Sojo et al., 2016). If this was the case, and prebiotic chemistry was so very different from modern biochemistry, then cells must have developed completely different methods for metabolism at some stage in their evolution to explain this discontinuity from the origin of life to modern processes. Finding a link between modern biochemistry and prebiotic chemistry would seem to be a more logical way of predicting what processes could have driven phosphorylation and condensation reactions in a prebiotic system. A simpler precursor to ATP would be more analogous to modern systems than most of the alternative processes mentioned above.

If ancestral metabolic pathways are considered, along with corresponding geochemical environments, one plausible prebiotic precursor to ATP stands out; acetyl phosphate (AcP). This is a molecule that has been discussed by many previously as a possible prebiotic energy molecule (Decker et al., 1970; Hartman, 1975; de Duve, 1991). Phylogenetic studies suggest that the earliest cells were autotrophic, meaning that they generated both organics and energy needed for growth from simple inorganic molecules (Stetter, 2006; Martin and Russell, 2007; Say and Fuchs, 2010). There are six known carbon fixation pathways across all life, and acetyl coenzyme A (acetyl-CoA) is at the centre of metabolism in all of them (Fuchs, 2011). Of these six pathways, only the acetyl-CoA pathway is found in both primary domains of life, the bacteria and archaea. This suggests that a form of this pathway was present in their common ancestor (Sousa et al., 2013; Martin et al., 2014; Sojo et al., 2014; Sousa and Martin, 2014; Sojo et al., 2016). This pathway has other properties that make it plausible as an ancient metabolic pathway; it is a short, linear, and exergonic pathway, generating acetyl-CoA from simple starting compounds, such as H_2 and CO_2, and using enzymes that contain

Fe(Ni)S clusters with structures very similar to minerals such as greigite and mackinawite (Russell and Martin, 2004; Nitschke and Russell, 2013; Kim et al., 2013; Harel et al., 2014; Burcar et al., 2015). Cells that use this pathway, like all autotrophs, depend on an electrochemical ion gradient across their membrane to drive carbon fixation. The electrochemical circuit in this case is very simple, needing neither quinones nor cyctochromes (Buckel and Thauer, 2013).

As mentioned previously these factors point to the significance of the acetyl-CoA pathway, and its deep evolutionary origin (Fuchs, 2011; Sousa et al., 2013; Sousa and Martin, 2014; Martin et al., 2014). Four billion years ago, in the absence of oxygen, alkaline hydrothermal systems may have contained conditions analogous to those required to drive the acetyl-CoA pathway. Sulphur compounds, such as methyl sulphide (CH_3SH), may have been produced geochemically in hydrothermal vents systems, through serpentinisation, or through the reduction of CO_2 in the presence of hydrogen sulphide (as discussed in Chapter 4.1, Equation 4.1.4), and should have been more abundant in early Earth environments than today (Russell et al., 1994; Schulte and Rogers, 2004; Martin et al., 2008; Nitschke and Russell, 2009; Lane and Martin, 2012; Russell et al., 2014). It is interesting to note that CH_3SH is very readily oxidised today, and has not been detected experimentally so far in our hands, even in concentrated standards.

The acetyl-CoA thioester is a very complex molecule, and like ATP it probably arose later in biochemical history. A primitive, inorganically catalysed analogue of acetyl-CoA, methyl thioacetate (CH_3COSCH_3), has been proposed to occur within hydrothermal vents, synthesised from formate or CO (both occur at the same redox state so could be interchangeable as seen in Figure 4.14) and CH_3SH as starting products (Figure 5.1) (de Duve, 1988; Huber and Wächtershäuser, 1997; de Duve, 1991; Martin and Russell, 2007). When sulphur is included in thermodynamic simulations of H_2/CO_2 equilibria in hydrothermal systems, high concentrations of methyl sulphide are expected in the hydrothermal fluid (Schulte and Rogers, 2004). This contradicts the view that condensation reactions do not occur easily in aqueous environments, this could be due to

the thermodynamics and kinetic barriers that are present in the vent system. Sulphur compounds are thought to play a key role in abiotic organic synthesis in modern hydrothermal environments, and may also have been important in prebiotic systems (Wächtershäuser, 1990; de Duve, 1991). In addition to CH_3SH being present in the vents, it has been suggested there could have been some CO, as the first reduction step from CO_2, however, it also has the same redox state as formate (Seewald et al., 2006; Figure 4.14, shown in Chapter 4), suggesting they could have been interchangeable. Huber and Wächtershäuser (1997) investigated the transition metal sulphide-catalysed synthesis of acetyl thioesters. They were able to synthesise methyl thioacetate from CH_3SH and CO, in the presence of FeS, Fe(Ni)S or NiS clusters, similar to the reductive acetyl-CoA pathway.

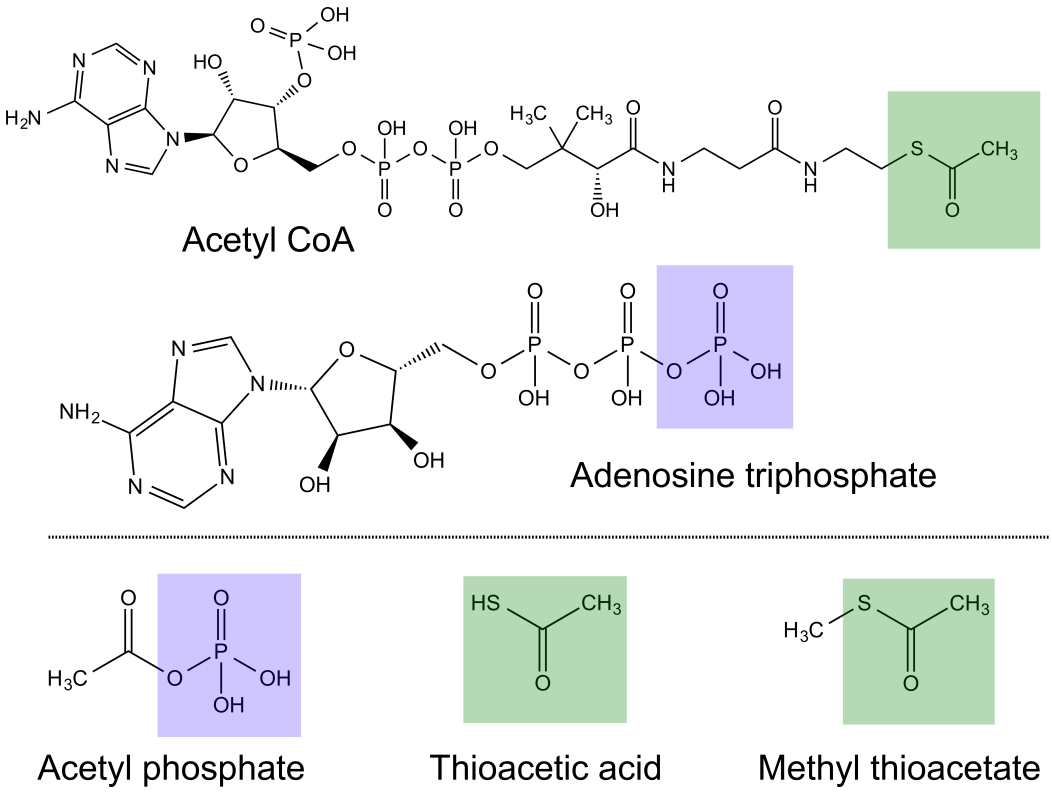

Figure 5.1. Molecular structures of key biotic and prebiotic molecules. Acetyl-CoA is the hub of metabolism in all six known pathways of carbon fixation. The important part of the molecule is the reactive thioester or thiol group (green shaded section) which has prebiotic analogues in methyl thioacetate and thioacetic acid. Adenosine triphosphate (ATP) is the universally conserved energy currency in modern metabolism; acetyl phosphate (AcP) could have been a simple precursor, driving similar reactions. The blue shading highlights equivalent phosphoanhydride bonds in both molecules.

Acetyl-CoA is a thioester, which is a class of energy-rich molecules that

have the ability to drive metabolic reactions when the thioester bond is broken. Acetyl-CoA can be phosphorylated to form acetyl phosphate (AcP), therefore the phosphorylation of simple thioesters should also take place to form AcP. de Duve (1991) proposed that along with the hydrolysis of the thioester bond in simple thioesters (producing free acetate), phosphorylation was also possible, leading to the formation of AcP and a free thiol.

Phosphate is a key element in biology, to the extent that the ratio of phosphorus to nitrogen and carbon are the limiting factors for growth in any ecosystem (Pasek and Kee, 2011; Gull, 2014). Activated phosphorus has specific chemical and physical features that make it important for life, in addition to its central role in bioenergetics, it has a specific role in nucleic acids where it can link two nucleotides and still ionise; the resulting negative charge both stabilises the diesters against hydrolysis, but also retains the molecules within a lipid membrane. Phosphate participates in nearly all biochemical functions, and no other residue appears to fulfil the multiple roles that it can take (Westheimer, 1987). The formation of phosphorylated biomolecules has been a major focus of origin of life research, due to its key importance in biochemistry and therefore prebiotic synthesis (Pasek and Kee, 2011; Kee et al., 2013). Phosphate could have been supplied to the oceans by a number of processes discussed in Chapter 1.4.2. The presence of inorganic phosphate and simple thioesters would enable the continuous synthesis of AcP within the alkaline vents.

AcP could then have driven prebiotic phosphorylations and condensations when its energy-rich phosphoanhydride bond is broken, in the same way that ATP does today. AcP is still used as an equivalent to ATP in some bacteria (Decker et al., 1970; Thauer et al., 1977). It is an excellent candidate as a source of primordial metabolic energy, phosphoryl donor, and acetyl donor for acetylation (Figure 5.1); it is chemically much simpler than ATP and has a higher phosphorylating potential (Martin and Russell, 2007).

Acetyl phosphate $\Delta G'_o = -43\ \mathrm{kJ\,mol^{-1}}$

ATP (to ADP) $\Delta G'_o = -31\ \mathrm{kJ\,mol^{-1}}$

These values are the standard free energy of the substrates at pH 7 and 1 M concentrations. The free energy can increase with displacement from equilibrium, in the case of ATP/ADP, the free energy is more than doubled in the negative direction. The same would be true to acetyl phosphate if there was a mechanism to push it far from equilibrium with acetate, for example high concentration of thioesters. Despite this AcP has been overlooked experimentally due to it being considered too unstable to persist for long enough to drive prebiotic chemical reactions, especially at either high or low temperatures and pH, both of which are found in hydrothermal vents (Barge et al., 2014). AcP has been used in the synthesis of more stable, but less reactive, products such as pyrophosphate (PPi), but not as an energy molecule itself (Barge et al., 2014; de Zwart et al., 2004).

In theory AcP should be reactive enough, due to its high energy phosphoanhydride bond, to facilitate metabolic-like reactions in aqueous conditions. In this study temperatures from $20 - 60\,^{o}$C and pH values from 6 to 12, which correspond to ranges found in alkaline hydrothermal vents, were considered in all experiments (Russell et al., 1994; Martin et al., 2008; Nitschke and Russell, 2009; Russell et al., 2014; Lane and Martin, 2012). As mentioned in Chapter 1.4, the vents would have been composed of a network of interconnected micropores, which had inorganic walls transecting hydrothermal fluids (pH 9 - 12) and ocean waters. The ocean waters would have been mildly acidic (pH 5 - 7) in the Hadean, due to higher levels of CO_2 (Pinti, 2005; Arndt and Nisbet, 2012). Mixing within the vent's microporous system occurs via thermal diffusion and convection, which is important for a number of reasons. Convective cycling means that products that form in cool, neutral conditions can cycle through warm, alkaline conditions, which would potentially drive other reactions, including simple hydrolysis (Braun and Libchaber, 2002). Organics might not always form in warm and strongly alkaline conditions, so cycling through cooler neutral pH, or mildly acidic areas is also important. Thermal cycling can concentrate small organics in cooler regions via a process known as thermophoresis (Braun and Libchaber, 2002). It has been shown that molecules as large as nucleotides, such as quinine or fluorescein, can be concentrated up to 5000-fold via thermophoresis in open hydrothermal systems

(Herschy et al., 2014). This could feasibly convert low yields (μM range) into high concentrations (high mM range), which would favour the polymerisation of amino acids and nucleotides (Baaske et al., 2007; Herschy et al., 2014). This process of concentration cannot be replicated for each experiment here, therefore relatively high concentrations of reagents were used in these experiments.

The aim of this chapter was to recreate simple metabolic reactions that could have taken place prebiotically in an alkaline hydrothermal vent setting, using compounds that have been synthesised by the reduction of CO_2 by H_2, and could have been present in alkaline hydrothermal vents 4 Ga. The order of experimentation was aiming to follow the predicted pathway thought to have occurred within the vent system:

1. The synthesis of methyl thioacetate, as a precursor to acetyl-CoA, from formate ($CHOO^-$) and methyl sulphide (CH_3SH), in the presence of FeS clusters as a catalyst. CO was used by Huber and Wächtershäuser (1997) to synthesise methyl thioacetate, and similar methods of detection were were used in this investigation. However, in this study formate, instead of CO, was used as the carboxylating agent, due to it having the same redox state as CO, and it being produced as a step in the reduction of CO_2 by H_2 (Herschy et al., 2014 detected formate and not CO in this reduction step), it could also have been a more viable molecule to have occurred in the vent setting, due to it being the 'hydrated' form of CO, therefore more likely to be produced in an aqueous setting.

2. The synthesis of AcP under ambient or mild hydrothermal conditions, from simple precursors of acetyl-CoA such as, methyl thioacetate (CH_3COSCH_3), or thioacetetic acid (CH_3COSH) with inorganic phosphate. Thioacetic acid was chosen as an alternative to methyl thioacetate, when AcP was not successfully produced using methyl thioacetate. Thioacetic acid is suggested to have occurred by carbonylation of methyl sulphide on a catalytic surface of (Ni,Fe)S as proposed by Huber and Wächtershäuser (1997) (Figure 5.2). It is therefore considered to be a valid thiol to have occurred in alkaline

hydrothermal vents, and is more reactive than methyl thioacetate due to $-SH$ being a better leaving group compared to $-SCH_3$.

3. Once AcP had been synthesised the aim was to see if it could imitate some of the functions of ATP in water, acting as an energy currency as ATP does today. The formation of nucleosides from their simple building blocks, a sugar and a base, was investigated to see if AcP could act as an activated phosphate group to enable this formation. The phosphorylation of nucleotide precursors under a range of alkaline hydrothermal conditions was a another logical consideration to help answer the question of AcP's ability to act as an energy currency molecule. The ability of AcP to drive condensation reactions in water, was also investigated by other members of the group. The purpose of these experiments was to assess if AcP was able to act as a prebiotic mimetic to ATP, the energy currency of all extant life. If AcP can act as an energy currency it could be an ideal link between prebiotic chemistry and biochemistry.

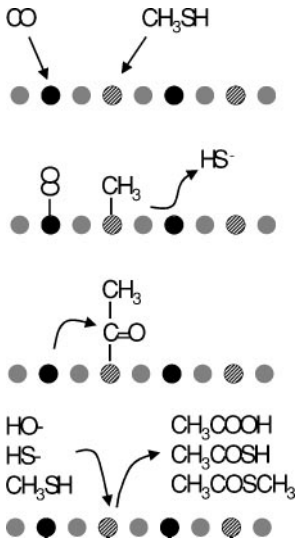

Figure 5.2. A schematic representation of the reaction between methyl sulphide (CH_3SH) and carbon monoxide on a NiS-FeS catalytic surface as proposed by Huber and Wächtershäuser (1997). A methyl group from methyl sulphide is transferred to a nickel atom and carbon monoxide to an iron atom. Carbonyl insertion leads to the formation of the nickel-bound acetyl group. Nucleophilic attack by either hydroxyl, bisulphide, or methyl sulphide yields acetic acid, thioacetic acid, or methyl thioacetate respectively. Image taken from Cody (2004).

One consideration when planning these experiments was the lack of pressure. As mentioned Chapter 4, Le Chatelier's principle states that a shift in pressure or volume will shift the equilibrium of the system (Le Chatelier and Boudouard, 1898). Overall, pressure should increase reaction rates and the potential for reactions to take place. To overcome the lack of pressure the concentration of reactants used was very high in the hope this would increase reaction efficiencies.

5.2 Formation of methyl thioacetate

For this study experiments were designed to investigate the synthesis of methyl thioacetate, similar to one experiment carried out by Huber and Wächtershäuser (1997). Experiments attempted to synthesise methyl thioacetate under mild hydrothermal conditions (50 - 80 °C, various pH conditions) from methyl sulphide and formate (as apposed to CO) in the presence of FeS and NiS catalysts.

Acetanilide was the detection product, which is produced when aniline reacts with acetic acid (Figure 5.3). Acetic acid is produced as methyl thioacetate is hydrolysed, therefore can be used as a detection product of methyl thioacetate. This method was used by Huber and Wächtershäuser (1997), and they were able to detect 7 - 9 μM of methyl thioacetate after 20 hours at pH 1.6.

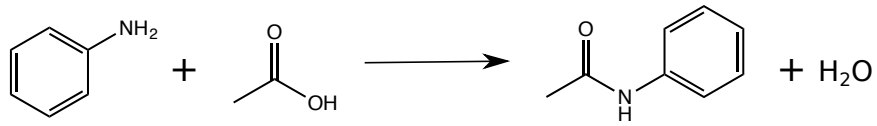

Figure 5.3. Reaction of aniline with acetic acid (produced when methyl thioacetate hydrolyses) to produce acetanilide and water.

In this study it was thought acetanilide was detected after 6 hours at 80 °C and pH 5 (very acidic conditions is what Huber and Wächtershäuser used, however a more moderate acidity was thought more plausible, reflecting ocean acidity convecting through alkaline vents), with both FeS and NiS catalysts, and quantified by HPLC (Figure 5.4). However, it was subsequently discovered that formanilide (formate reacting with analine) had the same elution time as acetanilide, which was 6 minutes (with the steeper gradient of H_2O:ACN used

initially, detailed in Methods Chapter 2.3). This was discovered when the reaction was carried out with sodium formate (CHOONa) and aniline as a negative control, where a peak was seen eluting at the same time as the acetanilide standards (Figure 5.5). The results were very similar in this negative control as to when the reaction was carried out in the presence of methyl sulphide, suggesting the compound seen was not the product of interest, acetic acid, reacting with aniline to produce acetanilide, but the reactant, formate, reacting with aniline to produce formanilide.

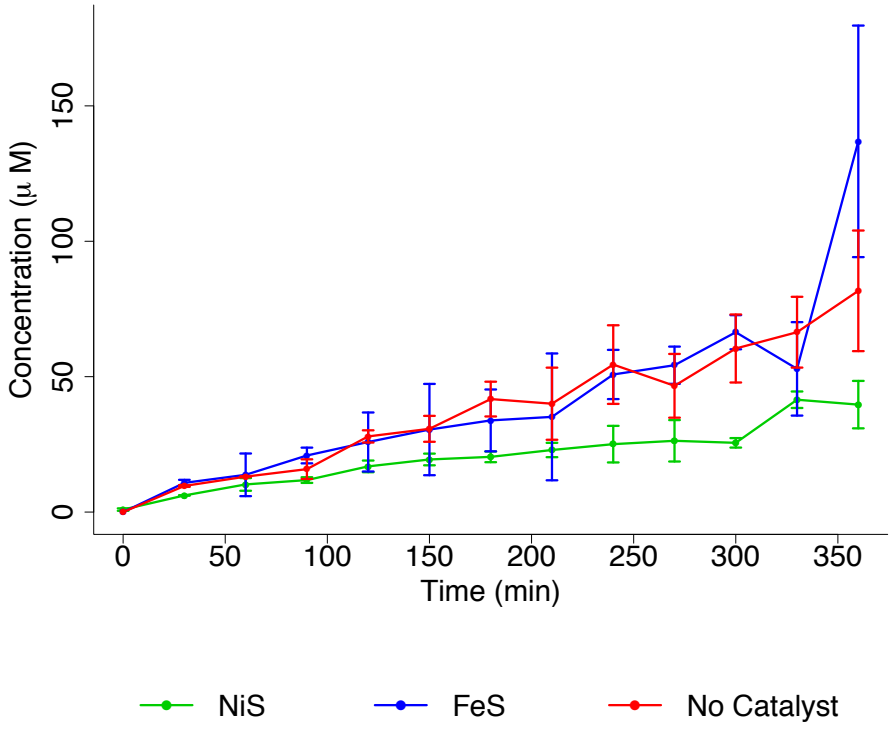

Figure 5.4. Acetanilide, as a measure of methyl thioacetate, production over time at 80 °C, pH 5. Measured by HPLC with NiS catalyst, FeS catalyst and no catalyst. Concentrations were calculated from standard calibration curve for acetanilide. It was later found out this was actually formanilide and probably not acetanilide. N = 3 ±SD.

Subsequent separation of formanilide and acetanilide detection, developed with a shallower solvent gradient on the HPLC (detailed in Chapter 2.3), enabled a better understanding of whether formate was reacting with aniline and if there was any methyl thioacetate being produced. Acetanilide eluted at 3.6 minutes

and formanilide at 3.5 minutes. This was the best separation that was achieved with the HPLC used, which is still not a good separation distance to accurately differentiate between the two compounds. Methyl thioacetate standards were also detected by HPLC (4.7 minutes), enabling multiple analysis assays to be developed (Figure 5.6).

The experiment was conducted at pH 5 with all the different catalytic conditions at once (No catalyst, FeS, NiS, and Fe(Ni)S), and samples were taken at 0 minutes and 5 hours. Parallel experiments were run with aniline to look for acetanilide, and without aniline too look for methyl thioacetate alone. Figure 5.7 shows the HPLC traces for no catalyst and FeS catalyst, at 0 and 5 hours. Figure 5.8 shows traces for NiS and Fe(Ni)S catalysts, at 0 and 5 hours. No acetanilide was detected when aniline was added, only formanilide at 3.5 minutes. When aniline was not added no methyl thioacetate was detected either, only methyl sulphide at 4 minutes (HPLC traces show no peak for methyl thioacetate at 4.7 minutes when no aniline was added, and traces were equivalent to the previous two figures so are not shown here).

The experiment was repeated three times each at pH 10 and pH 2, both with and without aniline added. Again no acetanilide or methyl thioacetate was detected with any catalytic conditions, only formanilide or methyl sulphide (results were equivalent to those seen at pH 5, wth no peaks identified for the analytes of interest. All graphs were similar to Figures 5.7 - 5.8, so are not shown here).

Detection of acetic acid and methyl thioacetate standards by GC-MS head-space was possible, but it was hard to distinguish between the compounds, as they eluted so closely together in time. Detection of any products in the experimental samples was not observed. Detection by GC-MS liquid injection for the standards was not very sensitive (possibly due to extraction not being effective enough at such low concentrations). After consideration of multiple methods of detection, this experiment was abandoned as the detection methods used did not yield any product, and it was decided that time could be spent more productively developing different experiments.

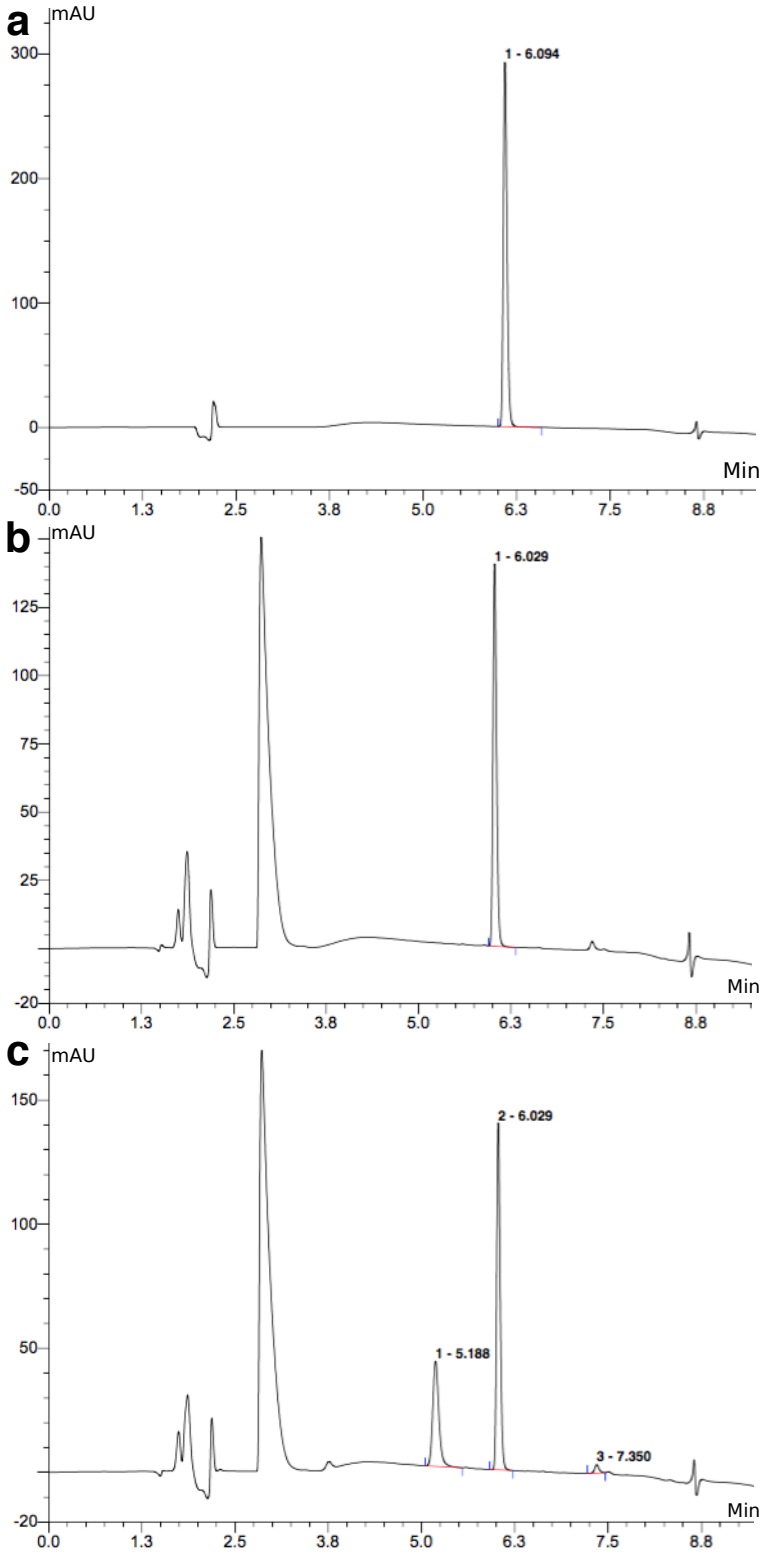

Figure 5.5. HPLC traces for standards of formate and acetanilide to compare to experimental sample, all at 80 °C and pH 5, using initial steeper solvent gradient on the HPLC. **(a)** HPLC trace for formate (CHOONa) with aniline as a control after 6 hours; formanilide product eluting at 6 minutes. **(b)** HPLC trace for 100 μM acetanilide standard, elutes at 6 minutes (large peak at 2.6 minutes is aniline). **(c)** HPLC trace for experimental sample after 6 hours, also see peak at 6 minutes indicating formanilide production, as the formate reagent is reacting with the aniline. Peak at 5.1 minutes is methyl sulphide.

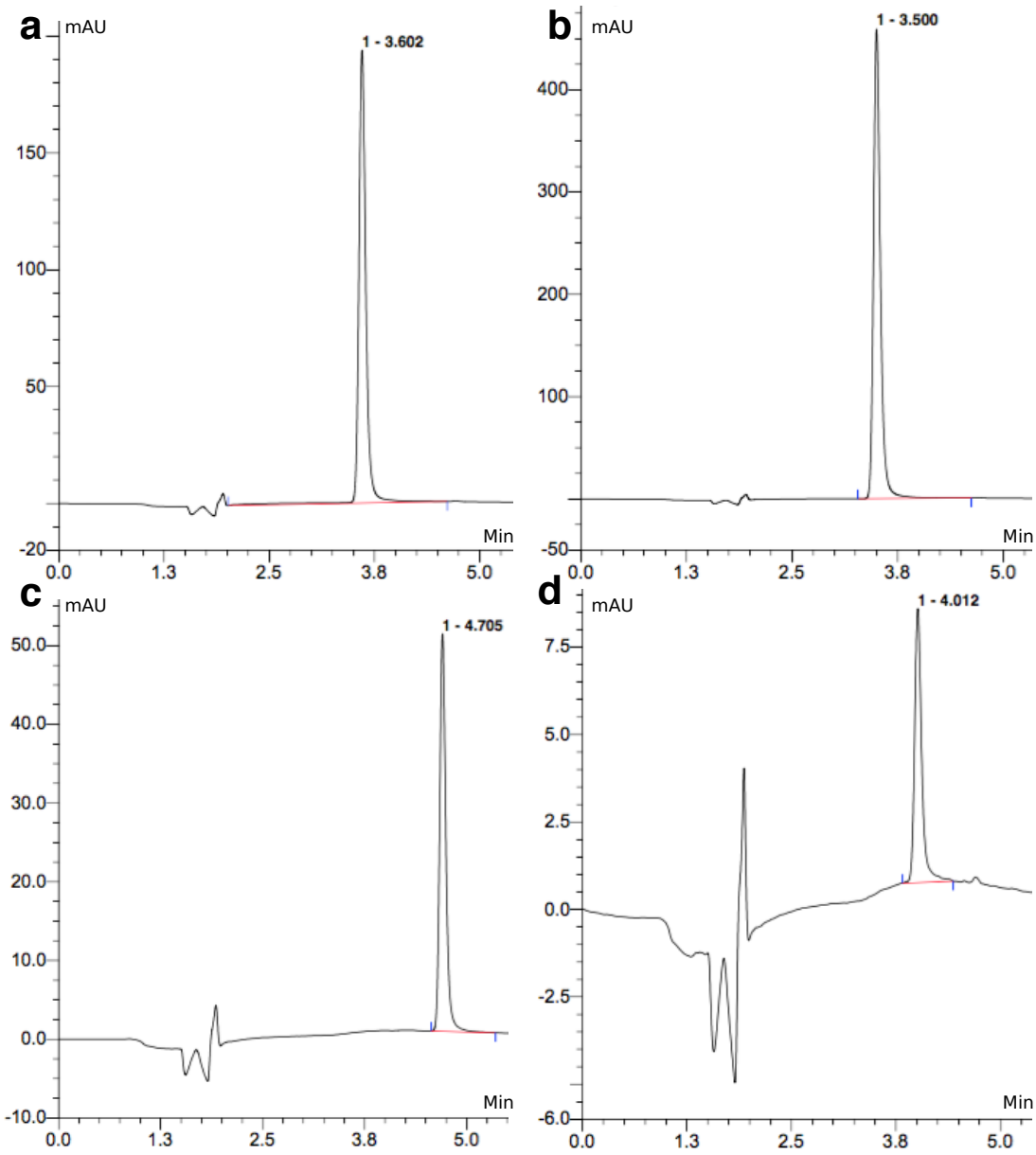

Figure 5.6. HPLC traces for standards using shallower solvent gradient. **(a)** Acetanilide (100 μM) elutes at 3.6 minutes. **(b)** Formanilide (100 μM) elutes at 3.5 minutes. **(c)** Methyl thioacetate (100 μM) elutes at 4.7 minutes when no aniline is added. **(d)** Methyl sulphide (1 mM) elutes at 4 minutes.

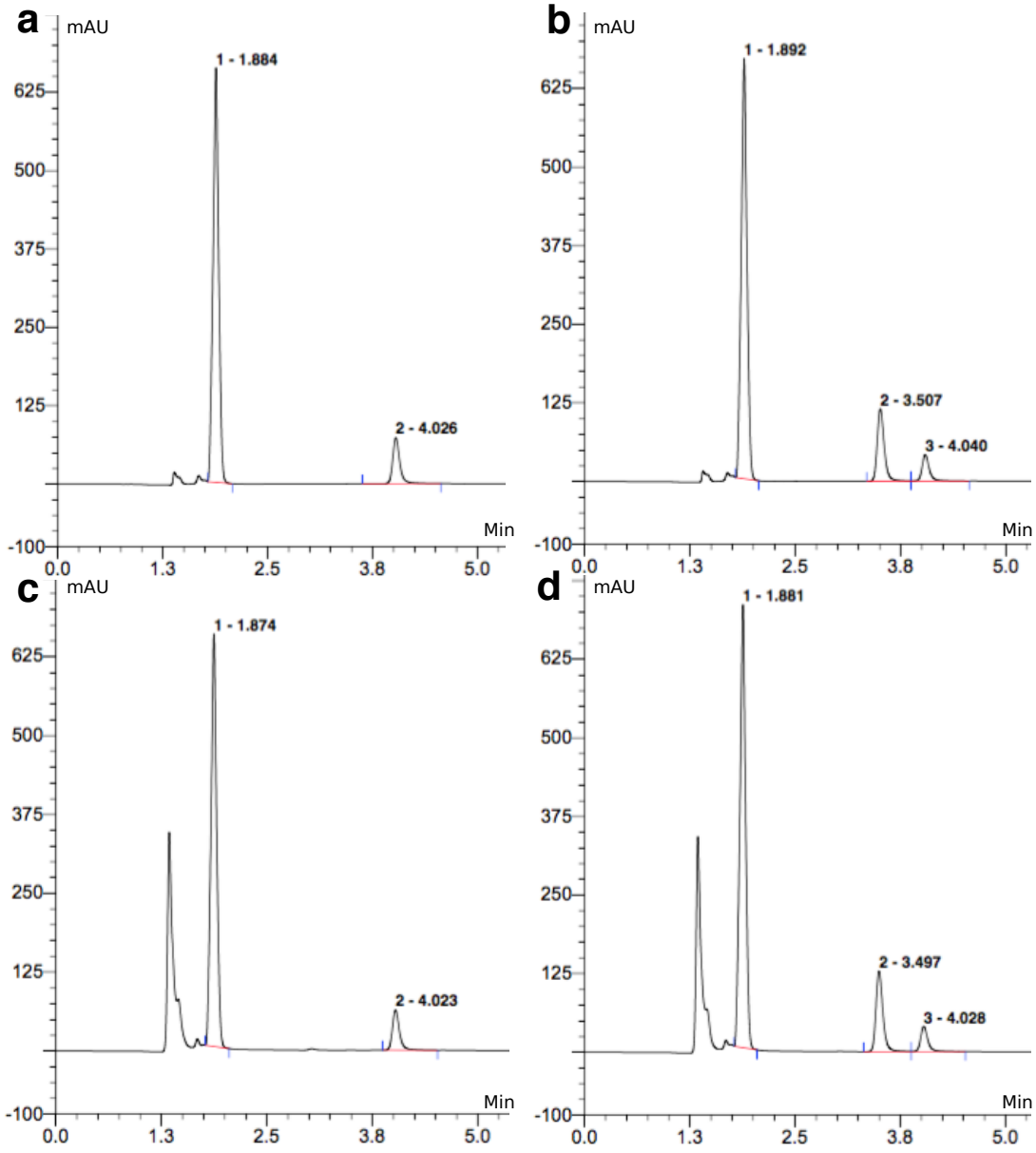

Figure 5.7. HPLC trace for experiment at pH 5, 80 °C, with aniline added to look for acetanilide. No catalyst and FeS experiments. **(a)** No catalyst at 0 minutes. **(b)** No catalyst at 5 hours. **(c)** FeS at 0 minutes. **(d)** FeS at 5 hours. Aniline eluted at 1.8 minutes, formanilide at 3.5 minutes and methyl sulphide at 4 minutes.

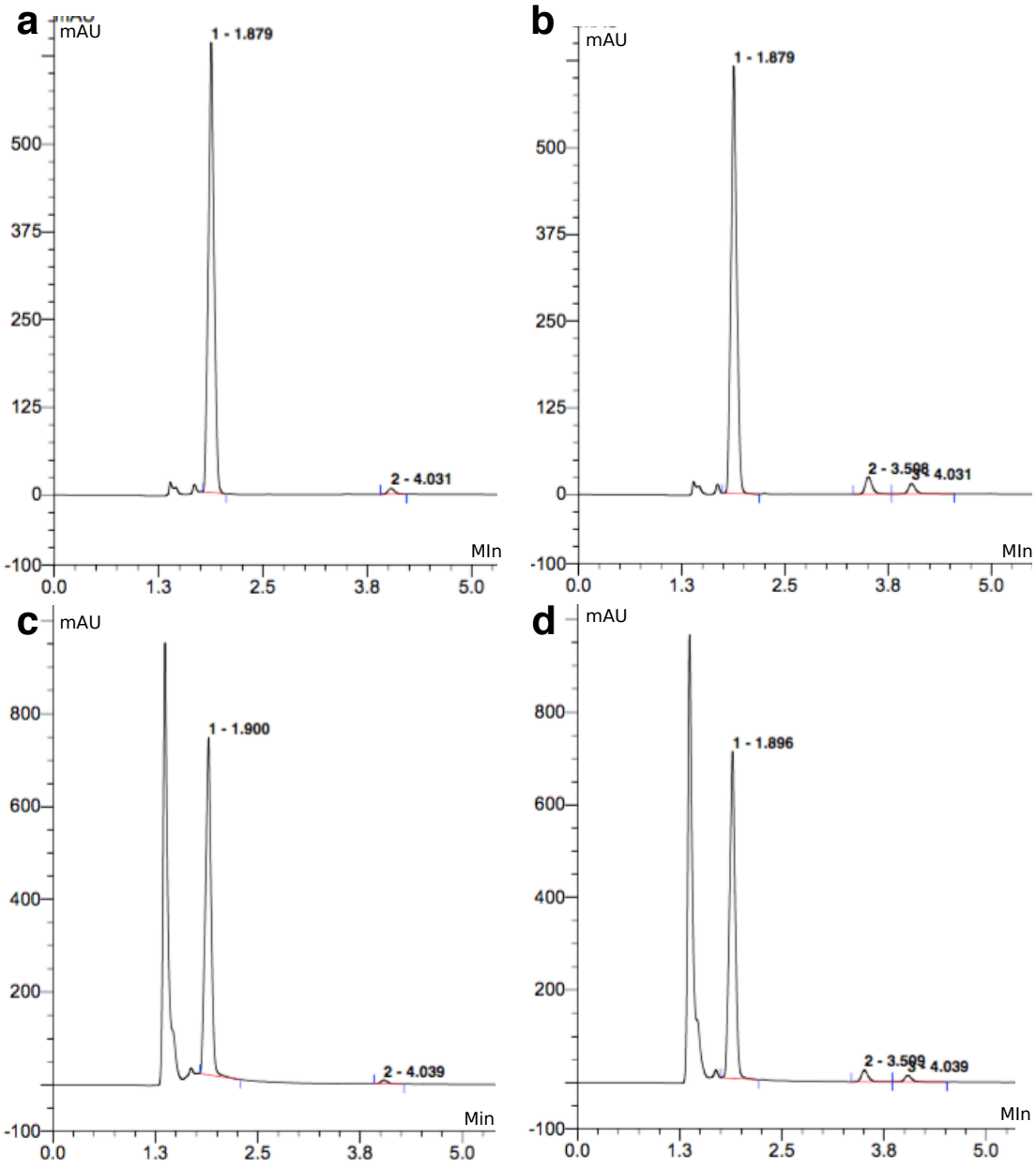

Figure 5.8. HPLC trace for experiment at pH 5, 80 °C, with aniline added to look for acetanilide. NiS and Fe(Ni)S experiments. **(a)** NiS at 0 minutes. **(b)** NiS at 5 hours. **(c)** Fe(Ni)S at 0 minutes. **(d)** Fe(Ni)S at 5 hours. Aniline eluted at ∼1.89 minutes, formanilide at 3.5 minutes and methyl sulphide at 4 minutes.

5.3 Synthesis of acetyl phosphate

Initial experiments investigated the synthesis of AcP by phosphorylating methyl thioacetate in the presence of inorganic phosphate. The reaction was attempted at pH 6, 7 and 8, at 50 °C and 20 °C, with three repeats per pH condition, however, no AcP was detected after 5 hours. Experiments were carried out alone or with Mg^{2+} and Ca^{2+} ions, due to their importance in cells today, (20 mM or 2 mM) added either together or separately as catalysts. Figure 5.9a shows the $^{1}H-NMR$ traces for all time points when the reaction was conducted using 20 mM with both catalysts at 50 °C; no AcP peak is seen at 2.11 ppm at any time point. Figure 5.9b shows the $^{1}H-NMR$ traces for all time points when the reaction was conducted using 2 mM with both catalysts at 20 °C; again no AcP peak is seen at 2.11 ppm at any time point. All other experiments (no catalysts, Mg^{2+} and Ca^{2+} ions added together or separately, and both 50 °C and 20 °C) showed similar traces to this, with no AcP detected at 2.11 ppm.

Because AcP was not synthesised from methyl thioacetate under the conditions tested the simpler activated thiol, thioacetic acid (CH_3COSH), was chosen as a potentially reactive alternative (as mentioned in the Introduction, investigation plan). With thioacetic acid as the reactive thiol, yields of up to 2 % AcP were detected within 1 - 2 hours, with yields being dependant on pH, temperature, and ions present. Under mildly acidic conditions and cooler temperatures (pH 6, 20 °C), equimolar mixtures of Ca^{2+} and Mg^{2+} ions promoted AcP synthesis, compared with no ions (Figure 5.10a). Under more alkaline conditions $Ca^{2+}$and Mg^{2+} ions together lowered the AcP synthesis, because Ca^{2+} precipitated out the phosphate, meaning it was no longer available for AcP formation (Figure 5.10b and c). Mg^{2+} alone precipitated relatively little phosphate below pH 11, and doubled yields of AcP under neutral or mildly alkaline conditions, presumably by promoting the synthesis of AcP (Figure 5.10d – f). AcP was formed at barely detectable concentrations, or not at all, at pH 11, even in the presence of Mg^{2+} ions at 20 °C (Figure 5.11) Experiments at pH 11 and 50 °C were not carried out, due to the fact that AcP was degraded very quickly at the more

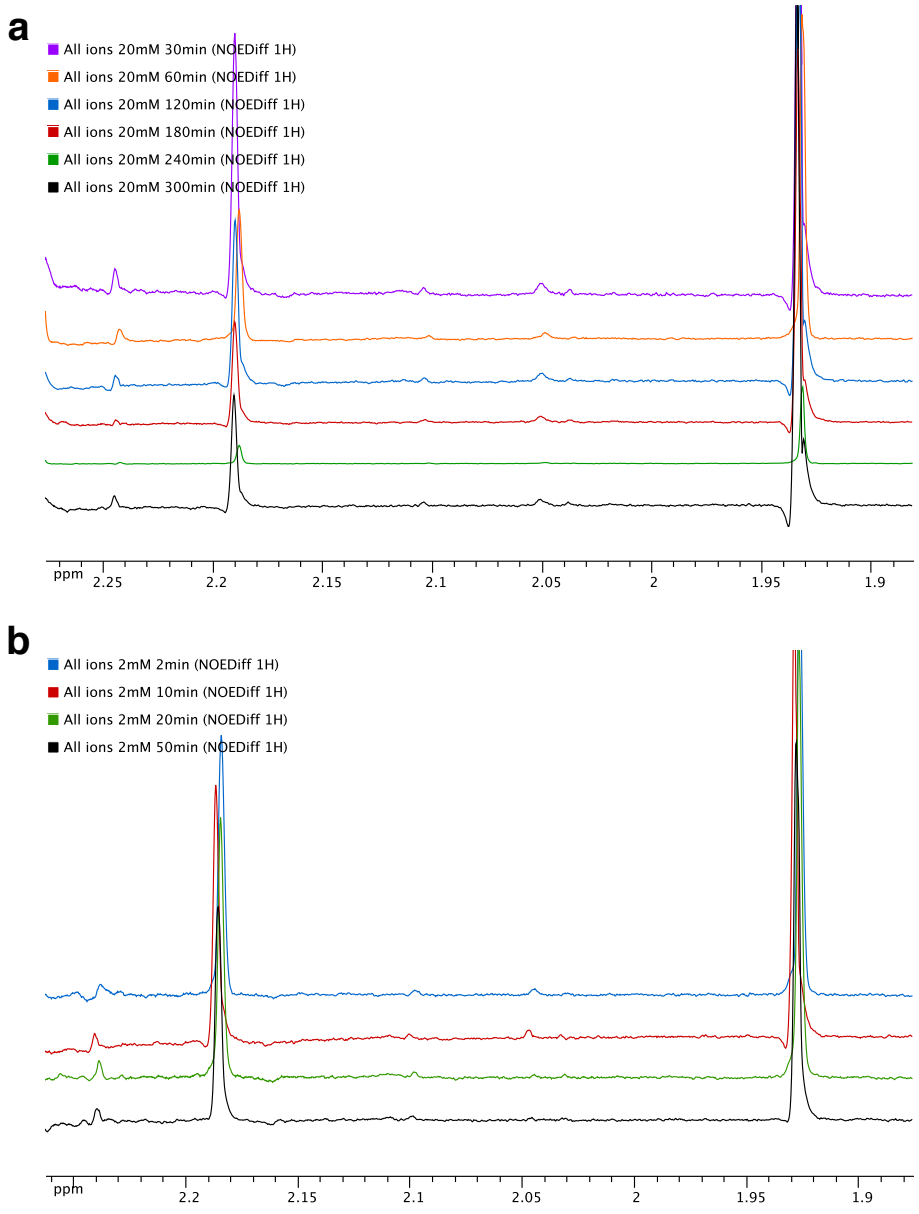

Figure 5.9. ^{1}H−NMR trace (600 Hz) of samples from reaction between methyl thioacetate and inorganic phosphate, in the presence of both Mg^{2+} and Ca^{2+} ions at 50 °C and 20 °C. **(a)** Experiment conducted at pH 7 at 50 °C, with 20 mM of both catalysts added, samples taken at 30, 60, 120, 180, 240 and 300 minutes. **(b)** Experiment conducted at pH 7 at 20 °C, with 2 mM of both catalysts added, samples taken at 2, 10, 20 and 50 minutes. Samples were analysed for AcP, which has a peak at 2.11 ppm. There is a very small peak at 2.10 ppm, however it is not large enough to quantify and is assumed to be an artefact of the trace not the presence of AcP, due its appearance and disappearance at different time points.

ideal pH conditions, and even at pH 8 the synthesis of AcP was very low at 50 °C, therefore it was assumed that the production at pH 11 at 50 °C would be even lower than at 20 °C. When Ca^{2+} ions were used alone they interfered with NMR measurements, producing a very noisy trace, therefore the results were thought to not be representative of the actual AcP production (Figure 5.12). The results had much greater variation within experiments (large error bars) and apparently produced a much higher concentration than Mg^{2+} ions alone, which also contradicts what was seen when the ions were used together, where Ca^{2+} ions reduced the production of AcP.

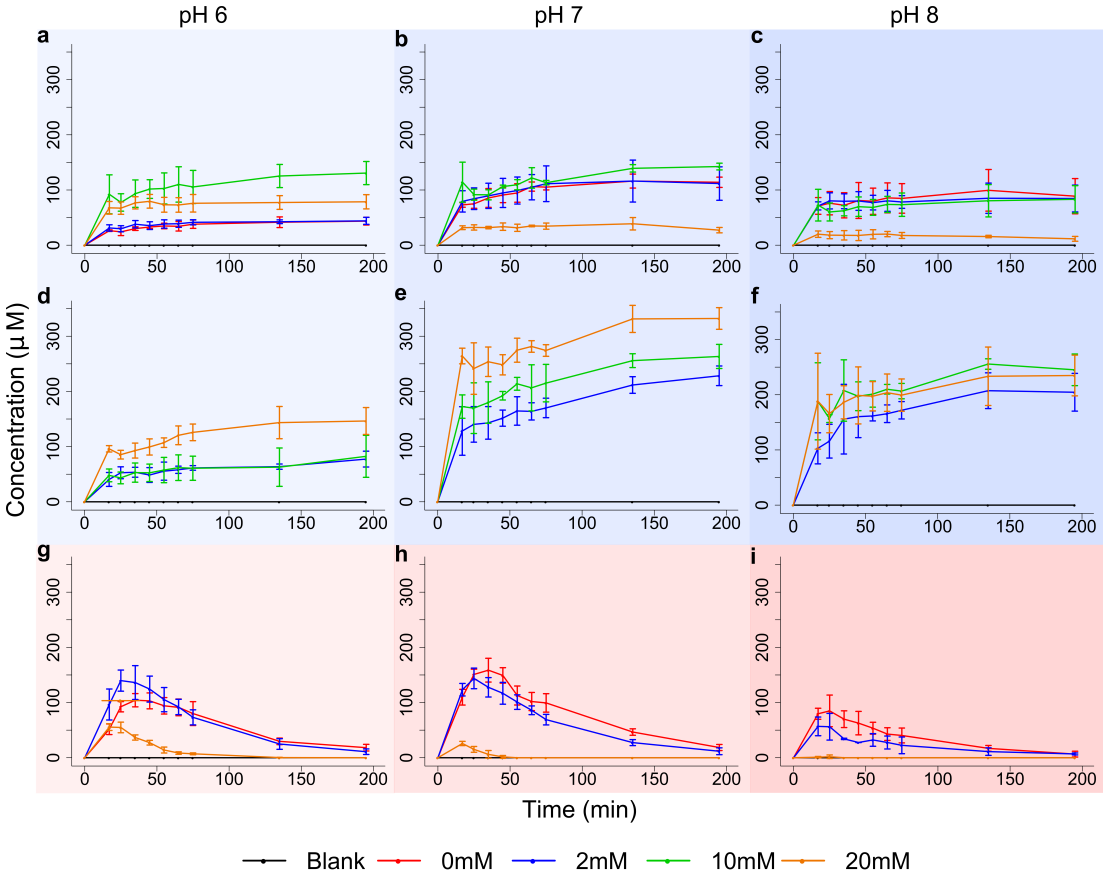

Figure 5.10. Synthesis of AcP from thioacetic acid and inorganic phosphate at pH 6, 7 and 8, at either 20 °C or 50 °C. **(a – c)** AcP synthesis at pH 6, 7 and 8, respectively, with equimolar concentrations of Ca^{2+} and Mg^{2+} ions; 0, 2, 10 or 20 mM of Ca^{2+} plus the same of Mg^{2+}, at 20 °C. **(d – f)** Mg^{2+} ions alone, 2, 10 and 20 mM, at 20 °C. **(g – i)** Equimolar concentrations of both Ca^{2+} and Mg^{2+} ions; 0, 2, 10 and 20 mM of Ca^{2+} plus the same of Mg^{2+}, at 50 °C. N = 3 ±SD.

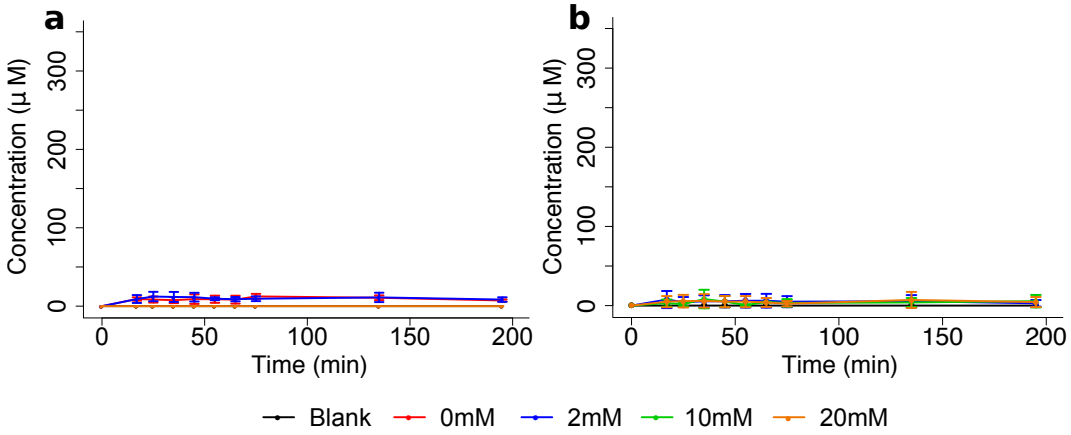

Figure 5.11. Synthesis of AcP from thioacetic acid and inorganic phosphate at pH 11 at 20 °C. **(a)** AcP synthesis in the presence of Ca^{2+} and Mg^{2+} ions; 0, 2, 10 or 20 mM of Ca^{2+} plus the same of Mg^{2+}, (N = 3 ±SD). **(b)** Mg^{2+} ions alone; 0, 2, 10 or 20 mM, (N = 2 ±SD).

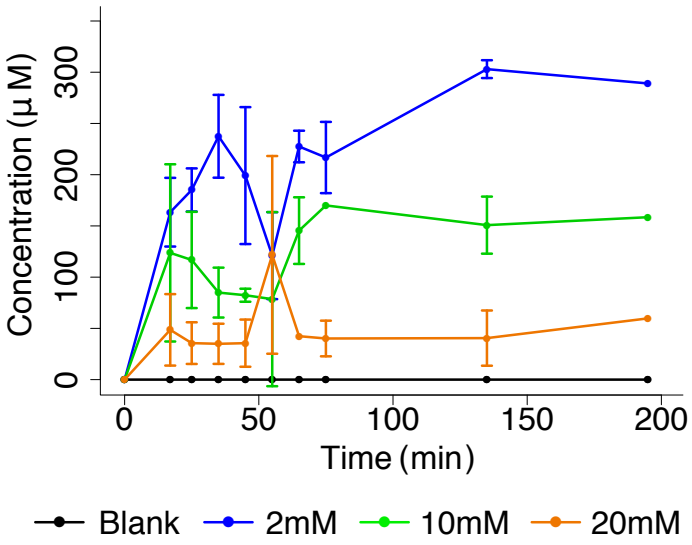

Figure 5.12. Synthesis of AcP from thioacetic acid and inorganic phosphate with Ca^{2+} ions alone, 2, 10 and 20 mM, at pH 7 and 20 °C. Ca^{2+} ions interfered with the NMR magnetism, producing a very noisy trace, resulting in seemingly very high concentrations of AcP synthesis with this catalyst. N = 3 ±SD.

Previous work has suggested that iron is the most predominant catalyst in the Archaean ocean, showing that Fe^{2+} ions had major effects on metabolite stability and increased reaction rates and efficiency (Keller et al., 2014). AcP synthesis was therefore simulated in anaerobic conditions, with Fe^{2+} ions added to the same reaction method carried out previously. The results did not indicate any significant difference in AcP production in the presence or absence of Fe^{2+} at any concentration (Figure 5.13a). The overall concentration of AcP produced was slightly higher than from previous experiments (Figure 5.10), but this cannot be stated as conclusive as the NMR detection can vary over time. Controls carried out in aerobic conditions at the same time (Figure 5.13b) suggested that the sensitivity may have increased, explaining the increase in detected AcP. It is therefore assumed that Fe^{2+} ions had no significant affect on AcP production rate or concentration.

To investigate the effect of oxic or anoxic conditions on the reactivity of thioacetic acid, the experiment was run with no ions present in aerobic and anaerobic conditions in parallel. There was no significant difference between the concentrations of AcP synthesised in either environment, indicating that thioacetic acid is equally reactive in anoxic conditions as oxic (Figure 5.13b).

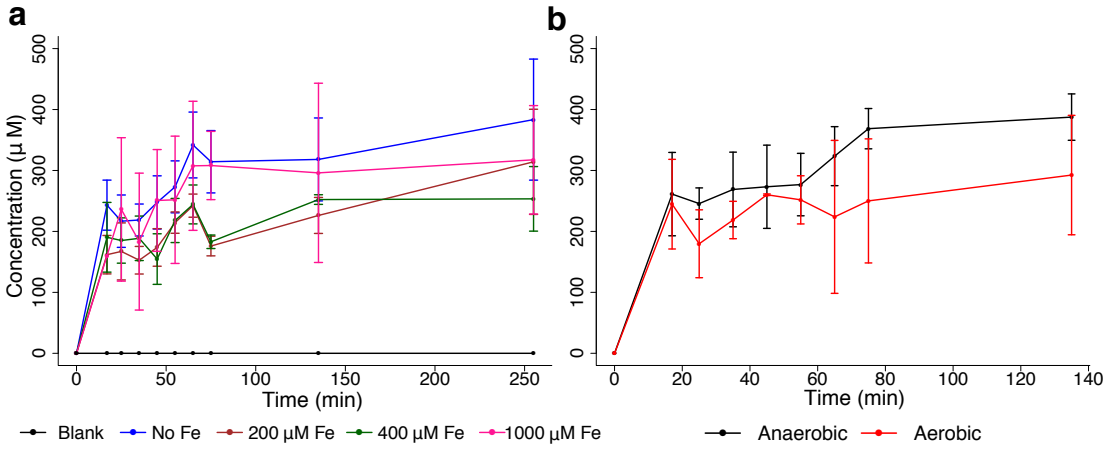

Figure 5.13. Synthesis of AcP from thioacetic acid and inorganic phosphate in the presence of Fe^{2+} ions, and a comparison of anaerobic and aerobic conditions at pH 7 and 20 °C. **(a)** Anaerobic experiments carried out in the presence of different concentrations of Fe^{2+} ions (0, 200, 400 and 1000 μM). In the absence of thioacetic acid no AcP was produced. **(b)** Anaerobic and aerobic conditions with no ions present. N = 3 ±SD.

AcP is surprisingly stable at ambient temperatures, with around 20 % hydrolysed over 5 hours at 20 °C under all pH conditions tested; 7, 9 and 11 (Figure 5.14). The rate of hydrolysis was highly dependant on temperature; AcP was completely hydrolysed within 3 - 5 hours at 50 °C, and within 1 hour at 60 °C. This can also be seen in the balance between AcP synthesis and hydrolysis, shifting towards hydrolysis at higher temperatures, which was observed in the synthesis experiments conducted at 50 °C (Figure 5.10g-i). Although the initial rate of synthesis was slightly faster in these experiments, AcP was almost completely hydrolysed within 3 hours, especially under mildly alkaline conditions (pH 8; Figure 5.10i). In contrast, pH had surprisingly little effect at any temperature on pure AcP degradation (Figure 5.14). In the presence of Mg^{2+} (Figure 5.14b) and Ca^{2+} (Figure 5.14c) ions also had little effect, slightly speeding the initial rate of hydrolysis at both 20 °C and 50 °C, but not changing the overall proportion hydrolysed over 5 hours. At 60 °C degradation was the same in all conditions; AcP was fully degraded within 1 hour.

5.4 Phosphorylation reactions with acetyl phosphate

5.4.1 Synthesis of adenosine

Preliminary tests were carried out to see if nucleosides could be formed from their building blocks; a sugar, a base and an activated phosphate group, such as AcP. Previously Cafferty et al. (2016) showed they were able to form glycosidic linkages with melamine and barbituric acid with ribose and ribose-5-phosphate in water to produce nucleosides and nucleotides in good yields. Adenine was used here as the base given its significant relevance to AMP and to RNA synthesis, as well as its close association to ATP. Adenine was added to ribose in the presence of AcP, which would act as both the phosphate donor and the source of energy to drive the reaction, at pH 7, 9 and 11 at 20 °C and 50 °C. No peaks for adenosine or AMP where seen in any of the pH or temperature conditions (Figure 5.15, which

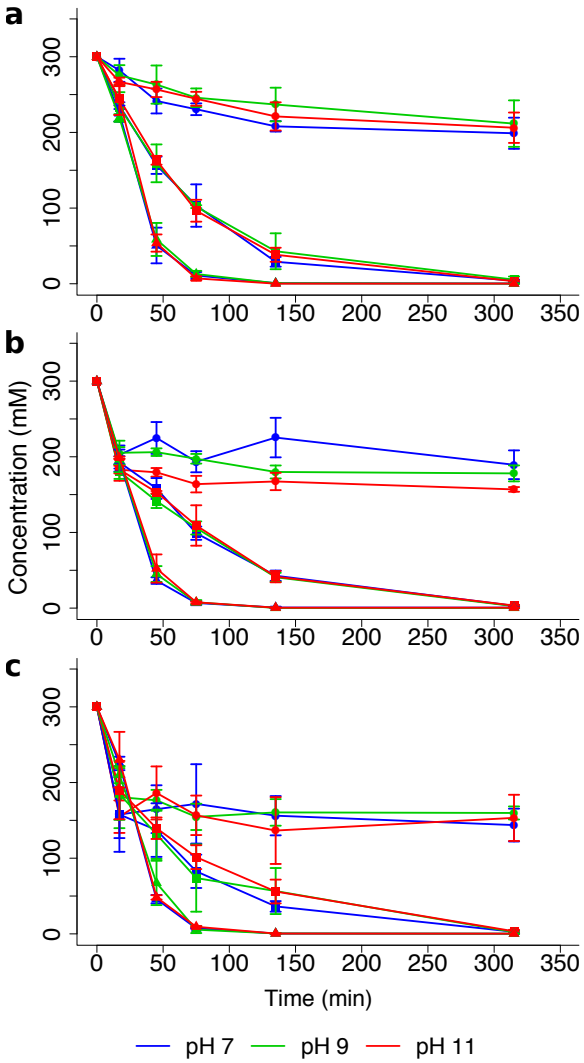

Figure 5.14. Degradation profile for AcP over 5 hours with and without ions at pH 7, 9 and 11, at 20 °C (circles), 50 °C (squares) and 60 °C (triangles). **(a)** no metal ions added to the reaction. **(b)** with 20 mM Mg^{2+} ions added. **(c)** with 20 mM Ca^{2+} ions added. N = 3 ±SD.

shows an example of the HPLC traces for the experiment conducted at pH 7 at 20 °C. All the other conditions produced similar traces with no peaks).

The reaction was also conducted by adding adenine at pH 11 drop-wise into the ribose solution at pH 7, in this way hoping to create a pH gradient (although neutralised instantly) that could drive the reaction. A transient pH gradient was thought to increase the likelihood of the reaction occurring due to the sugar needing to be in the linear form as this enables the aldehyde group to be open to attack, which only occurs at neutral to acidic pH, and the phosphorylation being more likely to occur at alkaline pH, as the base would have a lone pair on one of

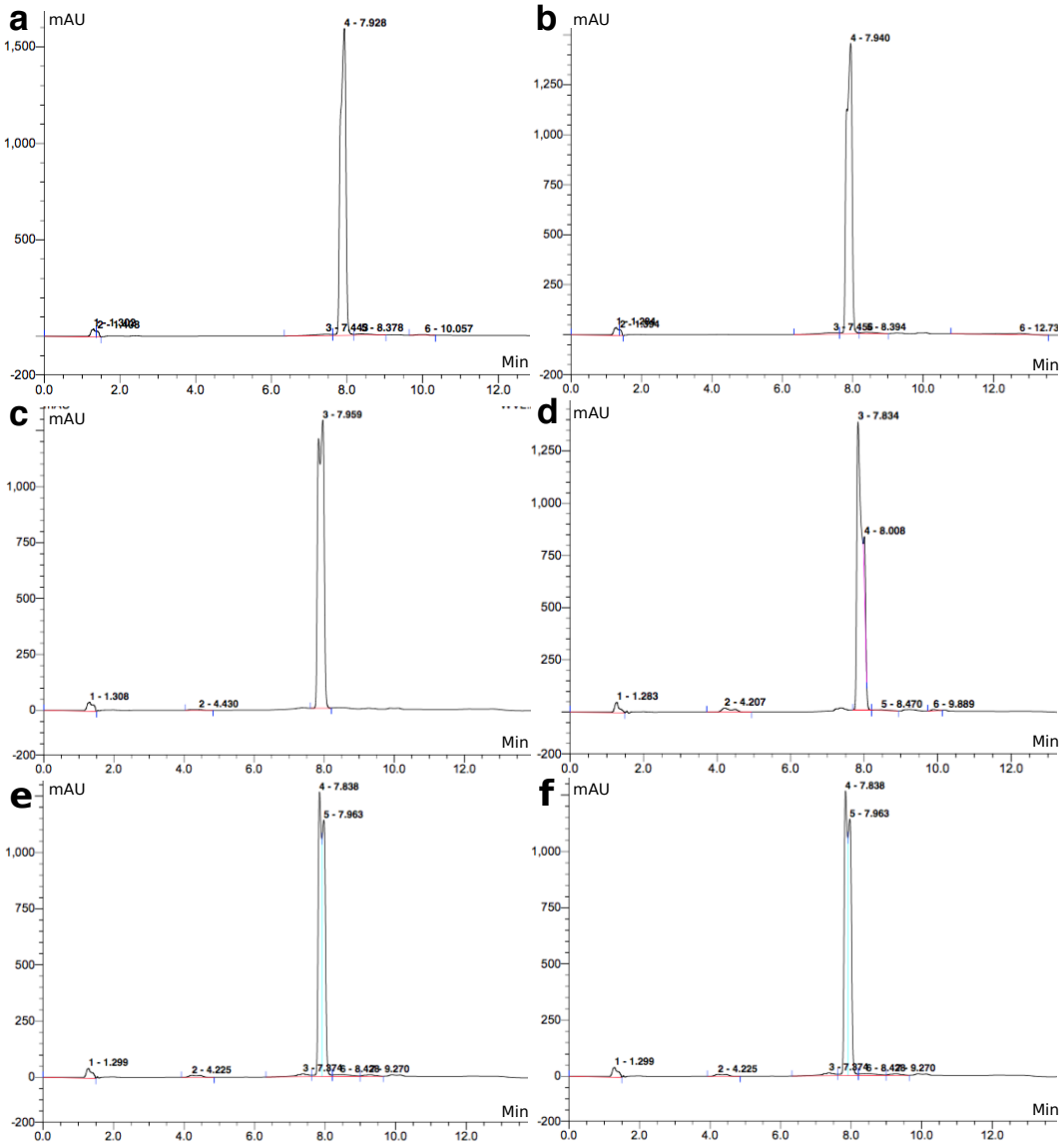

Figure 5.15. HPLC traces for experiment reacting adenine with ribose in the presence of AcP, at pH 7 and 20 °C. **(a)** Sample taken at 0 hours. **(b)** Sample taken at 1 hour. **(c)** Sample taken at 5 hours. **(d)** Sample taken at 24 hours. **(e)** Sample taken at 48 hours. **(f)** Sample taken at 6 days. No peak seen on the HPLC trace at 10.8 minutes for adenosine or 4.2 minutes for AMP. All three repeats and subsequent experiments at pH 9 and 11, all at 20 °C and 50 °C produced no peaks, and had traces similar to the examples shown here. The peak seen at 7.9 minutes in all traces was adenine.

the carbons (Figure 5.16). This would allow the base to react with the carbonyl of ribose-5-phosphate (Russell, 2011) This was carried out in the presence of Mg^{2+} ions to see if this increased the rate and concentration of products. In all cases no adenosine or adenosine monophosphate (AMP) was detected by HPLC (traces showed no peak, as seen in the example shown in Figure 5.15); either the reaction

did not occur or the detection method was not sensitive enough.

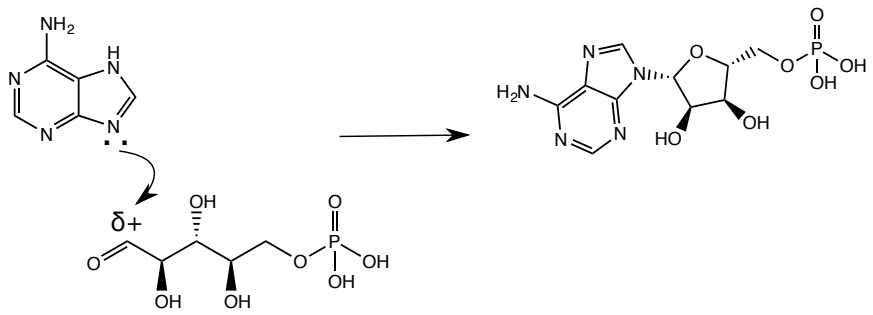

Figure 5.16. The interaction between adenine and ribose-5-phosphate in alkaline conditions, producing adenosine monophosphate (AMP).

These same experiments were carried out using ribose-5 phosphate (instead of ribose) with adenine, at constant pH (no drop-wise addition) to see if the phosphate group would enable the coupling of the base to the sugar. Again this was carried out in the presence of AcP to act as the phosphorylating agent. Analysis was carried out by LC-MS, however, the peak separation between reagents and products was very poor. A small amount of adenosine was detected, but with little or no significant increase over time (Figure 5.17). Repeats did not show a good correlation between runs, with large error bars between the three repeats for each pH condition (pH 5, 7, 9 and 11 tested). Even with such large error bars there seems to be an identifiable difference between pH 5 and pH 11, this however, may be a artefact of the instrument. The peaks detected were very close to the start of the trace, which is very inaccurate for detection due to the build up of contaminants from previous analyses. It can also be observed that there is adenosine presumably detected at time zero, this cannot be the case and therefore it was assumed this detection was contamination or noise within the LC-MS system, and AcP was not enabling the phosphorolysis of ribose.

No previous experimentation has accomplished this reaction in aqueous conditions, therefore continuation of this experiment was halted in the interest of time.

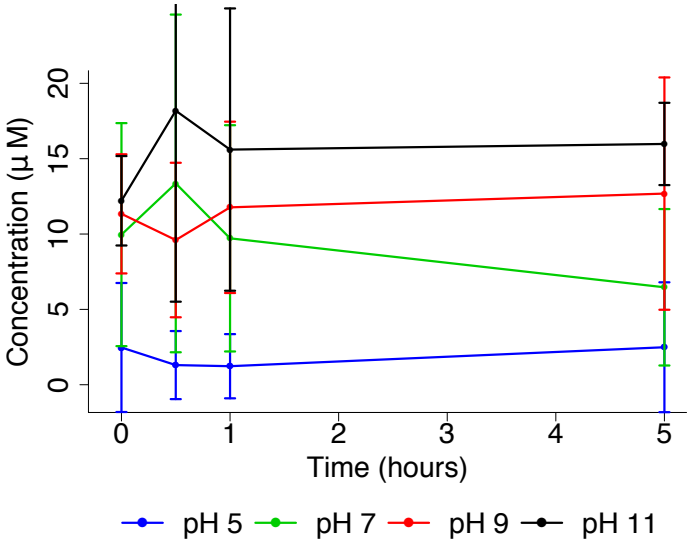

Figure 5.17. Synthesis of adenosine from ribose-5 phosphate and adenine in the presence of AcP, at pH 5, 7, 9 and 11 at 20 °C. N = N = 3 ±SD.

5.4.2 Phosphorylation of adenosine to AMP

The phosphorylation of nucleotide precursors under a range of alkaline hydrothermal conditions was considered to see if AcP could carry out some of the same reactions that ATP does today. The synthesis of adenosine monophosphate (AMP) from adenosine, as mentioned previously, was examined due to its relevance to RNA synthesis and its close association with ATP.

The phosphorylation of adenosine to AMP by AcP achieved yields of around 2 %, and was relatively slow compared to the synthesis of AcP, taking several hours even at 50 °C (Figure 5.18). This low yield may reflect the reaction conditions, in that adenosine has a very limited solubility in water (maximum solubility ∼10 mM). The concentration of AMP formed at pH 11 was slightly lower than pH 7; but in general pH had little effect on phosphorylation in the case of AMP. In the absence of AcP phosphorylation did not occur.

It has previously been shown that Mg^{2+} ions can dramatically increase the production of AMP from adenosine (Yamagata et al., 2005), due to the complex that it forms with the phosphates and the -OH groups on the sugar. Therefore, the same experiments were carried out in anaerobic conditions with Fe^{2+} (200 μM) and Mg^{2+} ions (2 mM) (Figure 5.19). As previously stated, it has been suggested that ferrous iron can increase reaction rates and product concentrations (Keller

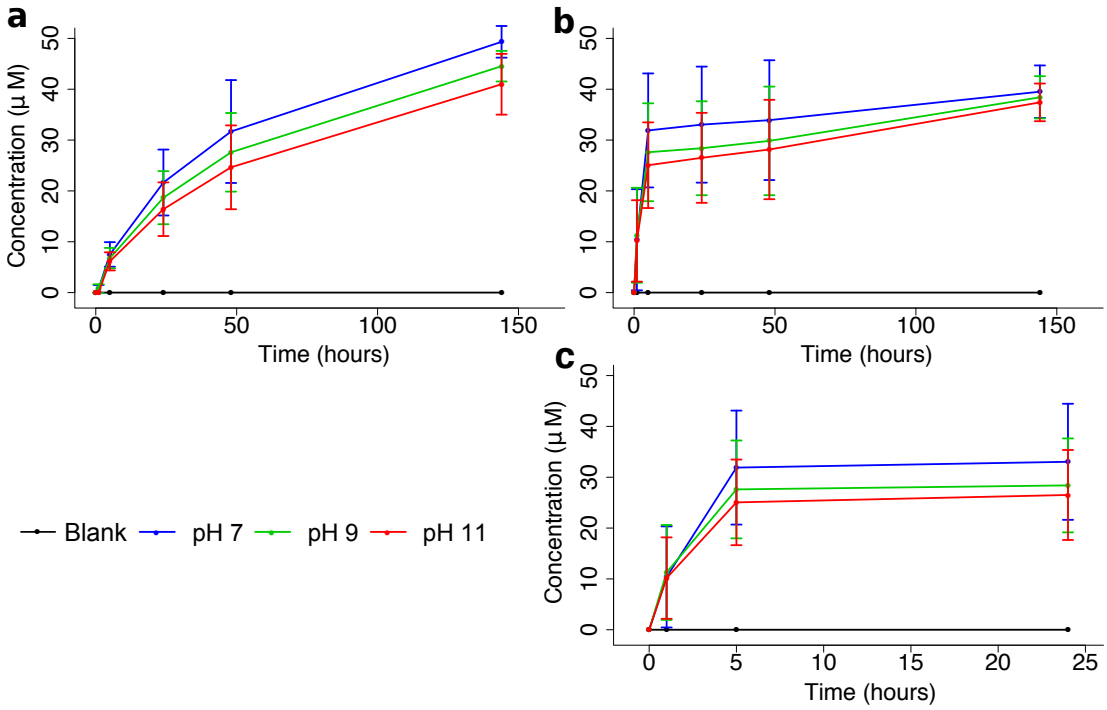

Figure 5.18. Phosphorylation of adenosine to adenosine monophosphate (AMP) by AcP at pH 7, 9 and 11. **(a)** At 20 °C. **(b)** At 50 °C. **(c)** The first 24 hours of the reaction at 50 °C, showing the fast rate of increase in the initial part of the reaction. N = 3 ±SD.

et al., 2014). Mg^{2+} ions were also used in aerobic conditions to give a comparison to anaerobic conditions. With these concentrations of ions Mg^{2+} had no effect on reaction rates or product concentration. Consequently the concentration of Mg^{2+} ions was increased from 2 mM to 20 mM, 100 mM and 200 mM, to see how concentration affected AMP synthesis. The concentration of Mg^{2+} ions were increased because of previous work by Keller et al. (2014), who used high mM concentrations of Mg^{2+} ions in their 'Hadean' ocean water as opposed to the 2 mM concentrations used initially here. They reported a marked difference in their product concentration relative to no ions (even though they were not looking directly at AMP production, the use of Mg^{2+} ions as a catalyst was thought to be analogous). The Mg^{2+} concentrations were varied as it was thought Mg^{2+} might have more effect on AMP production than Fe^{2+} (as this was shown earlier not to have much effect of product concentration, at least in the case of AcP; Figure 5.13). Initial concentrations of Mg^{2+} ions used were in line with those used by Yamagata et al., 2005 when they synthesised AMP from adenosine and

trimetaphosphate. It can be seen in Figure 5.19b that an increased concentration of Mg^{2+} ions does not affect the synthesis of AMP, either positively or negatively.

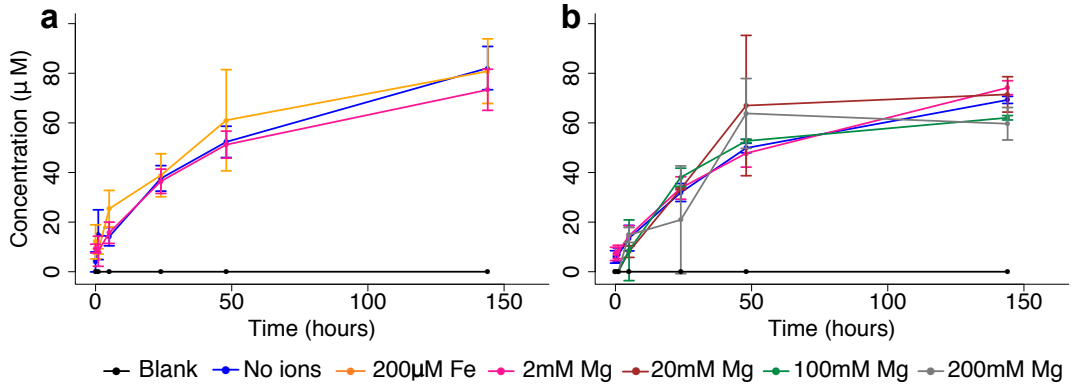

Figure 5.19. Phosphorylation of adenosine to adenosine monophosphate (AMP) by AcP, with the addition of metal ions (Fe^{2+} and Mg^{2+}). Experiments at pH 7 and 20 °C. **(a)** Anaerobic conditions with Fe^{2+} at 200 μM and Mg^{2+} ions at 2 mM. **(b)** Aerobic conditions with Mg^{2+} ions at 2, 20, 100 and 200 mM. In both experiments phosphorylation did not occur in the absence of AcP. N = 3 ±SD.

5.5 Further phosphorylation and condensation reactions

Alternative phosphorylation and condensation reactions where investigated by other members of my group; investigating phosphorylation of ribose to ribose phosphate and the condensation of glycine to glycine anhydride in aqueous conditions. These results will be discussed in this section and will be published with the results presented in this chapter (Whicher et al., 2016).

Eloi Camprubi has shown that AcP can phosphorylate ribose to ribose phosphate, in a similar way to that in which it phosphorylates adenosine to AMP. Again given its symbolic relevance to RNA synthesis, the formation of ribose-5 phosphate (R5P) from ribose was investigated, and measured by GC-MS. It was not confirmed if the ribose phosphate synthesised was actually R5P due to ^{31}P-NMR not being sensitive enough to the low yields being synthesised. Overall the yield for ribose phosphate was low (∼0.1 %) but the rate of synthesis was rapid, with >200 μM produced within 8 minutes at 20 °C in the absence of ions (Figure 5.20). The yield of ribose phosphate was slightly higher at 50 °C,

with concentrations reaching 300 μM. The concentration remained stable at 200-300 μM over several hours; this was thought in part to reflect an equilibrium between ribose and ribose phosphate, in which the high concentration of ribose inhibits the breakdown of the ribose phosphate. This was also thought to be the case with AcP, where the high acetate concentration slows AcP hydrolysis. The pH had little effect on ribose phosphate synthesis, albeit slightly lower at pH 11, similar to that of AMP synthesis.

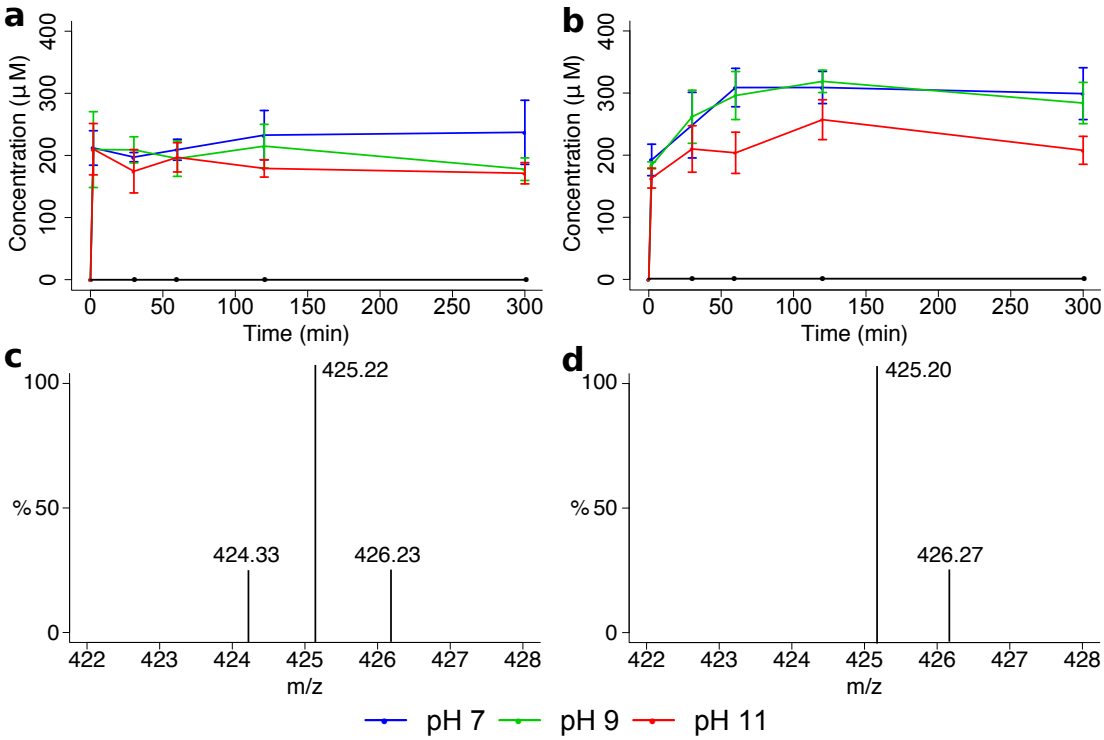

Figure 5.20. Synthesis of ribose phosphate from D-ribose and AcP at pH 7, 9 and 11. **(a)** 20 °C. **(b)** 50 °C. **(c – d)** Molecular ion monitored for derivatised ribose-5-phosphate (425.2 m/z): **(c)** standard and **(d)** experimental sample. N = 3 ±SD.

Barry Herschy examined the ability of AcP to drive condensation reactions in water. It was found that AcP can rapidly condense the amino acid glycine to form the polypeptide glycine anhydride (2,5-diketopiperazine; DKP) at very high yields in water (Whicher et al., 2016). Glycine was selected due to its relevance historically, being the focus of the majority of work over the last few decades (Rabinowitz et al., 1969; Chung et al., 1971; Bujdák and Rode, 1996). It was found here that AcP was a very effective condensing agent, with the main product being DKP rather than long-chain polypeptides. Both the amino and carboxyl groups

condense to form a ring structure that must open before further polymerisation can occur. The yield of DKP from glycine was 32 % within 1 hour, reaching >40 % over 1 week, with high stability levels (Figure 5.21). Neither temperature nor Mg^{2+} ions had much effect on yields. Other, previously tested condensing agents, such as cyanamide, linear polyphosphates and cyclic trimetaphosphate (cTMP) achieved lower conversions over longer periods, typically 1 - 4 % over 1 week (Rabinowitz, 1970; Chung et al., 1971; Bujdák and Rode, 1996). The effect of cTMP was tested here and the results were similar to those of earlier studies, corroborating a yield of 4 % in just over 1 hour (Figure 5.21a). Both cTMP and AcP produced the greatest yields at pH 12, however, unlike cTMP, AcP was still able to drive DKP synthesis even at neutral pH.

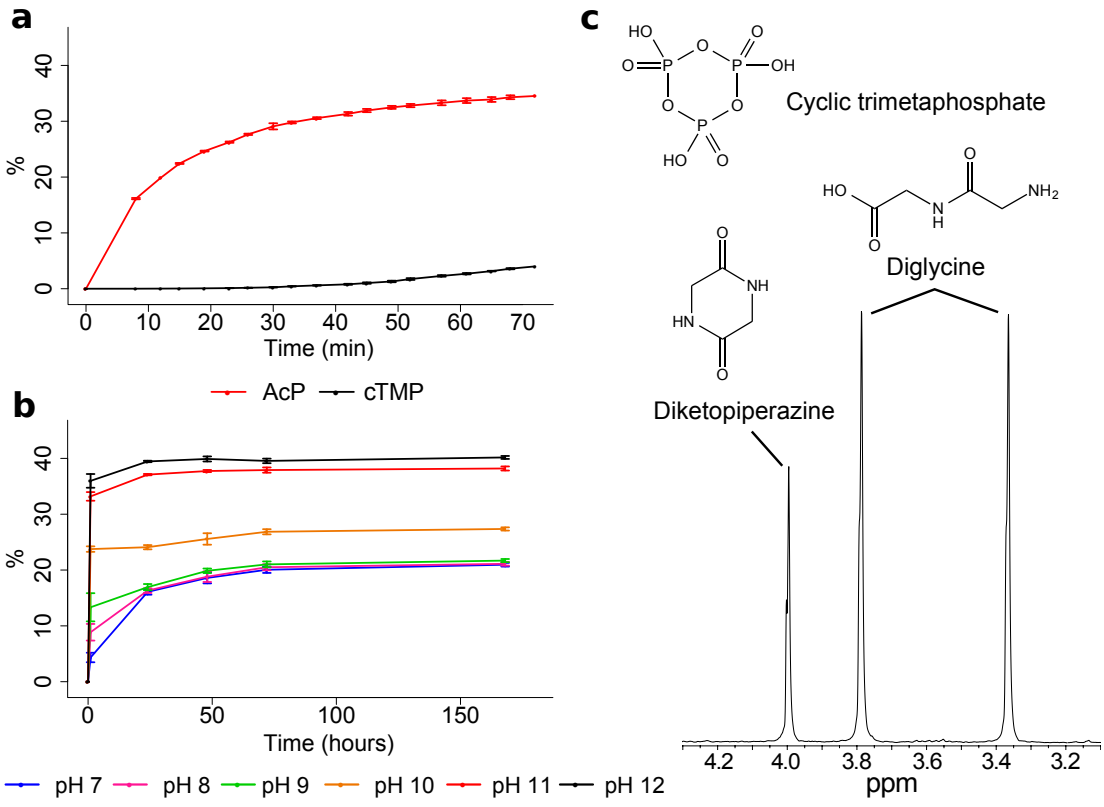

Figure 5.21. Condensation of glycine in water by AcP. **(a)** Condensation of glycine to diketopiperazine (DKP) by AcP and cTMP at 20°C and pH 12 over 72 minutes. **(b)** Condensation of glycine to DKP by AcP at varying pH over 7 days. **(c)** ^{1}H-NMR spectrum for the hydrolysis of DKP to diglycine, shown with molecular structures for cTMP, DKP and diglycine. N = 3 ±SD.

5.6 Discussion

It has been shown here that AcP can be formed at good yields under ambient conditions (neutral pH and 20 °C) or mild hydrothermal conditions from thioacetic acid, a simple 2-carbon precursor. Thioacetic acid and methyl thioacetate have themselves been synthesised from C_1-organic precursors under mild hydrothermal conditions in previous investigations (Huber and Wächtershäuser, 1997). It was hoped that methyl thioacetate could be synthesised from formate, instead of previously used CO, and CH_3SH. Formate is produced as a step in the reduction of CO_2 by H_2 under aqueous hydrothermal conditions, and has the same redox state as CO, as discussed earlier (Figure 4.14, shown in Chapter 4). It was detected in low concentrations in previous investigations by Barry Herschy (Herschy et al., 2014). The synthesis of methyl thioacetate proved not to be possible in this investigation. I was also unable to synthesise AcP from methyl thioacetate and inorganic phosphate. Due to these two factors, thioacetic acid was investigated as an alternative activated thiol. Thioacetic acid was chosen as an alternative to methyl thioacetate, as it is suggested to have occurred by carboxylation of methyl sulphide on a catalytic surface of (Ni,Fe)S as proposed by Huber and Wächtershäuser (1997) (Figure 5.2). It is therefore considered to be a plausible thiol to have occurred in alkaline hydrothermal vents, and is more reactive than methyl thioacetate due to the -SH being a better leaving group compared to $-SCH_3$. Liu and Orgel (1997) also use thioacetic acid as an acetylating agent in aqueous solution, in the formation of activated amino acids as substrates for prebiotic peptide synthesis. Hagan (2010) used thioacetic acid to form AcP photochemically from inorganic phosphate. Although these studies are not related to what is being investigated here, the use of thioacetic acid as an activated thiol was one of the reasons it was chosen as an alternative to methyl thioacetate. A future experimental investigation might consider the synthesis of thioacetic acid from CO or formate and methyl sulphide in the presence of (Fe,Ni)S, in the same way that methyl thioacetate was attempted here, and has been suggested to occur by Huber and Wächtershäuser (1997).

When using thioacetic acid the synthesis of AcP was possible, especially under mild or neutral conditions. It was observed that Mg^{2+} ions increased the synthesis of AcP, unlike Ca^{2+} ions, which when used in equimolar concentrations of Mg^{2+} it reduced synthesis. This corresponds with extant cellular processes, where Mg^{2+} ions have a close association with AcP, ATP and nucleotides, whereas Ca^{2+} ions are typically extruded from the cell. When Ca^{2+} ions were used alone they seemed to increase the synthesis of AcP, however this was not considered to be reliable as the NMR trace produced was very noisy and therefore any data used was thought not to be reliable.

AcP delivers an ideal balance between stability and reactivity; being stable over more than 5 hours under ambient conditions, even at high pH and in the presence of Ca^{2+} and Mg^{2+} ions. Evidence that AcP could have been a plausible precursor to ATP has been shown through a number of metabolic reactions; it can phosphorylate important intermediates in nucleotide synthesis, such as adenosine to adenosine monophosphate (AMP), along with phosphorylating ribose to ribose phosphate and condensing glycine to DKP.

The formation of DKP is significant, as it requires not one, but two condensation reactions. The high yields of DKP found using AcP as a condensing agent, compared to other condensing agents, such as cTMP, was very promising. However, the stability of the ring structure that DKP forms meant that there was no further polymerisation to longer polypeptides. At high pH and in the absence of AcP DKP partially hydrolyses back to diglycine, and due to the hydrolysis of AcP at warmer temperatures ($>50\,^{o}$C), thermal cycling within the vent system could facilitate the opening of the DKP ring structure to diglycine, potentially enabling the polymerisation to polyglycine. This polymerisation is known to occur at more neutral pH (Rabinowitz et al., 1969), which could also be facilitated by cycling of fluids within the vent. Few environments on Earth are known to cycle between pH and temperature at the same time. This work primarily shows that AcP is a powerful driver of amino acid condensation in water (Whicher et al., 2016).

These phosphorylation and condensation reactions required high concentrations of reagents, which could be criticised for being prebiotically implausible. While these concentrations are similar to those reported for most other studies (Yamagata et al., 1991; Morasch et al., 2014; Burcar et al., 2015; DeGuzman et al., 2014; Costanzo et al., 2007; Lohrmann and Orgel, 1968; Liu and Orgel, 1997; Leman et al., 2004; Huber et al., 2003; Chung et al., 1971; Rabinowitz et al., 1969; Bujdák and Rode, 1996), there are other factors that make such high concentrations more realistic in alkaline hydrothermal systems. The high pressure at the depth of these deep-sea hydrothermal vents (100 - 300 Bar) could drive condensation reactions at lower concentrations than in these experiments at atmospheric pressure (Imai, 1999; Wu et al., 2014). Thermal gradients and convection currents in alkaline vents should concentration organics by thermophoresis, a process where molecules concentrate in cooler areas (as discussed in Chapter 1). Heat gradients produced by lasers in closed glass capillaries have been shown to concentrate nucleotides and small RNAs by $10^{3}-10^{12}$ fold (Baaske et al., 2007; Mast and Braun, 2010; Mast et al., 2013; Braun and Libchaber, 2002). It has also been shown in an inert microporous matrix that organics can be concentrated by at least 5000-fold (Herschy et al., 2014) in an open flow system, as opposed to in a closed system. Thermophoresis should concentrate organics such as ribose phosphate and AMP, converting low yields into high concentrations, which would favour polymerisation. The far-from-equilibrium flux of H_2 and CO_2 in alkaline hydrothermal systems should also theoretically drive the synthesis of AcP to relatively high concentrations (Sojo et al., 2016). The disequilibria of H_2, CO_2 and proton concentrations are sustained by a continuous hydrothermal flow, providing a natural proton gradient across semi-conducting Fe(Ni)S barriers, which regulates their reduction potential. This should promote the synthesis of small organics such as thioacetic acid, which is shown here to phosphorolyse to form AcP. Finally, the charge on the phosphorylated biomolecules such as AcP makes them more likely to interact with the mineral ions within the surfaces of the vents, increasing their retention within the pores of the vents, rather than escaping like uncharged molecules such as methane. These four factors together

justify in part the high concentrations of reagents used here, meaning they are not necessarily unreasonable.

In conclusion, AcP was readily synthesised under ambient as well as mild hydrothermal conditions, and acted as a plausibly prebiotic ATP analogue in enabling phosphorylation and condensation reactions in water, without the need for catalysts and under a range of different conditions. The ability of AcP to drive these reactions in water eliminates the need for other processes suggested in previous investigations, such as wet-dry cycles, alternative solvents, or extremely reactive abiological dehydrating agents (also geologically implausible) such as cyanamide or carbonyl sulphide (Lohrmann and Orgel, 1968; Yamagata et al., 1991; Liu and Orgel, 1997; Huber et al., 2003; Leman et al., 2004; Costanzo et al., 2007; DeGuzman et al., 2014; Morasch et al., 2014), none of which bear any resemblance to the chemistry of modern cells. By acting as an analogue of ATP, AcP could drive prebiotic chemistry towards a form of protometabolism that precedes the metabolic pathways of cells, in which precursors are activated by phosphorylation, and polymers such as RNA, DNA and proteins are formed by condensation reactions in aqueous solution.

The conclusions drawn here apply not only the hydrothermal vent systems, but could also apply to a range of other prebiotic environments (except for peptide polymerisation, which might depend on pH gradients and thermal cycling). All the reactions carried out here occurred over time scales of minutes to hours, under ambient conditions even in the absence of enzymes, giving dynamics more similar to those of extant cells, than most geological systems. It can therefore be concluded that AcP is uniquely credible as a primordial energy currency, coupling carbon and energy flux at the origin of life, and so bridging the gap between abiotic chemistry and the biochemistry of extant cells.

Chapter 6

Conclusions and future work

6.1 Arguments for or against the hypothesis of congruence

This study has been an investigation into the transition from prebiotic to biotic chemistry, and has looked in both directions, bottom-up and top-down, to try and find a congruent progression from prebiotic chemical reactions to modern biochemical processes. As mentioned in Chapter 1, not everyone in the field agrees with this hypothesis for the origin of life, and some of the main reasons for this disagreement will be discussed here. The RNA world hypothesis suggests that if RNA came first it must have 'invented' metabolism later, therefore there would then be no link between modern metabolic processes and the chemistry before RNA, as RNA would have taken on the functionalities that proteins perform today (Orgel, 2004). The chemistry that works the most efficiently and produces the highest yields of products, with substrates such as cyanamide or formamide, organic solvents and reactive catalysts like iron pyrites, borate and zinc sulphides (Lohrmann and Orgel, 1968; Ricardo et al., 2004; Costanzo et al., 2007), does not look anything like life today. This presents an argument against prebiotic chemistry that looks like modern biochemistry, such as the chemistry presented in this thesis, starting with CO_2 and H_2. This reaction is difficult, slow and produces low yields compared to reactions starting with formamide or cyanide.

The problem of low yields in metabolic cycles has made people tend to favour chemistry with high yields, and therefore chemistry that uses more reactive substrates (Orgel, 2004, 2008). If prebiotic chemistry was very different from today, any number of experiments could be utilised, bringing substrates together from many diverse places, even delivered from meteorites, to produce high yields, but not equivalent to any cellular processes we see today. Further arguments against continuity are that it is very difficult to constrain the deep branches in the phylogenetic tree, and therefore to characterise what traits LUCA might have possessed, or what metabolic cycles it may have had. There is very little agreement on the properties of LUCA, and added to this the distance between prebiotic chemistry and a cellular LUCA with genes and proteins is so great there is some debate as to whether LUCA holds any relevance to the origin of life, can we really extrapolate back from an organism we know little about and was so far evolved from how life started?

Most prebiotic experimental chemistry looks nothing like life as we know it, which means at the very least there is a serious discontinuity between prebiotic chemistry and the origins of true metabolism. Despite strong arguments against the hypothesis of congruence between life today and the origin of life, there are many, and some may say even more persuasive, arguments for it. One of the main arguments advocating the congruence hypothesis is the absence of a difficult gap between the origin of life and modern biochemistry (de Duve, 1991, 1994; Morowitz et al., 2000; Martin and Russell, 2007). de Duve (1991; 1994) states that the only explanation for the appearance of catalysts with appropriate properties is that they arose by selection, and so they must have improved some form of protometabolism, therefore metabolism must have grown from protometabolism and reflect a similar geochemical flux. If life today evolved directly from processes at the beginning then we have a much simpler and more direct progression from chemical processes to the metabolic cycles and first organisms that resemble extant life. Leading on from this we can look at the structure and processes of cells and find environments where these processes could have started prebiotically, such as membranes in the alkaline hydrothermal vent pores, and the use of proton

gradients, which all life utilises today (Russell et al., 1993; Russell and Hall, 1997; Lane et al., 2010). Minerals found in alkaline hydrothermal vent walls, such as Fe(Ni)S clusters, are also involved in enzymes associated with metabolic cycles today, such as ferredoxin (Russell et al., 1988, 1989). The metabolic cycles suggested to have occurred at the origin of life are actually linear, not cyclic, therefore they are much simpler, with no dependance on autocatalysis, they only depend on the continued reduction of reduced CO_2 (Martin and Russell, 2007). This linearity means that high yields are no longer needed as the addition of CO_2 at each step introduces a carbon into the organic chain, and therefore more complexity (Figure 6.3). If we take into account evolution low yields are expected as chelation, complex enzymes and ultimately genes need to have the scope to improve a process that was at one time less efficient (de Duve, 2005).

The hypothesis of congruence between prebiotic chemistry and modern biochemistry has been the focus of the work in this thesis. Important metabolic processes have been considered and experiments designed to replicate them under prebiotic conditions, considering environments that might have provided the conditions and ingredients needed for this metabolism. The key to almost all extant life is the simple reduction of CO_2 with H_2 that we see occurring directly in ancient prokaryotes, notably methanogens and acetogens. Even though H_2 comes in the form of H_2O or H_2S in some processes, such as photosynthesis, the involvement of electron exchange (redox chemistry) and a flow of protons is still congruent (Maden, 2000; Stetter, 2006; Fuchs, 2011). The most ancient pathway of carbon reduction, arguably the acetyl-CoA pathway, uses H_2 to reduce CO_2 via membrane proteins that contain Fe(Ni)S clusters capable of electron transfer, and is powered by the proton-motive force, electrochemical differences in ion concentration, across a membrane (Russell and Martin, 2004; Lane et al., 2010; Sousa et al., 2013). Alkaline hydrothermal vents provide remarkably similar conditions to this pathway, even down to the magnitude and polarity of the pH gradients across their internal inorganic barriers (Lane et al., 2010; Sojo et al., 2016). For this reason, since their discovery, these vents have been of keen interest as a particularly promising location for the origin of life (Russell et al., 1989,

1993). They form spontaneously on the ocean floor, building huge systems of tiny interconnected micropores, having the potential to concentrate organics and protect molecules from the outside environment (Russell and Hall, 1997; Kelley et al., 2001). These vents continuously sustained far-from-equilibrium conditions, and harboured similar conditions and substrates required for the acetyl-CoA pathway, making the argument that these environments could have functioned as electrochemical reactors, enabling carbon reduction and energy metabolism at the origin of life. However, there have been no experiments thus far using proton gradients or acetyl phosphate (AcP) to drive potential prebiotic metabolic cycles, suggesting it cannot be ruled out as a potential process at the origin of life. The research in this thesis has provided some preliminary and original experimental investigations into these statements.

6.2 Formation of C_1-organics from CO_2 and H_2

The alkaline hydrothermal vent hypothesis suggests that natural proton gradients are produced by alkaline fluids coming into close contact with acidic ocean fluids percolating into the vent. In the Hadean, these two fluids would have been separated by thin, inorganic barriers containing catalytic semi-conducting FeS minerals, which could catalyse the synthesis of organic molecules within the vent's microporous system. Specifically the inorganic walls could act as semi-conducting barriers to facilitate the reduction of CO_2 by H_2 producing simple C_1-organics, such as formaldehyde, analogous to autotrophic CO_2 fixation in modern methanogens (Russell et al., 1988; Russell and Hall, 1997; Nitschke and Russell, 2009; Lane et al., 2010; Sojo et al., 2016).

To model the internal barriers of the vent system a simple flow-reactor was designed, and placed in an anaerobic chamber, where dynamic FeS or Fe(Ni)S precipitates were formed and characterised as disordered mackinawite (as reported in Chapter 3). These precipitates were then used to investigate the possibility of reducing CO_2 with H_2 across a catalytic, inorganic barriers transecting pH gradients.

As a proof-of-principle investigation, the precipitates were capable of reducing CO_2 to form μM concentrations of simple C_1-organics, specifically formaldehyde, once the contamination within the chamber had been reduced significantly and the GC-MS sensitivity increased (as reported in Chapter 4). It was found that the formaldehyde was mainly produced in association with, and possibly remained bound to, the FeS precipitates (although it had to be detached by derivatisation to enable detection). It was expected that the formaldehyde would be produced in close proximity to the precipitates as they were enabling the reduction of CO_2, however, it was not expected that it might remain bound to them. This gave useful insight into the dynamics of the precipitates, enabling a better understanding of how organics might be formed across the catalytic barriers. This understanding could enable more effective planning of future experiments, enabling a consideration for the importance of the mineral surface not just the pH conditions of the aqueous solutions, resulting a more in-depth investigation into increasing their efficiency at reducing CO_2.

Microfluidics is one experimental setup that has been considered for future investigations to decrease the variability in structure of the precipitates but also to reduce the number of variables in the system. In this setup the volume and flow rates of the two different fluids could be constrained in a small area, the precipitate could then be allowed to form between the two fluids for a selected length (in theory, however, this might be more difficult in reality). After the precipitate is formed the fluids could be allowed to mix, enabling a more neutral pH to occur at one end of the system, thereby stopping the build up of a charge on the precipitate, which would inhibit the flow of electrons once it became too great. This setup would also mean that any organics that formed and detached from the precipitate would not break down in the acid conditions but would remain at more neutral pH (Figure 6.1). There could also be the possibility to follow pH gradients under a fluorescence microscope with pH-sensitive dyes, enabling an investigation into how conditions might be changing in different areas of the modelled vent pores, giving clues about where organics might be most likely to form. There is the issue that this system might just fill up with precipitate,

rather than forming a nice thin barrier as designed, this was seen to happen in the flow-reactor when the precipitate was left to form over a number of hours. This could possibly be solved by having very low concentrations of Fe^{2+} and HS^- ions, or gradually lowering them over time.

Other future experiments could focus on using a high pressure flow-reactor system for the synthesis of vent-like precipitates, CO_2 reduction and thermophoresis experiments. Increasing the pressure would increase the partial pressure of the dissolved gases in the fluids and therefore the concentration of products, as described by Le Chatelier's Principle (Le Chatelier and Boudouard, 1898) and discussed in Chapter 4.5. The low concentrations of H_2 and CO_2 are one of the most significant problems for the experiments modelling CO_2 reduction. The challenge would be designing a highly pressurised system that is still an open flow reactor, allowing for the continuous flow of fluids throughout the system. A microfluidic system could also have the capability of being pressurised to around 20 atmospheres. This is not much, but better than atmospheric pressure for dissolving higher concentrations of H_2.

It was hoped that CO or formate ($CHOO^-$), and methyl sulphide (CH_3SH) might be formed and detected within the reactor. None of these products were detected in the experiments in the reactor; however, these compounds are very hard to detect due to their volatility. Interestingly there is a lack of methyl sulphide detected in modern alkaline vents. On the one hand this could be due to it being a thermodynamically difficult product to form, because it is a condensation reaction occurring in aqueous conditions, or it could be because it is easily oxidised in oxygenated systems, making it hard to detect once removed from the anaerobic chamber. If so it could actually be more likely to occur in anoxic systems than oxic, such as the alkaline vents 4 Ga.

6.3 Formation of C_2-organics from C_1-organics

The next step in this investigation was to see if it was possible to synthesise larger C_2-organics from the initial CO_2 reduction products, such as CO, formate

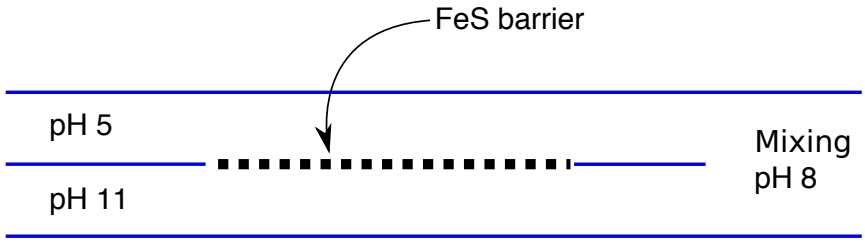

Figure 6.1. Schematic showing FeS barriers forming in a potential microfluidic setup. When fluids of different pH meet a FeS barrier would form between the two, potentially in a more controlled way than in the flow reactor. The mixing at the end prevents a charge building up on the precipitate wall (this would prevent any further electron transfer from occurring once the charge in each fluid was equalised). Mixing at the end of the tube prevents this charge from building up on the barrier, maintaining a continuous flow of the fluids at different pH. One problem that may be encountered is the FeS barrier becoming too thick and blocking up the whole system.

or formaldehyde. Experiments conducted by Eloi Camprubí showed that sugars, such as ribose and deoxyribose (key building blocks of nucleotides), can be synthesised from formaldehyde under mild alkaline hydrothermal conditions by the formose reaction, which has been shown in previous literature (Kopetzki and Antonietti, 2011), but here also.

Previous experiments by Huber and Wächtershäuser (1997) assumed the presence of methyl sulphide in volcanic hydrothermal systems, and successfully synthesised methyl thioacetate (possible precursors to acetyl-CoA) from methyl sulphide and CO. Consequently the focus of the experiments in this study was to investigate the possibility of reactive thiol synthesis from initial products of CO_2 reduction, using formate instead of CO. One reason for using formate instead of CO is due to it being the intermediate reduction product between CO_2 and formaldehyde, potentially making it more plausible in these systems than CO, and it also has the same redox state as CO suggesting it could carry out the same reactions. However, this was found not to be the case, and unfortunately no methyl thioacetate was found from the reaction of formate with methyl sulphide in this investigation.

6.4 Formation of AcP from C_2-organics

ATP is a key molecule for metabolism in all extant life although complex, therefore a more simple prebiotic precursor, which can be synthesised from simple organic molecules, is important for modelling protometabolism. Previous literature has suggested AcP as a possible precursor to ATP (Ferry, 2006; Martin and Russell, 2007; Martin et al., 2014; Sojo et al., 2016), therefore experiments moved on to look at synthesising AcP from methyl thioacetate or thioacetic acid (which is also thought to be a possible prebiotic precursor to acetyl-CoA). AcP was successfully synthesised in good yields from the simple thioacetic acid (as opposed to methyl thioacetate which did not produce any AcP under the conditions used here) and was shown to be stable over at least 5 hours at mild temperatures, regardless of pH.

Future experiments could go back and investigate synthesising AcP from methyl thioacetate under the conditions used with thioacetic acid, as the ideal conditions needed for the reaction with thioacetic acid are now better understood and may correspond to methyl thioacetate. Methyl thioacetate would have been the preferred molecule to use for this reaction as it is a thioester, and so more relevant to the thioester world as suggested by de Duve (1991), and has already been synthesised from CO and methyl sulphide by Huber and Wächtershäuser (1997). Due to it not reacting in the experiments conducted, thioacetic acid, which was more reactive under the conditions tested here, was used in the interest of time.

6.5 AcP to drive a prebiotic Krebs cycle

The incomplete reverse Krebs cycle produces important intermediates for amino acid and nucleoside biosynthesis today, and it does so from the acetyl-CoA pathway in methanogens and acetogens (Fuchs, 1989; Martin and Russell, 2007). In the abiotic version of the acetyl-CoA pathway a version of the incomplete reverse Krebs cycle could have been driven by the reaction of methyl thioacetate or thioacetic acid with the addition of CO_2 and H_2 to produce pyruvate.

Pyruvate (C_3) is then converted to phosphoenolpyruvate (C_3), and oxaloactate (C_4) with the addition of CO_2 (Figure 6.2). Phosphoenolpyruvate goes onto produce glyceraldehyde-3-phosphate, an important intermediate in the formose reaction, and therefore the synthesis of sugars, needed for the building of sugar phosphates and nucleotides. Oxaloacetate carries out two more carboxylations to form C_5, alpha-keto-glutarate, and then C_6, isocitrate, by stepwise reactions in the incomplete reverse Krebs cycle (Figure 6.3). Today this cycle is driven by enzymes and ATP (indicated by a red star in both figures), prebiotically these carboxylations might be possible without enzymes under hydrothermal conditions, with AcP acting as the energy molecule instead of ATP (Martin and Russell, 2007), and FeS minerals acting as the catalysts. Whenever CO_2 is added to the reaction H_2 is also needed to reduce it, resulting in one more carbon being added to the resulting organic molecule, building up the number of carbons in the organic chains. The reduction of CO_2 by H_2 utilised in these carboxylations could again be driven by pH differences, the same way as it was able to drive the formation of C_1-organics discussed in section 6.1. Consequently, could the Krebs cycle be linked to the cell membrane and proton gradients? If so could a prebiotic form of this reaction occur in the alkaline hydrothermal vents, driven by pH gradients and AcP, instead of ATP and enzymes?

Future work could concentrate on investigating the ability of pH gradients, and even sodium gradients, which are important in cells today, to drive the carboxylations in the incomplete reverse Krebs cycle, and the eventual production of key compounds needed for amino acid and nucleoside synthesis.

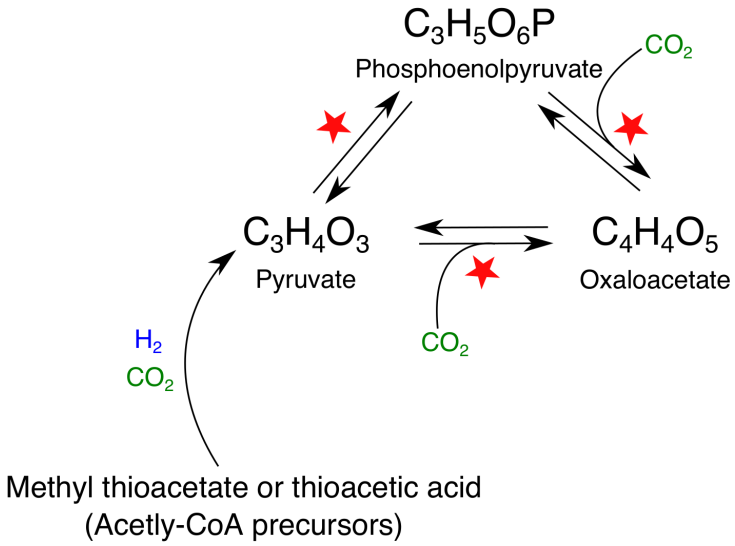

Figure 6.2. The cyclic reaction of pyruvate, phosphoenolpyruvate and oxaloacetate, with modern enzymatic reactions labelled with a red star. Pyruvate could be formed by the reaction of reduced CO_2 with methyl thioacetate or thioacetic acid (as indicated in Figure 6.4) where the incomplete Krebs cycle is indicated in a green box. Once pyruvate is formed could AcP and FeS minerals in the vent act together to enable the formation of phosphoenolpyruvate and, then with the addition of CO_2, the formation of oxaloacetate, as modern enzymatic reactions do today? It can be observed that oxaloacetate has one more carbon that pyruvate or phosphoenolpyruvate, and is enabled by the addition of CO_2, which could potentially be driven by pH gradients within the vent setting.

6.6 AcP drives condensation and phosphorylation reactions

Today ATP carries out phosphorylation and condensation reactions of key substrates needed to synthesise the building blocks of life, such as proteins and nucleic acids. To investigate whether AcP could have acted as a prebiotic energy currency, an analogue of ATP, a number of preliminary phosphorylation and condensation reactions were conducted.

Previously Cafferty et al. (2016) showed they were able to form glycosidic linkages with melamine and barbituric acid with ribose and ribose-5-phosphate in water to produce nucleosides and nucleotides in good yields. It was therefore hoped that AcP might be able to condense a sugar and a base to form a nucleoside, specifically adenosine, where the high energy phosphoanhydride bond might activate the ribose and adenine to ultimately join. This was not found to work in the experimental setup used here. However, AcP was found to

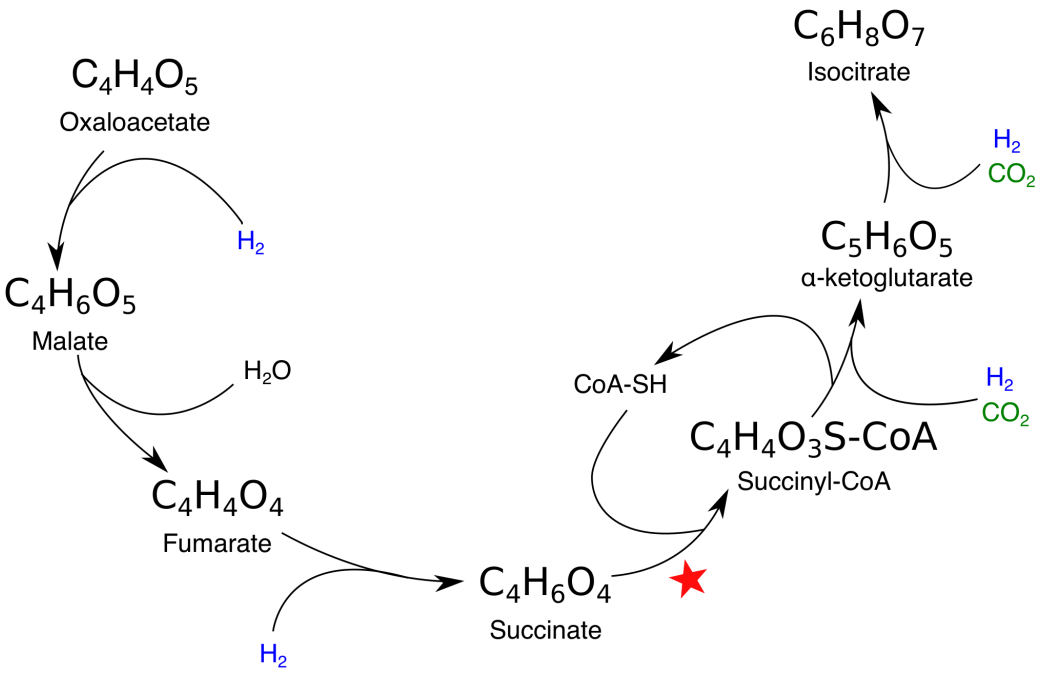

Figure 6.3. The incomplete reverse Krebs cycle, starting from oxaloacetate and ending with isocitrate. As the cycle progresses reduced CO_2 enables the addition of one carbon to the product formed, enabling a progression from C_4-organics to C_6-organics. The red star indicates modern enzymatic reactions, which could be driven by AcP in a prebiotic setting. The alkaline hydrothermal vents could provide pH gradients, which modulates the reduction potentials and enables CO_2 and H_2 to drive carboxylation reactions. This cycle could then provide some of the building blocks needed for the formation of simple amino acids and nucleotides, providing the substrates for polymerisation and condensation of larger organics, as shown at the end of the metabolic pathway shown in Figure 6.4.

successfully carry out phosphorylation reactions, specifically the phosphorylation of adenosine to adenosine monophosphate (a key nucleotide for the formation of nucleic acids). Additionally experiments by Eloi Camprubí showed that AcP can also phosphorylate ribose and deoxyribose to form ribose phosphate (reported in Chapter 5; Whicher et al., 2016).

6.7 Condensation reactions to synthesise nucleotides and amino acids

The incomplete reverse Krebs cycle, originating from precursors of acetyl-CoA, such as methyl thioacetate or thioacetic acid, via pyruvate, and powered by AcP,

could have provided the key carbon intermediates for the biosynthesis of amino acids and nucleosides, as it does today in methanogens and acetogens, with acetyl-CoA and ATP. If the polymerisation of nucleotides and then condensation of amino acids can take place in conditions likely to have occurred in the vent, there is a feasible process for further polymerisation to more complex biopolymers, such as RNA and DNA, further advocating the vents as a plausible location for chemiosmotic coupling and organic synthesis to have originated.

Nucleoside and amino acid synthesis is difficult, and little experimental research has been conducted in the hydrothermal vent setting. In this investigation it was shown that AcP was able to carry out condensation reactions; condensing the amino acid glycine to DKP, the ring form of diglycine, which can be broken open by partial hydrolysis to linear diglycine at alkaline pH in the absence of AcP. As AcP is rapidly hydrolysed at warmer temperatures (50–60°C) thermal cycling of DKP could open the DKP ring to regenerate diglycine. Few known environments are capable of cycling between strongly alkaline and neutral pH, except for alkaline hydrothermal vents, which do just this, indicating that these systems might be uniquely able to promote amino acid polymerisation in water.

The critical point is that AcP is a powerful driver of amino acid condensations in water, and future work needs to further investigate its ability to condense more complex amino acids, and polymerise them into longer chain polypeptides. This would be the next step in the synthesis of the building blocks of life, such as proteins. Investigations also need to look into the condensation of nucleotides into nucleic acids by AcP, which would become the building blocks of RNA and later DNA.

6.8 Summary

The reduction of CO_2 by H_2 to form organics is exergonic under alkaline hydrothermal conditions, and the characteristics of the acetyl-CoA pathway, which seem analogous to conditions within alkaline hydrothermal vents, advocates this autotrophic pathway as having geochemical origins (Sojo et al., 2016). Research

in this study has suggested that primordial carbon-reducing pathways could have preceded that which is used by methanogens and acetogens today, where CO_2 is reduced by H_2 to form simple thioesters and AcP, under abiotic, alkaline hydrothermal conditions, which might have gone on to drive energy and carbon metabolism, as ATP does today. A simple schematic summary can be used to explain this process (Figure 6.4); how the different reactions and pathways investigated fit together into a progression from reduction of CO_2 by H_2 across inorganic, catalytic barriers following an equivalent to the acetyl-CoA pathway, with methyl thioacetate or thioacetic acid acting as an acetyl-CoA mimetic. This is followed by the synthesis of AcP, a potential ATP precursor, which could theoretically facilitate the phosphorylation and condensation of key organic substrates, such as sugars (derived from reactions involving pyruvate), nucleosides and amino acids (which are formed by sequential carboxylations in the reverse incomplete Krebs cycle). AcP could then further assist in polymerisation of these smaller organics to nucleotides, nucleic acids and polypeptides, the key building blocks of life.

The combined bottom-up, top-down approach is what has driven the ideas and experiments within this investigation. The results acquired here have given some insight into how alkaline hydrothermal vents could have facilitated the origin of core metabolic processes that are universally conserved across all extant life, and further polymerisation of key organics into the building blocks of life that are utilised today. In this way the gap between the origin of life and modern biochemistry can be at least partially explained, and we can see some congruence between life's origin and evolution.

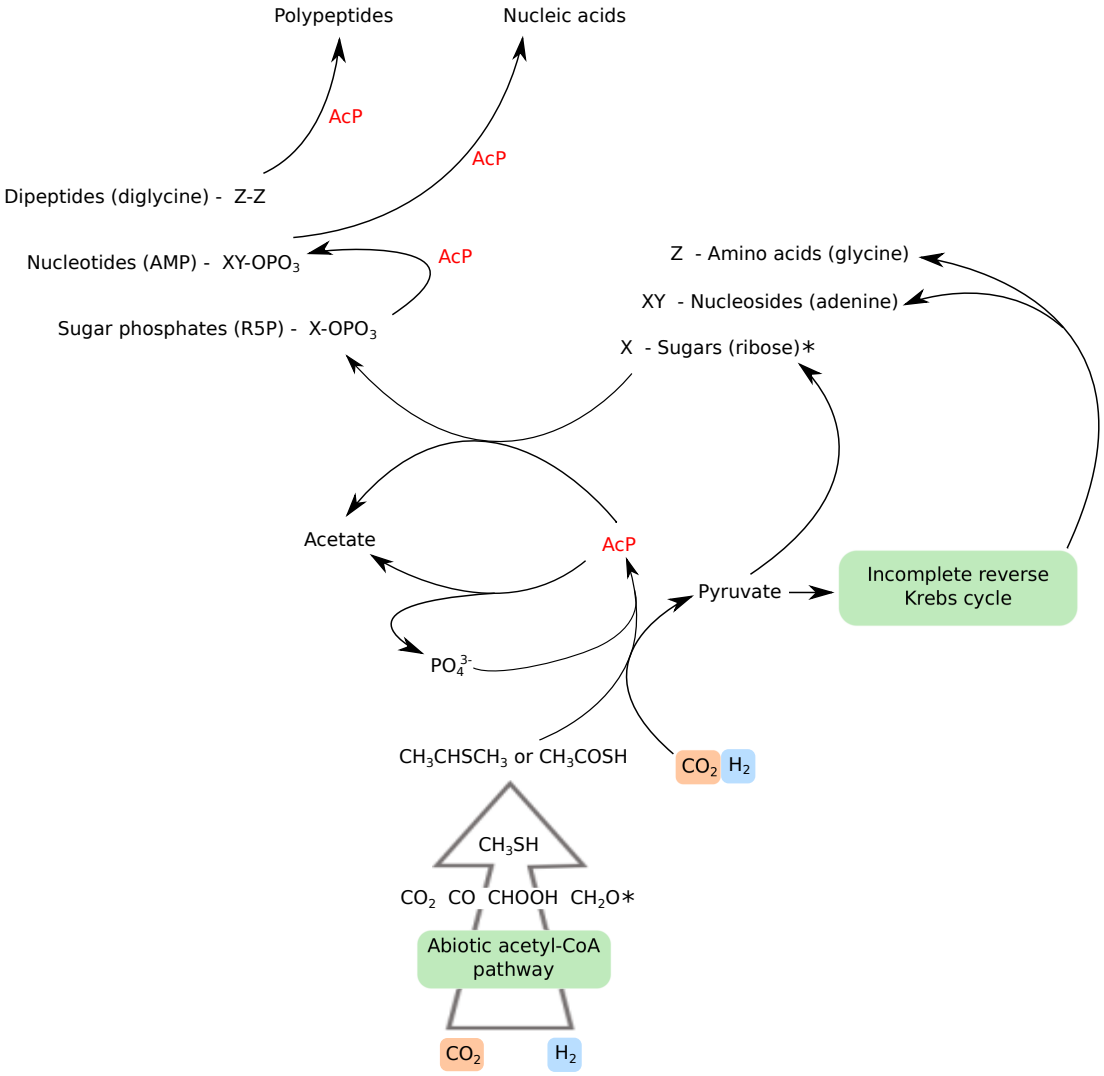

Figure 6.4. Schematic summary of the core abiotic carbon and energy metabolism congruent to the prebiotic chemistry proposed in this study. The initial steps of this chemistry is an abiotic analogue of the acetyl-CoA pathway; starting with the reduction of CO_2 by H_2, using proton gradients across catalytic inorganic barriers within alkaline hydrothermal vents, which produces C_1 intermediates, along with methyl sulphide from bisulphide ions. These intermediates go on to produce simple thiol analogues of acetyl-CoA; methyl thioacetate or thioacetic acid. In hydrothermal conditions these reactive thiols are phosphorolysed to synthesise acetyl phosphate (AcP), a plausible mimetic of ATP. The pathway then splits into energy metabolism and carbon metabolism. On the carbon metabolism branch (right-hand side) methyl thioacetate or thioacetic acid would react with CO_2 and H_2 to produce pyruvate (described in Figure 6.2), which goes on to produce sugars such as ribose. From pyruvate a prebiotic form of the incomplete reverse Krebs cycle could then be driven by AcP, as ATP does today, potentially supplying key intermediates for amino acid and nucleoside synthesis (described in Figure 6.3). On the energy metabolism branch (left-hand side) AcP phosphorylates or condenses key substrates, such as sugars, nucleotides and amino acids (X, XY and Z), when its high energy phosphoanhydride bond hydrolyses to produce acetate and inorganic phosphate (which can then go on to synthesise more AcP). The phosphorylated or condensed substrates can then be further polymerised by AcP, to nucleic acids and polypeptides. Sugars can be produced from the formose reaction with formaldehyde in hydrothermal conditions (indicated with a *).

Bibliography

Abbott DH, Hoffman SE (1984) Archaean plate tectonics revisited 1. Heat flow, spreading rate, and the age of subducting oceanic lithosphere and their effects on the origin and evolution of continents. *Tectonics* 3:429–448.

Abe Y, Ohtani E, Okuchi T, Righter K, Drake M (2000) Water in the Earth Earth In Canup R, Righter K, editors, *Origin of the Earth and Moon*, pp. 413 – 433. Tuscon: University of Arizona Press.

Amend JP (1998) Energetics of amino acid synthesis in hydrothermal ecosystems. *Science* 281:1659–1662.

Amend JP, LaRowe DE, McCollom TM, Shock EL (2013) The energetics of organic synthesis inside and outside the cell. *Philosophical transactions of the Royal Society of London. Series B, Biological sciences* 368:20120255.

Amend JP, McCollom TM (2009) Energetics of biomolecule synthesis on early earth. *ACS Symposium Series* 1025:63–94.

Arndt NT, Nisbet EG (2012) Processes on the young earth and the habitats of early life. *Annual Review of Earth and Planetary Sciences* 40:521–549.

Arrhenius S (1908) *Worlds in the making: the evolution of the universe.* Haper and brothers.

Baaske P, Weinert FM, Duhr S, Lemke KH, Russell MJ, Braun D (2007) Extreme accumulation of nucleotides in simulated hydrothermal pore systems. *Proceedings of the National Academy of Sciences* 104:9346–9351.

Barge LM, Doloboff IJ, Russell MJ, VanderVelde D, White LM, Stucky GD, Baum MM, Zeytounian J, Kidd R, Kanik I (2014) Pyrophosphate synthesis in iron mineral films and membranes simulating prebiotic submarine hydrothermal precipitates. *Geochimica et Cosmochimica Acta* 128:1–12.

Barge LM, Doloboff IJ, White LM, Stucky GD, Russell MJ, Kanik I (2012) Characterization of iron-phosphate-silicate chemical garden structures. *Langmuir : the ACS journal of surfaces and colloids* 28:3714–21.

Baross JA, Hoffman SE (1985) Submarine hydrothermal vents and associated gradient environments as sites for the origin and evolution of life. *Origins of Life and Evolution of the Biosphere* 15:327–345.

Bell C, Taber D, Clark A (2000) *Organic Chemistry Laboratory: with qualitative analysis and microscale experiments* Cengage Learning, 3rd edition.

Benner SA (2013) Planets, minerals and life's origin. *Minerological Magazine* 77:686.

Benner SA, Kim HJ, Kim MJ, Ricardo A (2010) Planetary organic chemistry and the origins of biomolecules. *Cold Spring Harbor perspectives in biology* 2:a003467.

Blake RE, Chang SJ, Lepland A (2010) Phosphate oxygen isotopic evidence for a temperate and biologically active Archaean ocean. *Nature* 464:1029–1032.

Bourdoiseau JA, Jeannin M, Sabot R, Rémazeilles C, Refait P (2008) Characterisation of mackinawite by Raman spectroscopy: Effects of crystallisation, drying and oxidation. *Corrosion Science* 50:3247–3255.

Boyd SR (2001) Ammonium as a biomarker in Precambrian metasediments. *Precambrian Research* 108:159–173.

Braun D, Libchaber A (2002) Trapping of DNA by thermophoretic depletion and convection. *Physical review letters* 89:188103.

Buckel W, Thauer RK (2013) Energy conservation via electron bifurcating ferredoxin reduction and proton/Na^+ translocating ferredoxin oxidation. *Biochimica et Biophysica Acta - Bioenergetics* 1827:94–113.

Budin I, Bruckner RJ, Szostak JW (2009) Formation of protocell-like vesicles in a thermal diffusion column. *Journal of the American Chemical Society* 131:9628–9629.

Bujdák J, Rode BM (1996) The effect of smectite composition on the catalysis of peptide bond formation. *Journal of molecular evolution* 43:326–333.

Burcar BT, Barge LM, Trail D, Watson EB, Russell MJ, McGown LB (2015) RNA oligomerization in laboratory analogues of alkaline hydrothermal vent systems. *Astrobiology* 15:509 – 522.

Cafferty BJ, Fialho DM, Khanam J, Krishnamurthy R, Hud NV (2016) Spontaneous formation and base pairing of plausible prebiotic nucleotides in water. *Nature Communications* 7:11328.

Cairns-Smith A, Hall AJ, Russell MJ (1992) Mineral Theories of the Origin of Life and an Iron Sulfide Example. *Origins of life and evolution of the biosphere* 22:161–180.

Catling DC, Claire MW (2005) How Earth's atmosphere evolved to an oxic state: A status report. *Earth and Planetary Science Letters* 237:1–20.

Charlou JL, Donval JP, Fouquet Y, Jean-baptiste P, Holm N (2002) Geochemistry of high H_2 and CH_4 vent fluids issuing from ultramafic rocks at the Rainbow hydrothermal field (36°14' N, MAR). *Chemical Geology* 191:345–359.

Chung N, Lohrmann R, Orgel L, Rabinowitz J (1971) The mechanism of the trimetaphosphate-induced peptide synthesis. *Tetrahedron* 27:1205–1210.

Cleland CE, Chyba CF (2002) Defining 'life'. *Origins of Life and Evolution of Biospheres* 32:387–393.

Cody GD (2004) Transition metal sulfides and the origins of metabolism. *Annual Review of Earth and Planetary Sciences* 32:569–599.

Cody GD, Mysen B, Sághi-Szabó G, Tossell JA (2001) Silicate-phosphate interactions in silicate glasses and melts: I. A multinuclear (^{27}Al, ^{29}Si, ^{31}P) MAS NMR and ab initio chemical shielding (^{31}P) study of phosphorous speciation in si. *Geochimica et Cosmochimica Acta* 65:2395–2411.

Costanzo G, Saladino R, Crestini C, Ciciriello F, Di Mauro E (2007) Nucleoside phosphorylation by phosphate minerals. *The Journal of biological chemistry* 282:16729–16735.

Crans D, Whitesides GM (1983) A convenient synthesis of disodium acetyl phosphate for use in in situ ATP cofactor regeneration. *Journal of organic chemistry* 48:3130–3132.

de Duve C (1988) Did God make RNA? *Nature* 336:209–210.

de Duve C (1991) Blueprint for a Cell - The Nature and Origin of Life. *Biochemical Education* 19:159.

de Duve C (1994) From protometabolism to metabolism In *Origins of Life and Evolution of Biospheres*, Vol. 24, pp. 346–362.

de Duve C (1995) *Vital dust: life as a cosmic imperative* Basic Books, New York, NY.

de Duve C (2005) *Singularities: landmarks on the pathways* Cambridge University Press, New York.

de Leeuw NH, Catlow CRA, King HE, Putnis A, Muralidharan K, Deymier P, Stimpfl M, Drake MJ (2010) Where on Earth has our water come from? *Chemical communications (Cambridge, England)* 46:8923–8925.

de Ronde CE, Channer DM, Faure K, Bray CJ, Spooner ET (1997) Fluid chemistry of Archean seafloor hydrothermal vents: Implications for the

composition of circa 3.2 Ga seawater. *Geochimica et Cosmochimica Acta* 61:4025–4042.

de Zwart II, Meade SJ, Pratt AJ (2004) Biomimetic phosphoryl transfer catalysed by iron(II)-mineral precipitates. *Geochimica et Cosmochimica Acta* 68:4093–4098.

Deamer D, Weber AL (2010) Bioenergetics and life's origins. *Cold Spring Harbor perspectives in biology* 2:a004929.

Decker K, Jungermann K, Thauer RK (1970) Energy production in anaerobic organisms. *Angewandte Chemie (International ed. in English)* 9:138–158.

DeGuzman V, Vercoutere W, Shenasa H, Deamer D (2014) Generation of oligonucleotides under hydrothermal conditions by non-enzymatic polymerization. *Journal of Molecular Evolution* 78:251–262.

Ducluzeau AL, van Lis R, Duval S, Schoepp-Cothenet B, Russell MJ, Nitschke W (2009) Was nitric oxide the first deep electron sink? *Trends in Biochemical Sciences* 34:9–15.

Eck RV, Dayhoff MO (1966) Evolution of the structure of ferredoxin based on living relics of primitive amino acid sequences. *Science* 152:363–366.

Eschenmoser A, Loewenthal E (1992) Chemistry of potentially prebiological natural products. *Chemical Society Reviews* 21:1–16.

Ferry JG (2006) The stepwise evolution of early life driven by energy conservation. *Molecular Biology and Evolution* 23:1286–1292.

Follmann H, Brownson C (2009) Darwin's warm little pond revisited: From molecules to the origin of life. *Naturwissenschaften* 96:1265–1292.

Franck S (1998) Evolution of the global mean heat flow over 4.6 Gyr. *Tectonophysics* 291:9–18.

Früh-Green GL, Connolly JA, Plas A, Kelley DS, Grobéty B (2004) *The Subseafloor Biosphere at Mid-Ocean Ridges*, Vol. 144 of *Geophysical Monograph Series* American Geophysical Union, Washington, D. C.

Fuchs G (1989) *Alternative pathways of autotrophic CO_2 fixation.* Berlin, Germany: Springer Verlag.

Fuchs G (1994) Variations of the acetyl-CoA pathway in diversely related microorganisms that are not acetogens. *Acetogenesis* pp. 507 – 520.

Fuchs G (2011) Alternative pathways of carbon dioxide fixation: insights into the early evolution of life? *Annual Review of Microbiology* 65:631–658.

Fyfe W (1988) Granites and a wet convecting ultramafic planet. *Earth and Environmental Science Transactions of the Royal Society of Edinburgh* 79:339–346.

Fyfe W (1994) The water inventory of the Earth: fluids and tectonics. *Geological Society, London, Special Publications* 78:1–7.

Geptner A, Kristmannsdóttir H, Kristjánsson JK, Marteinsson VT (2002) Biogenic saponite from an active submarine hot spring, Iceland. *Clays and Clay Minerals* 50:174–185.

Goldschmidt V (1952) Geochemical aspects of the origin of complex organic molecules on the Earth, as precursors to organic life. *New Biology* 12:97–105.

Gull M (2014) Prebiotic Phosphorylation Reactions on the Early Earth. *Challenges* 5:193–212.

Hagan WJ (2010) Uracil-catalyzed synthesis of acetyl phosphate: a photochemical driver for protometabolism. *Chembiochem : a European journal of chemical biology* 11:383–7.

Haldane J (1929) The origin of life. *Rationalist Annual* .

Hallis LJ, Huss GR, Nagashima K, Taylor GJ, Halldórsson SA, Hilton DR, Mottl MJ, Meech KJ (2015) Evidence for primordial water in Earth's deep mantle. *Science (New York, N.Y.)* 350:336–339.

Harel A, Bromberg Y, Falkowski PG, Bhattacharya D (2014) Evolutionary history of redox metal-binding domains across the tree of life. *Proceedings of the National Academy of Sciences* 111:7042–7047.

Hartman H (1975) Speculations on the origin and evolution of metabolism. *Journal of molecular evolution* 4:359–70.

Heinen W, Lauwers AM (1996) Organic sulfur compounds resulting from the interaction of iron sulfide, hydrogen sulfide and carbon dioxide in an anaerobic aqueous environment. *Origins of life and evolution of the biosphere* 26:131–150.

Henderson-Sellers A, Henderson-Sellers B (1988) Equable climate in the early Archaean. *Nature* 336:117–118.

Herschy B, Whicher A, Camprubi E, Watson C, Dartnell L, Ward J, Evans JRG, Lane N (2014) An origin-of-life reactor to simulate alkaline hydrothermal vents. *Journal of Molecular Evolution* 79:213–227.

Holland HD (1962) Model for the evolution of the Earth's atmosphere. *Petrologic Studies: A volume in honor of AF Buddington* 30:726 – 732.

Holland HD (2002) Volcanic gases, black smokers, and the great oxidation event. *Geochimica et Cosmochimica Acta* 66:3811–3826.

Holland HD (2009) Why the atmosphere became oxygenated: A proposal. *Geochimica et Cosmochimica Acta* 73:5241–5255.

Holm NG (2012) The significance of Mg in prebiotic geochemistry. *Geobiology* 10:269–279.

Holm NG (2014) Glasses as sources of condensed phosphates on the early earth. *Geochemical transactions* 15:8.

Holm NG, Baltscheffsky H (2011) Links between hydrothermal environments, pyrophosphate, Na^+, and early evolution. *Origins of Life and Evolution of Biospheres* 41:483–493.

Holm NG, Dumont M, Ivarsson M, Konn C (2006) Alkaline fluid circulation in ultramafic rocks and formation of nucleotide constituents: a hypothesis. *Geochemical transactions* 7:7.

Huber C, Wächtershäuser G (1997) Activated acetic acid by carbon fixation on (Fe,Ni)S under primordial conditions. *Science* 276:245–247.

Huber C, Eisenreich W, Hecht S, Wächtershäuser G (2003) A possible primordial peptide cycle. *Science (New York, N.Y.)* 301:938–940.

Imai E (1999) Elongation of oligopeptides in a simulated submarine hydrothermal system. *Science* 283:831–833.

Jaffrés JB, Shields GA, Wallmann K (2007) The oxygen isotope evolution of seawater: A critical review of a long-standing controversy and an improved geological water cycle model for the past 3.4 billion years. *Earth-Science Reviews* 83:83–122.

Jeong HY, Lee JH, Hayes KF (2008) Characterization of synthetic nanocrystalline mackinawite: crystal structure, particle size, and specific surface area. *Geochimica et cosmochimica acta* 72:493–505.

Kasting JF (1993) Earth's early atmosphere. *Science* 259:920–926.

Kaye G, Laby T (1986) *Tables of physical and chemical constraints* Longman, New York, 15th edition.

Kee T, Bryant D, Herschy B, Marriott K, Cosgrove N, Pasek M, Atlas Z, Cousins C (2013) Phosphate activation via reduced oxidation state phosphorus (P). Mild routes to condensed-P energy currency molecules. *Life* 3:386–402.

Keefe AD, Miller SL (1995) Are polyphosphates or phosphate esters prebiotic reagents? *Journal of molecular evolution* 41:693–702.

Keller MA, Turchyn AV, Ralser M (2014) Non-enzymatic glycolysis and pentose phosphate pathway-like reactions in a plausible Archean ocean. *Molecular systems biology* 10:725.

Kelley DS, Karson JA, Blackman DK, Früh-Green GL, Butterfield DA, Lilley MD, Olson EJ, Schrenk MO, Roe KK, Lebon GT, Rivizzigno P (2001) An off-axis hydrothermal vent field near the Mid-Atlantic Ridge at 30° N. *Nature* 412:145–9.

Kelley DS (2005) From the mantle to microbes: The Lost City hydrothermal field. *Oceanography* 18:32–45.

Kelley DS, Karson JA, Früh-Green GL, Yoerger DR, Shank TM, Butterfield DA, Hayes JM, Schrenk MO, Olson EJ, Proskurowski G, Jakuba M, Bradley A, Larson B, Ludwig KA, Glickson D, Buckman K, Bradley AS, Brazelton WJ, Roe K, Elend MJ, Delacour A, Bernasconi SM, Lilley MD, Baross Ja, Summons RE, Sylva SP (2005) A serpentinite-hosted ecosystem: the Lost City hydrothermal field. *Science (New York, N.Y.)* 307:1428–34.

Kieber RJ, Mopper K (1990) Determination of picomolar concentrations of carbonyl compounds in natural waters, including seawater, by liquid chromatography. *Enivironmental, Science and Technology Research* 24:1477–1481.

Kim JD, Senn S, Harel A, Jelen BI, Falkowski PG (2013) Discovering the electronic circuit diagram of life: structural relationships among transition metal binding sites in oxidoreductases. *Philosophical transactions of the Royal Society of London. Series B, Biological sciences* 368:20120257.

Klein AH, Shulla A, Reimann SA, Keating DH, Wolfe AJ (2007) The intracellular concentration of acetyl phosphate in Escherichia coli is sufficient for direct phosphorylation of two-component response regulators. *Journal of bacteriology* 189:5574–5581.

Knauth LP, Lowe DR (2003) High Archean climatic temperature inferred from oxygen isotope geochemistry of cherts in the 3.5 Ga Swaziland Supergroup, South Africa. *Geological Society of America Bulletin* 115:566–580.

Koonin EV, Martin W (2005) On the origin of genomes and cells within inorganic compartments. *Trends in Genetics* 21:647–654.

Kopetzki D, Antonietti M (2011) Hydrothermal formose reaction. *New Journal of Chemistry* 35:1787 – 1794.

Lambert D, Foster J, Frick L (1998) Geodynamics of magmatic Cu-Ni-PGE sulfide deposits: New insights from the Re-Os isotope system. *Bulletin of the Society of Economic Geologists* 93:121–136.

Lane N (2014) Bioenergetic constraints on the evolution of complex life. *Cold Spring Harbor perspectives in biology* 6:a015982.

Lane N (2015) *The Vital Question* Profile Books Ltd., London.

Lane N, Allen JF, Martin W (2010) How did LUCA make a living? Chemiosmosis in the origin of life. *BioEssays : news and reviews in molecular, cellular and developmental biology* 32:271–280.

Lane N, Martin W (2012) The origin of membrane bioenergetics. *Cell* 151:1406–1416.

Le Chatelier H, Boudouard O (1898) Limits of flammability of gaseous mixtures. *Bulletin de la Société Chimique de France (Paris)* 19:483 – 488.

Leduc S (1911) The Mechanism of Life. *Archives of the Roentgen Ray* 16:30 – 31.

Leman L, Orgel L, Ghadiri MR (2004) Carbonyl sulfide-mediated prebiotic formation of peptides. *Science (New York, N.Y.)* 306:283–286.

Lennie A, Redfern S, Champness P, Stoddart C, Schofield P, Vaughan D (1997) Transformation of mackinawite to greigite: an in situ X-ray powder diffraction and transmission electron microscope study. *American Mineralogist* 82:302–309.

Ligon B (2002) Biography: Louis Pasteur: A controversial figure in a debate on scientific ethics. *Seminars in Pediatric Infectious Diseases* 13:134–141.

Lipmann F, Tuttle LC (1944) Acetyl phosphate: chemistry, determination and synthesis. *J. Biol. Chem.* 153:571–582.

Liu R, Orgel LE (1997) Oxidative acylation using thioacids. *Nature* 389:52–54.

Lohrmann R, Orgel LE (1968) Prebiotic synthesis: phosphorylation in aqueous solution. *Science (New York, N.Y.)* 161:64–66.

Lombard J, López-García P, Moreira D (2012) The early evolution of lipid membranes and the three domains of life. *Nature Reviews Microbiology* 10:507–515.

Ludwig KA, Kelley DS, Butterfield DA, Nelson BK, Früh-Green G (2006) Formation and evolution of carbonate chimneys at the Lost City Hydrothermal Field. *Geochimica et Cosmochimica Acta* 70:3625–3645.

Ludwig KA, Shen CC, Kelley DS, Cheng H, Edwards RL (2011) U-Th systematics and ^{230}Th ages of carbonate chimneys at the Lost City Hydrothermal Field. *Geochimica et Cosmochimica Acta* 75:1869–1888.

Macleod G, Mckeown C, Hall A, Russell MJ (1994) Hydrothermal and oceanic pH conditions of possible relevance to the origin of life. *Origins of life and evolution of the biosphere* 24:19–41.

Maden BE (2000) Tetrahydrofolate and tetrahydromethanopterin compared: functionally distinct carriers in C_1 metabolism. *The Biochemical journal* 350:609–29.

Marteinsson VT, Kristjánsson JK, Kristmannsdóttir H, Dahlkvist M, Saemundsson K, Hannington M, Pétursdóttir SK, Geptner A, Stoffers P (2001) Discovery and description of giant submarine smectite cones on the seafloor in Eyjafjordur, northern Iceland, and a novel thermal microbial habitat. *Applied and environmental microbiology* 67:827–833.

Martin W (1999) Mosaic bacterial chromosomes: a challenge en route to a tree of genomes. *BioEssays : news and reviews in molecular, cellular and developmental biology* 21:99–104.

Martin W (2011) Early evolution without a tree of life. *Biology Direct* 6:36.

Martin W (2012) Hydrogen, metals, bifurcating electrons, and proton gradients: the early evolution of biological energy conservation. *FEBS letters* 586:485–493.

Martin W, Baross J, Kelley D, Russell MJ (2008) Hydrothermal vents and the origin of life. *Nature reviews. Microbiology* 6:805–814.

Martin W, Russell MJ (2003) On the origins of cells: a hypothesis for the evolutionary transitions from abiotic geochemistry to chemoautotrophic prokaryotes, and from prokaryotes to nucleated cells. *Philosophical transactions of the Royal Society of London. Series B, Biological sciences* 358:59–83; discussion 83–5.

Martin W, Russell MJ (2007) On the origin of biochemistry at an alkaline hydrothermal vent. *Philosophical transactions of the Royal Society of London. Series B, Biological sciences* 362:1887–1925.

Martin W, Sousa FL, Lane N (2014) Evolution. Energy at life's origin. *Science (New York, N.Y.)* 344:1092–1093.

Mast CB, Braun D (2010) Thermal trap for DNA replication. *Physical Review Letters* 104:1–4.

Mast CB, Schink S, Gerland U, Braun D (2013) Escalation of polymerization in a thermal gradient. *Proceedings of the National Academy of Sciences of the United States of America* 110:8030–8035.

McCollom TM (2013) Miller-Urey and beyond: what have we learned about prebiotic organic synthesis reactions in the past 60 years? *Annual Review of Earth and Planetary Sciences* 41:207–229.

McCollom TM, Seewald JS (2007) Abiotic Synthesis of Organic Compounds in Deep-Sea Hydrothermal Environments on Abiotic Synthesis. *Chemical reviews* 107:382–401.

Mielke RE, Robinson KJ, White LM, McGlynn SE, McEachern K, Bhartia R, Kanik I, Russell MJ (2011) Iron-sulfide-bearing chimneys as potential catalytic energy traps at life's emergence. *Astrobiology* 11:933–50.

Mielke RE, Russell MJ, Wilson PR, McGlynn SE, Coleman M, Kidd R, Kanik I (2010) Design, fabrication, and test of a hydrothermal reactor for origin-of-life experiments. *Astrobiology* 10:799–810.

Miller SL (1953) A production of amino acids under possible primitive Earth conditions. *Science* 117:528–529.

Miller SL (1957) The mechanism of synthesis of amino acids by electric discharges. *Biochimica et Biophysica Acta* 23:480–489.

Mitchell P (1961) Coupling of phosphorylation to electron and hydrogen transfer by a chemi-osmotic type of mechanism. *Nature* 191:144 – 148.

Morasch M, Mast CB, Langer JK, Schilcher P, Braun D (2014) Dry polymerization of 3',5'-cyclic GMP to long strands of RNA. *ChemBioChem* 15:879–883.

Morowitz HJ, Kostelnik JD, Yang J, Cody GD (2000) The origin of intermediary metabolism. *Proceedings of the National Academy of Sciences* 97:7704–7708.

Mullet M, Boursiquot S, Abdelmoula M, Génin JM, Ehrhardt JJ (2002) Surface chemistry and structural properties of mackinawite prepared by reaction of sulfide ions with metallic iron. *Geochimica et Cosmochimica Acta* 66:829–836.

Mysen BO, Cody GD (2001) Silicate-phosphate interactions in silicate glasses and melts: II. quantitative, high-temperature structure of P-bearing alkali aluminosilicate melts. *Geochimica et Cosmochimica Acta* 65:2413–2431.

Navarro-Gonzalez R, McKay CP, Mvondo DN (2001) A possible nitrogen crisis for Archaean life due to reduced nitrogen fixation by lightning. *Nature* 412:61–64.

Nisbet EG (1985) The geological setting of the earliest life forms. *Journal of Molecular Evolution* 21:289–298.

Nisbet EG, Cheadle MJ, Arndt NT, Bickle MJ (1993) Constraining the potential temperature of the archean mantle - a review of the evidence from komatiites. *Lithos* 30:291–307.

Nisbet EG, Sleep NH (2001) The habitat and nature of early life. *Nature* 409:1083–91.

Nitschke W, Russell MJ (2009) Hydrothermal focusing of chemical and chemiosmotic energy, supported by delivery of catalytic Fe, Ni, Mo/W, Co, S and Se, forced life to emerge. *Journal of molecular evolution* 69:481–496.

Nitschke W, Russell MJ (2013) Beating the acetyl coenzyme A-pathway to the origin of life. *Philosophical transactions of the Royal Society of London. Series B, Biological sciences* 368:20120258.

Oparin A (1924) The origin of life. *Proiskhozhdenie zhizny, Moscow, Trad* .

Orgel LE (1998) The origin of life-a review of facts and speculations. *Trends in Biochemical Sciences* 23:491–495.

Orgel LE (1999) Are you serious, Dr Mitchell? *Nature* 402:17.

Orgel LE (2004) Prebiotic chemistry and the origin of the RNA world. *Critical Reviews in Biochemistry and Molecular Biology* 39:99–123.

Orgel LE (2008) The implausibility of metabolic cycles on the prebiotic Earth. *PLoS biology* 6:e18.

Oró J (1960) Synthesis of adenine from ammonium cyanide. *Biochemical and Biophysical Research Communications* 2:407–412.

Pasek M, Harnmeijer JP, Buick R, Gull M, Atlas Z (2013) Evidence for reactive reduced phosphorus species in the early Archean ocean. *Proceedings of the National Academy of Sciences of the United States of America* 110:10089–94.

Pasek M, Kee T (2011) On the origin of phosphorylated biomolecules In *Origins of Life: The Primal Self-Organization*, pp. 57–84. Springer Berlin Heidelberg.

Pasek M, Lauretta D (2008) Extraterrestrial flux of potentially prebiotic C, N, and P to the early earth. *Origins of Life and Evolution of Biospheres* 38:5–21.

Pasteur L (1862) *Mémoire sur les corpuscules organisés qui existent dans l'atmosphère: examen de la doctrine des générations spontanées* Mallet-Bachelier.

Peretó JG, Velasco AM, Becerra A, Lazcano A (2010) Comparative biochemistry of CO_2 fixation and the evolution of autotrophy. *International Microbiology* 2:3–10.

Peters JW, Williams LD (2012) The Origin of Life: Look Up and Look Down. *Astrobiology* 12:1087–1092.

Pinti DL (2005) The origin and evolution of the oceans In *Lectures in Astrobiology*, Vol. I, pp. 83–112. Springer Berlin Heidelberg.

Powner MW, Gerland B, Sutherland JD (2009) Synthesis of activated pyrimidine ribonucleotides in prebiotically plausible conditions. *Nature* 459:239–242.

Rabinowitz J (1970) Peptide and amide bond formation in aqueous solutions of cyclic or linear polyphosphates as a possible prebiotic process. *Helvetica chimica acta* 53:1350–1355.

Rabinowitz J, Flores J, Krebsback R, Rogers G (1969) Peptide formation in the presence of linear or cyclic polyphosphates. *Nature* 224:795–796.

Rajamani S, Vlassov A, Benner S, Coombs A, Olasagasti F, Deamer D (2008) Lipid-assisted synthesis of RNA-like polymers from mononucleotides. *Origins of Life and Evolution of Biospheres* 38:57–74.

Reineck P, Wienken CJ, Braun D (2010) Thermophoresis of single stranded DNA. *Electrophoresis* 31:279–286.

Ricardo A, Carrigan M, Olcott A, Benner S (2004) Borate minerals stabilize ribose. *Science* 303:196–196.

Richter FM (1988) A major change in the thermal state of the Earth at the Archean-Proterozoic boundary: Consequences for the nature and preservation of continental lithosphere. *Journal of Petrology* pp. 39–52.

Robert F, Chaussidon M (2006) A palaeotemperature curve for the Precambrian oceans based on silicon isotopes in cherts. *Nature* 443:969–72.

Russell MJ, Arndt NT (2005) Geodynamic and metabolic cycles in the Hadean. *Biogeosciences* 2:97–111.

Russell MJ (2011) *Abiogenesis and the Origins of Life.*

Russell MJ, Barge LM, Bhartia R, Bocanegra D, Bracher PJ, Branscomb E, Kidd R, McGlynn S, Meier DH, Nitschke W, Shibuya T, Vance S, White L, Kanik I (2014) The drive to life on wet and icy worlds. *Astrobiology* 14:308–343.

Russell MJ, Daniel RM, Hall AJ (1993) On the emergence of life via catalytic iron-sulphide membranes. *Terra Research* 5:343–347.

Russell MJ, Daniel RM, Hall AJ, Sherringham J (1994) A hydrothermally precipitated catalytic iron sulphide membrane as a first step toward life. *Journal of Molecular Evolution* 39:231–243.

Russell MJ, Hall AJ (1997) The emergence of life from iron monosulphide bubbles at a submarine hydrothermal redox and pH front. *Journal of the Geological Society* 154:377–402.

Russell MJ, Hall AJ, Martin W (2010) Serpentinization as a source of energy at the origin of life. *Geobiology* 8:355–71.

Russell MJ, Hall AJ, Boyce AJ, Fallick AE (2005) 100th anniversary special paper: on hydrothermal convection systems and the emergence of life. *Economic Geology* 100:419–438.

Russell MJ, Hall AJ, Cairns-Smith A, Braterman P (1988) Submarine vents and the origin of life. *Nature* 336:117.

Russell MJ, Hall AJ, Turner D (1989) In vitro growth of iron sulphide chimneys: possible culture chambers for origin-of-life experiments. *Terra Nova* 1:238–241.

Russell MJ, Martin W (2004) The rocky roots of the acetyl-CoA pathway. *Trends in biochemical sciences* 29:358–363.

Say RF, Fuchs G (2010) Fructose 1,6-bisphosphate aldolase/phosphatase may be an ancestral gluconeogenic enzyme. *Nature* 464:1077–1081.

Schimadzu (2016) TOC-L TOC Analyzers.

Schoepp-Cothenet B, van Lis R, Atteia A, Baymann F, Capowiez L, Ducluzeau AL, Duval S, ten Brink F, Russell MJ, Nitschke W (2013) On the universal core of bioenergetics. *Biochimica et biophysica acta* 1827:79–93.

Schoonen Maa, Xu Y, Bebie J (1999) Energetics and kinetics of the prebiotic synthesis of simple organic acids and amino acids with the FeS-H_2S/FeS_2 redox couple as reductant. *Origins of Life and Evolution of Biospheres* 29:5–32.

Schulte MD, Rogers KL (2004) Thiols in hydrothermal solution: standard partial molal properties and their role in the organic geochemistry of hydrothermal environments. *Geochimica et Cosmochimica Acta* 68:1087–1097.

Schwartz M (2001) The life and works of Louis Pasteur. *Journal of Applied Microbiology* 91:597–601.

Seewald JS, Zolotov MY, McCollom T (2006) Experimental investigation of single carbon compounds under hydrothermal conditions. *Geochimica et Cosmochimica Acta* 70:446–460.

Shields Ga, Kasting JF (2007) Palaeoclimatology: evidence for hot early oceans? *Nature* 447:969–972.

Shock EL, Schulte MD (1998) Organic synthesis during fluid mixing in hydrothermal systems. *Journal of Geophysical Research* 103:28513.

Simoncini E, Kleidon A, Gallori E (2010) Thermodynamics of chemical free energy generation in off-axis hydrothermal vent systems and its consequences for compartmentalization and the emergence of life. *Journal of Cosmology* 10:3325–3344.

Sleep NH, Meibom A, Fridriksson T, Coleman RG, Bird DK (2004) H_2-rich fluids from serpentinization: geochemical and biotic implications. *Proceedings of the National Academy of Sciences of the United States of America* 101:12818–23.

Sleep NH, Zahnle K, Neuhoff PS (2001) Initiation of clement surface conditions on the earliest Earth. *Proceedings of the National Academy of Sciences of the United States of America* 98:3666–3672.

Sleep NH, Bird DK, Pope EC (2011) Serpentinite and the dawn of life. *Philosophical transactions of the Royal Society of London. Series B, Biological sciences* 366:2857–69.

Sojo V, Herschy B, Whicher A, Camprubi E, Lane N (2016) The origin of life in alkaline hydrothermal vents. *Astrobiology* 16:181–197.

Sojo V, Pomiankowski A, Lane N (2014) A bioenergetic basis for membrane divergence in archaea and bacteria. *PLoS Biology* 12:e1001926.

Sousa FL, Martin W (2014) Biochemical fossils of the ancient transition from geoenergetics to bioenergetics in prokaryotic one carbon compound metabolism. *Biochimica et Biophysica Acta - Bioenergetics* 1837:964–981.

Sousa FL, Thiergart T, Landan G, Nelson-Sathi S, Pereira IAC, Allen JF, Lane N, Martin W (2013) Early bioenergetic evolution. *Philosophical transactions of the Royal Society of London. Series B, Biological sciences* 368:20130088.

Spiess F, Macdonald K, Atwater T, Ballard B, Carranza A, Cordoba D, Cox C, Diaz Garcia M, Francheteau J, Guerrera J, Hawkins J, Haymon R, Hessler R, Juteau M, Kastner M, Larson R, Luyendyk B, Macdougall J, Miller S, Normak W, Orcutt J, Rangin C (1980) East Pacific Rise: Hot springs and geophysical experiments. *Science* 207:1421–1433.

Spudis PD, Wilhelms DE, Robinson MS (2011) The Sculptured Hills of the Taurus Highlands: Implications for the relative age of Serenitatis, basin chronologies and the cratering history of the Moon. *Journal of Geophysical Research E: Planets* 116:1–9.

Stetter KO (2006) Hyperthermophiles in the history of life. *Philosophical Transactions of the Royal Society B: Biological Sciences* 361:1837 – 1843.

Sugaya N, Nakagawa T, Sakurai K, Morita M, Onodera S (2001) Analysis of Aldehydes in Water by Head Space-GC/MS. *Journal of Health Science* 47:21–27.

Sutherland JD, Whitfield JN (1997) Prebiotic Chemistry: A Bioorganic. *Tetrahedron* 53:11493–11527.

Thauer RK, Jungermann K, Decker K (1977) Energy conservation in chemotrophic anaerobic bacteria. *Bacteriological reviews* 41:100–180.

Thauer RK (1998) Biochemistry of methanogenesis: a tribute to Marjory Stephenson. *Microbiology* 144:2377–2406.

Trail D, Watson EB, Tailby ND (2011) The oxidation state of Hadean magmas and implications for early Earth's atmosphere. *Nature* 480:79–82.

Turcotte D (1980) On the thermal evolution of the Earth. *Earth and Planetary Science Letters* 48:53–58.

Wächtershäuser G (1990) Evolution of the first metabolic cycles. *Proceedings of the National Academy of Sciences* 87:200–204.

Wächtershäuser G (1988) Before enzymes and templates: theory of surface metabolism. *Microbiological Reviews* 52:452–484.

Wang W, Song Y, Wang X, Yang Y, Liu X (2015) Alpha-oxo acids assisted transformation of FeS to Fe_3S_4 at low temperature: Implications for abiotic, biotic, and prebiotic mineralization. *Astrobiology* 15:1043–1051.

Westheimer FH (1987) Why nature chose phosphates. *Science* 235:1173–1178.

Whicher A, Camprubi E, Herschy B, Lane N (2016) Acetyl phosphate as the primordial energy currency at the origin of life. *Origins of Life and Evolution of Biospheres* Under cons.

Wilde SA, Valley JW, Peck WH, Graham CM (2001) Evidence from detrital zircons for the existence of continental crust and oceans on the Earth 4.4 Gyr ago. *Nature* 409:175–178.

Williams TA, Foster PG, Cox CJ, Embley TM (2013) An archaeal origin of eukaryotes supports only two primary domains of life. *Nature* 504:231–236.

Woese CR (2000) Interpreting the universal phylogenetic tree. *Proceedings of the National Academy of Sciences of the United States of America* 97:8392–8396.

Wolthers M, Charlet L, van Der Linde PR, Rickard D, van Der Weijden CH (2005) Surface chemistry of disordered mackinawite (FeS). *Geochimica et Cosmochimica Acta* 69:3469–3481.

Wu J, Zhang Z, Yu X, Pan H, Xu X, Tang R (2014) Mechanism of promoted dipeptide formation on hydroxyapatite crystal surfaces. *Chinese Science Bulletin* 56:633–639.

Yamagata Y, Inoue H, Inomata K (2005) Specific effect of magnesium ion on 2', 3'-cyclic amp synthesis from adenosine and trimeta phosphate in aqueous solution. *Origins of Life and Evolution of the Biosphere* 25:47–52.

Yamagata Y, Watanabe H, Saitoh M, Namba T (1991) Volcanic production of polyphosphates and its relevance to prebiotic evolution. *Nature* 352:516–519.

Yamaguchi A, Yamamoto M, Takai K, Ishii T, Hashimoto K, Nakamura R (2014) Electrochemical CO_2 reduction by Ni-containing iron sulfides: How is CO_2 electrochemically reduced at bisulfide-bearing deep-sea hydrothermal precipitates? *Electrochimica Acta* 141:311–318.

Zahnle K, Arndt N, Cockell C, Halliday A, Nisbet E, Selsis F, Sleep NH (2007) Emergence of a habitable planet. *Space Science Reviews* 129:35–78.

Zahnle K, Schaefer L, Fegley B (2010) Earth's earliest atmospheres. *Cold Spring Harbor perspectives in biology* 2:a004895.